

ADA 037259

EM-4883

DESIGN AND DEVELOPMENT OF A
SEGMENTED MAGNET HOMOPOLAR TORQUE CONVERTER.

FINAL TECHNICAL REPORT.

10 May 72 - 30 Jun 76

Submitted to ARPA in Sept 1976

Principal Investigator:

G. J. Mole, Manager
Superconducting Electric Machinery Systems
Phone: (412) 256-3612

C. J. /Mole, F. G. /Arcella, E. /Berkey,
D. J. /Boes V. B. /Doshi

Sponsored by:

Advanced Research Projects Agency

✓ ARPA Order No. - 2174

This research was supported by the Advanced Research Projects Agency of the Department of Defense under Contract No. DAH015-72-C-0229. Effective date of Contract - 10 May 1972. Contract expiration date 30 June 1976. Amount of contract - \$2,368,670.

WESTINGHOUSE ELECTRIC CORPORATION
ELECTRO-MECHANICAL DIVISION
P.O. BOX 217
CHESWICK, PENNSYLVANIA 15024

390 359

D D C
RECEIVED
MAR 22 1977
A

DISTRIBUTION STATEMENT A
Approved for public release;
Distribution Unlimited

The views and conclusions contained in this document are those of the authors and should not be interpreted as necessarily representing the official policies, either expressed or implied, of the Advanced Research Projects Agency or the U.S. Government.

Unclassified

Security Classification

DOCUMENT CONTROL DATA - R & D

(Security classification of title, body of abstract and indexing annotation must be entered when the overall report is classified)

1. ORIGINATING ACTIVITY (Corporate author) Westinghouse Electric Corporation Electro-Mechanical Division Cheswick Avenue, Cheswick, PA 15024		2a. REPORT SECURITY CLASSIFICATION Unclassified	
3. REPORT TITLE DESIGN AND DEVELOPMENT OF A SEGMENTED MAGNET HOMOPOLAR TORQUE CONVERTER		2b. GROUP	
4. DESCRIPTIVE NOTES (Type of report and inclusive dates) Final Technical Report for Contract from 10 May 1972 through 30 June 1976.			
5. AUTHOR(S) (First name, middle initial, last name) C.J.Mole/F.G.Arcella/E.Berkey/D.J.Boes/V.B.Doshi/R.A.Feranchak/D.L.Greene/H.E.HallerIII J.L.Johnson/S.A.Karpathy/A.R.Keeton/D.C.Litz/I.R.McNab/L.E.Moberly/E.Mullan/P.Reichner/ R.D.Schultz/R.M.Slepian/R.E.Stillwagon/O.S.Taylor/T.C.Tsu/A.Ulke/T.J.Webb/L.N.Wedman/			
6. REPORT DATE September 1976		7a. TOTAL NO. OF PAGES 318	7b. NO. OF REFS 47
8a. CONTRACT OR GRANT NO. DAHC 15-72-C-0229		9a. ORIGINATOR'S REPORT NUMBER(S) E.M. 4883	
b. PROJECT NO.		9b. OTHER REPORT NO(S) (Any other numbers that may be assigned)	
c.		10. DISTRIBUTION STATEMENT Qualified requesters may obtain copies of this report from Defense Documentation Center, Cameron Station, Alexandria, Virginia 22314	
d.		11. SUPPLEMENTARY NOTES	
		12. SPONSORING MILITARY ACTIVITY Advanced Research Projects Agency Department of Defense 1400 Wilson Blvd., Arlington, VA 22209	
13. ABSTRACT This program was for the research and development of a new mechanical power transmission concept: the segmented magnet homopolar torque converter. The purpose of this device is to convert unidirectional torque of constant speed (such as from a steam turbine prime mover) into variable speed output torque in either the forward or reverse directions. The concept offers an efficient, lightweight low volume design with potential application over a wide range of speeds and power ratings in the range from hundreds to tens of thousands of horsepower. This machine concept can be applied to commercial and military advanced concept vehicles for both terrain and marine environments. In Phase I the technical problems were reviewed, the machine concepts were studied, and a detailed technical plan was evolved for the entire program. In Phase II, a reliable constant speed current collection system was developed and demonstrated in an actual segmented magnet homopolar generator (SEGMAG). The objective of Phase III was to extend the technology developed in Phase II for constant speed machines to the case of the torque converter which must operate at variable and reversing speeds. The program places particular emphasis on the technology of advanced current collection systems for the reason this is essential for the success of the homopolar machine concept. Phases I, II, and the initial Phase III effort were based on the use of liquid metal current collectors. In Phase III-A (beginning 1 July 1975) work was redirected toward the use of a promising current collection concept utilizing a solid brush-gas-vapor additive system. This report encompasses the completion of the contractual workscope.			

DD FORM 1 NOV 65 1473

Unclassified

Security Classification

Unclassified

Security Classification

14 KEY WORDS	LINK A		LINK B		LINK C	
	ROLE	WT	ROLE	WT	ROLE	WT
alkali metals						
current collectors						
dc motor						
drive						
drive motor						
electric brushes						
electric drive						
electric machine						
homopolar						
liquid metals						
motor						
propulsion						
ship propulsion						
torque converter						

Lettron file

A

Unclassified

Security Classification

E.M. 4883

DESIGN AND DEVELOPMENT OF A
SEGMENTED MAGNET HOMOPOLAR TORQUE CONVERTER

FINAL TECHNICAL REPORT

Submitted to ARPA in September 1976

Principal Investigator:

C. J. Mole

C. J. Mole, Manager
Superconducting Electric Machinery Systems
Phone: (412) 256-3612

Sponsored by:

Advanced Research Projects Agency
ARPA Order No. 2174

This research was supported by the Advanced Research Projects Agency of the Department of Defense under Contract No. DAHC 15-72-C-0229. Effective date of Contract - 10 May 1972. Contract expiration date 30 June 1976. Amount of contract - \$2,368,670.

WESTINGHOUSE ELECTRIC CORPORATION
ELECTRO-MECHANICAL DIVISION
P.O. BOX 217
CHESWICK, PENNSYLVANIA 15024

THIS FINAL TECHNICAL REPORT CONSISTS OF TWO VOLUMES:

VOLUME I: COMPLETION OF PHASE III-A SOLID BRUSH CURRENT COLLECTOR DEVELOPMENT FOR HIGH CURRENT DENSITY APPLICATIONS, encompassing the period from December 1, 1975 through June 30, 1976.

VOLUME II: SUMMARY OF TECHNICAL ACCOMPLISHMENTS FOR ENTIRE CONTRACT, from its inception - May 10, 1972 to its completion - June 30, 1976.

TABLE OF CONTENTSPage

VOLUME I: COMPLETION OF PHASE III-A SOLID BRUSH CURRENT COLLECTOR
DEVELOPMENT FOR HIGH CURRENT DENSITY APPLICATIONS

SECTION 1	INTRODUCTION AND SUMMARY.	I 1-1
1.0	BACKGROUND	I 1-1
1.1	OBJECTIVES	I 1-1
1.2	PRIOR AND RELATED WORK	I 1-2
1.3	SUMMARY OF CURRENT PROGRESS.	I 1-2
1.3.1	Current Collector Test Rigs	I 1-2
1.3.2	Current Collector Contact Material/Performance.	I 1-3
1.3.3	Current Collector Mechanical Load Systems.	I 1-3
1.3.4	Current Collector Interface Cooling Systems	I 1-4
1.3.5	Current Collector Gaseous Environment/Control	I 1-4
1.3.6	Application Studies for Solid Brush SEGMAG Machines	I 1-4
SECTION 2	CURRENT COLLECTOR TEST RIGS	I 2-1
2.0	GENERAL.	I 2-1
2.1	LABORATORY BRUSH TESTERS	I 2-1
2.1.1	Objectives.	I 2-2
2.1.2	Prior and Related Work.	I 2-2
2.1.3	Current Progress.	I 2-2
2.2	MACHINE ENVIRONMENT BRUSH TESTER (MEB)	I 2-2
2.2.1	Objectives.	I 2-2
2.2.2	Prior and Related Work.	I 2-5
2.2.3	Current Progress.	I 2-5
SECTION 3	CURRENT COLLECTOR CONTACT MATERIAL/PERFORMANCE.	I 3-1
3.1	OBJECTIVES	I 3-1
3.2	PRIOR AND RELATED WORK	I 3-1
3.3	CURRENT PROGRESS	I 3-1
3.3.0	General	I 3-1
3.3.1	Brush Materials	I 3-2
3.3.2	Ring Material	I 3-3
SECTION 4	CURRENT COLLECTOR MECHANICAL LOAD SYSTEMS	I 4-1
4.1	OBJECTIVES	I 4-1
4.2	PRIOR AND RELATED WORK	I 4-1
4.3	CURRENT PROGRESS	I 4-1
4.3.1	Electrical Shunts	I 4-2
4.3.2	Actuation System.	I 4-5
4.4	REFERENCES	I 4-5

VOLUME 1 (Cont'd.)	Page
SECTION 5 CURRENT COLLECTOR INTERFACE COOLING SYSTEMS. . . .	I 5-1
5.1 OBJECTIVES.	I 5-1
5.2 PRIOR AND RELATED WORK.	I 5-1
5.3 CURRENT PROGRESS.	I 5-1
SECTION 6 CURRENT COLLECTION GASEOUS ENVIRONMENT/CONTROL . .	I 6-1
6.1 OBJECTIVES.	I 6-1
6.2 PRIOR AND RELATED WORK.	I 6-1
6.3 CURRENT PROGRESS.	I 6-1
SECTION 7 APPLICATION STUDIES FOR SOLID BRUSH SEGMAG MACHINES.	I 7-1
7.1 OBJECTIVES.	I 7-1
7.2 PRIOR AND RELATED WORK.	I 7-1
7.3 CURRENT PROGRESS.	I 7-1

VOLUME II: SUMMARY OF TECHNICAL ACCOMPLISHMENTS FOR ENTIRE CONTRACT

SECTION 1 INTRODUCTION AND SUMMARY	II 1-1
1.0 GENERAL	II 1-1
1.1 BACKGROUND.	II 1-1
1.2 OBJECTIVES.	II 1-1
1.3 SUMMARY OF CONTRACTUAL ACCOMPLISHMENTS. . . .	II 1-2
1.3.1 Summary of Contractual Accomplishments in Phases I, II, III	II 1-2
1.3.2 Summary of Contractual Accomplishments in Phase III-A	II 1-8
1.4 ORGANIZATION OF FINAL REPORT.	II 1-10

PART A: LIQUID METAL SEGMAG DEVELOPMENTS

SECTION 2 CURRENT COLLECTOR TEST RIGS.	II 2-1
2.0 GENERAL	II 2-1
2.1 SEGMENTED MAGNET HOMOPOLAR TORQUE CONVERTER (SMHTC).	II 2-1
2.1.1 Objectives	II 2-1
2.1.2 Prior and Related Work	II 2-2
2.1.3 Summary of Accomplishments	II 2-2
2.1.4 Conclusions.	II 2-12
2.1.5 References	II 2-13
2.2 SEGMENTED MAGNET HOMOPOLAR MACHINE (SEGMAG) . .	II 2-14
2.2.1 Objectives	II 2-14
2.2.2 Prior and Related Work	II 2-14
2.2.3 Summary of Accomplishments	II 2-14
2.2.4 Conclusions.	II 2-38
2.2.5 References	II 2-38

VOLUME II (Cont'd.)

Page

2.3	GEC GENERATOR.	II 2-40
2.3.1	Objectives.	II 2-40
2.3.2	Prior and Related Work.	II 2-40
2.3.3	Summary of Accomplishments.	II 2-40
2.3.4	Conclusions	II 2-50
SECTION 3	APPLICATION STUDIES FOR SEGMAG MACHINERY WITH CURRENT COLLECTORS	II 3-1
3.1	OBJECTIVES	II 3-1
3.2	SUMMARY OF ACCOMPLISHMENTS	II 3-1
3.2.0	General	II 3-1
3.2.1	Ship Propulsion	II 3-2
3.2.2	Torpedo Drive	II 3-2
3.2.3	High Power Pulsing Generators	II 3-4
3.2.4	Heavy Vehicle Drive	II 3-4
3.2.5	Variable Speed Input/Constant Speed Output Aviation Drives.	II 3-5
3.2.6	Homopolar Servomotor.	II 3-6
3.2.7	Tank Propulsion System.	II 3-6
3.2.8	Amphibious Vehicles Propulsion Systems	II 3-9
3.2.9	Miscellaneous Applications.	II 3-10
3.3	CONCLUSIONS.	II 3-11
SECTION 4	LIQUID METAL CURRENT COLLECTION SYSTEMS TECHNOLOGY AND EXPERIMENTAL PROGRAM	II 4-1
4.1	OBJECTIVES	II 4-1
4.2	PRIOR AND RELATED WORK	II 4-1
4.3	SUMMARY OF ACCOMPLISHMENTS	II 4-2
4.3.0	General	II 4-2
4.3.1	Power Losses in Current Collectors.	II 4-4
4.3.2	Confinement of Liquid Metal	II 4-9
4.3.3	Current Collector Evaluation Program and Test Facilities	II 4-13
4.4	CONCLUSIONS.	II 4-21
4.5	REFERENCES	II 4-22
SECTION 5	LIQUID METAL CURRENT COLLECTION SYSTEMS COLLECTOR DESIGN STUDIES.	II 5-1
5.1	OBJECTIVES	II 5-1
5.2	PRIOR AND RELATED WORK	II 5-1
5.3	SUMMARY OF ACCOMPLISHMENTS	II 5-2
5.3.0	General	II 5-2
5.3.1	High Speed Collectors	II 5-3
5.3.2	Flooded Collectors.	II 5-3
5.3.3	Unflooded Collectors.	II 5-3
5.3.4	Hybrid Collectors	II 5-56
5.4	CONCLUSIONS.	II 5-78
5.5	REFERENCES	II 5-79

VOLUME 11 (Cont'd.)

Page

SECTION 6	LIQUID METAL SUPPORT SYSTEMS.	II 6-1
6.1	OBJECTIVES	II 6-1
6.2	PRIOR AND RELATED WORK	II 6-1
6.3	SUMMARY OF ACCOMPLISHMENTS	II 6-1
6.3.1	Machine Materials Selection	II 6-4
6.3.2	Liquid Metal Systems.	II 6-14
6.3.3	Cover Gas Systems	II 6-19
6.3.4	Support System Summary.	II 6-22
6.4	CONCLUSIONS.	II 6-22
6.5	REFERENCES	II 6-22
SECTION 7	SEAL STUDY.	II 7-1
7.1	OBJECTIVES	II 7-1
7.2	PRIOR AND RELATED WORK	II 7-1
7.3	SUMMARY OF ACCOMPLISHMENTS	II 7-3
7.3.0	General	II 7-3
7.3.1	Test Stand Construction	II 7-5
7.3.2	Material Studies of Candidate Seal Composites	II 7-5
7.3.3	Face Seal Screening Tests	II 7-9
7.3.4	Functional Testing: Tandem Circumferential Seal	II 7-12
7.4	CONCLUSIONS.	II 7-18
7.5	REFERENCES	II 7-19

PART B: SOLID BRUSH SEGMAG DEVELOPMENTS

SECTION 8	SOLID BRUSH CURRENT COLLECTOR TEST RIGS	II 8-1
8.1	OBJECTIVES	II 8-1
8.2	PRIOR AND RELATED WORK	II 8-1
8.3	SUMMARY OF ACCOMPLISHMENTS	II 8-2
8.3.0	General	II 8-2
8.3.1	Brush Testers B1 and B2 -- For Testing Sub-Size Brushes.	II 8-3
8.3.2	High Speed Brush Testers HS1 and HS2 -- For Testing Full-size Brushes	II 8-5
8.3.3	Machine Environment Brush Tester (MEB).	II 8-8
SECTION 9	CURRENT COLLECTOR CONTACT MATERIAL/PERFORMANCE.	II 9-1
9.1	OBJECTIVES	II 9-1
9.2	PRIOR AND RELATED WORK	II 9-1
9.3	SUMMARY OF ACCOMPLISHMENTS	II 9-2
9.3.0	General	II 9-2
9.3.1	Testing Procedure	II 9-2
9.3.2	High Current Density (500-2500 A/in ²) Brush Material Test Results	II 9-4
9.3.3	Medium-High Current Density (to 500 A/in ²) Brush Material Test Results.	II 9-10
9.3.4	Brush Power Loss and Wear Characteristics	II 9-10

VOLUME II (Cont'd.)

Page

	9.3.5 Ring Materials.	II 9-14
	9.3.6 Additive Materials.	II 9-15
9.4	CONCLUSIONS.	II 9-15
9.5	REFERENCES	II 9-15
SECTION 10	CURRENT COLLECTOR MECHANICAL LOAD SYSTEMS	II 10-1
10.0	OBJECTIVES.	II 10-1
10.1	PRIOR AND RELATED WORK.	II 10-1
10.2	SUMMARY OF ACCOMPLISHMENTS.	II 10-1
	10.2.0 General	II 10-1
	10.2.1 Brush Holding System.	II 10-2
	10.2.2 Electrical Shunts	II 10-4
	10.2.3 Actuation System.	II 10-9
10.3	CONCLUSIONS	II 10-9
10.4	REFERENCES.	II 10-9
SECTION 11	CURRENT COLLECTOR INTERFACE COOLING SYSTEMS	II 11-1
11.1	OBJECTIVES.	II 11-1
11.2	PRIOR AND RELATED WORK.	II 11-1
11.3	SUMMARY OF ACCOMPLISHMENTS.	II 11-1
	11.3.0 General	II 11-1
SECTION 12	CURRENT COLLECTOR GASEOUS ENVIRONMENT/CONTROL	II 12-1
12.1	OBJECTIVES.	II 12-1
12.2	PRIOR AND RELATED WORK.	II 12-1
12.3	SUMMARY OF ACCOMPLISHMENTS.	II 12-1
	12.3.0 General	II 12-1
	12.3.1 Gaseous Environment Control System.	II 12-1
	12.3.2 General Operating Procedure	II 12-6
12.4	CONCLUSIONS	II 12-7
SECTION 13	APPLICATION STUDIES FOR SOLID BRUSH SEGMAG MACHINERY	II 13-1
13.1	OBJECTIVES.	II 13-1
13.2	PRIOR AND RELATED WORK.	II 13-1
13.3	DETAIL OF ACCOMPLISHMENTS	II 13-1

LIST OF FIGURESVOLUME I: COMPLETION OF PHASE III-A SOLID BRUSH CURRENT COLLECTOR
DEVELOPMENT FOR HIGH CURRENT DENSITY APPLICATIONS

<u>Figure</u>		<u>Page</u>
2.1.1	Test Chamter of B1 and B2 Brush Testers	I 2-3
2.1.2	Test System for B1 Brush Tester	I 2-3
2.1.3	Physical Arrangement of Components of Type HS1 and HS2 High Speed Brush Testers	I 2-4
2.1.4	High Speed Brush Testers (HS1 and HS2)	I 2-4
2.1.5	Machine-Environment Brush Tester (MEB)	I 2-6
2.1.6	Machine Environment Brush Tester (MEB) - Permits testing of solid brush systems in an actual SEGMAG machine environment.	I 2-7
2.1.7	MEB rotor showing copper drum, bearing housing and coolant seal system.	I 2-8
2.1.8	Water Cooled excitation coil positioned in stator drum.	I 2-10
2.1.9	Coolant cross-over tube, which is inserted into the rotor bore to provide controlled coolant flow to the rotor.	I 2-11
2.1.10	The MEB mounted on its test stand, showing (1 to r) the MEB, gear box and drive motor. Below the stand are components of the water cooling system.	I 2-12
3.1	Metal graphite brush copper ring contact loss characteristics. 500 A/in ² , 10-12 lb _f /in ² , 42-83 ft/s, inert gas ambient.	I 3-4
3.2	Metal graphite brush wear characteristics. Copper ring, 500 A/in ² , 10-12 lb _f /in ² , 42-83 ft/s, inert gas ambient.	I 3-5
4.1	Experimental shunt using silver plated metal fibers.	I 4-4
4.2	Metal fiber shunt electrical test site; current path in foreground shows shunt test block mounted to heat sink and shunt mating piece suspended from ceiling. Mating piece is pressed against shunt by cantilevered strain gauge assembly.	I 4-6

LIST OF FIGURES (Cont'd.)VOLUME I

<u>Figure</u>		<u>Page</u>
6.1	Environment gas control system for the Machine Environment Brush Tester (MEB).	I 6-2
6.2	Current collection gaseous environment control system for use with the Machine Environment Brush Tester (MEB).	I 6-3

VOLUME II: SUMMARY OF TECHNICAL ACCOMPLISHMENTS FOR ENTIRE CONTRACT

1.1	SEGMAG Generator, utilizing NaK liquid metal current collectors.	II 1-4
1.2	SEGMAG Generator on its test stand - the drive system and gas purification system are both on the right. The six NaK purification and supply loops are below. To their right are the gas subsystems for intercollector pressure balancing and shaft sealing.	II 1-4
1.3	GEC homopolar generator with GaIn current collection.	II 1-5
1.4	GEC homopolar machine in its test area showing the cover gas system (right), and the control panel (left).	II 1-5
1.5	Test stand used in evaluating liquid metal current collectors for SEGMAG machine.	II 1-6
1.6	Assembled NaK purification loop for servicing each current collector in the prototype SEGMAG machine.	II 1-7
1.7	Internal components of central gas purifier station for the SEGMAG homopolar machine.	II 1-7
1.8	High speed brush testers, for screening of prototypic brushes.	II 1-9

PART A: LIQUID METAL SEGMAG DEVELOPMENTS

2.1.1	Disk-Type homopolar machine (DISKMAG)	II 2-7
2.2.1	Principle of SEGMAG machine operation.	II 2-17
2.2.2	Benefits of axial segmentation of magnetic field (equivalent power machines).	II 2-17

LIST OF FIGURES (Cont'd.)VOLUME II

	<u>Page</u>
2.2.3 Typical current collector.	II 2-18
2.2.4 Circumferential force due to load current and axial magnetic field.	II 2-19
2.2.5 Load current force in magnified detail.	II 2-19
2.2.6 3000 hp prototype SEGMAG generator.	II 2-21
2.2.7 SEGMAG with top half of stator removed, showing field excitation coils.	II 2-22
2.2.8 Close-up of Fig. 2.2.7 showing SEGMAG current collector detail.	II 2-22
2.2.9 Half module of SEGMAG.	II 2-26
2.2.10 Thermal model of SEGMAG half module.	II 2-26
2.2.11 SEGMAG excitation coil.	II 2-27
2.2.12 SEGMAG Generator - The current collector terminals are shown in the foreground. The leads to the excitation coils are on top.	II 2-31
2.2.13 SEGMAG Generator on its test stand - The drive system and gas purification system are both on the right. The six NaK purification and supply loops are below. To their right are the gas subsystems for intercollector pressure balancing and shaft sealing.	II 2-31
2.2.14 SEGMAG no-load losses.	II 2-34
2.2.15 SEGMAG open circuit voltage.	II 2-34
2.2.16 Losses in SEGMAG due to short circuit current.	II 2-35
2.3.1 GEC vertical shaft homopolar machine schematic.	II 2-41
2.3.2 Front view of GEC test area in the Westinghouse Liquid Metal Laboratory. The cover gas impurity monitoring system is on the right. The machine control and test panel is on the left. Below the machine is a cover gas flowmeter, and also flowmeters and pressure regulator for the cooling water system.	II 2-43

LIST OF FIGURES (Cont'd.)VOLUME II

	<u>Page</u>
2.3.3 Side view of the test area showing the GaIn electrolytic purification cell, to the left of the GEC machine.	II 2-43
2.3.4 GEC open circuit test losses.	II 2-46
2.3.5 GEC total flux calculated from open circuit voltage and speed.	II 2-46
2.3.6 GEC short circuit test losses.	II 2-46
2.3.7 GEC motor test losses.	II 2-46
2.3.8 GEC calculated losses due to friction windage on liquid metal viscosity.	II 2-48
2.3.9 GEC calculated MHD losses.	II 2-48
2.3.10 GEC calculated I^2R losses.	II 2-48
2.3.11 GaIn purification cell schematic.	II 2-49
4.1 Model of liquid metal current collector.	II 4-5
4.2 Magnetic field effect on power losses (NaK-78). Axial field effect based upon Eqs. (4.3) and (4.6); radial field effects upon Eq. (4.7).	II 4-7
4.3 Calculated collector power loss, based upon assumed load current (100 kA), radial magnetic field (0.03T), peripheral velocity (67 m/s), and liquid metal (NaK-78).	II 4-9
4.4 Calculated pressure variation caused by load and circulating currents.	II 4-11
4.5 Effect of contact resistance (ϵ) on calculated pressure caused by load and circulating currents.	II 4-11
4.6 Calculated liquid metal velocity characteristics.	II 4-12
4.7 Test stand with auxiliary systems.	II 4-14
4.8 Current collector test rig.	II 4-14
4.9 Typical viscous torque-NaK flow characteristics: Collector radius, $r = 17.8$ cm; radial gap, $d = 1.59$ mm; width, $w = 1.91$ cm.	II 4-16

LIST OF FIGURES (Cont'd.)

		<u>Page</u>
4.10	Ordinary fluid dynamic power loss-speed characteristics for collector of Fig. 4.9.	II 4-16
4.11	Rotor speed and width effects on ordinary fluid dynamic power loss.	II 4-17
4.12	Torque temperature -- characteristics related to collector gap filling.	II 4-17
4.13	Critical performance dependency on temperature and speed.	II 4-18
4.14	Indication of collector fluid flow instability.	II 4-19
4.15	ϵ valves determined from radial field experiments with 17.8 cm radius collectors.	II 4-20
5.1	Lip-seal collector configuration.	II 5-8
5.2	Hydrostatically-positioned seal (sealed drain).	II 5-13
5.3	Hydrostatically-positioned seal.	II 5-13
5.4	Power-leakage relationship for a single annular seal lip (at $\Delta p = 20,700$ N/m ² , 3 psi).	II 5-15
5.5	Hydrodynamically-positioned seals.	II 5-22
5.6	Self-field electromagnetic (E.M.) containment.	II 5-32
5.7	Adaptation of pad design to annular collector ring.	II 5-42
5.8	Hybrid pad current collector schematic.	II 5-58
5.9	Typical hybrid pad.	II 5-58
5-10	Axial and radial current collector schematic.	II 5-60
5-11	Homopolar motor schematic.	II 5-61
5-12	Schematic of collector regions for the homopolar motor.	II 5-62
5-13	Hydrostatically positioned pad.	II 5-64
5-14	Hybrid pad geometry.	II 5-65

LIST OF FIGURES (Cont'd.)

VOLUME II

		<u>Page</u>
6.1	Phase diagram for the NaK binary system.	II 6-5
6.2	Glove box facilities utilized for the preparation and handling of materials being evaluated for NaK compatibility.	II 6-9
6.3	Simplified flow chart of materials compatibility test plan.	II 6-9
6.4	Surface and volume resistivity values obtained on heat aged and NaK exposed electrical insulation systems.	II 6-11
6.5	The change in maximum stress of candidate laminate materials as a result of NaK exposure at 140°C.	II 6-13
6.6	The change in elastic modulus of candidate laminate materials as a result of NaK exposure at 140°C.	II 6-13
6.7	Small NaK loop concept for servicing each current collector independently.	II 6-17
6.8	Assembled NaK loop of a current collector service in prototype SEGMAG machine.	II 6-17
6.9	3000 HP segmented magnet homopolar generator (SEGMAG) on test bed. The NaK loops are located below the SEGMAG and the diagnostic dials. The gas systems are to the lower right and far right of the test bed.	II 6-18
6-10	Calibration of NaK flowmeter.	II 6-18
6-11	SEGMAG cover gas systems.	II 6-20
7.1	Schematic of typical tandem circumferential seal.	II 7-4
7.2	Tandem circumferential seal test rig.	II 7-4
7.3	Shaft/Containment Seal Test Stand.	II 7-6
7.4	Details of Seal Test Device.	II 7-6
7.5	Seal Test Stand.	II 7-7
7.6	Face seal test stand.	II 7-7
7.7	Face seal screening test apparatus.	II 7-11

LIST OF FIGURES (Cont'd.)

VOLUME II

		<u>Page</u>
7.8	Operating temperature and friction coefficient vs. time for W Se ₂ /GaIn seal material - 15 psi 2360 fpm-N ₂ .	II 7-13
7.9	Operating temperature vs. time for SP-3 seal material - 2.6 psi - 2360 fpm - He.	II 7-13
7.10	Operating temperature and friction coefficient vs. time for SP-211 seal material - 2.6 psi - 2360 fpm-N ₂ .	II 7-14
7.11	Operating temperature and friction coefficient vs. time for Meldin PI-30 seal material - 15 psi - 2360 fpm - N ₂ .	II 7-14
7.12	Photograph of tandem circumferential seal; bore 3.97° diameter.	II 7-15
7.13	Leak rate vs. running time for Tandem Circumferential seal operating in dry N ₂ 2100 rpm - 5 psig feed gas.	II 7-15
7.14	Leak rate versus running time for tandem circumferential Stein Seal; carbon-graphite USG67 3600 RPM-N ₂ gas feed < - 45°C Dew pt.	II 7-17
7.15	Leak rate versus running time for tandem circumferential Stein seal; carbon-graphite USG67 3600 RPM - N ₂ gas feed < - 45°C Dew pt.	II 7-17
7.16	Leak rate vs. running time for tandem circumferential Stein seal - VespeI SP-211 3600 RPM - 5 psig N ₂ gas feed < - 45°C Dew pt.	II 7-19
8.1	Test chamber of Type B1 brush tester.	II 8-4
8.2	Type B1 brush test system.	II 8-6
8.3	Physical arrangement of components of type HS1 and HS2 high speed brush testers.	II 8-7
8.4	High speed brush testers (HS1 and HS2).	II 8-9
8.5	Machine-environment brush tester (MEB).	II 8-10
9.1	Contact voltage drop vs. load pressure for various brush materials.	II 9-6

LIST OF FIGURES (Cont'd.)

VOLUME II

		<u>Page</u>
9.2	Friction coefficient vs. load pressure for various brush materials.	II 9-7
9.3	Metal graphite brush-copper ring contact loss characteristics 500 A/in ² , 10-12 lbf/in ² , 42-83 ft/s, inert gas ambient.	II 9-12
9.4	Metal graphite brush wear characteristics, copper ring, 500 A/in ² , 10-12 lbf/in ² , 42-83 ft/s, inert gas ambient.	II 9-13
10.1	Brush holder used in HSl brush test rig.	II 10-3
10.2	Brush holder arrangement for the Machine-Environment Brush Tester (MEB).	II 10-5
10.3	Experimental shunt using silver plated metal fibers.	II 10-8
10.4	Metal fiber shunt electrical test site; current path in foreground shows shunt test block mounted to heat sink and shunt mating piece suspended from ceiling. Mating piece is pressed against shunt by cantilevered strain gauge assembly.	II 10-8
11.1	Brush holder used in HSl brush test rig.	II 11-3
12.1	Front panel view of gas control system.	II 12-2
12.2	Rear view of gas control system.	II 12-3
12.3	Current collection gaseous environment control system for use with the Machine Environment Brush Tester (MEB).	II 12-5

LIST OF TABLESVOLUME I: COMPLETION OF PHASE III-A SOLID BRUSH CURRENT COLLECTOR
DEVELOPMENT FOR HIGH CURRENT DENSITY APPLICATIONS

<u>Table</u>		<u>Page</u>
3.1	Loss Characteristics of Sliding Contact Material Combinations: Copper-Graphite Brush, 500 A/in ² , 12 lb _f /in ² , 51 ft/s, Inert Gas Ambient.	I 3-6

VOLUME II: SUMMARY OF TECHNICAL ACCOMPLISHMENTS FOR ENTIRE CONTRACTPART A: LIQUID METAL SEGMAG DEVELOPMENTS

2.1.1	Weights and Losses of Typical Machines for an 8000 HP, 3600/500 RPM Torque Converter.	II 2-5
2.1.2	8000 HP, 3600/500 RPM Torque Converter Options.	II 2-6
2.1.3	Dimensions and operating conditions for typical design 8,000 hp normal temperature and 40,000 hp SC Dick-Type "Flooded Gap" (DISKMAG) Homopolar Motors.	II 2-10
2.1.4	Seal Pressure and Rotor Thrust Forces for a Typical 8000 hp Normal Temperature and 40,000 hp SC Disk Type Motor (DISKMAG).	II 2-11
2.1.5	Calculated Power Losses for the 40,000 hp SC and 8,000 hp NT DISKMAGS.	II 2-12
2.2.1	Efficiency Tabulation.	II 2-37
3.1	Typical Application Parameters.	II 3-3
3.2	SEGMAG Machines Considered for Tank Drive.	II 3-8
5.1	Unflooded Motor Reference Design - Collector Requirements.	II 5-5
5.2	Classification of Unflooded Reversing Collector Concepts.	II 5-6
5.3	Evaluation Criteria for Current Collectors.	II 5-7

LIST OF TABLES (Cont'd.)VOLUME II

		<u>Page</u>
5.4	General Requirements for Reversing Collectors.	II 5-57
5.5	Specific Requirements for Typical Applications.	II 5-57
5.6	Typical Design Information.	II 5-74 and 5-75
5.7	Summary of Current Collector Component Power Losses.	II 5-76
5.8	Summary of Calculated Current Collector MHD Pressures.	II 5-77
6.1	Typical Electrical Machine Insulating Systems.	II 6-6
6.2	Rotor Banding Material 431-S-2 (Epoxy Novolac Resin/Glass Fibers) Tensile Test Data.	II 6-10
6.3	Braze Alloys Evaluated for NaK Compatibility at 140°C.	II 6-12
6.4	Materials Compatibility Summary.	II 6-15
6.5	NaK Loop Capabilities.	II 6-19
7.1	Seal Material Procured For Friction-Wear and Compatibility Studies.	II 7-8
7.2	Candidate Seal Materials for use in SEGMAG Primary Rotor Shaft Seals.	II 7-9
7.3	Face Seal Test Results on Candidate Seal Materials.	II 7-12
7.4	Friction-Wear Characteristics of Candidate Seal Materials Pre-and Post NaK Exposure.	II 7-13

PART B: SOLID BRUSH SEGMAG DEVELOPMENTS

9.1	Silver-Graphite Material Brush Test Results (2000 A/in ²) Ring Speed 2500 ft/min.	II 9-5
9.2	Performance Characteristics of SG216(1) Material Brushes, Ring Speed 2500 ft/min, Test Duration to 60 h.	II 9-8
9.3	Performance Characteristics of Selected Metal-Graphite Material Brushes, Ring Speed 5000 ft/min.	II 9-9

LIST OF TABLES (Cont'd.)VOLUME II

		<u>Page</u>
9.4	Performance Characteristics of Brush Materials (500 A/in ²) (Medium-High Current Density Applications).	II 9-11
9.5	Loss Characteristics of Sliding Contact Material Combinations Copper-Graphite Brush, 500 A/in ² , 12 lb _f /in ² , 51 ft/s, inert gas ambient.	II 9-14

E.M. 4883

VOLUME I

COMPLETION OF PHASE III-A
SOLID BRUSH CURRENT COLLECTOR
DEVELOPMENT FOR HIGH CURRENT
DENSITY APPLICATIONS

VOLUME I
COMPLETION OF PHASE III-A SOLID BRUSH CURRENT COLLECTOR
DEVELOPMENT FOR HIGH CURRENT DENSITY APPLICATIONS

SECTION 1

INTRODUCTION AND SUMMARY

1.0 BACKGROUND

Part I describes the completion of the work performed under Phase III-A of this contract, for the period of December 1, 1975 through June 30, 1976. Phase III-A involves the initiation of research and development of advanced current collection technology using a solid brush-gas-vapor-additive system. This development will have great potential value for reversing and other machine current collector systems.

The new current collection concept has demonstrated extremely good performance using individual brushes in a humidified inert atmosphere, and represents an ideal reversing collector system for the torque converter and other machines. The technology may be extended to high speed generators and allow the development of a high voltage SEGMAG, thus reducing current transmission problems substantially and enhancing the utilization of SEGMAG by DOD.

1.1 OBJECTIVES

The principal objective of the Phase III-A program is to initiate the development of high-power current collection systems for electrical machines, in order to increase the performance, life, and reliability of such machines. The individual steps are to: (1) investigate the materials and atmospheres of current collection systems; (2) to select preferred technical approaches in terms of the materials system and requirements; (3) to develop slip ring and commutator current collection systems appropriate to reasonably large machines; and finally (4) to conduct extensive testing to determine the performance and life of such systems. The specific objectives of Phase III-A are summarized below:

- 1) Using suitable parameters for typical machines, evaluate promising materials and atmospheres, in terms of velocity, current density, pressure, life, losses, and voltage drop. Select suitable combinations for continued evaluation.
- 2) From the materials selected, construct large brushes and test in the preferred atmosphere.
- 3) Construct a slip ring system using a suitable array of solid brush materials and test for bulk properties at variable speed. Evaluate load current sharing problems.

- 4) Determine the brush loading and cooling system requirements for selected materials. Evolve a system concept and fabricate a model for initial tests.
- 5) Design and construct a model system using two slip rings to evaluate the solid brush SEGMAG concept, and to determine the potential future technical problems with such a system. Testing over a wide range of speeds and loadings will be accomplished in a related program (ONR/ARPA Contract N00014-76-C-0683).
- 6) Conduct a continuous application study to correlate brush research with machine requirements and potential utilization. Assist in materials selection.

1.2 PRIOR AND RELATED WORK

Westinghouse has for many years been investigating the problems of power transfer across sliding electrical contacts (solid brushes). One of the results of this research was the demonstration that brush life can be increased 10 to 15 times by operating brushes in a humidified inert gas atmosphere rather than in air. These brushes are now in practical machine applications at current densities of 60 apsi.

Recent experimental work at Westinghouse has shown that very high current densities (3 MA/m^2 , 2 kA/in.^2) can be achieved when solid brushes are operating in controlled inert gas atmospheres with water and/or other additives. Furthermore, substantially reduced friction coefficients and voltage drops across the interface have been achieved simultaneously, resulting in a predicted brush life in the range of 20,000 to 200,000 hours.

The improved operating performance of these and other new brush systems will improve the performance of existing commercial machines, and will improve the applicability and maintainability of advanced concept machines, such as SEGMAG. However, before these new solid brush systems can be fully utilized it is important to characterize and understand their performance, and this is the central feature of the investigations planned here.

1.3 SUMMARY OF CURRENT PROGRESS

1.3.1 Current Collector Test Rigs

In support of those program objectives requiring experimental evaluation of brush and slip ring materials and current collector environment, five test rigs are required. These include four laboratory test rigs for the initial screening of materials and environments, as well as a Machine Environment Brush Tester (MEB) which can be utilized for more controlled and extensive examination of selected brush and slip ring materials.

1.3.1.1 Laboratory Brush Testers

In addition to the B1 and HS1 brush testers reported previously (E.M. 4790), two further Westinghouse brush testers, B2 and HS2, were modified and made ready for operation.

1.3.1.2 Machine Environment Brush Tester (MEB)

Construction and assembly of the MEB tester was completed. In addition, a test plan was drafted for utilization of MEB in the analysis of promising brush materials. The MEB test rig was subjected to hydrostatic test and mounted on its test stand. The first set of MEB test brushes was received and prepared for testing.

1.3.2 Current Collector Contact Material/Performance

Useful developmental information was obtained from recent screening tests of brush, ring, and vapor additive materials.

Based on screening test data, commercially available graphite brushes containing 65-75 w/o copper are reasonable candidates for more extensive testing and evaluation on the larger, more sophisticated test machines.

Based on a fixed set of operating conditions, contact resistance is lowest when copper-graphite brushes are run on copper rings. Friction coefficients are lower when the same brushes are run against either nickel or steel collector rings.

1.3.3 Current Collector Mechanical Load Systems

A multi-contact electrical-shunt for use in solid brush holders was analyzed in this reporting period. Several shunts were fabricated and statically tested, with encouraging results. The metal fiber construction of these shunts is also being considered for use in multi-contact brushes.

To achieve minimum power loss under low-load operating conditions, it is necessary to maintain high current density per brush. This can be accomplished by lifting some of the brushes during low load. A full-scale model of such a brush actuation system was constructed in order to facilitate evaluation of this concept.

1.3.4 Current Collector Interface Cooling Systems

The thermal data from the HSI tester was evaluated. The results indicate that the present HSI brushholder meets the program thermal objectives. This basic brushholder thermal information will be utilized as a guideline for the evaluation of future brushholder concepts.

1.3.5 Current Collector Gaseous Environment/Control

A gas recirculating system called "the current collector gaseous environment control" was constructed for the purpose of controlling the internal ambient atmosphere of the Machine Environment Brush Tester (MEB). Capabilities of the gas system include operation with a variety of non-oxidizing gases over a wide range of flow rates and preset moisture concentrations, removal of particulate debris and vapor contaminants from test facility outgassing, and maintenance of a predetermined positive pressure level.

1.3.6 Application Studies for Solid Brush SEGMAG Machines

All work was completed in the previous reporting period (E.M. 4790).

VOLUME I

SECTION 2

CURRENT COLLECTOR TEST RIGS

2.0 GENERAL

The development of solid brush SEGMAG machines requires extensive experimental facilities to evaluate two principal areas:

- Brush Material Selection
- Current Collection System Evaluation

The program scope required the use of five brush test rigs, four of which were employed in the initial stages of the brush screening work, while the fifth was constructed in preparation for more extensive parametric experimental tests in a related program (ONR/ARPA Contract #N00014-76-C-0683):

B1 = Brush Tester #1

B2 = Brush Tester #2

HS1 = High Speed Tester #1

HS2 = High Speed Tester #2

MEB = Machine Environment Brush Tester

The four laboratory testers (B1, B2, HS1, HS2) evaluate individual brushes to determine coefficient of friction, double voltage drop, brush pressure, and wear rate in specified environments. These four rigs provide an initial screening of brush and slip ring material performance.

B1 and B2 are duplicate testers for initial screening of prototypic materials in small (sub-size) brush configurations. HS1 and HS2 are duplicate testers for advanced screening of prototypic full-size brushes under higher speed and higher current conditions than B1 and B2. During this report period, B1, B2, HS1 and HS2 were operational.

The fifth test rig, the Machine Environment Brush Tester (MEB) was constructed to study current sharing in multiple parallel connected brushes in flux leakage fields anticipated in machine applications. Concepts of brush restraint, brush shunting and brush cooling will also be examined with this rig. MEB will expose the brush and slip ring materials to an actual machine environment, including high currents, multi-brush systems and ambient magnetic fields.

2.1 LABORATORY BRUSH TESTERS

2.1.1 Objectives

The objective of the laboratory test rigs is to aid in the selection and development of contact system materials for use in advanced electro-mechanical machines. This task is accomplished initially by sequentially screening potential brush, slip ring, gas, and additive materials over acceptable ranges of current density and speed. The test response parameters of particular importance are contact voltage, friction coefficient, and brush wear rate. Finally, (in a related ONR/ARPA Contract N00014-76-C-0683) the best combined contact system materials will be evaluated in more sophisticated test rigs and machines, capable of higher speeds, higher currents, larger numbers of brushes and with forced cooling of both brushes and rings.

2.1.2 Prior and Related Work

Two existing small laboratory brush testers, available from other Westinghouse-funded programs, were modified and placed in operation. These test rigs, B1 and HS1, were modified primarily to accommodate larger electrical load currents. Descriptions of these "bell jar" type testers and their capabilities are given in the previous semi-annual report (E.M. 4790).

2.1.3 Current Progress

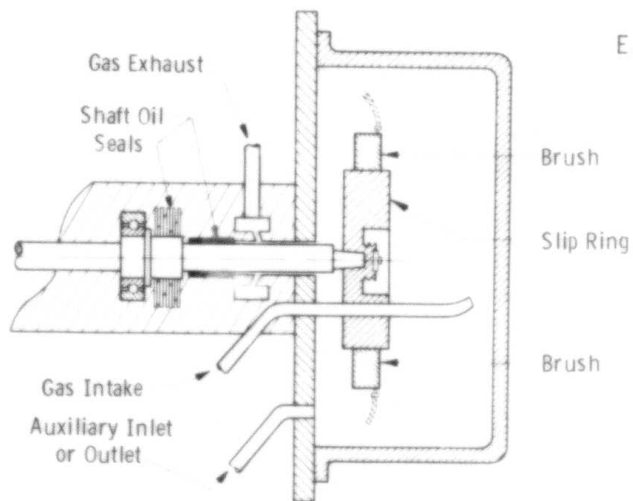
Two additional Westinghouse laboratory brush testers, B2 and HS2, were modified and made ready for operation during the reporting period. These are essentially identical to test rigs B1 and HS1 previously mentioned and described. See Figs. 2.1.1, 2.1.2, 2.1.3, and 2.1.4.

2.2 MACHINE ENVIRONMENT BRUSH TESTER (MEB)

2.2.1 Objectives

The objective of this task is to develop a tester to evaluate solid brush current collection systems in an actual machine environment. This tester will consist of a single module segmented magnet homopolar machine concept with capabilities of 6 volts and 20,000 amps.

The Machine Environment Brush Tester (MEB) will subject the current collectors to current densities, leakage flux and other conditions associated with operation in a machine environment. In addition, the unit will provide for long-term testing of current collectors, their attendant support systems, and the machine itself to develop operational data for solid brush machines.



E.M. 4883

Fig. 2.1.1: Test Chamber of B1 and B2 Brush Testers

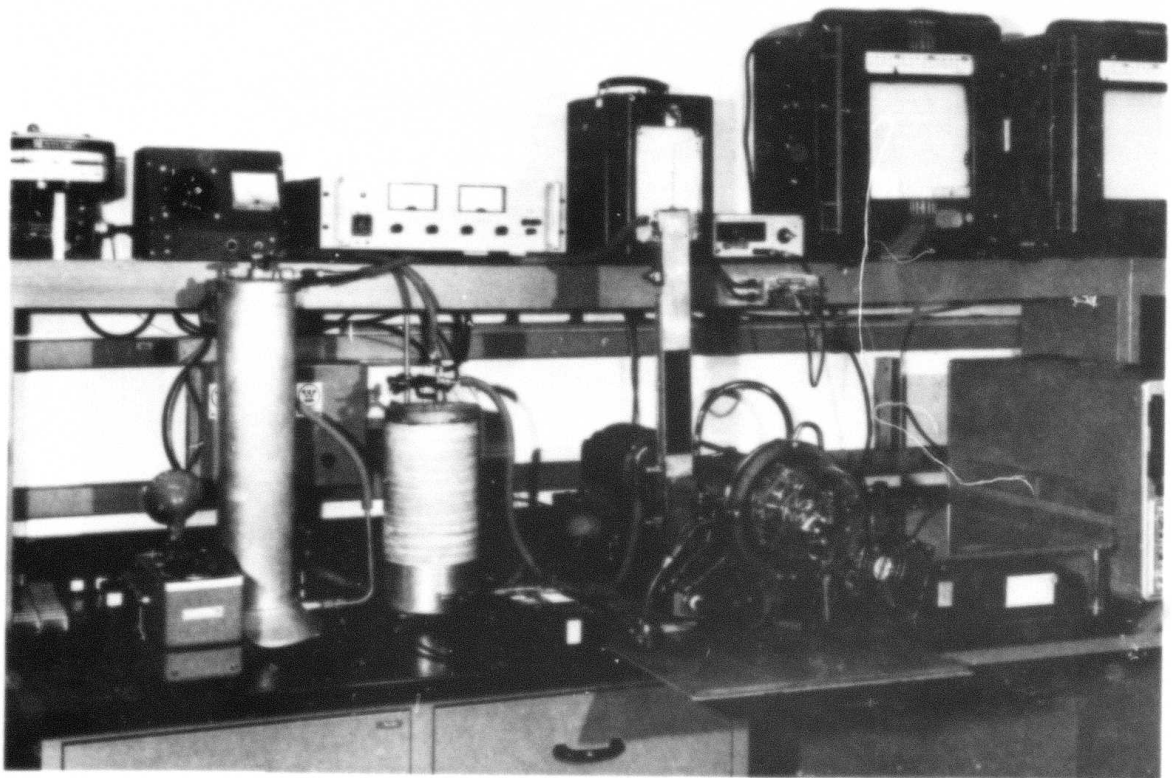


Fig. 2.1.2: Test System for B1 Brush Tester

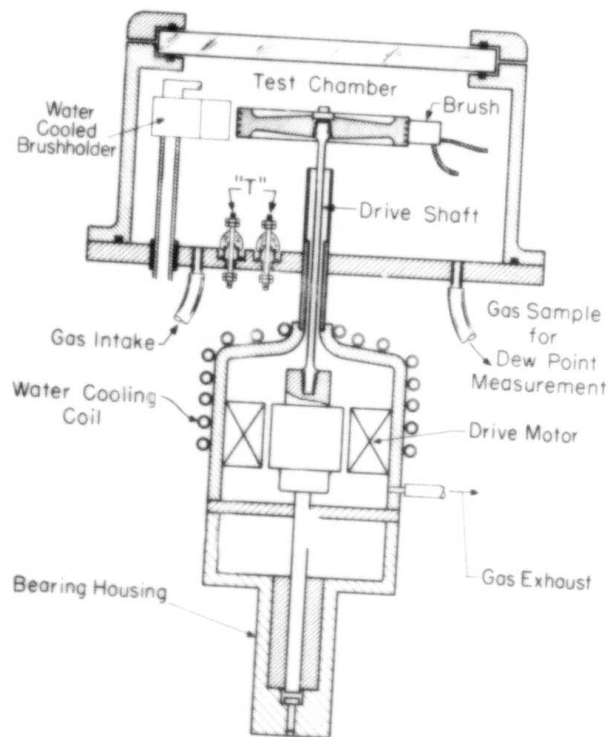


Fig. 2.1.3: Physical Arrangement of Components of Type HS1 and HS2 High Speed Brush Testers

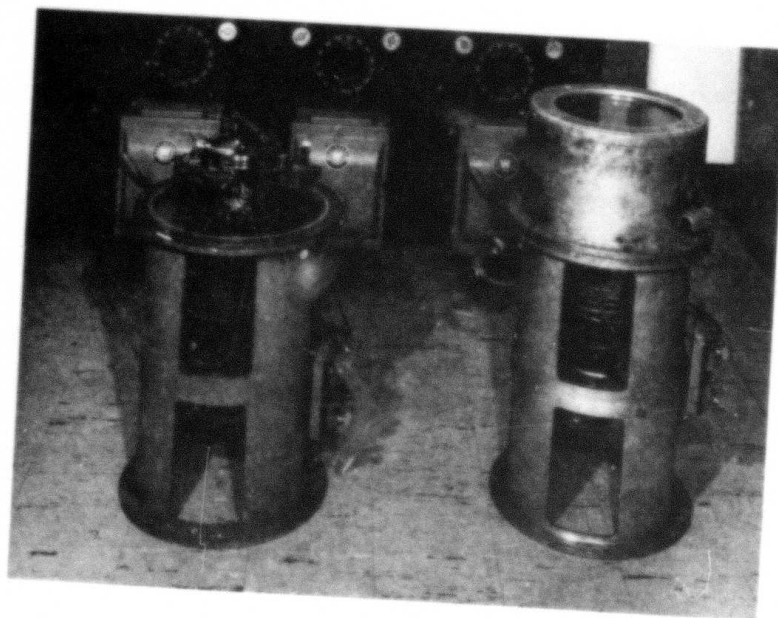


Fig. 2.1.4: High Speed Brush Testers (HS1 and HS2)

2.2.2 Prior and Related Work

The previous ARPA supported effort under this contract lead to the successful development of the water-cooled, liquid metal Segmented Magnet Homopolar Generator (SEGMAG) and proved the basic SEGMAG concept. The use of solid brush systems will result in a reliable reversing collector for motor applications, will remove the complications associated with liquid metal current collectors, and will simplify the overall system.

The result of various studies indicates that the minimum current density for a solid brush homopolar with equal volume to a liquid metal collector homopolar is 1000 A/in² (apsi). Since the initial solid brush-gas-vapor testing indicates solid brush current densities up to 2000 apsi, the solid brush SEGMAG machine will have a volume that is equal to or less than the equivalent liquid metal SEGMAG.

2.2.3 Current Progress

The Machine Environment Brush Tester (MEB) consists of a single module SEGMAG configuration incorporating solid brushes in the current collection areas as shown in Figs. 2.1.5 and 2.1.6.

The mechanical design of the MEB considered the same factors as those for the design of conventional rotating electrical machinery. In addition to the current collection system, the design of the MEB incorporates simplicity and maximum flexibility of its components to minimize the down time between test sequences.

The following factors were considered:

- 1) Mechanical conductor support,
- 2) Rotor to stator alignment,
- 3) Removal of losses,
- 4) Machine environment,
- 5) Erosion of cooling system components,
- 6) Electrical insulation,
- 7) Instrumentation.

The rotor conductor drum is restrained to withstand both centrifugal forces due to rotation and torsional forces due to the machine torque reaction. The torsional forces (8,000 in/lb) are restrained by shrinking the copper conductor drum onto the iron rotor. Since the rotor conductor drum and rotor iron have the same electrical potential, no insulation is required. Figure 2.1.7 shows the rotor with the copper drum in position.

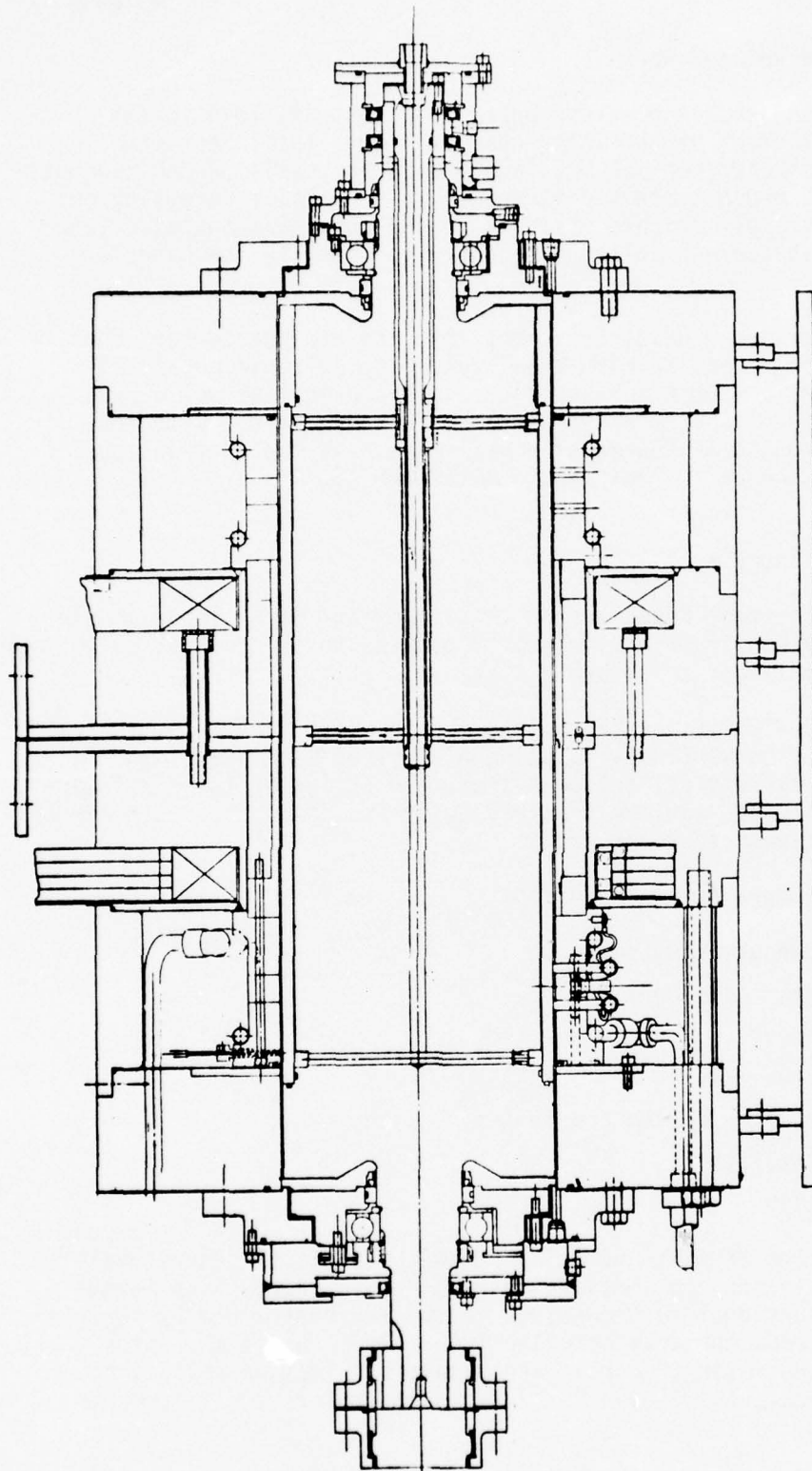


Fig. 2.1.5 Machine-Environment Brush Tester (MEB)

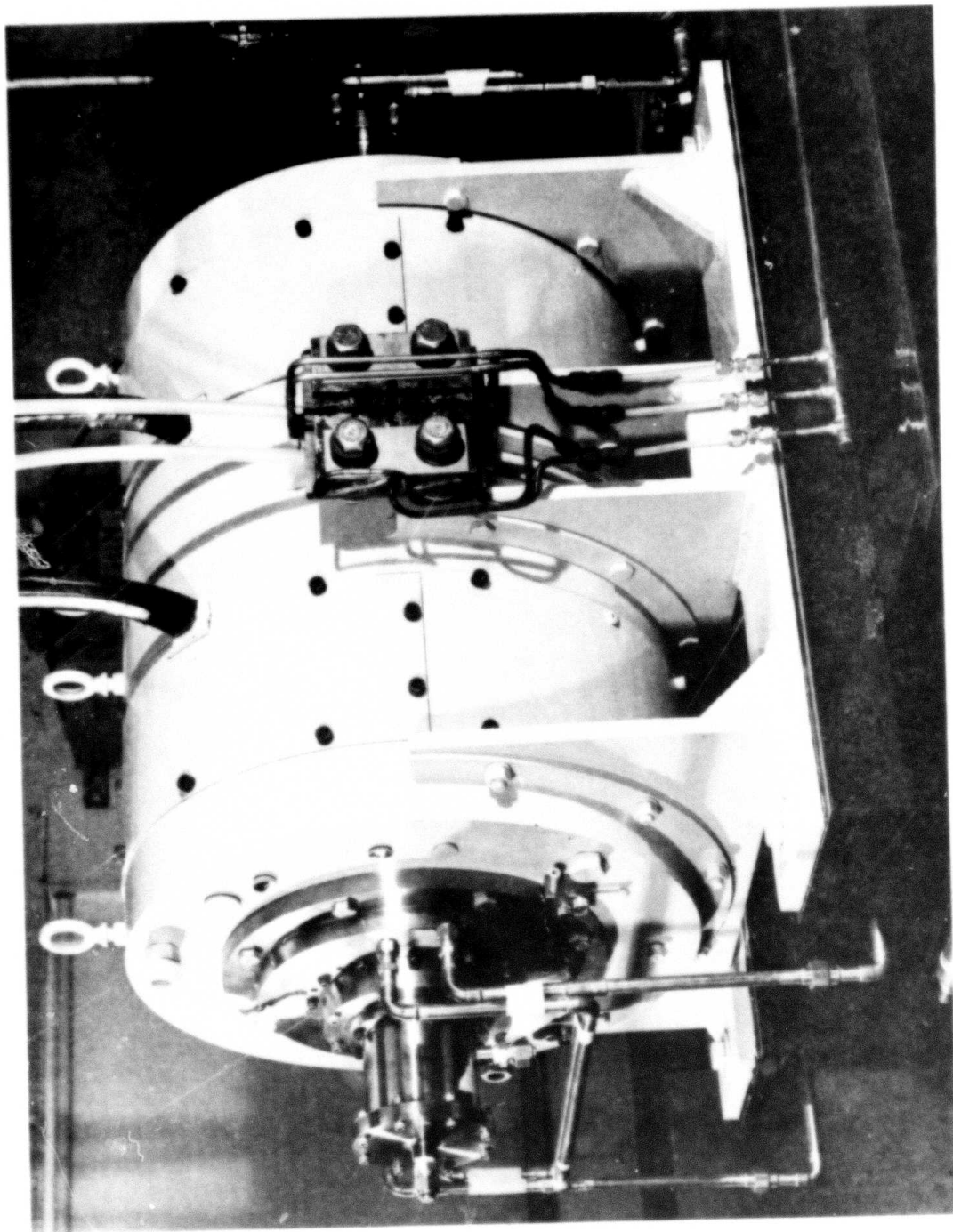


Fig. 2.1.6: Machine Environment Brush Tester (MEB) - Permits testing of solid brush systems in an actual SEGMAG machine environment.

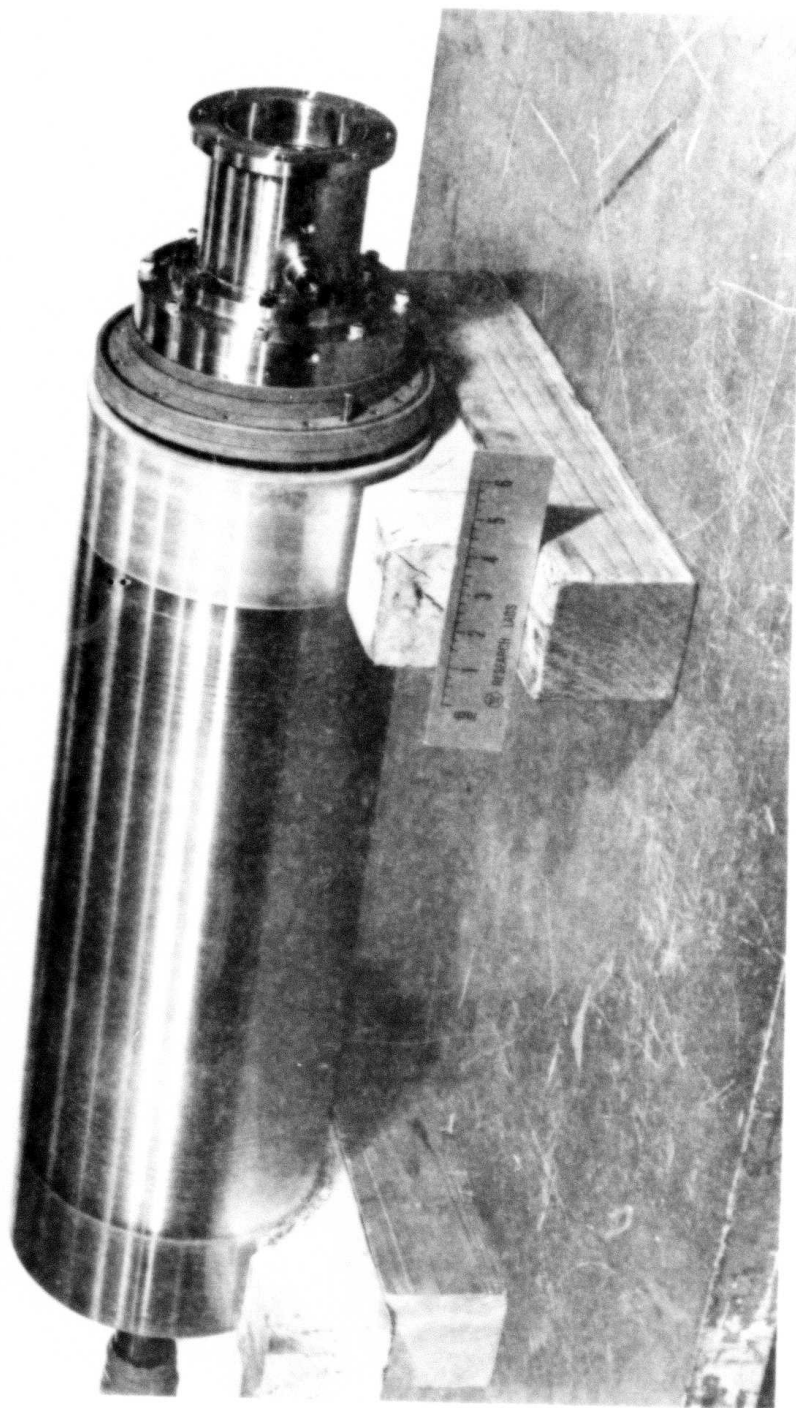


Fig. 2.1.7: MEB rotor showing copper drum, bearing housing and coolant seal system.

The support of the stator conductor is somewhat simpler since there are no rotational forces. The conductor drum will be restrained by an interference fit between it and the ferromagnetic stator iron. This concept provides adequate support to meet the 3/unit torque design criterion. Each stator conductor is insulated from the iron as well as from each other.

The alignment of the rotor in the stator is accomplished by four (4) positioning blocks, two (2) at each end of the test stand. These blocks provide vertical and horizontal adjustment capability. To measure the alignment, four (4) viewing ports are provided at each end of the machine at 3, 6, 9 and 12 o'clock positions. Measurements can be made of the rotor to stator gap at these locations and the proper adjustment can be made with the blocks. This arrangement provides maximum positioning flexibility for the systems including the possibility of testing brush operation with the rotor deliberately misaligned.

This test capability is very important since the run-out of the slip ring surface can adversely effect brush performance. Such run-outs result in radial acceleration of the brush known as "brush bounce". This condition must be accommodated in the brush actuation gear to ensure proper contact pressure on the slip ring for optimum life with minimum losses.

Rotor alignment is a function of the stator alignment provided by the rotor support structure, and dynamic deflection during operation. The MEB incorporates rolling element bearings which are adequate for the design loads and speed. Since the total flux of the machine must be carried by the ferromagnetic iron in the rotor, there is a substantial structural member in the active length and flux return path, thus resulting in a high critical speed for the machine. Because of high rotor stiffness, the dynamic deflection of the rotor is small.

Water cooling was adopted to remove machine losses from the MEB in the brush bearing area, machine leads, the field coils and the rotor conductor drum. Figure 2.1.8 shows the configuration of the water-cooled field coils.

The major losses requiring removal from the MEB include:

- Armature joule heating
- Brush friction
- Brush joule heating
- Friction and windage losses

The cooling system is designed to remove 80% of the machine losses through the rotor and 20% through the stator. The losses generated in the brush account for the majority of the total machine losses, and they must be removed through a sliding surface.

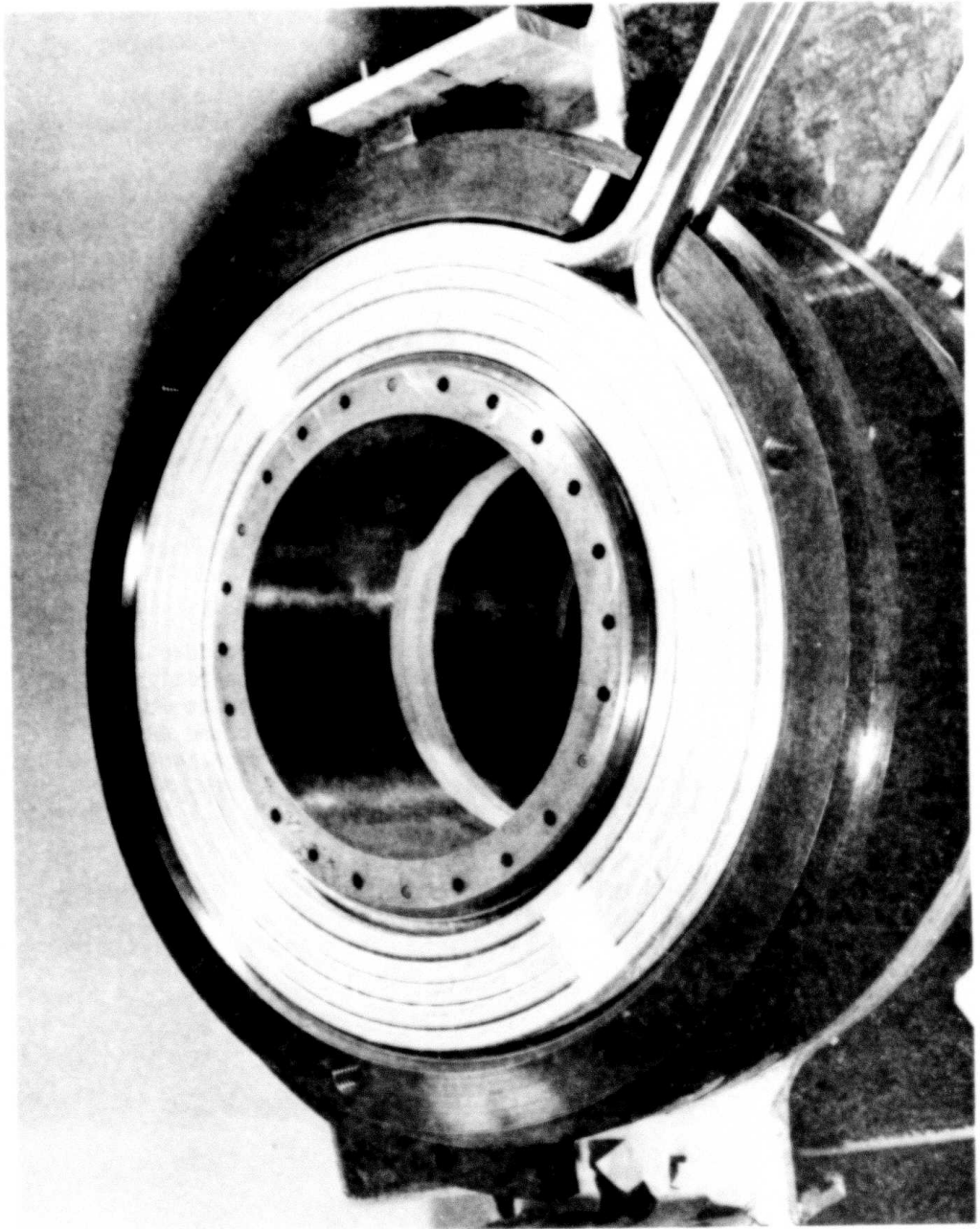


Fig. 2.1.8: Water cooled excitation coil positioned in stator drum.

In the rotor the coolant is passed immediately below the rotor conductor drum in small channels (.38"W x .03"D) and provides parallel cooling paths for the two collector areas. In this way the slip ring temperature can be regulated to give optimal brush performance. Figure 2.1.9 shows the coolant cross-over tube which provides an inlet/outlet path to the rotor.

To control the environment within the MEB, shaft seals are used. The shaft seals are mounted in-board to the bearings to prevent contamination from the bearing lubricants. Since the environment will be adjusted for low brush friction, the conventional rubbing face seals will perform adequately.

The design provides for measurement of the important parameters. Temperature measurements of the rotor conductor, ferromagnetic iron, and slip ring surface are accomplished by thermocouples placed inside the rotor and brought out through slip rings. Brush temperature and potential drops from brush to brush are measured by instruments imbedded in specified brushes. The machine torque is measured by a torque meter installed between the MEB and the prime mover. Associated instrumentation of the stator, gas system, and the cooling water system is also provided.

A view of the completed MEB installed on its test stand is shown in Fig. 2.1.10.

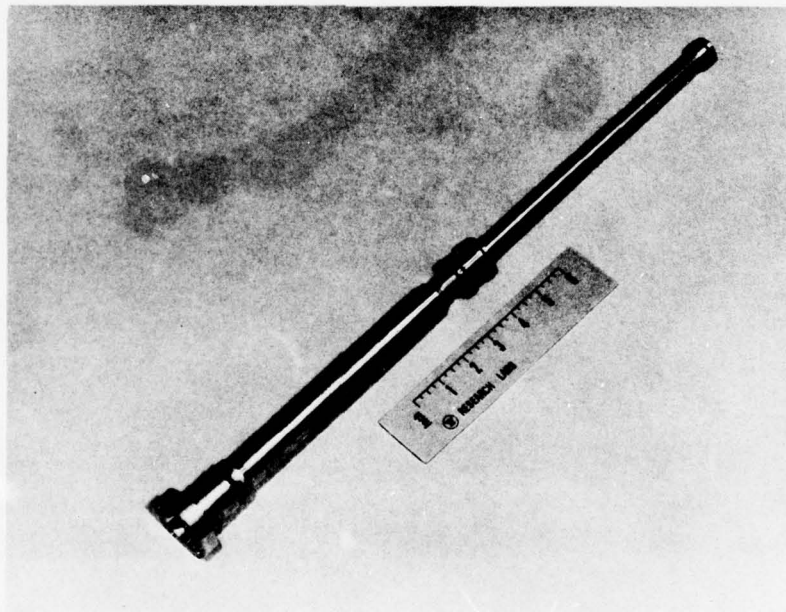


Fig. 2.1.9: Coolant cross-over tube, which is inserted into the rotor bore to provide controlled coolant flow to the rotor.

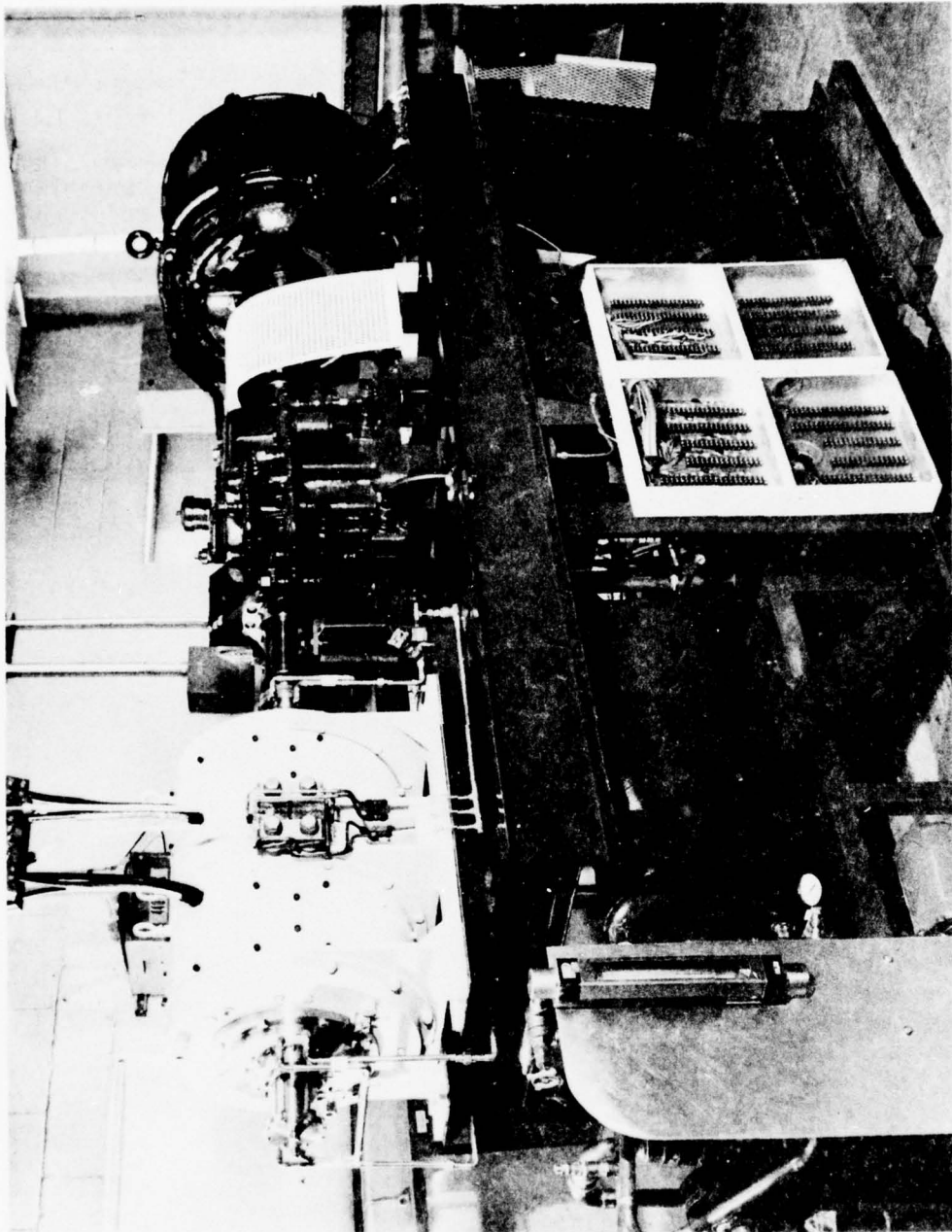


Fig. 2.1.10: The MEB mounted on its test stand, showing (1 to r) the MEB, gear box and drive motor. Below the stand are components of the water cooling system.

VOLUME I

SECTION 3

CURRENT COLLECTOR CONTACT MATERIAL/PERFORMANCE

3.1 OBJECTIVES

The objective of this task is to develop sliding contact system materials for use in advanced electromechanical machines. The principal elements of an electrical contact system include the brushes, collector rings, environmental gas, and vapor additives. Important requirements are capability of high current density, low power loss, and long life.

3.2 PRIOR AND RELATED WORK

Test procedures were established and existing test rigs were modified for evaluating contact system materials. Screening tests were initiated to evaluate candidate brush, ring, additive, and gas materials.

A few brush materials were evaluated for high (to 500 A/in²) and ultra high (to 2500 A/in²) current density application. Small size electro-graphitic brushes performed with long life and reasonably low energy losses in the high current density range. Metal-graphite brushes showed best overall feasibility for the ultra high current density application. In general, brush performance appeared to be affected by the base graphite material, percentage metal content, and applied mechanical load.

Additional testing is required to evaluate the effect of greater numbers of brushes, larger load currents, higher ring speeds, and the presence of ambient magnetic fields such as will be imposed by actual electro-mechanical machines. Test rigs are being readied for such investigations. In addition to the test features mentioned, provision for forced cooling of the contact system is also included.

3.3 CURRENT PROGRESS

3.3.0 General

A number of brush and ring materials were evaluated during this report period. Detailed descriptions of the screening test rigs employed, testing procedure, parametric operating conditions, and the performance-evaluation responses of interest may be found in the previous semi-annual technical report (E.M. 4790). Useful developmental information obtained from recent screening tests of brush, ring, and vapor additive materials is presented here.

3.3.1 Brush Materials

Copper and silver-graphite brush materials, representing a wide range in metal content (0-97 w/o), were subjected to screening-type evaluation tests. The contact resistance of graphite brushes is relatively high, leading to high electrical power loss when transferring large load currents. Additions of metal to such graphite structures reduce contact resistance and electrical loss, but excessive amounts lead to increased mechanical friction loss and wear and will more than offset the former advantage. The optimum metal content is dependent upon the relative importance of achieving lowest total power loss on one hand, and highest brush life on the other.

The brush materials evaluated were selected from available state-of-art grades, and they were fabricated with typical powder metallurgy compaction/sintering techniques. Based upon direction obtained from recent test results, new experimental brush materials were specified for evaluation and further development. Such materials are presently being fabricated for evaluation as improved brushes.

Power loss and wear expressions were modified to expedite comparisons of the candidate brush materials. Here, an attempt was made to account, in part, for the effect of differences in collector ring velocity among testers on brush power loss and brush wear performance. Based on such performance values, contact material comparisons are more meaningful.

The power loss expression (k_L) combines the friction coefficient, contact voltage drop, and ring velocity, yielding units of energy loss density per unit distance traveled. The wear expression (k_W) combines linear wear rate, brush area, and ring velocity, giving final units of volume brush wear per unit distance traveled.

$$k_L = 1.356 \mu p + \frac{jV_c}{v} \quad (3.1)$$

where: k_L = brush energy loss density per unit distance traveled, J/in² · ft.

μ = coefficient of friction.

p = load pressure, lb_f/in².

j = current density, A/in².

V_c = contact voltage drop, V.

v = ring velocity, ft/s.

$$k_W = \frac{w a}{3600 v} \quad (3.2)$$

where: k_w = volume of brush wear per unit distance traveled, in³/ft,
 w = linear wear rate, in/h,
 a = brush area, in²,
 v = ring velocity, ft/s.

Based on test results, power loss (mechanical and electrical components) and wear characteristic values were calculated for 26 metal-graphite brush materials. These values are plotted for each material as a function of its metal content in Figs. 3.1 and 3.2. Average curves are drawn through the points to show trends in performance as a function of brush metal content. Based on these data, the following conclusions are made:

- The performance characteristics of copper and silver-graphite brushes of comparable metal content are similar. Thus, economies in brushes can be realized by employing copper rather than silver.
- Total contact energy loss (mechanical plus electrical) is minimal when the metal content of graphite brushes is near 75 w/o.
- Total contact energy loss is dominated by the electrical component when the metal content of brushes is less than about 70 w/o, but by the mechanical component at larger percentages.
- Brush wear is very low for small additions of metal, increasing at a modest rate up to about 75 w/o. At higher metal percentages brush wear increases sharply.
- Based on the screening test data, it appears that commercially available graphite brushes containing 65 to 75 w/o copper are reasonable candidates for more extensive testing and evaluation on larger, more sophisticated test machines.

The next generation of experimental brush materials is currently being fabricated. The objective, of course, is to develop brushes with improved performance capability for high current density application.

3.3.2 Ring Material

Copper, nickel, and steel metals were selected for initial evaluation as candidate collector ring materials for advanced current collection systems. The significant screening evaluation test results obtained for these ring materials are reported and compared in this report. Other metals, including super copper alloys, brasses, and special steels, were selected, machined, and are available for testing.

Physical properties of ring materials such as strength, hardness, and conductivity appear to be important factors which affect contact

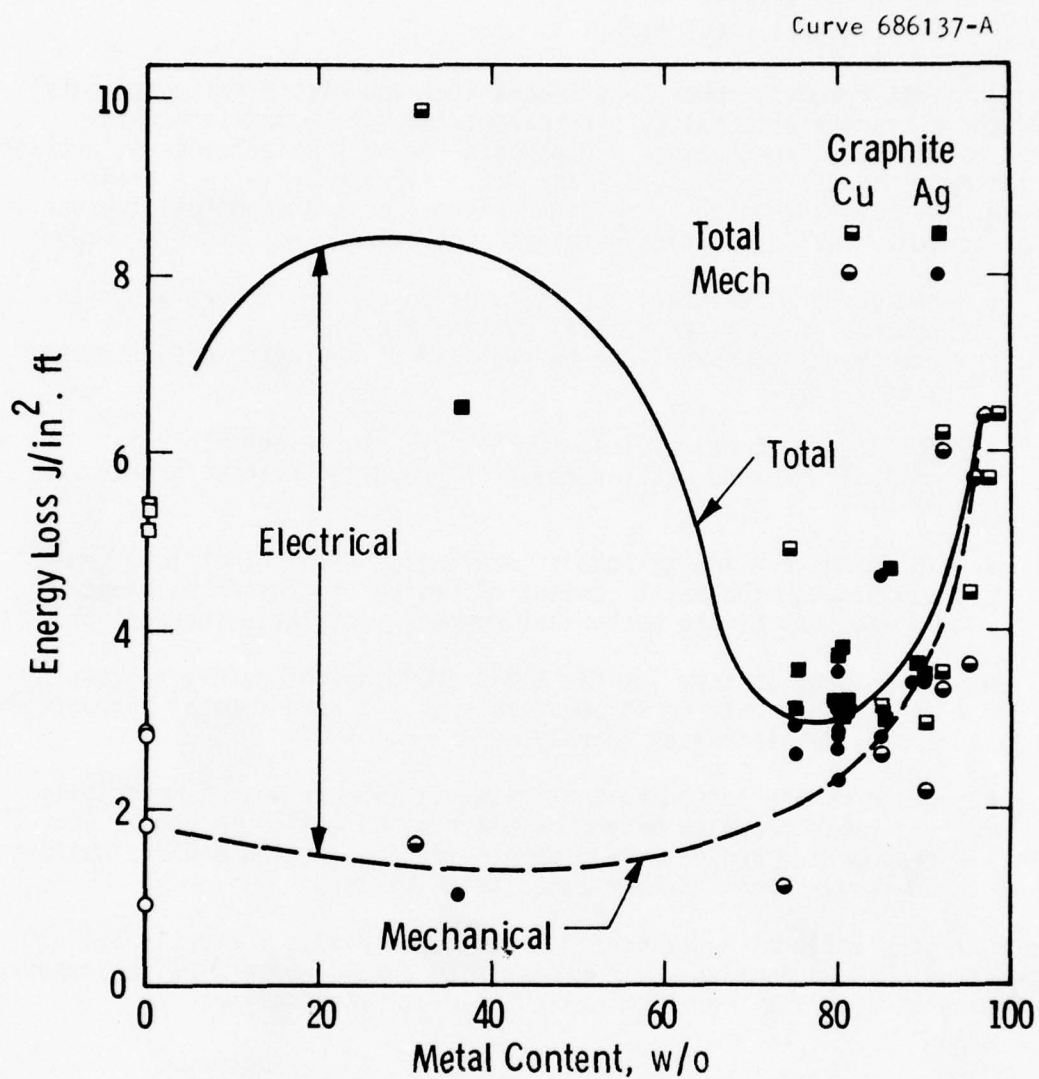


Fig. 3.1: Metal graphite brush-copper ring contact loss characteristics. 500 A/in², 10-12 lb_f/in², 42-83 ft/s, inert gas ambient.

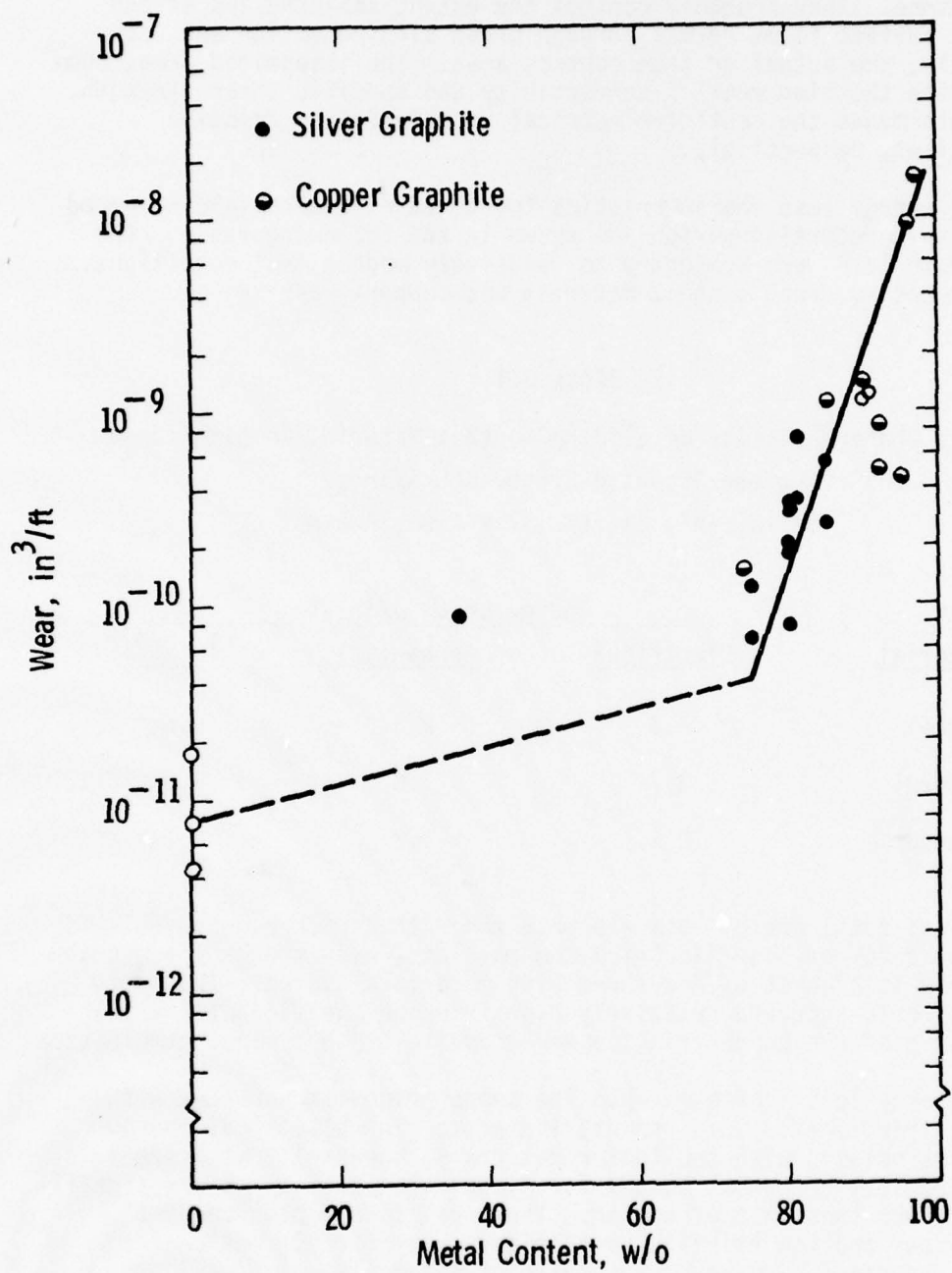


Fig. 3.2: Metal graphite brush wear characteristics. Copper ring, 500 A/in², 10-12 lbf/in², 42-83 ft/s, inert gas ambient.

performance. They probably control the extent and adhesion of the complex surface films formed through brush sliding action and, consequently, the actual or true contact area. The integrated area, combined with the ring metal's conductivity and specific shear strength, then determines the contact electrical resistance and friction coefficient, respectively.

Contact energy loss characteristics for three ring materials screened during this reporting period are shown in the following table. The three materials were subjected to relatively modest test conditions, and the mating brush contact material was copper-graphite.

TABLE 3.1

Loss Characteristics of Sliding Contact Material Combinations:
Copper-Graphite Brush, 500 A/in²,
12 lb_f/in², 51 ft/s, Inert Gas Ambient

Ring Material	Energy Loss, J/in ² ·ft		
	Electrical	Mechanical	Total
Steel	7.3	2.3	9.6
Nickel	3.7	1.6	5.3
Copper	0.8	3.3	4.1

The lowest total energy loss was obtained with copper rings. This is attributed to very low electrical energy loss, even though the mechanical loss is highest of the three ring materials tested. Thus, low contact resistance and relatively high friction coefficient are characteristic of the copper ring/copper-graphite brush contact combination.

Total energy loss increased when the copper ring was replaced with nickel, then steel. This was attributed to high electrical energy losses associated with the latter materials, especially with steel. The mechanical component losses for nickel and steel rings are significantly lower than that of copper. Thus, relatively high contact resistances and low friction coefficients are characteristic of the nickel and steel ring/copper-graphite brush contact combinations.

Long brush life was obtained for each of the three ring materials evaluated. The longest and shortest brush life was found for copper and steel rings, respectively.

VOLUME I

SECTION 4

CURRENT COLLECTOR MECHANICAL LOAD SYSTEMS

4.1 OBJECTIVES

The objective of the mechanical load system program is to develop a system capable of controlling the brush loads to acceptable values, as specified in Section 3. The contact material performance program will determine what is required of the brush system for efficient current transfer and the mechanical load system will determine how to achieve these requirements.

4.2 PRIOR AND RELATED WORK

The basic function of a current collection system is to transfer electrical power between stationary and rotating contact members efficiently, reliably, and with long life. Much experience in the application of solid brush current collectors for this purpose has been accumulated over the years at Westinghouse and elsewhere, for brush systems operating at conventional current densities (93 KA/m^2 , 60 A/in^2) in ambient air environments. This work has been used as a foundation with the present effort utilized to extend the technology to the high current densities ($3.1 \times 10^6 \text{ A/m}^2$, 2000 A/in^2).

High current density brush holders were designed and built as a brush test vehicle for use in the High Speed Test rigs (HS1 and HS2). The design configuration consisted of a water-cooled holder surrounding a rectangularly shaped solid brush. The brush loading was provided by constant force springs, and conventional (pig tail) electrical shunts carried current between the brush and holder.

Brush holders were designed and built for the Machine Environment Brush Tester (MEB). The design philosophy was similar to that used for the High Speed Testers. The cooling configurations differed, however, in that the rotor of the MEB also has a water-cooled rotor, in addition to water-cooled brush holders.

4.3 CURRENT PROGRESS

In the area of mechanical load systems the two principal concerns are the electrical shunts and the solid brush actuation system.

4.3.1 Electrical Shunts

The purpose of the electrical shunt is to transfer current from the solid brush to the stator conductor with low loss, and with free radial motion.

Conventional pigtail shunts were analyzed and were found to impose excessive mechanical load on the brush when designed for low electrical loss. The size of these conventional shunts becomes excessive for high current density brushes.

Another disadvantage of the pigtail shunt is the substantial electrical resistance (I^2R) loss in the solid brush. These losses are inherent in this configuration since pigtail shunts cannot be fastened near the brush-slip ring interface. Ideally, current should be transferred from immediately behind the rotor-brush interface directly into the stator conductor. However, since the pigtail is permanently attached to the solid brush and since there is a specific brush length allowance for wear, the current must pass through the wear length prior to entering the pigtail shunt.

Investigation of alternate concepts resulted in the attractive multi-contact shunt concept, which has the following features:

- 1) Low electrical resistance at a low total contact force.
- 2) The capability for solid brush sliding on the multi-contact provides close contact with the brush-slip ring interface.

The resistance of a single point contact is given by Holm¹ as:

$$R_s = \frac{a}{(F_s)^m} \quad (4.1)$$

where: R_s = Single contact resistance,

a = Constant,

F_s = Total force applied to the single contact,

m = Constant.

The resistance of a number of identical contacts arranged in parallel is:

$$R_M = \frac{a}{n (f)^m} \quad (4.2)$$

where: R_M = Multi-contact resistance,

a = Constant,

f = Force per multi-contact point,

m = Constant.

$$F_M = n f \quad (4.3)$$

where: F_M = Total force applied to the multi-contact,
 n = Number of contacts.

$$R_M = \frac{a}{n^{(1-m)} (F_M)^m}$$

$$\text{Setting: } R_S = R_M$$

$$\text{Yields: } F_S/F_M = n^{(1-m/m)} \quad (4.4)$$

Equation (4.4) reveals that for a given electrical resistance, the total force required for a multi-contact is less than the total force required for a single contact when $m < 1$. For $m = 0.33$ which corresponds to non-oxidized, lightly loaded, copper-on-copper contacts:

$$F_M = \frac{F_S}{(n)^{2.03}} \quad (4.5)$$

For $n = 10$ contacts the total multi-contact force required is approximately 100 times less than a single contact force (at equal electrical resistance).

The presence of alien films on the contacts reduces the advantage of multi-contacts. These films are usually oxides and tend to cause not only higher resistance but also a higher constant m . For oxidized, lightly loaded, copper-on-copper contacts, $m = .65^1$, and

$$F_M = \frac{F_S}{(n)^{.54}} \quad (4.6)$$

For $n = 10$ contacts the total multi-contact force required is approximately four times less than a single contact force (at equal electrical resistance). The advantage of multi-contacts although still present, has been reduced 25 times due to the oxidized surfaces.

Several metal fiber shunts were made in order to investigate manufacturing techniques and to obtain test data for multi-contacts. The metal fiber shunts were made of brass tufts drawn into a brass base with a brass tie wire. The electrical connection between the fiber tuft and the base was found to be inadequate. The use of soft solder provided an acceptable electrical junction. Figure 4.1 is a photograph of a typical metal fiber shunt, with the tufts angled into the base. This particular shunt was also silver plated.



Fig. 4.1: Experimental shunt using silver plated metal fibers.

Figure 4.2 is a photograph of the experimental setup for static testing of the metal fiber shunt. The fiber shunt is attached to a large metal heat sink. The mating part of the shunt is a long metal bar suspended from the ceiling. The long length of the suspension cable results in practically perpendicular motion of the bar to the fiber shunt base. The suspended bar completes the electrical circuit with the fiber shunt. The load to the multi-contact was applied through a cantilevered beam and strain guage assembly. Mechanical loading is provided by adjusting a screw threaded through the end of the cantilever.

The static tests were initiated in order to establish the empirical constants in the resistance-force relationship.

Following the static tests the design of the metal fiber shunts will be reviewed and updated. The redesigned fiber shunt will be utilized in a related program (ONR/ARPA Contract N00014-76-C-0683) in one of the solid brush test rigs. The test data from the dynamic rigs should yield information valuable in the design of full-size SEGMAG machines.

4.3.2 Actuation System

The actuation system is that part of the brush holder system which mechanically loads or lifts the brushes. The brush is loaded; that is, pressed against the rotor slip ring, through the use of constant force springs. The mechanism which lifts the solid brush is a cable attached to the solid brush and spring assembly. The cable is pneumatically actuated by a cylinder located outside the brush area. A full-size model of this solid brush holder actuation system was constructed for use in evaluating potential brush holder problems.

4.4 REFERENCES

- ¹ Holm, Ragnar; Electric Contacts Theory and Application; Springer-Verlag; 1967; Germany.

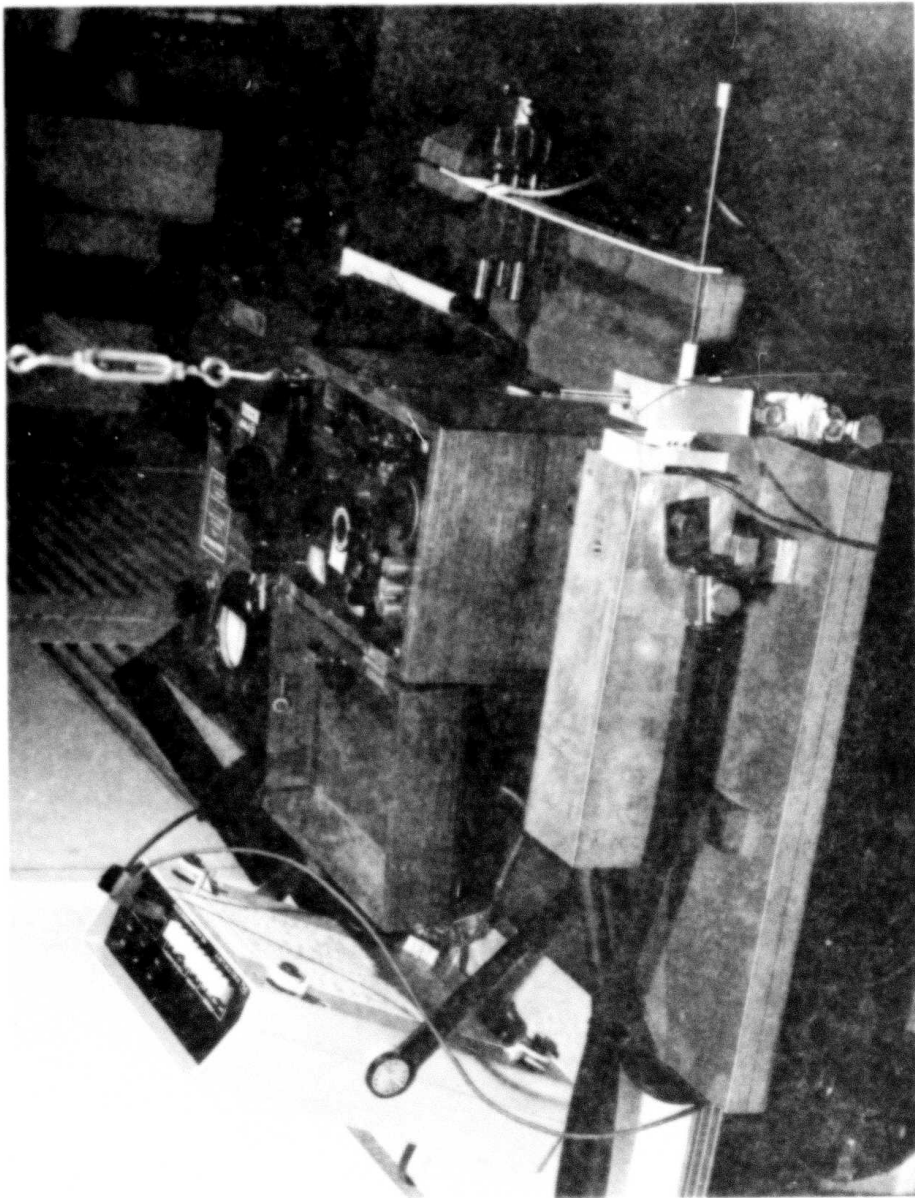


Fig. 4.2: Metal fiber shunt electrical test site; current path in foreground shows shunt test block mounted to heat sink and shunt mating piece suspended from ceiling. Mating piece is pressed against shunt by cantilevered strain gauge assembly.

VOLUME I

SECTION 5

CURRENT COLLECTOR INTERFACE COOLING SYSTEMS

5.1 OBJECTIVES

The objective of the interface cooling system program is to determine the heat transfer characteristics of the high current density brushholders. These heat transfer characteristics will be correlated with the solid brush objectives in order to determine high current density brushholder heat transfer design requirements and procedures.

5.2 PRIOR AND RELATED WORK

Westinghouse has accumulated much experience over the years in the application of solid brush current collectors. This experience has been with conventional current densities (93 KA/m^2 , 60 A/in^2) where transferring the heat from the brushholder was not considered a problem area. The high current densities ($3.1 \times 10^6 \text{ A/m}^2$, 2000 A/in^2) increase the power density in the brushholder area to a point where heat transfer has become an area of concern. The intent of the on-going work is to utilize the Westinghouse experience to support the evaluation of the heat transfer in the brushholder area for high current density brushes.

5.3 CURRENT PROGRESS

The brushholder heat transfer characteristics of the HSl Brush Tester and the Machine Environment Brush Tester (MEB) were analyzed. The holders and brushes were instrumented in an effort to determine the thermal resistance. The experimental data was then correlated with theory in an effort to understand the heat transfer mechanism between the brush and holder.

The thermal data from the HSl test was evaluated, with the result that the present HSl brushholder meets the program thermal objectives. The brushholder is capable of extracting 30% of the heat generated as a result of brush losses. The remaining heat will be extracted through the rotor cooling system.

VOLUME I

SECTION 6

CURRENT COLLECTION GASEOUS ENVIRONMENT/CONTROL

6.1 OBJECTIVES

The objective of this task is to provide a controllable atmosphere of non-oxidizing gas to the machine environment brush tester. The gaseous environment control system must have the ability to flow preconditioned non-oxidizing gas through the test system including separate flows through the brush chambers (two) and flow in the rotor stator gap. The gas system is required to remove both solid wear debris and vapor contaminants and to maintain preset pressure conditions.

6.2 PRIOR AND RELATED WORK

Results of tests performed at the Westinghouse Research Laboratories reveal that the performance of graphite brushes sliding on copper rings is greatly improved if the usual air ambient is replaced with a humidified carbon dioxide gas atmosphere. This allows operation of the brushes at much higher current density with relatively low power loss and long life. Adsorbed gas and water vapor on the contact surfaces provides lubricity but does not significantly interfere with conduction of electrical current.

6.3 CURRENT PROGRESS

A recirculating gas control system (see Figs. 6.1 and 6.2) was built and shakedown-tested for use with the MEB. Design, construction, and operation of this system is reported in Volume III, Section 12 of this report.

After completing construction of the gas control system, a series of shakedown tests was run to characterize its performance. Besides leak testing, tests were made to determine pump capacity, flow control, moisture saturation level, and moisture probe response. The unit performed well and will be used with the MEB test facility in a related program (ONR/ARPA Contract N00014-76-C-0683).

Improvements made to the unit following shakedown testing included:

- 1) The addition of a self-draining aerosol trap after the water bubbler to prevent aerosols from entering the main gas stream.
- 2) The addition of a 15 μ filter after the aerosol trap to remove any dust that might be carried from the charcoal adsorbing column.

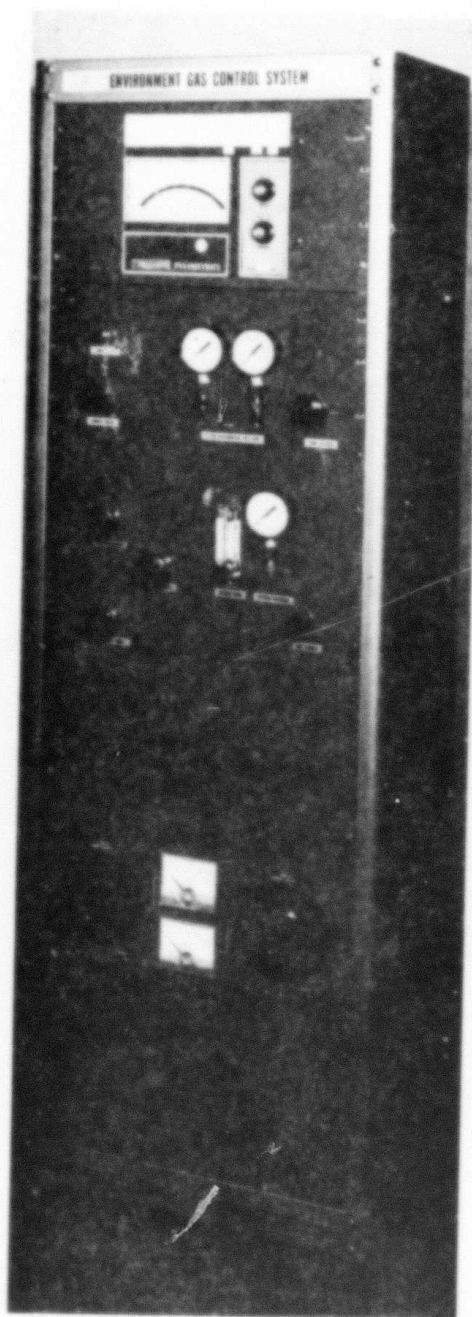
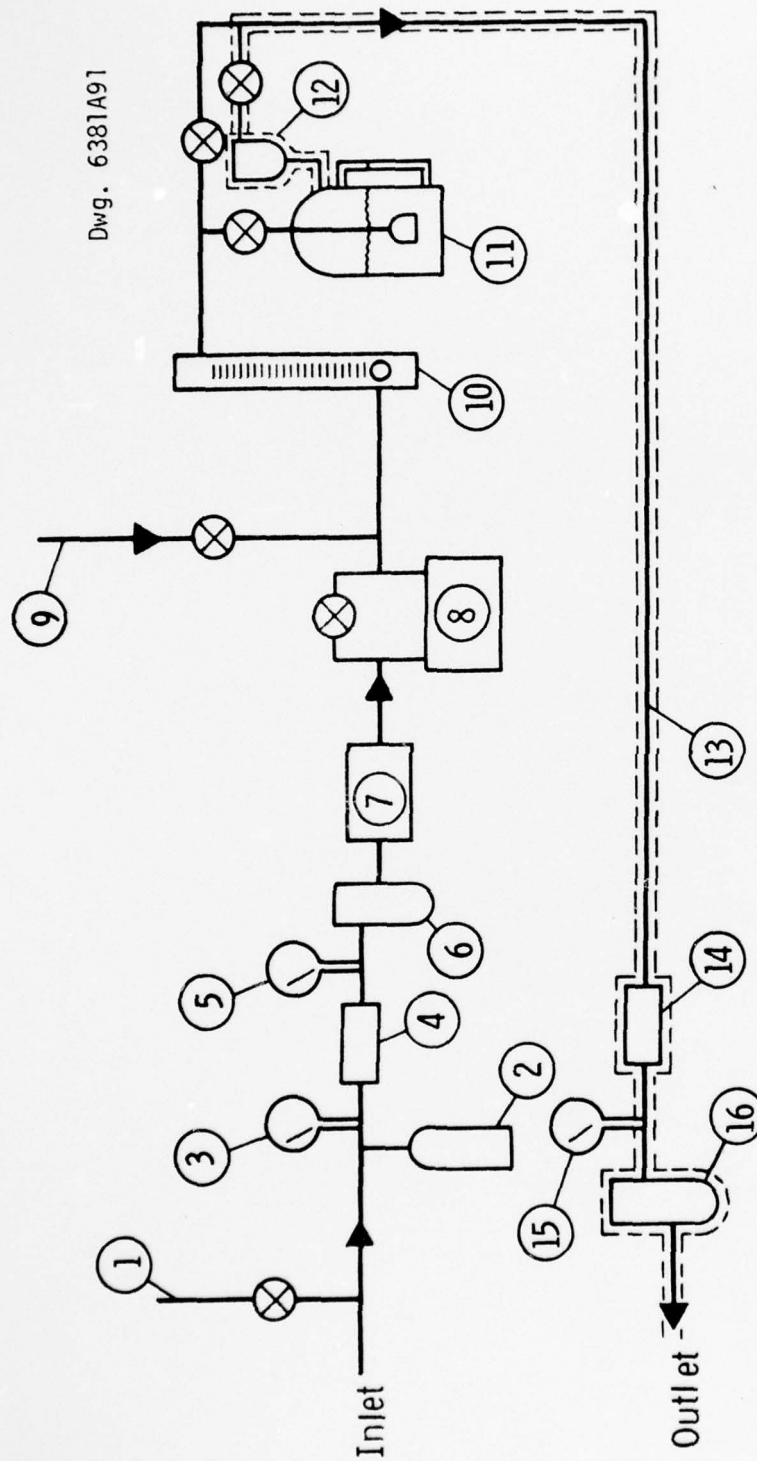


Fig. 6.1: Environment gas control system for the Machine Environment Brush Tester (MEB)



- | | |
|---------------------------|-------------------------------------|
| 1. Sample Port | 9. Make Up Gas |
| 2. Dust Trap | 10. Flow Meter |
| 3. Pressure Before Filter | 11. Water Bubbler |
| 4. 60 μ Filter | 12. Aerosol Trap |
| 5. Pressure After Filter | 13. Return Gas Line With Trace Heat |
| 6. Moisture Probe | 14. 15 μ Filter |
| 7. Charcoal Filter | 15. System Pressure |
| 8. Bellows Pump | 16. Moisture Probe |

Fig. 6.2: Current collection gaseous environment control system for use with the Machine Environment Brush Tester (MEB).

VOLUME I

SECTION 7

APPLICATION STUDIES FOR SOLID BRUSH SEGMAG MACHINES

7.1 OBJECTIVES

The purpose of this study is to correlate brush research with machine requirements and potential utilization. This will ensure that the electrical machine requirements, operating parameters, and machine environment effects are effectively translated into the solid brush research program.

7.2 PRIOR AND RELATED WORK

The range of slip ring and commutator peripheral speeds for both motors and generators were initially defined, with a maximum velocity of 250 ft/second for generators.

The range of operating current levels and overload levels were carefully considered with relation to the brush research program.

The problems of loading very high current density brushes to the machine contact surface are complex and required considerable attention to innovative approaches to shunting and cooling.

The effects of magnetic fields, vibration and other transient effects were carefully considered with reference to the brush loading system.

All of the above information was utilized in the current collection and brush developments of this contract and in related ONR/ARPA Contract N00014-76-C-0683.

7.3 CURRENT PROGRESS

Work on this task was completed in the previous reporting period.

E.M. 4883

VOLUME II
SUMMARY OF TECHNICAL
ACCOMPLISHMENTS FOR
ENTIRE CONTRACT

II a

VOLUME II

SECTION 1

INTRODUCTION AND SUMMARY

1.0 GENERAL

This is the final technical report under ARPA Contract #DAHC 15-72-C-0229. The work was performed over a period of four years from program inception, 10 May 1972 to its termination. During this period the work was completed, in accordance with the agreed plan as specified in the contract and its amendments.

1.1 BACKGROUND

This program was for the research and development of a Westinghouse-proposed mechanical power transmission concept: the segmented magnet homopolar torque converter (SMHTC). The purpose of this device is to convert unidirectional torque of constant speed (such as from a steam turbine prime mover) into variable speed output torque in either the forward or reverse directions. The concept offers an efficient, light-weight, low volume design with potential application over a wide range of speeds and power ratings in the range from hundreds to tens of thousands of horsepower. Initial analysis indicates that this machine concept can be applied to commercial and military advanced concept vehicles for both terrain and marine environments over a wide range of applications with considerable benefit to the U.S. Government, provided the complex current collection, and materials problems can be completely solved.

The present contract is part of a proposed three phase program to develop the segmented magnet homopolar torque converter (SMHTC). The aims of this program are: a) solve the operational problems relating to current collection systems for segmented magnet machines; b) demonstrate the solution of these problems in a small segmented magnet homopolar machine (SEGMAG); c) utilize the developed technology to design, construct and test a segmented magnet homopolar torque converter (SMHTC).

The program placed particular emphasis on the materials technology of current collection systems for the reason that this is essential to the success of the homopolar machine concept for high power density applications. Both liquid metal and solid brush current collection systems were studied.

1.2 OBJECTIVES

In Phase I, completed on January 9, 1973, all of the technical problems were reviewed, the machinery concepts studied, and a detailed technical plan was evolved for Phase II.

Phase II had the primary purpose of providing the necessary theoretical and engineering design work, as well as the supporting experimental tasks, to develop a reliable and efficient current collection system for the successful operation of a segmented magnet (SEGMAG) homopolar generator. Key task areas include: (a) the design, construction, and operation of a SEGMAG generator having sodium-potassium (NaK) current collectors and all necessary support systems for liquid metal handling and purification, cover gas purity maintenance, and shaft seals; and (b) the procurement and testing of a GEC Ltd. homopolar generator with its Gallium-Indium (GaIn) current collector system.

The objectives of Phase III were to extend the technology developed in Phase II for constant speed machines (such as generators) to the case of a torque converter which operates at low speed, zero speed, or reversing conditions and then to construct and test a demonstration machine.

Phases I, II, and the initial Phase III effort were based on the use of liquid metal current collectors. In Phase III-A (begun on July 1, 1975) work was redirected toward the use of a promising current collection concept utilizing a solid brush-gas-vapor-additive system.

1.3 SUMMARY OF CONTRACTUAL ACCOMPLISHMENTS

The work performed under this contract falls into two categories: (1) work involving liquid metal current collection, encompassing Phases I, II, and III (Section 1.3.1), and, (2) work involving solid brush current collection of Phase III-A (Section 1.3.2).

1.3.1 Summary of Contractual Accomplishments in Phases I, II, III

This work related to the use of liquid metal current collection:

- 1) Segmented Magnet Homopolar Torque Converter (SMHTC) System Studies. SMHTC system studies were made of various possible machine configurations. A conceptual design was prepared of a 6000 HP machine to deliver constant torque from zero speed to 200 RPM in forward and reverse directions, from a 1200 rpm input shaft.
- 2) Application Studies for SEGMAG Machines with Liquid Metal Current Collectors. A Survey was made of the most promising applications for segmented magnet torque converters, motors, and generators. Several of the applications resulting from the Phase II application studies were reviewed and the most useful applications for segmented magnet homopolar machines or torque converters were selected.
- 3) Machine Developments. A SEGMAG generator utilizing NaK current collectors and a GEC (England) machine which employed GaIn as the current collection fluid.

The SEGMAG (Figs. 1.1 and 1.2) was rated 3000 HP, 3600 rpm and served to prove both the SEGMAG machine concept and the practicability of the NaK current collection system developed under related subtasks of this contract. This machine was used in evaluating the components and materials required for the SMHTC.

The prime purpose of the GEC machine (Figs. 1.3 and 1.4) was to obtain operational experience with GaIn as a current collector liquid. This machine's mechanical and electrical design and performance were studied as a basis for evaluating presently used mathematical models for predicting machine performance.

- 4) Liquid Metal Current Collection Systems. A study was conducted of liquid metal current collection system technology. The preferred system and liquid metal were identified for the segmented magnet homopolar machine arrangement.

The principal areas of study concerned the handling, containment and measure of power losses associated with liquid metal use in current collectors. The preferred system configuration was employed in the prototype SEGMAG machine. Figure 1.5 shows the test stand used to evaluate prototypic current collectors developed under this program.

Under Phase III the unidirectional SEGMAG current collectors of Phase II were further refined and extended to higher speed applications. In addition, collectors suitable for reversible and variable speed applications were developed.

- 5) Liquid Metal Support Systems. The purpose of this task area was to develop, design, fabricate, and instrument a liquid metal recirculation loop (Fig. 1.6) and a cover gas recirculation system (Fig. 1.7) to provide maximum protection to the liquid metal in the current collector region. Both the liquid metal and the cover gas are recirculated for contaminant removal and purity maintenance. Consideration was also given to use of these systems for removal of waste heat from the machine.

This task included a compatibility study of all machine materials (insulation, lubricants, and structural materials) with the liquid metal current collection fluid.

A fundamental studies program was part of this task area and was concerned with those aspects of liquid metal technology necessary to optimize the current collection electrodes to provide long term reliability for stable current conduction. Topics included surface wetting by liquid metals, aerosol formation, corrosion or alloying reactions, effect of high current transfer, and chemistry control in liquid metals using soluble getters.

In Phase III the SEGMAG liquid metal system was further developed and simplified. Support systems were developed for use in torque converter and motor applications where reversible and variable speeds are encountered.

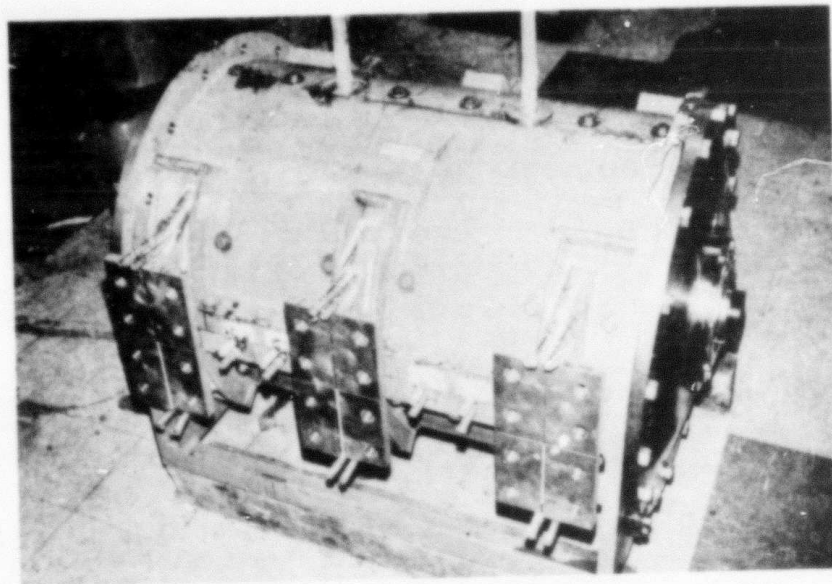


Fig. 1.1: SEGMA Generator, Utilizing NaK liquid metal current collectors.

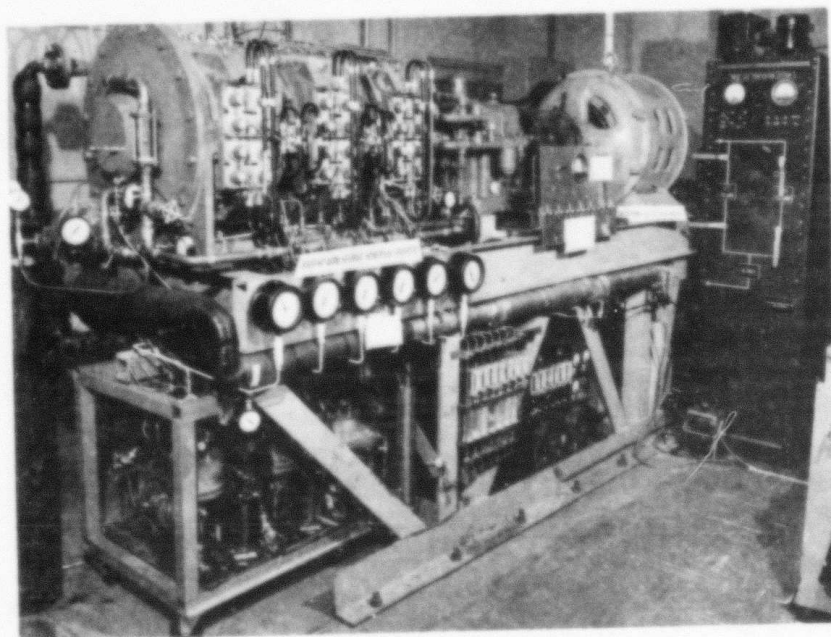


Fig. 1.2: SEGMA Generator on its test stand - The drive system and gas purification system are both on the right. The six NaK purification and supply loops are below. To their right are the gas subsystems for intercollector pressure balancing and shaft sealing.

II 1-4

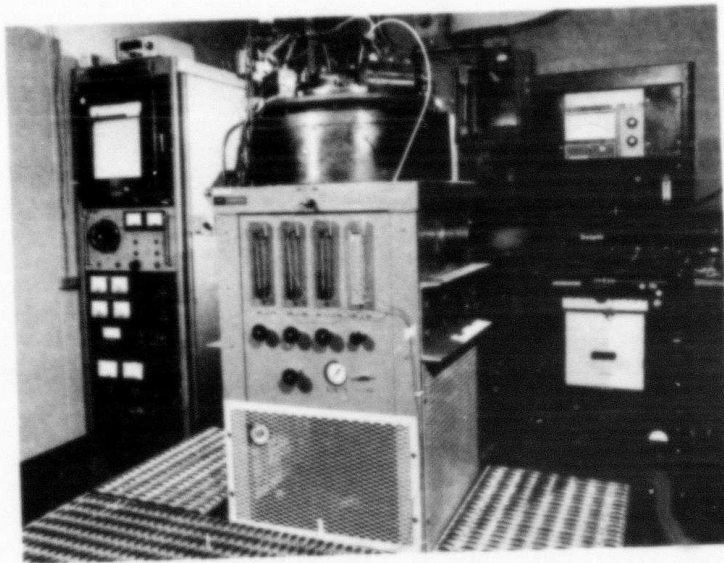


Fig. 1.3: GEC homopolar generator with GaIn current collection.

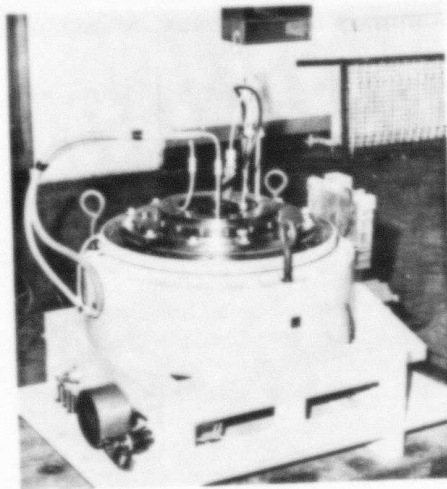


Fig. 1.4: GEC homopolar machine in its test area showing the cover gas system (right), and the control panel (left).

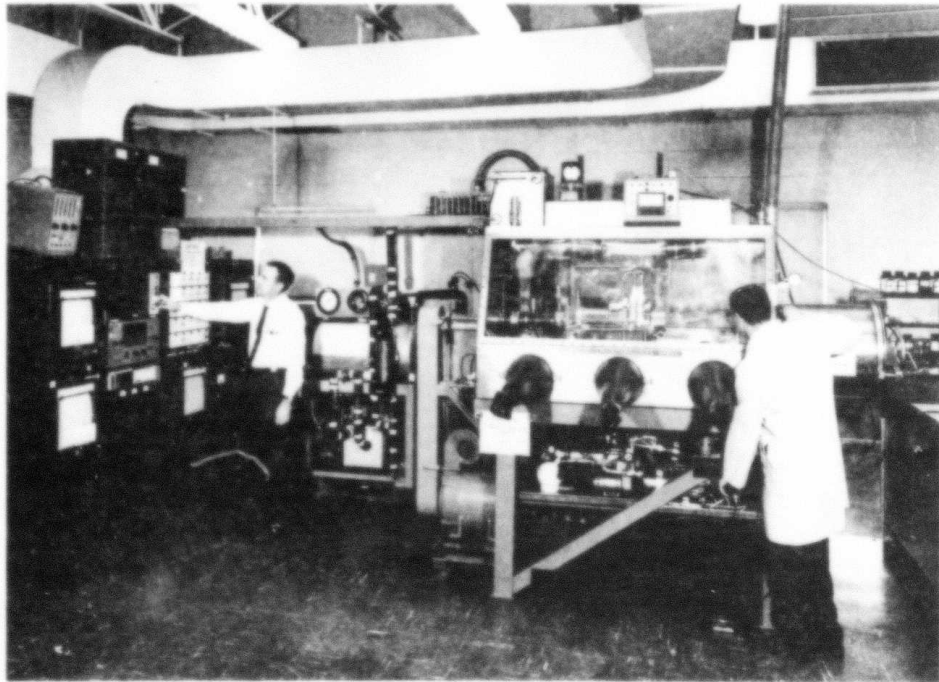


Fig. 1.5: Test stand used in evaluating liquid metal current collectors for SEGMAG machine.

- 6) Seal Study. A study of the sealing problems between the liquid metal, bearing oil system, and the environment was conducted. Seal system conceptual designs were evolved for both the SMHTC and SEGMAG machines.

Seal systems were developed for SEGMAG machines to: (a) confine the liquid metal to the collector zone; and (b) prevent air contamination of the liquid metal and loss of its protective cover gas atmosphere. Test rigs were constructed to simulate actual machine operating conditions.

The seal technology of Phases I and II was extended to higher speed unidirectional applications in Phase III. Seals for reversible and variable speed applications remain to be developed for motors and torque converters.

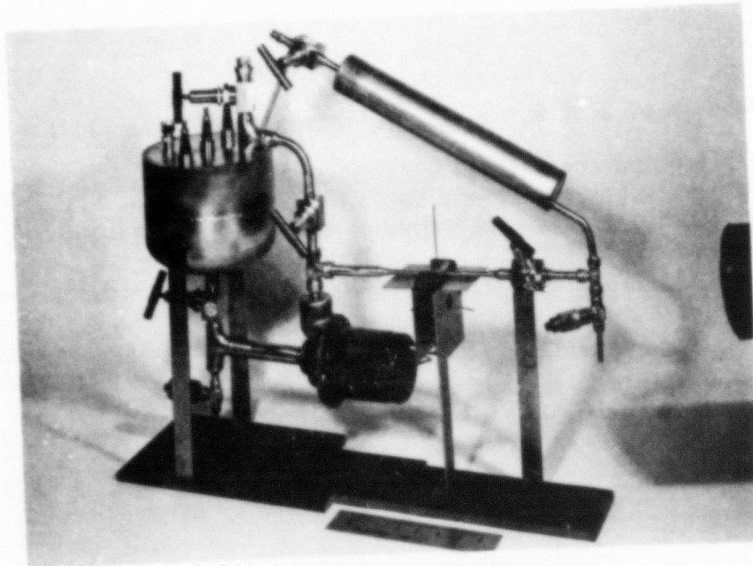


Fig. 1.6: Assembled NaK purification loop for servicing each current collector in the prototype SEGMAG machine.



Fig. 1.7: Internal components of central gas purifier station for the SEGMAG homopolar machine.

1.3.2 Summary of Contractual Accomplishments in Phase III-A

In Phase III-A the contractual workscope was redirected to investigate promising new, highly efficient solid brushes for homopolar machines as an alternative to liquid metal current collection systems.

- 1) Current Collector Test Rigs. Brush test rigs of reduced and full size were constructed for the purpose of evaluating various brush materials and brush systems. The small testers were used to determine coefficient of friction, double voltage drop, brush pressure and wear rate of various brush materials in specified environments. The larger rigs (Fig. 1.8) enabled the testing of these brushes under higher speed and higher current conditions. Finally the Machine Environment Brush Tester (Fig. 1.9), which is a SEGMAG machine, will expose the brushes and slip rings to an actual machine environment.
- 2) Current Collector Contact Material/Performance. Experiments were performed to evaluate potential brush and slip ring materials characterized by medium to high current density ratings, low wear rate, and low power loss. Silver and copper graphite composites comprised the bulk of brushes tested. An expression was also developed to predict brush life, based on brush wear and geometrical considerations. This work is continuing under a related contract (ONR/ARPA Contract #N00014-76-C-0683).
- 3) Current Collector Mechanical Load Systems. In order to optimize the performance of the newly developed brushes and slip rings, special brushholders were developed in order to facilitate the transfer of load current from brushes to machine output terminals.
- 4) Current Collector Interface Cooling Systems. This task established the heat transfer characteristics between the brush, its holder, and the slip ring interface. High current density applications make brush cooling requirements a more critical performance parameter here than in conventional machines. Heat flow data from the brushes led to the design of a water cooling system for the MEB.
- 5) Current Collector Gaseous Environment Control. A gas recirculating system was designed and constructed to control the internal ambient atmosphere of the Machine Environment Brush Tester. Capabilities of the gas system include: operation with a variety of non-oxidizing gases over a wide range of flow rates and preset moisture concentrations; removal of particulate debris due to brush wear; removal of vapor product contaminants from test facility outgassing; and maintenance of a predetermined positive gas pressure level. A controlled gaseous environment is necessary to the operation of the brush system being developed under this contract and the related ARPA/ONR Contract #N00014-76-C-0683.

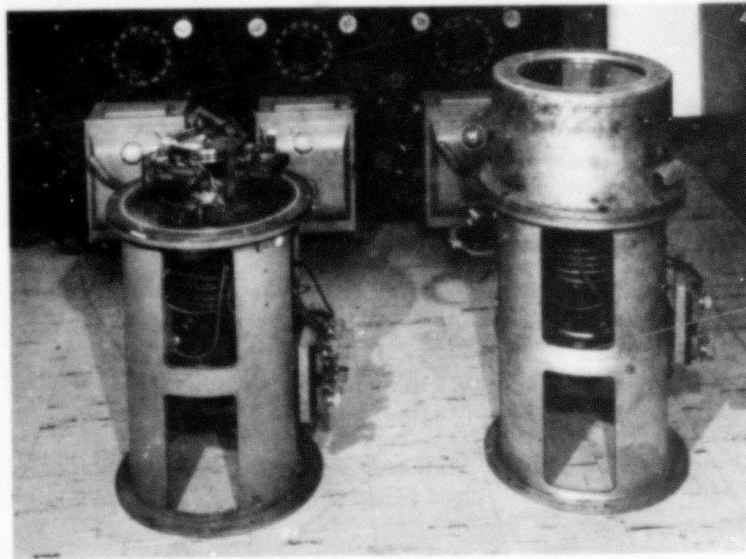


Fig. 1.8: High Speed Brush Testers, for screening of prototypic brushes.

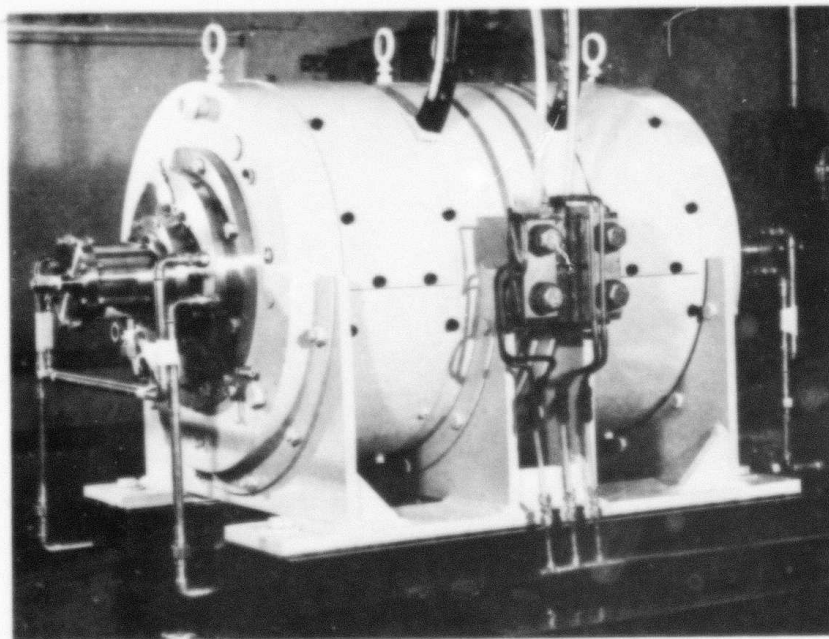


Fig. 1.9: Machine Environment Brush Tester (MEB); will be used in a related program (ONR/ARPA Contract #N00014-76-C-0683) to expose brush and slip ring materials to an actual SEGMAG machine environment.

- 6) Application Studies for Solid Brush SEGMAg Machines. In this study the results of brush research were correlated with the machine design and utilization requirements. This provided the necessary interface between the solid brush research program and the operational requirements of the machines.

1.4 ORGANIZATION OF FINAL REPORT

The balance of this final report has been organized into two parts, A and B, as follows:

Part A: Liquid Metal SEGMAg Developments. This includes all of the work under Phases I, II and III arranged by subtask. Part A consists of Sections 2 through 7.

Part B: Solid Brush SEGMAg Developments. This includes the work of Phase III-A. Part B is comprised of Sections 8 through 13.

E.M. 4883

VOLUME II

PART A

LIQUID METAL SEGMAG DEVELOPMENTS

A1

VOLUME II
PART A
SECTION 2
CURRENT COLLECTOR TEST RIGS

2.0 GENERAL

Three machines employing liquid metal current collection were examined under this contract:

- 1) Conceptual designs for Segmented Magnet Homopolar Torque Converter (SMHTC) were evaluated. The SMHTC converts constant speed inputs to variable speed output in either the forward or reverse direction.
- 2) A Segmented Magnet Homopolar Generator (SEMGAG) was designed, constructed, and tested extensively. The SEMGAG machine successfully demonstrated both the segmented magnet machine concept and the reliability of NaK liquid metal current collectors.
- 3) A General Electric Company (England) homopolar generator was purchased and tested to provide operating experience with GaIn current collection fluid.

2.1 SEGMENTED MAGNET HOMOPOLAR TORQUE CONVERTER (SMHTC)

2.1.1 Objectives

The objective of this program was to investigate the segmented magnet homopolar torque converter (SMHTC), within the framework of some of the more promising applications. This concept will then be demonstrated (in a later program) in a torque converter which will operate at constant input speed (as from a prime mover), and will provide variable output speeds, in both forward and reverse directions, at variable torque up to full power rating.

Our objective in Phase I was to study the various configurations proposed for the SMHTC, and the technical problems involved in developing the prototype machine.

In Phase III a conceptual design was evolved for the prototype torque converter.

2.1.2 Prior and Related Work

The SMHTC concept was derived from a unique modular DC homopolar machine being investigated at Westinghouse. This machine, known as a segmented magnet homopolar machine (SEGMAG) uses series connected DC modules to obtain the design output. The characteristics of SEGMAGs were investigated under another contract (N000 14-72-C-0393).

2.1.3 Summary of Accomplishments

2.1.3.0 General

The SMHTC consists basically of two homopolar machines connected as a generator-motor set. Two basic configurations are being considered: (1) a radial design which uses a generator mounted within a motor; and (2) an axial design which consists of inline generator and motor. The inline configuration is preferred.

Two basic homopolar machine types are being considered: (1) the drum-type (SEGMAG), and (2) the disk-type (DISKMAG).

During Phase I of this contract, electrical analyses of large (30,000 HP) and small (6000 HP) machines were completed.¹ These were of the drum-type (SEGMAG) homopolar machine configuration. Two conceptual designs (radial and axial) were also prepared for the 6000 HP machine, as part of the Phase I effort.

More recent studies (in Phase III) have shown that a rating of 8000 HP, 3600/500 RPM is typical of potential applications to small naval ship drives,² and this rating was therefore chosen for the prototype torque converter.

In Phase III, a number of 8000 HP designs for the disk-type "flooded gap" machine (DISKMAG) were investigated.² The power losses and internal machine fluid pressures associated with a particular "flooded gap" design were defined.

A conceptual design was prepared for an 8000 HP torque converter of the SEGMAG type.³ This machine is able to accept input power from a gas turbine prime mover at 3600 rpm and deliver power to a propeller load at variable speeds to 500 rpm in either forward or reverse directions.

In addition, conceptual studies of small (8000 HP) and large (40,000 HP) DISKMAG propulsion motors were performed. Electrical design and loss studies were performed to develop optimum configurations for maximum efficiency and power density.

2.1.3.1 8000 HP Torque Converter

A parametric study was done to optimize the design of the 8000 HP, 3600/500 rpm torque converter, in terms of low weight and size and high efficiency. Test results from the current collector test stand and the 3000 HP SEGMAG generator were incorporated in the analysis to provide a more realistic assessment of losses than had previously been considered. In particular, provision was made in each design to minimize tooth ripple losses on the rotor and stator surfaces, and to minimize total loss in the collectors, including contact resistance loss.

In a machine of this type, there are a large number of independent variables, and a true optimization was not possible in the time available. To further complicate the situation, the objectives of low weight and high efficiency are not compatible; i.e., that which tends to decrease weight also decreases efficiency, and vice versa. Therefore, a range of each variable to be considered was defined for both the generator and the motor part of the torque converter. Machines were designed which covered the ranges of variables defined, and appropriate pairings of motors and generators were made to produce torque converters.

The independent variables and their specified ranges were the following:

	<u>Motor</u>	<u>Generator</u>
Rated Current	150,000-400,000 Amps	150,000-500,000 Amps
Current Density	5,000-10,000 Amps/inch ²	5000-10,000 Amps/inch ²
Number of Modules	1-4	1-3
Number of Turns/Module	1-2	1-2
Rotor Diameter	No general specification.	

Because the generator and motor are not constrained to be the same in any of these variables except rated current, the total number of independent variables for a torque converter design is nine.

Current densities in the torque converter conductors of 10,000 amperes per square inch were first considered. However, no designs at this current density were found to have an efficiency greater than about 88%. Therefore, the design current density was reduced to 5000 amperes per square inch.

The weight and losses for typical designs from this study are shown in Table 2.1.1. The weights shown are for the electrical components of the machines, and are not intended to represent the total weight of complete

machines; the addition of housings, bearings, shafting, etc., may add 20-50% to the weights shown. In each case, the rotor diameter has already been "optimized", and thus has been removed as an independent variable.

The table shows the difficulty in choosing among the various machines. In some cases the choice is obvious; for example, 2-G is clearly superior to 1-G. However, it is not at all obvious which is superior between 4-M and 5-M.

Various combinations of these SEGMAG motors and generators were combined as torque converters. Table 2.1.2 illustrates a range of typical torque converters resulting from this process. Once again, the choice of an optimum is not obvious. For a particular application, a means could be determined to relate the benefits of a decrease in size and/or weight to the penalties of a decrease in efficiency. Without having such a relationship in general, objectives were established of an efficiency of about 94%, a weight of about 20,000 pounds, and a size compatible with a space approximately 6 feet long and 4 feet in diameter. Torque converter no. 6 comes closest to meeting these objectives, and thus was chosen for the conceptual design.

2.1.3.2 Typical 8,000 HP Disk-Type Motor Design (DISKMAG)

A number of designs for an 8000 HP disk-type "flooded gap" motor (DISKMAG) were considered during the study. The geometrical dimensions and operating conditions for a typical design are listed in Table 2.3 and illustrated in Figure 2.1.1.

A qualitative description of the fluid flow behavior in a "flooded gap" motor is given in Reference 2. The problem of fluid containment in the annular current collector gaps appears to be resolved by this machine concept. However, other problems associated with pressure and thrust loads placed on the machine seals and bearings, as well as power losses in the liquid metal, must be considered.

Unbalanced centrifugal pressures are induced in the liquid metal because of high velocity circumferential flow on one side of each disk and zero velocity on the other. Because of the required tandem arrangement, the unbalanced pressure created at each disk accumulates throughout the machine. If no axial circulation of fluid is allowed (as with a batch-loaded liquid metal system), the shaft seals and rotor bearings must withstand rather large pressures and thrust forces. On the other hand, if axial flow of liquid metal is permitted, such as under the action of the unbalanced centrifugal pressure, the fluid and mechanical loads on the seals and bearings will be reduced. This reduction is attributed to an electromagnetic pressure drop associated with movement of the conducting liquid metal in the machine's magnetic field. The following governing expressions which permit calculation of the machine seal and bearing pressures and forces were developed by Rhodenizer and acknowledged in Section 4.3.1.3.

Table 2.1.1

Weights and Losses of Typical Machines
for an 8000 HP, 3600/500 RPM Torque Converter

<u>Machine No.</u>	<u>Rated Current-kA</u>	<u>Generators</u>		<u>Weight, Pounds</u>	<u>Loss, Kilowatts</u>
		<u>Number Modules</u>	<u>Turns Per Module</u>		
1-G	150	1	2	3,900	240
2-G	150	2	1	3,800	158
3-G	200	1	1	3,500	147
4-G	200	2	1	3,100	183
5-G	250	1	1	3,000	159
6-G	250	2	1	2,900	207
 <u>Motors</u>					
1-M	150	1	2	26,700	157
2-M	150	2	2	22,300	209
3-M	150	3	2	21,000	259
4-M	200	2	2	18,000	255
5-M	200	3	1	23,400	172
6-M	250	1	2	17,600	219
7-M	250	2	1	20,600	156
8-M	250	2	2	15,700	312

TABLE 2.1.2
8000 HP, 3600/500 RPM Torque Converter Options

<u>Torque Conv. No.</u>	<u>Rated Current-kA</u>	<u>Generator</u>	<u>Motor</u>	<u>Weight, Pounds</u>	<u>Min. Length, Inches</u>	<u>Motor Dia. Inches</u>	<u>Efficiency</u>
1	150	2-G	1-M	30,500	66	57	94.7%
2	150	2-G	2-M	26,100	82	44	93.9%
3	200	3-G	4-M	21,500	68	41	93.3%
4	200	4-G	4-M	21,100	76	41	92.7%
5	200	4-G	5-M	26,500	75	43	94.1%
6	250	5-G	6-M	20,600	51	49	93.7%
7	250	5-G	7-M	23,600	59	47	94.7%
8	250	5-G	8-M	18,700	88	38	92.1%

Liquid metal is not allowed to flow through the motor from end to end:

$$p_s = p_i + \frac{N\rho\omega^2}{2} (R_o^2 - R_i^2), \quad 2.1.1$$

where: p_s = total pressure on seal, N/m^2

p_i = liquid metal inlet pressure, N/m^2

$$F_R = \frac{N\rho\omega^2\pi}{4} (R_o^2 - R_i^2)^2, \quad 2.1.2$$

Dwg. 6252A32

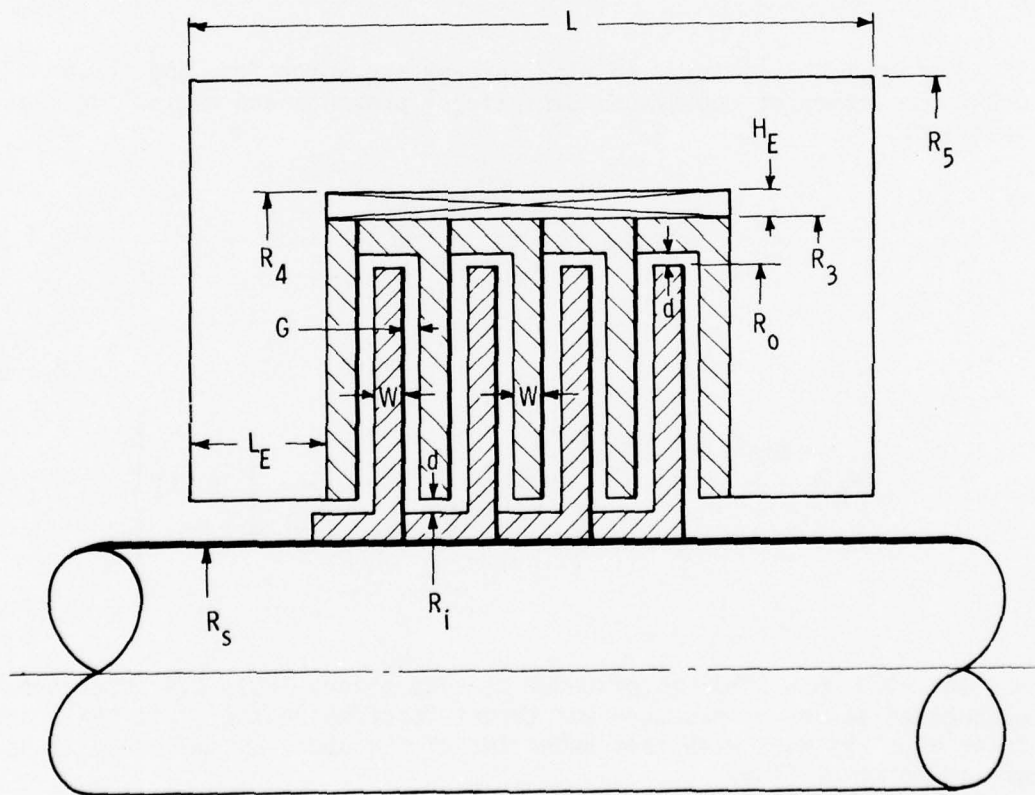


Fig. 2.1.1: Disk-Type homopolar machine (DISKMAG)

where: F_R = rotor bearing thrust force, N

If liquid metal is allowed to flow through the motor from end to end:

$$p_s = p_i + \underbrace{\frac{N\rho\omega^2}{2} (R_o^2 - R_i^2)}_{\text{Centrifugal press. rise}} - \underbrace{(2N-1) \frac{B_x^2 \sigma Q}{2\pi G} \ln \left(\frac{R_o}{R_i} \right)}_{\text{Electromagnetic press. drop}}, \quad 2.1.3$$

where Q = liquid metal volume flow, m^3/s .

$$F_R = \frac{N\rho\omega^2\pi(R_o^2 - R_i^2)^2}{4} - \frac{(2N-1)B_x^2\sigma Q}{2G} \left[\frac{(R_o^2 - R_i^2)}{2} - R_i^2 \ln \left(\frac{R_o}{R_i} \right) \right], \quad 2.1.4$$

If liquid metal is allowed to flow through the motor from end to end under the action of unbalanced centrifugal pressure and neglecting fluid friction:

$$Q = \frac{N}{(2N-1)} \frac{\rho\omega^2 G \pi (R_o^2 - R_i^2)}{B_x^2 \sigma \ln \left(\frac{R_o}{R_i} \right)}, \quad 2.1.5$$

$$p_s = p_i \quad 2.1.6$$

$$F_R = \frac{N\rho\omega^2\pi(R_o^2 - R_i^2)}{4} \left\{ (R_o^2 - R_i^2) \left[1 - \frac{1}{\ln \left(\frac{R_o}{R_i} \right)} \right] + 2R_i^2 \right\}. \quad 2.1.7$$

For the 8000 hp DISKMAG motor under consideration, Table 2.4 shows the calculated values of pressure and thrust force which the shaft seals and rotor bearings must withstand under two of the above assumed conditions of liquid metal flow.

2.1.3.3 40,000 hp Disk-Type SC Motor Design (DISKMAG)

An investigation was made to determine if a "flooded gap" motor having a superconducting (SC) excitation magnet may offer any advantages over machines with normal temperature (NT) winding magnets.

The disks of the SC motor were assumed to be of solid copper in order to reduce the complexity of construction as well as reduce electrical resistance. Consequently, without iron in the disks, a greater magnetic induction will appear in the current collector radial gaps. The expected increase in collector radial gap loss due to the larger induction will be compensated to some extent by the reduced ohmic loss in the disks.

The internal fluid pressures and machine power losses were calculated for a disk-type "flooded gap" superconducting 40,000 hp, 180 rpm motor. These characteristics are compared with those of a disk-type "flooded gap" NT design 8,000 hp, 500 rpm motor studied above.

A number of 40,000 hp disk-type SC "flooded gap" motor designs were considered during the study. The geometrical dimensions and operating conditions for a typical design are listed in Table 2.1.3 and illustrated in Fig. 2.1.1.

Fluid flow behavior in a "flooded gap" DISKMAG machine and governing expressions which permit calculation of the machine seal pressure, rotor bearing thrust forces, and machine power losses, are identical to those used for the 8,000 hp machine.

For the typical 40,000 hp DISKMAG SC motor under consideration, Table 2.1.4 shows the calculated values of pressure and thrust force which the shaft seals and rotor bearings must withstand under two conditions of liquid metal flow. These pressures and forces are significantly greater than the corresponding ones previously calculated for the 8,000 hp NT motor. This difference is attributed mainly to the greater number of disks used in the SC machine, required for the larger power rating.

Table 2.1.5 provides a comparison of calculated power losses for the 40,000 hp SC and 8,000 hp NT DISKMAGS. Larger radial gap losses for the SC machine were offset by lower machine losses, but afforded no advantage in reducing the overall loss rating as compared to the NT machine. The corresponding axial gap and collector ohmic losses remained fairly equal (in percent) for both designs considered. The net percentage of all power losses was identical (4.8%) for both designs.

Operating efficiency is generally a function of machine weight, (i.e., higher efficiency can generally be attained by making the machine heavier). The calculated specific power for the 40,000 hp SC design is 0.63 hp/kg compared to 0.69 hp/kg for the 8,000 hp NT design. Since it is heavier per unit power output than the 8,000 hp NT motor, but does not operate with higher efficiency, there does not appear to be an

TABLE 2.1.3

Dimensions and Operating Conditions for Typical Design 8,000 hp
Normal Temperature and 40,000 hp SC Disk-Type "Flooded Gap"
(DISKMAG) Homopolar Motors

A. Operating Conditions

P = machine rated power,	8,000 hp	40,000 hp
I = machine full-load current,	100,000 A	100,000 A
B_{xi} = axial magnetic induction at inner collector,	0.25 T	1.44 T
B_{xo} = axial magnetic induction at outer collector,	0.35 T	1.44 T
B_{yi} = radial magnetic induction at inner collector,	Essen. 0	Essen. 0
B_{yo} = radial magnetic induction at outer collector,	Essen. 0	Essen. 0
= rotor angular velocity,	8.33rad/s(500RPM)	18.8rad/s(180RPM)
B_x = axial magnetic induction in disks,	1.26 T	1.44 T

B. Geometrical Design (rectangular cross-section)

R_s = shaft radius,	-	.206m(8.11in)
R_i = radius of inner collector,	0.101m(6.34in)	.220m(8.68in)
R_o = radius of outer collector,	0.394m(15.507in)	.675m(26.6in)
W_i = width of inner collector,	$3.05 \times 10^{-2}m(1.2in)$.0140m(.55in)
W_o = width of outer collector,	$3.05 \times 10^{-2}m(1.2in)$.0140m(.55in)
d_i = radial gap of inner collector,	$1.65 \times 10^{-3}m(0.065m)$	$1.27 \times 10^{-3}m(0.05in)$
d_o = radial gap of outer collector,	$1.65 \times 10^{-3}m(0.065m)$	$1.27 \times 10^{-3}m(0.05in)$
N = number of disks,	14	54
G = axial gap between rotating and stationary disks,	$3.05 \times 10^{-3}m(0.065m)$	$1.40 \times 10^{-3}m(.055in)$
R_5 = outer radius of machine,	-	0.956m(37.6in)
L = machine length,	-	2.14m(84.3in)
S_p = specific power	-	0.63hp/kg(0.29hp/lb)

C. Constants and NaK Physical Properties (100°C)

$f(\delta < 1)$ = Fanning fric. factor, smooth surface,	0.7×10^{-2}	0.7×10^{-2}
$f(\delta > 1)$ = Fanning fric. factor, roughened sur,	1.8×10^{-2}	1.8×10^{-2}
ρ = mass density	850 kg/m ³	850 kg/m ³
σ = electrical conductivity,	$2.2 \times 10^6 mhos/m$	$2.2 \times 10^6 mhos/m$
ϵ_k = specific contact potential (Cu-NaK-Cu),	$4.1 \times 10^{-9} Vm^2/A$	$4.1 \times 10^{-9} Vm^2/A$
η = dynamic viscosity	$5.1 \times 10^{-4} N-s/m^2$	$5.1 \times 10^{-4} N-s/m^2$

TABLE 2.1.4

Seal Pressure and Rotor Thrust Forces for a Typical 8000 hp
Normal Temperature and 40,000 hp SC Disk Type Motor (DISKMAG)

Condition	Seal Pressure, p_s		Rotor Thrust, F_R	
	N/m^2	(psi)	N	(tons)
No liquid metal flow through motor.				
8,000 hp	$*2.11 \times 10^6$	*306	4.28×10^5	48.1
40,000 hp	$*3.32 \times 10^6$	*481	2.06×10^6	231.7
Liquid metal circulation by internal centrifugal pressure.				
**8,000 hp	p_i	p_i	1.21×10^5	13.6
[†] 40,000 hp	p_i	p_i	6.72×10^5	75.5

* pressure above inlet pressure, p_i .

** max. NaK flow rate (assuming no friction), $4.79 \times 10^{-4} m^3/s$ (7.6 gal/m).

[†] max. NaK flow rate (assuming no friction), $5.33 \times 10^{-5} m^3/sec$ (0.845 gal/min).

TABLE 2.1.5

Calculated Power Losses for the 40,000 hp SC and 8,000 hp NT DISKMAGS

Power Loss Mode	*40,000 HP Power Loss		**8,000 HP Power Loss	
	kw	%	kw	%
Radial Gap (P_{rg})	424	30	18.26	6
Axial Gap (P_{ag})	597	42	119.06	42
Ohmic (P_o)	173	12	31.01	11
Machine (conductor + excitation)	<u>237</u>	<u>16</u>	<u>115.49</u>	<u>41</u>
Total	1431	100	283.82	100
% of Machine Rating	4.8	4.8	8	4.8

* Superconducting (SC) excitation coil.

** Normal temperature (NT) winding excitation coil.

advantage in the use of a superconducting excitation magnet for "flooded-gap" disk-type homopolar machines.

2.1.4 Conclusions

As a result of this study, which included ranges in geometrical dimensions, load currents, and excitation levels, a number of problem areas associated with disk-type machines were found. A few of these concerns are summarized below:

- Complex construction of disks to obtain magnetic circuits with low axial and high circumferential reluctance.
- High machine power losses, attributed mainly to MHD effects in the axial gaps between disks.
- Probability for turbulent rather than laminar flow and high short circuit losses in the liquid along the flat side walls of the machine disks. Reynolds to Hartman number ratios >1000 are calculated for operating conditions down to 30% of rated full load speed. Thus, the assumption of laminar fluid flow employed in axial gap power loss expressions is in doubt except at low speeds.
- A need is recognized for large thrust bearings and high pressure shaft seals to assure a fail safe machine design.

The inherent low efficiency of this DISKMAG type of machine precludes its use in the applications of interest. Thus, the focus of the conceptual design study in the future should be concentrated on the SEGMAG drum-type torque converter configuration.

2.1.5 References

1. C. J. Mole, et. al., "Design and Development of a Segmented Magnet Homopolar Torque Converter," Semi-Annual Technical Report for May 31, 1973, June, 1973, E.M. 4518.
2. C. J. Mole, et. al., "Design and Development of a Segmented Magnet Homopolar Torque Converter," Semi-Annual Technical Report for May 31, 1974, Feb. 1975, E.M. 4648.
3. C. J. Mole, et. al., "Design and Development of a Segmented Magnet Homopolar Torque Converter," Semi-Annual Technical Report for May 31, 1975, July 1975, E.M. 4705.

2.2 SEGMENTED MAGNET HOMOPOLAR MACHINE (SEGMAG)

2.2.1 Objectives

The objective of this program is to demonstrate the SEGMAG concept and to provide a test vehicle for evaluation of the current collection systems, containment seals, and liquid metal handling systems developed in previous subassembly testing. The demonstration unit (rated 3000 HP, 3600 RPM) subjected the current collectors to current densities, leakage flux and other conditions associated with operation in a machine environment. In addition, the unit provided for long-term testing of current collectors, their attendant support systems, and the machine itself, in order to develop operational data for liquid metal machines.

2.2.2 Prior and Related Work

The SEGMAG concept was developed to provide a high performance DC machine without requiring superconducting magnet excitation. This low reluctance machine, using room temperature excitation, has capability for high output per unit weight and volume. The modular construction allows for higher outputs by using many modules connected in series. The characteristics of this machine were investigated thoroughly in another U.S. Government Contract (N00014-72-C-0393).

2.2.3 Summary of Accomplishments

2.2.3.0 General

The demonstration SEGMAG machine design was constructed and tested in January 1974. The initial series of tests was continued for 140 hours of SEGMAG operation. Short-circuit output of 90,000 amperes and 19 volts open-circuit was achieved. The testing validated both the SEGMAG machine concept and the liquid metal current collector system.

SEGMAG operation. Short-circuit output of 90,000 amperes and 19 volts open-circuit was achieved. The testing validated both the SEGMAG machine concept and the liquid metal current collector system.

As a current collector test vehicle, the performance of SEGMAG was excellent. The following objectives were accomplished:

- Techniques for filling the collectors were evaluated.
- Methods of detecting a filled collector were determined.
- High purity of both NaK and cover gas was maintained.
- Current collector filling was maintained, even in the presence of radial magnetic fields and high load currents.
- Liquid metal leakage from the current collectors was minimal except at highest open circuit excitation.
- The small NaK spillage that did occur was handled without difficulty, and without creating internal short circuits.
- Calculated viscous and eddy current losses were experimentally confirmed.

Following the test run the machine was disassembled and inspected. Decontamination was rapid and straightforward.

Several modifications were undertaken including:

- Insulation in the collector region to improve NaK containment.
- A strain gauge system on the rotor shaft to improve torque and power measurements.
- The air gap geometry was modified in order to reduce parasitic losses, and
- The current collectors were silver plated to enhance wetting.

The machine was then assembled and installed on the test stand, and the second test series was initiated in early 1975.

The tests for friction, windage, and NaK viscous loss were repeated for comparison with previous measurements. Series open-circuit and short-circuit tests were then performed with these favorable results:

- Successful operation of SEGMAG and auxiliary machine systems at or near rated design conditions for extended periods. Total running time 215 hours.

- Peak power demonstration of 107,000 amperes and 20.8 volts, corresponding to a rating of 2983 horsepower (versus a program target level of 3000 horsepower).
- Verification that steady state power levels of 90,000 amperes and 20 volts can be maintained, corresponding to a 2413 horsepower rating.
- Machine efficiency of 92.5%.
- Demonstration that these performance levels are primarily restricted by the capability of the present collector design to confine NaK against the magnetohydrodynamic ejection forces and to operate with low contact resistance.
- Identification of design improvements capable of producing 93,300 amperes at 30 volts (power rating = 3750 horsepower) with 97% efficiency within the volume of the present machine.
- Verification that the technology base developed earlier in the program could be successfully implemented in an operating machine.

2.2.3.1 General Design Considerations

The SEGMAG concept¹ is shown in Fig. 2.2.1 and 2.2.2. The field excitation for the machine is distributed or segmented along the axial length of the machine. This design produces flux in the air gap between magnets that alternate from radially inward to radially outward along the length of the machine. Voltage is generated in bars embedded in the rotor. The voltages of the rotor bars are connected in series so that the total machine voltage is equal to the voltage in each section or module times the number of modules. In order to minimize excitation requirements, a low reluctance path is provided in each module. This is accomplished by using magnetic teeth between bars in the active length of the stator and rotor and minimizing air gaps in the machine. This design requires therefore conductors mounted in magnetic teeth in the rotor and stator.

One of the most critical areas of design in homopolar machines is that of the current collector. These machines typically operate at low voltage and high current. This necessitates a current collector capable of carrying high currents from the rotor to the stator. If conventional brush slip ring configurations were used, the machine size and weight would be very high to accommodate the necessary brush gear and slip rings. In applications requiring high power densities, this would be undesirable. To reduce the size of the current collection system, liquid metal current collectors were developed and full sized prototypes were tested for this machine as part of the overall program.² The collector system consisted of a thin annulus of liquid metal retained in the current collection area as shown in Fig. 2.2.3. The high current density achievable in such devices permitted reduction in machine size and weight over machines with conventional brush gear.

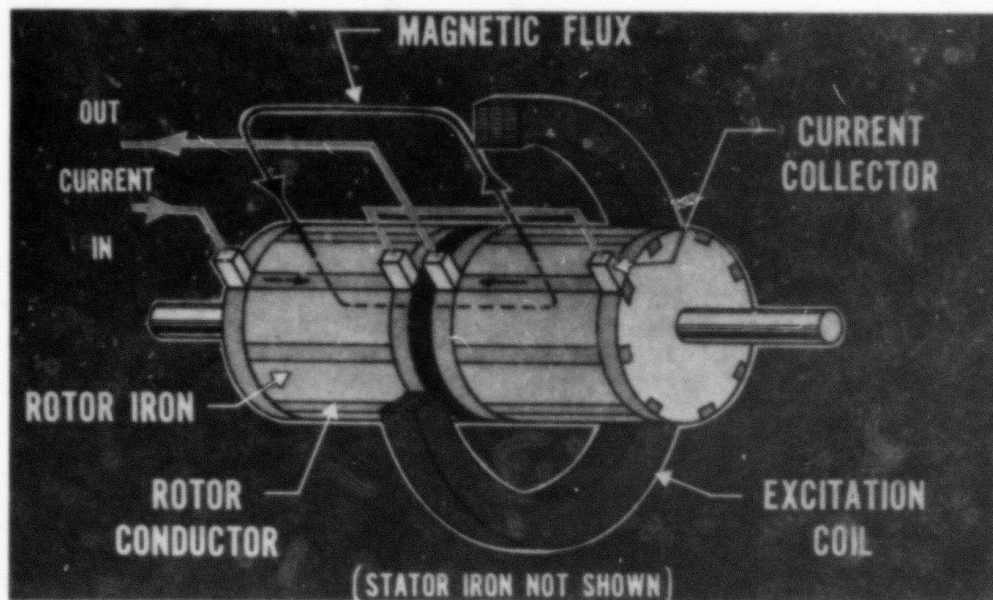


Fig. 2.2.1: Principle of SEGMAg machine operation.

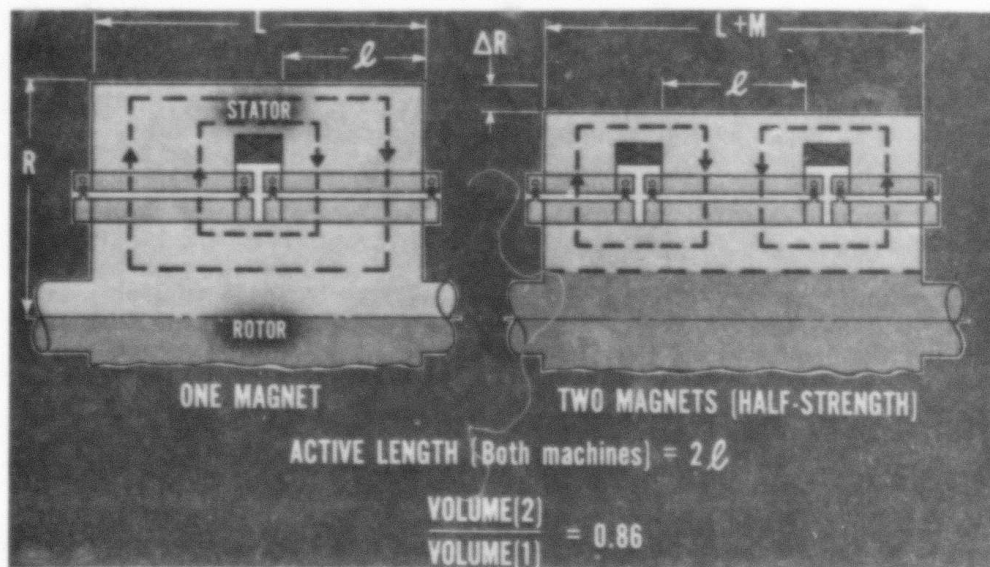


Fig. 2.2.2: Benefits of axial segmentation of magnetic field (equivalent power machines).

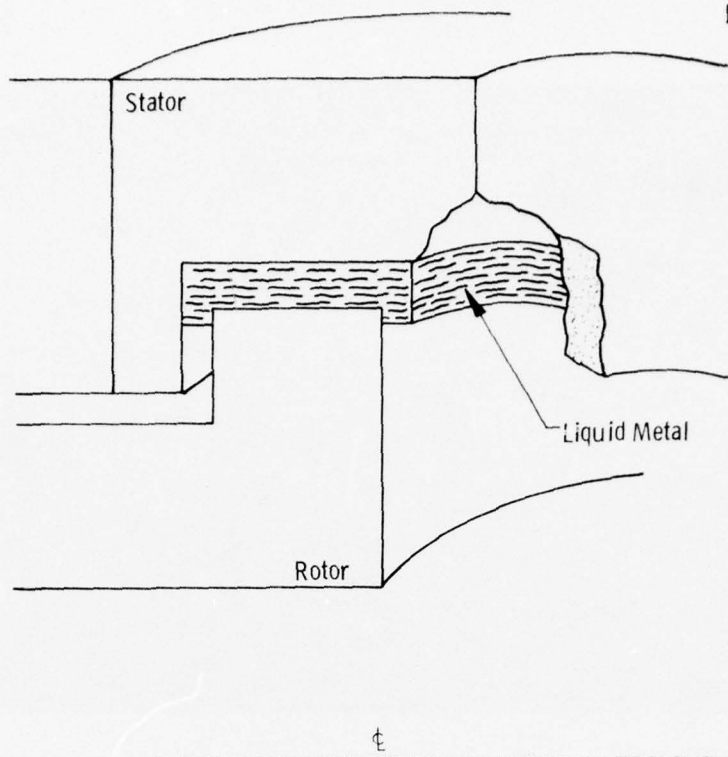


Fig. 2.2.3: Typical current collector.

The liquid metal chosen was NaK-78, an Eutectic alloy of sodium and potassium. This liquid metal was chosen because its conductivity and viscosity were acceptable from the standpoint of joule heating and viscous power losses for machines of this type. The losses in the current collectors, which are an important factor in machine efficiency, can be divided into three categories; viscous, MHD and joule losses.² The viscous losses are due to the fluid shear stress developed in the liquid metal due to the velocity gradient. The MHD losses are due to velocity changes due to the interaction of the transport current and the leakage flux through the collector and due to voltage gradients across the collector width as shown in Fig. 2.2.4. Axial flux leakage interacts with the transport current in the collector producing a body force that accelerates the liquid metal thus increasing the velocity gradient in the NaK.⁴ Radial leakage flux produces a voltage gradient axially across the rotor collector face, producing circulating currents and resulting in a joule heating loss in the liquid metal.

In addition to the MHD losses, two undesirable effects are produced by leakage flux in the current collector area.² Both of these effects produce body forces that tend to expel the liquid metal from the collector area. In the first effect the circumferential flux developed by the circulating currents produce body forces that put the liquid metal in tension thus tending to expel the NaK from each side of the collector. In addition, the machine load current produces a circumferential flux in the active length that interacts with the transport current to expel the liquid metal from one side of the collector. This results in an uneven distribution of liquid metal in the collector as shown in Fig. 2.2.5 or in an extreme case complete expulsion.

These effects must be minimized both from an efficiency and operational viewpoint. They can be reduced in several ways, including shielding of the current collector area to lower the leakage flux to an acceptable level. This was a major design objective in the SEGMAG program

The use of NaK in a machine requires design attention to areas not normally considered in electrical machinery. NaK reacts readily with oxygen to form an abrasive, insulating oxide that is detrimental to acceptable collector performance. In addition, NaK reacts with water forming the hydroxide with the subsequent evolution of heat and hydrogen with its attendant explosive hazard. Auxiliary systems are required to remove these impurities and to provide an inert environment within the machine.³

The machine power losses, both viscous losses in the collector and joule heating losses, must be removed. The cooling system within the machine must insure that the coolant is compatible with the liquid metal or provide complete isolation from the machine internals to prevent contamination. The rating of SEGMAG machines is strongly dependent upon the cooling capability.

The design of the SEGMAG machine was based on several requirements including:

- High current density in the collectors.
- High speed to duplicate tip speeds of typical full sized machines.
- Modular configuration to demonstrate feasibility.
- Segmented excitation coils to duplicate flux paths.

To satisfy these requirements, a machine rating of 3000 hp with rated current of 100,000 amps and 24 volts at 3600 rpm was chosen. The machine would consist of one center module and two end modules with two excitation coils. Since full scale machine studies have shown that water cooling is essential to achieve power density objectives, the SEGMAG prototype generator was designed for water cooling.

2.2.3.2 Mechanical Design of SEGMAG

The SEGMAG generator shown in cross-section on Fig. 2.2.6 is composed of four major assemblies; the rotor, the horizontally-split stator, the end-flange/bearing-housing assemblies, and the excitation coils. Since the two excitation coils are not split, these are positioned on the rotor prior to installation of the rotor, and subsequent assembly of the split-stator halves.

The SEGMAG machine, shown in Fig. 2.2.7 with the stator upper half removed, consists of one center module and two end modules. The end modules are half the center module length.

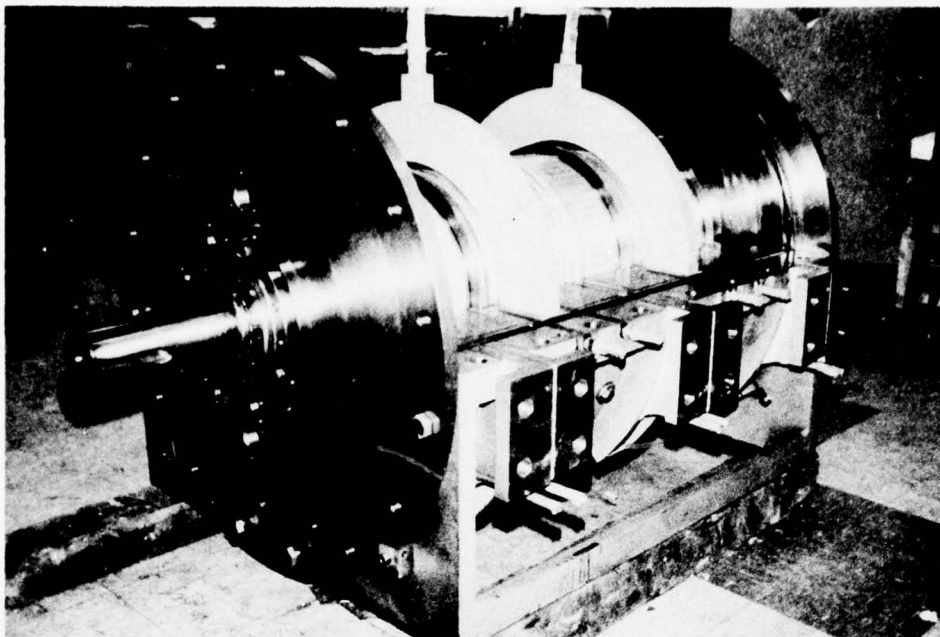


Fig. 2.2.7: SEGMAK with top half of stator removed, showing field excitation coils.

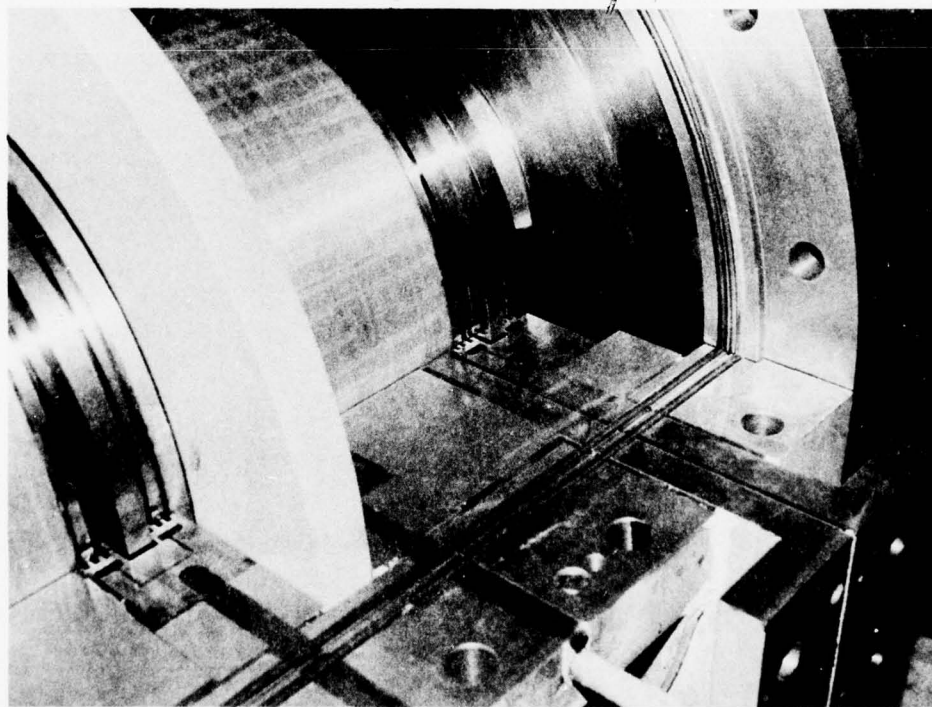


Fig. 2.2.8: Close-up of Fig. 2.2.7 showing SEGMAK current collector detail.

The center module of the rotor is integral with the rotor shaft and a cylindrical half-length module is shrunk onto each end of the rotor shaft. Within the outer iron shell of the housing, four similar stator half-modules are installed, with the two in the center corresponding to the one central rotor module. Each cylindrical stator module, which is split along the horizontal centerline, has lead plates which extend from one end, and a collector well embedded in the iron at the other end. The leads extend through both sides of the machine to improve electrical symmetry. An additional collector well, with attached leads, is positioned at each end of the machine to complete the electrical circuit for the end-modules.

Each module of the rotor or stator consists of a copper "squirrel-cage" assembly of conductor bars joined to two collector rings for the rotor or a collector ring (well) and lead plates for the stator. The squirrel-cage assemblies are brazed in position after installation around the magnetic iron of the module. The copper conductors and end-rings were not insulated from their adjacent iron segments, in either the rotor or the stator. This permitted insulation to be applied after the braze cycle was completed, and subsequent machining of the active length (along the machine gap) did not affect the insulation integrity.

The stator modules (including leads) and the inside surfaces of the iron housing were insulated by electro-static application of epoxy insulation prior to assembly. Three insulated bolts were used to position each module in the housing as it was cemented in place. Since the torque of the rotor end-modules was transmitted through the insulation gap, a more rugged insulation was employed in that area. A 0.002-0.005 in. thick coating of flame-sprayed alumina was applied to the bore of the end-module and the mating OD of the rotor and this was sealed with a thin epoxy coating. The shrink-fit interference of about 0.008 in. (diametral) was adequate to assure three times the rated module torque, even if the average module temperature were to rise about 150°F higher than that of the rotor shaft. Sample assemblies were used to demonstrate the capability of the flame-sprayed coating to withstand the pressure of the shrink-fit without damage. Final machining of the rotor assembly assured concentricity of the active length and collector periphery, to the bearing shaft locations. The active lengths of the rotor were sealed with a 0.005 in. layer of insulating epoxy paint to prevent penetration of liquid metal into spaces between the conductor bars and the slots in the iron. This made decontamination easier, during disassembly, and also provided electrical insulation of the rotor surface.

Circularity of the stator bore was also achieved through final machining, following installation of the stator modules and assembly of the upper and lower halves. A coating of epoxy paint was used to seal and insulate the stator bore. Transverse and vertical positioning of the rotor in the stator bore was accomplished by jack-screws, at each end, between the stator housing and the end-flange/bearing-housing assembly. The transverse positioning was completed prior to installation of the upper stator half, based upon measurements taken along the horizontal split, of the

lower half, with the rotor in place. Final vertical positioning by the jack screws was checked through specially enlarged gas inlet ports which permitted feeler gages to be inserted at the rotor/stator gap, at the top and bottom vertical centerline. Thus, accurate centering of the rotor in the stator was achieved.

The drive-end bearing was axially fixed in both the rotor and stator, and its position was shimmed to insure axial gaps of the rotor collectors in the stator wells, prior to installation of the upper stator half. The second bearing was tied to the rotor but was free to slide against a pre-load spring relative to the stator to accommodate relative axial expansion. Deep-grooved ball bearings were used with phenolic cages and grease packing. To prevent electrical current flow through the bearings, the bearing housing was insulated from the end-flange by a Micarta sleeve. The bearing housing was fabricated from non-magnetic stainless steel to minimize leakage flux in the vicinity of the bearings. To maintain separation between the bearing lubricant and the liquid metal, the bearings were located outside of the primary containment shaft seals which were dual, or tandem, segmented radial seals, with pressurized inert buffer gas fed into the center of each seal. A small leakage (2 SCFH) of this gas flows from the seal into and out of the machine. A stainless steel shield, which projects axially into a groove in the end of the rotor, protects each seal from direct impingement of any liquid metal droplets that might enter this area of the machine.

The primary closure sealing surfaces were those along the linear horizontal flange and at the circular joints between the stator and the two end-flanges. As shown in Fig. 2.2.8 a double "O"-ring seal of Buna-"N" material was used to assure reliability. A plenum region between the two "O"-rings was pressurized with the inert cover gas at 2-3 lb/in² above the internal cover gas pressure of the machine. Thus, any defect in the seal would result only in buffer cover gas leakage into or out of the machine, and the possibility of air leakage into the machine was minimized. The end of each linear horizontal "O"-ring was bonded to the mating circular "O"-ring in the end-flange, with silicone rubber cement. The sealed housing assembly was designed to contain a fault gas pressure rise of at least 100 lb/in².

The squirrel-cage conductor assemblies of the rotor consisting of two collector rings joined by 69 conductor bars were designed to be self-supporting under rotational loading. A portion of each 1.75 in. deep conductor bar was extended axially under the collector rings to provide mechanical constraint as a back-up for the braze shear strength. The braze area was about seven times the cross-sectional area of the bar, to assure adequate joint conductivity even with a partially effective braze joint. The central module conductor bars were 0.156 in. thick and 7.78 in. long between collector rings. A 0.3% Cr/0.3% Cd copper alloy was selected as the conductor bar material to improve post-braze strength and creep resistance over that for O.F.H.C. copper. The collector rings were machined from forgings of 0.1% Cr/0.15% Zr copper alloy. At design

operating conditions, the maximum centrifugal force-induced radial growth of the bars, at the band, was calculated to be about 0.004 in. Since the rotor assembly was quite rigid, bearing support stiffness was found to be a significant factor in determining the calculated critical speed, which was found to be greater than 12,000 rpm.

The need for liquid metal recirculation, machine cooling, cover gas circulation, and magnetic excitation, results in a large number of penetrations of the sealed machine. The two drain channels which surround each collector are joined internally, resulting in one NaK supply and one drain line penetration for each of the six collectors. A circulation of cover gas is introduced at two circumferential locations at the center of each three-inch active length (a total of eight inlet points), and is removed through the liquid metal drain lines. Additional inlet and exit ports are provided in the end flanges to sweep cover gas through each end of the machine.

There are three major sources of power losses in a SEGMA homopolar machine: 1) the electrical losses in the conductors; 2) the viscous and electrical losses in the liquid metal current collectors; 3) the eddy current losses in the iron. The heat generated by these losses was removed by water, with all coolant flow through the machine contained within stainless steel channels. Figures 2.2.7 and 2.2.8 show the stainless steel coolant tubes brazed in the collector well and lead of a stator module half. No coolant tube was used in the two collectors at the ends of the machine, since no stator conductor bars were attached to these, and the lead coolant flow tube alone was adequate. No additional penetrations were required for the lead cooling tubes, since they were carried through the housing with the lead penetrations. However, it was necessary to slot the housing along the horizontal flange at both sides of each stator collector half to permit the cooling tube penetration. These slots were filled with epoxy after installation of the stator modules.

Owing to the modular design, each half-module of the machine consisting of a collector, a cooling tube, and one half of the rotor and stator bars in a module could be treated as a unit identical in electrical and thermal performance to the others. A schematic drawing of one such unit is shown in Fig. 2.2.9. Figure 2.2.10 shows the thermal model of a half-module where the geometry has been simplified to a single spatial dimension, x . Assuming that the tangential temperature distribution is negligible, the temperature history along the current path, x , may be determined. The conductor temperature is governed by the differential equation,

$$\frac{d^2 T(x)}{dx^2} + \frac{\dot{q}}{k} + \frac{\dot{q}_I}{kA_c} = 0 \quad (2.2.1)$$

where: $T(x) - t(x) - t_1$

$t(x)$ is the conductor temperature at x ,

Dwg. 6177A07

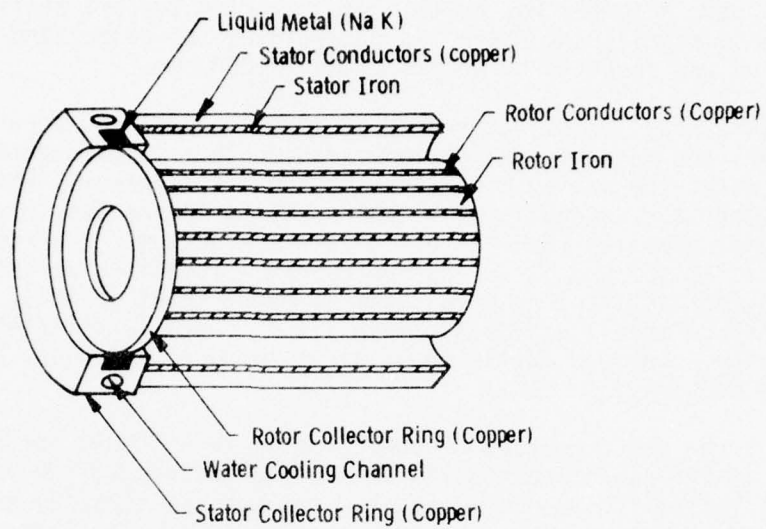


Fig. 2.2.9: Half module of SEGMAg.

Dwg. 6177A08

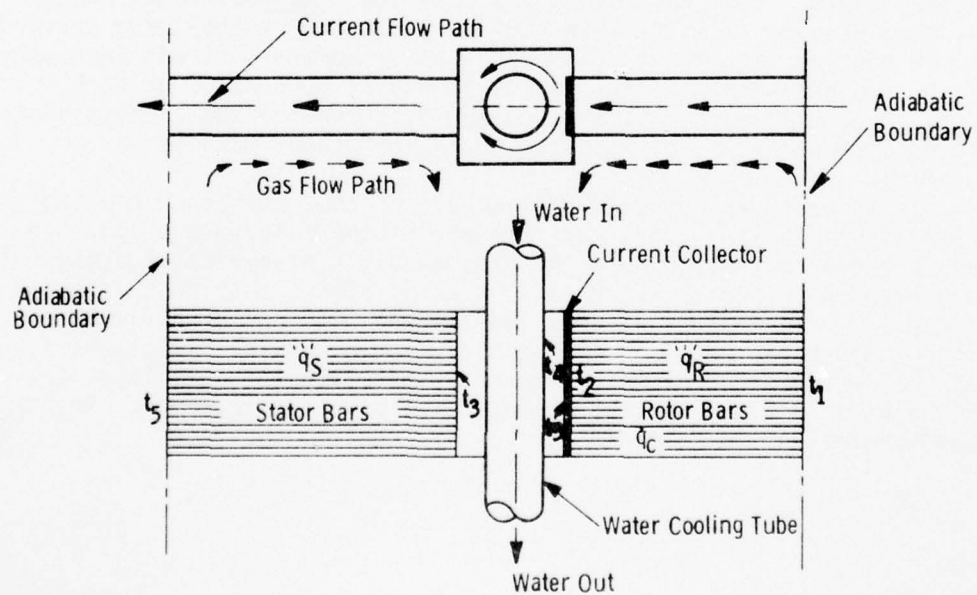


Fig. 2.2.10: Thermal model of SEGMAg half module.

E.M. 4883

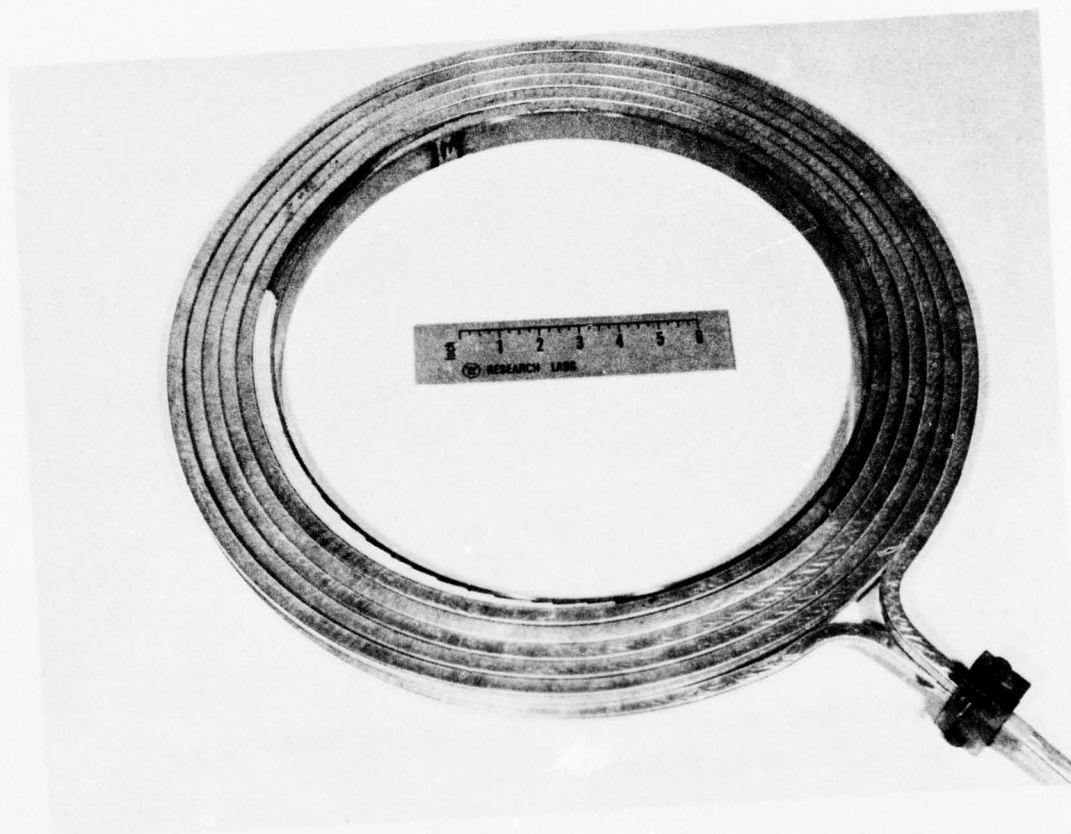


Fig. 2.2.11: SEGMAg excitation coil.

t_1 is the conductor temperature at the module center of symmetry,
 \dot{q} is the rate of iron loss per half-module.

The conductor heat generation rate q is given by

$$\ddot{q} = J^2 \rho_e(t) \quad (2.2.2)$$

where: J is the conductor current density,

ρ_e is the electrical resistivity of the conductors.

Solution of Equation 2.2.1 with a zero temperature gradient at $x = \ell$ yields,

$$t_2 - t_1 = - \frac{\phi_1}{c_1} (1 - \cos \sqrt{c_1} \ell_r) \quad (2.2.3)$$

$$\dot{q}_r = \frac{k A_r \phi_1}{\sqrt{c_1}} \sin \sqrt{c_1} \ell_r \quad (2.2.4)$$

where:

$$\phi_1 = \frac{\ddot{q}_1}{k} + \frac{\dot{q}_1}{k \ell_r A_r} \quad (2.2.5)$$

$$c = \frac{\ddot{q}_1}{k} \quad (2.2.6)$$

α is the temperature coefficient of electrical resistivity, ρ_e ,

\ddot{q}_1 has been evaluated at temperature, t_1 ,

ℓ_r is the equivalent length of rotor conductors,

A_r is the cross-sectional area of the rotor conductor,

\dot{q}_r is the rate of heat from the rotor conductors at the collector surface.

A similar set of equations is used for the stator conductors.

The viscous loss in the collector, P_c , was calculated assuming fully turbulent flow

$$P_c = \frac{1}{8} f \rho V_o^3 A_c \quad (2.2.7)$$

where: f is the Fanning friction factor.

ρ is the liquid metal (NaK-78) density,

t_1 is the conductor temperature at the module center of symmetry,
 \dot{q} is the rate of iron loss per half-module.

The conductor heat generation rate q is given by

$$\ddot{q} = J^2 \rho_e(t) \quad (2.2.2)$$

where: J is the conductor current density,
 ρ_e is the electrical resistivity of the conductors.

Solution of Equation 2.2.1 with a zero temperature gradient at $x = \ell$ yields,

$$t_2 - t_1 = -\frac{\phi_1}{c_1} (1 - \cos \sqrt{c_1} \ell_r) \quad (2.2.3)$$

$$\dot{q}_r = \frac{k A_r \phi_1}{\sqrt{c_1}} \sin \sqrt{c_1} \ell_r \quad (2.2.4)$$

where:

$$\phi_1 = \frac{\ddot{q}_1}{k} + \frac{\dot{q}_1}{k \ell_r A_r} \quad (2.2.5)$$

$$c = \frac{\ddot{q}_1}{k} \quad (2.2.6)$$

α is the temperature coefficient of electrical resistivity, ρ_e ,
 \ddot{q}_1 has been evaluated at temperature, t_1 ,
 ℓ_r is the equivalent length of rotor conductors,
 A_r is the cross-sectional area of the rotor conductor,
 \dot{q}_r is the rate of heat from the rotor conductors at the collector surface.

A similar set of equations is used for the stator conductors.

The viscous loss in the collector, P_c , was calculated assuming fully turbulent flow

$$P_c = \frac{1}{8} f \rho V_o^3 A_c \quad (2.2.7)$$

where: f is the Fanning friction factor.
 ρ is the liquid metal (NaK-78) density,

V_o is the collector surface velocity,
 A_c is the collector area.

The collector ohmic loss, P_e , is given by

$$P_e = J^2 d \rho_e \quad (2.2.8)$$

Modifications of Equation 2.2.7 for operation under magnetic fields was based on the work of Rhodenizer.⁴

The heat transfer coefficient, h , for the collector surfaces was calculated from Seban's⁵ equation for small gaps.

$$\frac{hd}{k_e} = 5.8 + 0.02 (R_e P_r)^{0.8}, \quad R_e \geq 10,000 \quad (2.2.9)$$

where: d is the collector gap

k_e is the liquid metal thermal conductivity

P_r is the Prandtl number.

$$R_e = \frac{V_o d}{\nu} \quad (2.2.10)$$

ν is the kinematic viscosity.

Then

$$t_2 - t_c = q_r / h_f A_c \quad (2.2.11)$$

$$t_c - t_3 = (\dot{q}_r + P_c + P_e) / h_m A_c \quad (2.2.12)$$

where: t_c is the mean liquid metal temperature.

h_f and h_m are calculated from Equation 2.2.9 for the fixed and the rotating walls of the collector respectively.

The collector ring which contains the cooling channel was approximated by a hollow cylinder of cross-sectional area equal to that of the ring.

The rate of heat generation in the ring and the temperature gradient to the cooling channel could then be calculated by standard methods. The water temperature rise was obtained from an energy balance on the coolant. Thus given the water inlet and the maximum allowable conductor temperature,

t, the problem could be set up to yield either the required water flow rate and the current, I , for a given geometry and rotor rpm or the geometrical values for a fixed water flow rate and output current.

The excitation coil was wound using Mylar-wrapped hollow copper conductor with a 0.410 square OD, two layers wide and six layers in the radial direction as shown in Fig. 2.2.11. The coil was enclosed in a stainless steel housing which was then welded and finish-machined to provide a second barrier to water leakage from the conductor bore, in the event of an accident. A collar which projected from the housing, surrounding the coil leads, penetrated the upper stator half at the top vertical centerline, and a seal was installed between the stator OD and the coil collar after assembly of the machine.

Collectors

The rotor collector was simply a 0.500 in. wide, 0.500 in. radial projection from each "squirrel-cage" end-ring (see Fig. 2.2.8). The corresponding stator collector well provided a 0.06 in. gap for the liquid metal, both axially and radially. To achieve accurate alignment between all six rotor collectors and their corresponding stator wells, these were machined after permanently fixing the modules in position. The circulating NaK was introduced tangentially to the annular radial gap and was removed by overflow into one of the labyrinth seals (shown in Fig. 2.2.8) on either side of the collector, and then drained through the annular channel behind each labyrinth. Additional drains were provided between stator modules along the active length of the machine, and at the excitation coil wells, to remove any accumulation of NaK aerosol or droplets that escaped the labyrinth seal.

Following the fabrication and assembly of the SEGMAG generator, the machine was no-load tested at the Westinghouse Research Center to determine machine performance characteristics and to demonstrate successful collector performance in a machine environment.

The SEGMAG machine and the test facility is shown in Figs. 2.2.12 and 2.2.13. The drive motor is a 150 hp, 1800 rpm wound-rotor induction motor with variable external resistance for speed control. A 2.2 to 1 gear box is also provided to achieve the design speed of 3600 rpm. The 150 hp rating of the test stand is sufficient to offset no-load losses encountered during the test program. The test facility is also equipped with auxiliary systems to provide cooling water, inert cover gas, field excitation and to process the NaK for the collectors.³

The cooling water system provides coolant for the current collectors, leads, excitation coils and during short circuit tests, the calibrated shunts. The system is a recirculation-type providing inlet coolant temperatures of 25°-85°C. The cooling water system has flow balance provisions to adjust the flow in each of the coolant passages. The system is instrumented to measure coolant flow, pressure drop, and inlet and outlet temperatures.

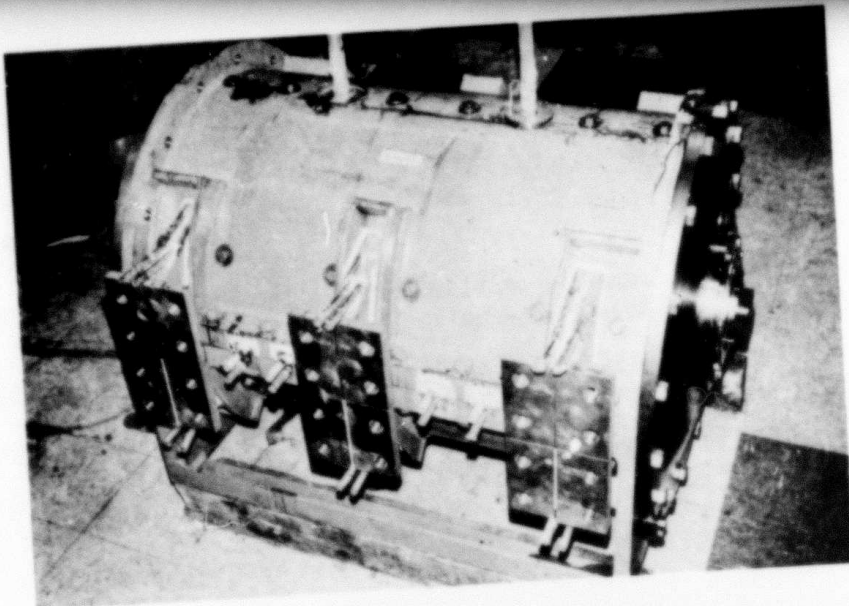


Fig. 2.2.12: SEGMA Generator - The current collector terminals are shown in the foreground. The leads to the excitation coils are on top.

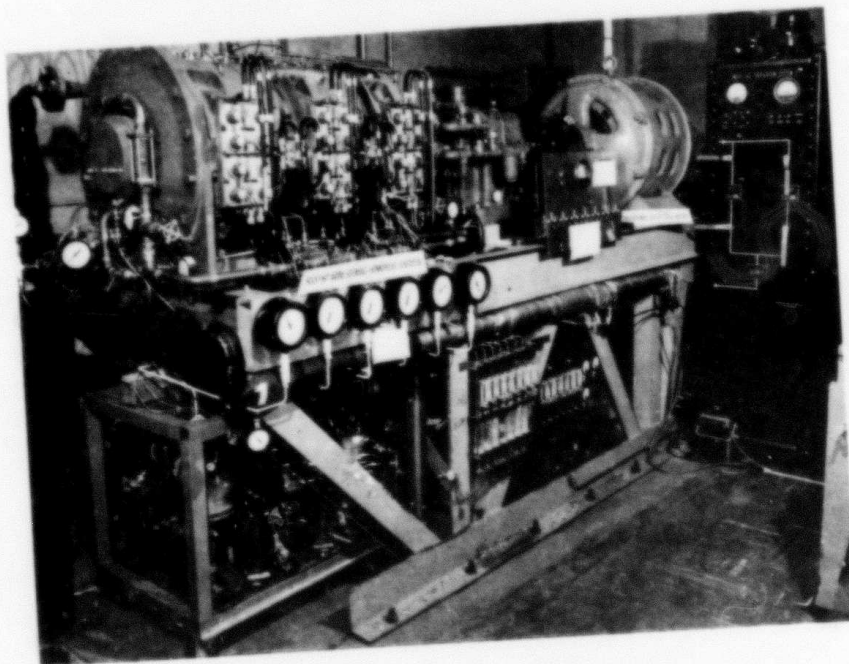


Fig. 2.2.13: SEGMA Generator on its test stand - The drive system and gas purification system are both on the right. The six NaK purification and supply loops are below. To their right are the gas subsystems for intercollector pressure balancing and shaft sealing.

An electrical break must be provided between the machine and cooling water system since the cooling coils in the machine are at machine potential.

The inert cover gas system provides high purity dry nitrogen gas to the machine internals. The gas is injected into the machine at the end bell cavity, between the dual shaft seals and into the air gap between each pair of collectors. The cover gas leaves the machine through the liquid metal system, from the end bell cavity and by leakage through the shaft seal into the bearing cavity. The gas purification loop removes moisture and oxygen from the gas extracted from the end-bell cavity. Makeup gas is provided to offset leakage through the shaft seals. The water vapor and oxygen content of the purification gas is continuously monitored and maintained below 1 ppm. Instrumentation is provided to monitor flow rates, pressures and temperatures in critical portions of the system.

The field excitation is provided by a motor generator set capable of providing 1500 amperes at 70 volts. This system is also provided with instrumentation required to control the field excitation during open circuit testing. For short circuit testing an auxiliary 30-amp power supply was available.

The NaK supply system provided several functions. The injection pressure was provided by a canned motor centrifugal vane pump. An MHD flow measuring device was used while flow control was achieved by throttle valves in the collector supply line and bypass piping. A sump was used on the current collector exit line to provide an adequate NaK reservoir during the test. This sump was also a place for the NaK oxides formed in the machine to separate from the clean NaK which was re-injected into the current collectors. A cold-trap and strainer was used to precipitate oxides and to remove particulate matter from the liquid metal prior to injection into the current collector. Instrumentation was provided to monitor NaK flow, temperature, inlet pressure and sump level during the machine test.

Instrumentation was provided to measure critical machine parameters during the test. Included were current collector temperatures, seal temperatures, bearing temperatures, bearing housing vibrations, rotor speed, and machine voltages. Calculated shunts were used during short circuit tests. These shunts were instrumented to measure shunt voltage drop and temperature to insure an accurate measurement of current. Four watt meters were used to measure the power in the three-phase stator and rotor circuit to determine total input power.

The machine was no-load tested in accordance with a test plan to determine:

- Machine open circuit and short circuit performance.
- Machine losses.
- Current collector performance.
- Mechanical performance of critical components.

The test plan consisted of the following tests to achieve these objectives.

The machine was operated at various speeds (to 3900 rpm) to determine rotor performance, machine vibrations and to run-in the shaft seals. The power input to the drive motor was used to determine the friction and windage losses as a function of machine speed.

The viscous losses associated with the NaK in the current collectors was measured by injecting NaK into individual collectors and measuring the change in drive motor input power. This test provided a means to develop operating procedures for the current collectors and to compare collector losses and performance with previous tests performed on full-scale mockups.

The open circuit test was designed to experimentally investigate three areas; open circuit voltage developed, MHD losses due to leakage fluxes in the collector and to investigate the expelling force due to eddy currents. The machine is connected in series and operated at various speeds and excitation, to design voltage and speed. Data was taken to determine the machine voltage, input power, and the current performance.

The short circuit test has a two-fold purpose; first to determine the joule losses in the machine at full rated current and to evaluate the expelling effect due to the load current. The power modules were shorted with calibrated water cooling shunts. Each of the shunts was instrumented to measure the shunt voltage drop and temperature. The machine was run at various load currents up to rated, with data recorded to measure input power and collector performance.

The SEGMAG generator was no-load tested to full open circuit voltage of 20.4 volts and stable short circuit current of 90,000 amperes at 3600 rpm. During these tests, data were taken to determine power losses, collector performance and mechanical performance of the machine.

The resulting SEGMAG friction and windage and current collector viscous losses are shown in Fig. 2.2.14. As seen, 92% of these losses are current collector viscous losses. The losses measured on SEGMAG correlated well with theoretical values and with test data obtained from full scale mockup testing of an identical current collector. This indicates that the operation within the machine environment has not seriously effected the hydraulic characteristics developed during prototype tests.

The results of the series open circuit tests are shown in Fig. 2.2.15, showing series connected open circuit voltage as a function of field

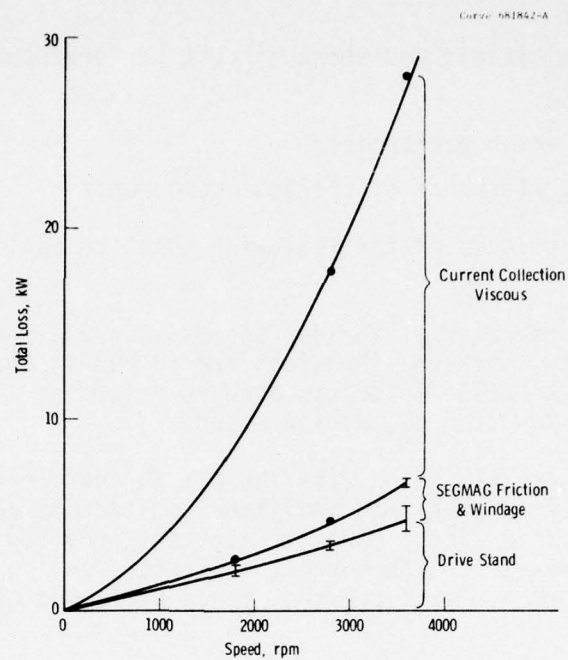


Fig. 2.2.14: SEGMA no-load losses.

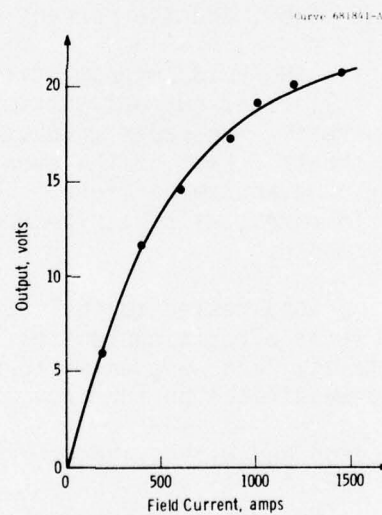


Fig. 2.2.15: SEGMA open circuit voltage.

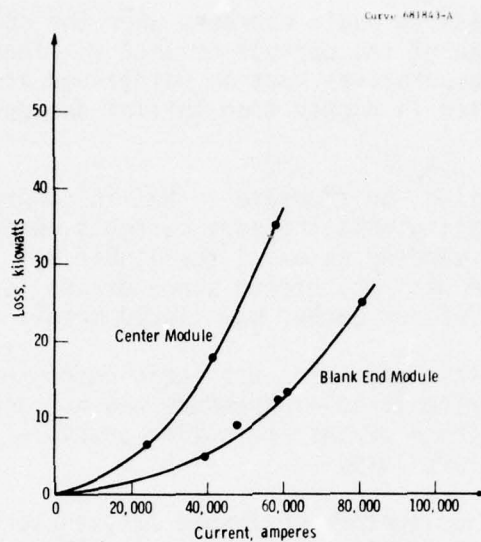


Fig. 2.2.16: Losses in SEGMAg due to short circuit current.

excitation current. As seen, full voltage of 20.4 volts was achieved with saturation effects becoming significant at 14 volts. Due to the limited choice of discrete speeds for the induction motor, the speed varied from 3400 to 3650 rpm requiring that all points be linearly adjusted for 3600 rpm.

There were two types of short circuit tests run; in the first, the center module was shorted and the end modules left open, and in the other the end modules were shorted and the center module left open. All three modules were not successfully tested simultaneously due to the difficulty in canceling the residual magnetism in the three modules using two excitation coils. Although a demagnetization of the machine was attempted following the open circuit test, there was still sufficient residual magnetism in the machine to circulate 50,000 to 100,000 amperes in the shorted condition. Due to the extremely low internal impedance of the SEGMAg, it takes an mmf to equivalent of only a few hundred ampere-turns to circulate these high currents, compared to the 22,000 ampere-turns reached during open circuit testing.

The power loss measured during the short circuit is shown in Fig. 2.2.16 as a function of load current. An analysis of these losses shows they are a function of the load current squared.

The current collectors were continuously monitored during the test program to insure proper performance. Complete filling of the current collector was deemed necessary for proper operation. Filling of the current collectors could be confirmed by observing collector temperatures, the machine power loss and the NaK inlet pressure. Prototype tests have

shown that NaK inlet pressure would decrease when the collector was filled due to the pumping action of the current collector. These tests also showed that collector temperatures must be maintained at 75°C or higher for proper operation which is higher than initial design value of 50°-60°C.

During open circuit testing, an increase in NaK inlet pressure was noted at 20 volts indicating that the eddy currents generated due to radial flux leakage was tending to expel the liquid metal from the collector. No expulsion was encountered since drains located on either side of the collectors did not gather any liquid metal.

During short circuit tests, expulsion was again encountered at 110,000 amperes. However, the rise in inlet pressure was not accompanied by loss of NaK into the machine drains indicating possible fragmentation in the collector without gross loss.

In general, the current collectors performed satisfactorily during all phases of the program. Retention of NaK in the collector annulus could be maintained without significant leakage at speeds as low as 600 rpm. The dropout speed, or speed at which the centrifugal forces cannot retain the liquid metal in the collector, could not be determined since the lowest drive motor speed achievable was 600 rpm.

The losses from the open circuit and short circuit tests have been analyzed and related to full load operation as defined by current capability (2412 hp) demonstrated by test, to full load operation using design changes (3000 hp). These losses are shown below. They have been used to compute the machine efficiencies derived from the losses, and to compare the most recent projection of design efficiency for various machines.

The losses measured during machine testing varied from the design objective for several reasons, which are discussed below:

- Winding Joule Losses. As a result of the high collector temperatures required for successful NaK containment, the overall average winding temperatures are increased by approximately 50°C. This results in extra losses due to winding temperature coefficient of approximately 20% or 10.1 kW or 0.56% in machine efficiency.
- Collector Losses. Viscous and radial field losses are higher than those measured during prototype testing. These differences result from the machine environment, and from collector modifications to improve NaK confinement within the machine at very high currents. The loss increase in this area amounts to 6 kW or 0.3% in machine efficiency.

In the very early stages of the program, contact resistance was considered to be negligible. Experimental work on this program yielded contact resistance levels under ideal conditions equivalent to 6.3 kW. The loss derived from the steady stage 90,000 ampere test was on the

order of 21 kW, which represents an efficiency penalty of 1.0%. However, since it is expected that the lower level can be achieved in the current machine, a range of machine loss and efficiency quantities is presented in Table 2.2.1.

TABLE 2.2.1
EFFICIENCY TABULATION

Design Loss KW	Design Objective 3000HP	Recent Test Data 20V, 90,000A 2400HP	Present Design Capability 24V, 93,300A 3000HP
Winding Joule	49.2	60.2	49.3
Collector	32.1	50.7-45.4	30.0
Mechanical Friction and Windage	2.6	2.0	2.0
Parasitic-Eddy Current	Small	6.7	1.0
Total	83.9	119.6-114.3	82.3
Rating-KW	2240	1800.0	2240.0
Input	2324	1920-1914	2322
Efficiency	96.4%	93.8-94.0	96.5

- Parasitic Losses. These losses which are due to eddy currents and flux pulsations in the armature windings were considered small at the design stage. However, tests indicate that these losses are 6.7 kW or 0.3% in terms of efficiency.

The ultimate capability of the SEGMAG machine subject to certain modifications is presented in the tabulation. This 3000 hp machine will have an efficiency about the same as originally projected. These modifications will reflect current parallel efforts in the current collection program. These efforts are directed at achieving the projected machine rating at the efficiency objective, and at the same time simplifying the auxiliary systems.

The mechanical performance of the SEGMAG machine can be divided into three critical areas; rotor characteristics, seal performance and bearing performance.

The SEGMAG rotor was balanced on its support bearings to zero imbalance in two planes at 300 rpm to insure stable operation. The performance of the rotor in the machine was determined by operating the machine at various speeds up to 3980 rpm and monitoring bearing vibration and power losses. At design operating speed of 3600 rpm the bearing vibration varied from 1.5 to 2.2 mils. This level of vibration is acceptable for a machine of SEGMAG's weight and speed.

The seals performed well over the entire test program. The seal temperature, leakage and running sound were monitored during the performance test program. Seal temperature remained in the range of 45°-85°C during the test which is normal for these units. Measured seal leakage rates varied from 1 to 2 SCFH which is also acceptable. The running sounds of both seals were determined using a machinery stethoscope indicating no significant change over the test period. Some leakage of NaK into the end bell region was detected during the test program. The presence of this leakage did not affect seal performance. Final evaluation of seal performance will be established when the machine is disassembled and seal wear is determined.

The bearings performed adequately over the test period. Bearing temperatures remained well within operating temperatures of 50°-100°C indicating acceptable performance. The bearing running sounds were monitored during the test and no significant change was noted. The final evaluation will be performed when SEGMAG is disassembled and the bearings can be inspected.

2.2.4 Conclusions

The results of the tests performed on SEGMAG indicate that a machine of this type is feasible and will deliver high current-low voltage power with high machine efficiency. The program has also shown that the current collectors can be operated stably in a machine environment with properly designed support systems. The mechanical components showed no signs of failure during the program.

The test program has also defined several technical problems that must be considered including:

- Current collector critical temperature.
- Contact resistance in the collectors.
- Parasitic losses in the machine.

Additional work is required to fully understand these areas so that they will have minimum impact on machine performance and efficiency.

2.2.5 References

- 1) Van Reuth, E.C., Mole, C.J., Berkey, E., and Haller, H.E., "The Segmented Homopolar Machine", Presented at IEEE Winter Meeting, New York, 1976.

2.2.5 References (Cont'd.)

- 2) Johnson, J.L., Hummert, G.T., Keeton, A.R., "Liquid Metal Current Collectors for Homopolar Machines", Presented at IEEE Winter Meeting, New York, 1976.
- 3) Arcella, F.G., Witkowski, R.E., Keeton, A.R., "Vital Support Systems for Liquid Metal Collector Homopolar Machines", Presented at IEEE Winter Meeting, New York, 1976.
- 4) Rhodenizer, R.L., "Development of Solid and/or Liquid Metal Collectors for Acyclic Machines", General Electric Co., Schenectady, New York, Final Report on Contract No. N00024-68-C-5415, Serial No. SF01 30 702, Task 11582, for Department of the Navy, September 1971.
- 5) Selan, R.A., "Heat Transfer to a Fluid Flowing Turbulently Between Parallel Walls with Asymmetric Wall Temperature", Trans. ASME, Vol. 72, 1950, p. 789.

2.3 GEC GENERATOR

2.3.1 Objectives

The General Electric Company, Ltd., of England has developed an experimental homopolar generator which utilizes a GaIn current collection system. This generator employs an electrochemical purification system to maintain the purity of the liquid metal and avoid the "black powder" problems of previous investigators who used this metal. ARPA has approved purchase of this generator for experimental evaluation under the contract. The machine will be used to provide operating and technical experience with GaIn as a current collector liquid and to supplement the main experimental studies which will be conducted with NaK. This experience is expected to be valuable in broadening the scope of the program beyond the alkali metals. The physical design of the machine and its performance will be investigated thoroughly, and the unit may also be employed as a high current dc source in the current collector test program.

2.3.2 Prior and Related Work

Liquid metal current collection systems have a high potential to function efficiently with long, trouble free life in the face of high electrical current loads and high rotational speeds conceived for homopolar machines of the advanced segmented magnet design.

Based on extensive study, NaK-78 was selected as the best liquid metal for current collectors employed in the SEGMAG machine, and GaIn was selected as the alternate choice.

Since GaIn has been identified as the back-up choice to NaK, the ability to work with and study a functioning GaIn unit is expected to be highly instructional in the general sense and also to shorten any subsequent development effort with GaIn.

Based on an extensive search of the market we have concluded that the GEC machine is the best vehicle to provide the GaIn experience needed for this program. No other liquid metal machine, to our knowledge has operated continuously longer than 40 hours without maintenance. Therefore, this machine, which has operated up to 1000 hours with no problems, represents a unique development.

2.3.3 Summary of Accomplishments

2.3.3.0 General

The GEC generator is a vertical shaft machine utilizing GaIn liquid metal eutectic as the slip ring contactor. The generator is rated at 16,000 amperes, 8 volts when driven at 3400-3600 rpm. Figure 2.3.1 displays schematically the GEC generator vertical shaft concept.

During Phase II, the acceptance tests were successfully performed in England at The General Electric Company, Ltd., and witnessed by Westinghouse personnel. These tests consisted of open circuit, short circuit, generator load, motor and an endurance test. The proper operation and maintenance of the unit were also demonstrated.

Dwg. 6251A96

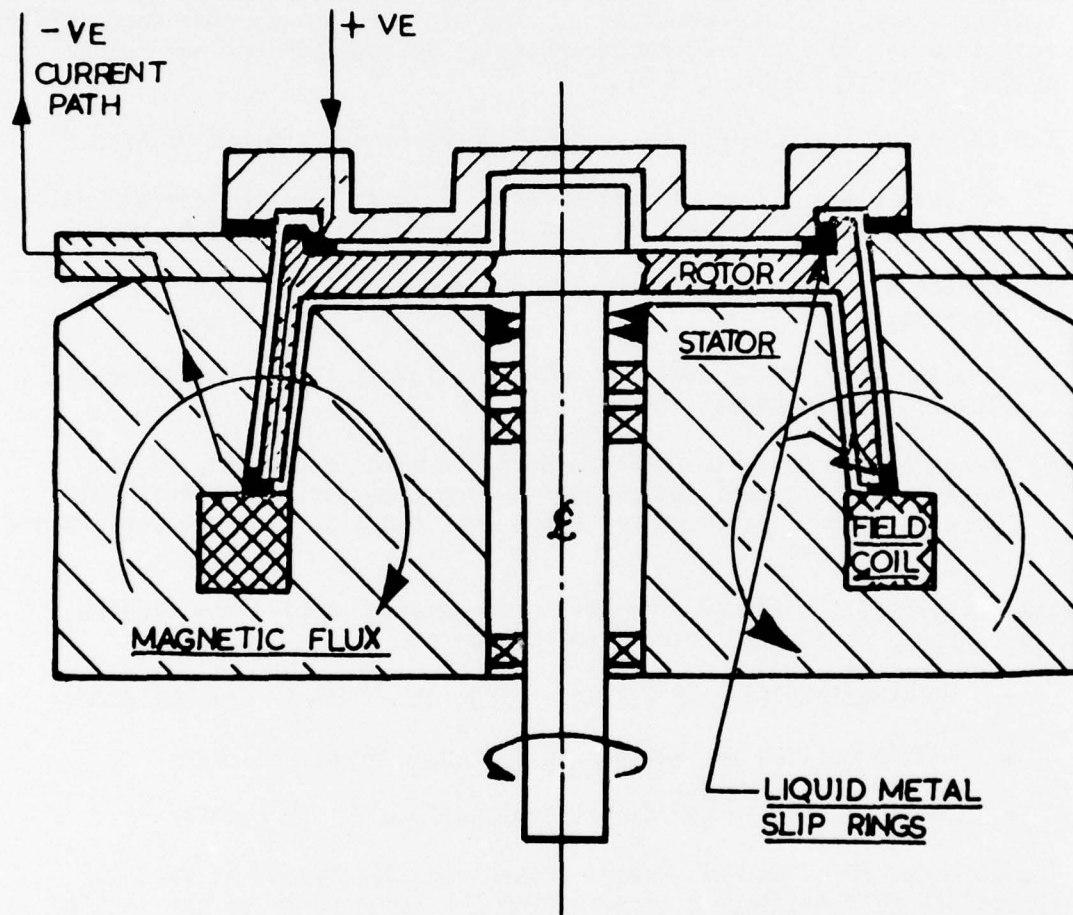


Fig.2.3.1: GEC vertical shaft homopolar machine schematic

The GaIn purification cell was severely damaged in shipment. A replacement cell was fabricated by Westinghouse using detailed drawings furnished by GEC Company.

The GEC generator test stand was completed in Phase II, and the machine was installed. The test stand is powered by a 50 HP 1750 rpm AC machine, and a drive train provides speeds of 1800 and 3600 rpm.

Installation of the auxiliary equipment was completed, including cover gas, cooling water, and instrumentation. The GEC machine was then successfully tested to verify its performance and to study the GaIn current collector system (Fig. 2.3.2 and 2.3.3).

The following are the four basic tests performed on the GEC machine:

- 1) An open circuit test, to determine no-load voltage and current collection magneto-hydrodynamic losses as a function of field current.
- 2) A machine short circuit test, to determine the I^2R losses in the machine.
- 3) A motor test, to measure the vibration levels, magnetohydrodynamic losses, and coastdown time.
- 4) An endurance test, to confirm the performance capability of the machine and its auxiliaries over a long time period. Liquid metal loss rate, cell performance, argon contamination and seal performance were monitored.

The test results obtained from this program have enabled the machine losses to be segregated into three categories:

- Machine friction and windage losses with GaIn in the collector.
- MHD losses due to leakage flux in the current collector.
- Joule heating losses due to current flow in the machine.

The viscous, friction and windage losses were determined at various speeds and zero excitation by measuring the input power to the coupled drive motor. The difference between this power and the uncoupled drive motor losses at each speed determined the generator losses. The friction and windage losses cannot be separated from the liquid metal viscous losses because gallium indium could not be completely excluded from the collector areas during the test to measure friction and windage losses (See Fig. 2.3.8).

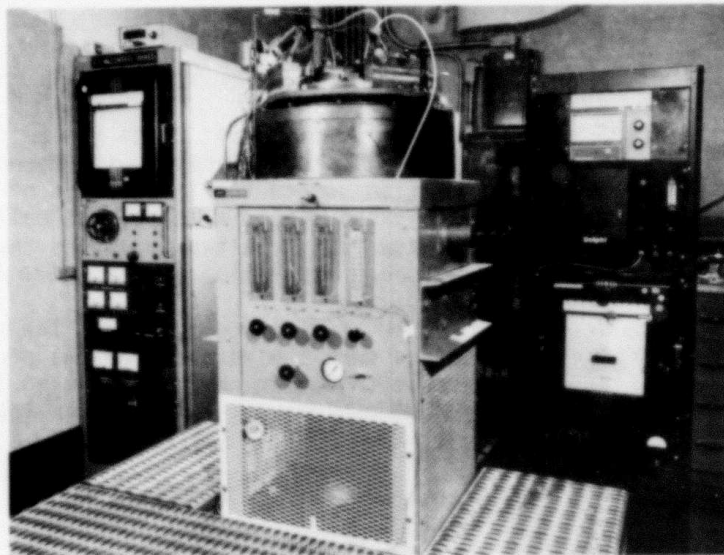


Fig. 2.3.2: Front view of GEC test area in the Westinghouse Liquid Metal Laboratory. The cover gas impurity monitoring system is on the right. The machine control and test panel is on the left. Below the machine is a cover gas flowmeter, and also flowmeters and pressure regulator for the cooling water system.

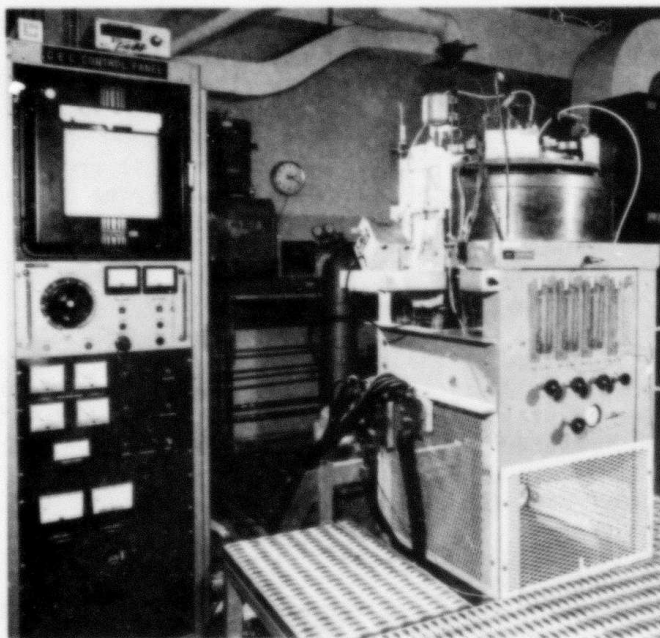


Fig. 2.3.3: Side view of the test area showing the GaIn electrolytic purification cell, to the left of the GEC machine.

The MHD losses were determined during open circuit tests at various speeds and field currents. The power losses increased with speed due to viscous losses, and with excitation due to the interaction of leakage flux with current induced in the liquid metal of the collector. These currents induced by the leakage flux resulted in losses that became significant at higher speeds and excitation levels (See Fig. 2.3.9).

The I^2R losses were determined by the short circuit tests. The sum of friction, windage and viscous losses were subtracted from the power losses measured during short circuit to determine joule heating losses in the machine. The MHD losses were neglected because of the low machine flux during short circuit (See Fig. 2.3.10).

The losses measured during the test program at 3600 rpm are:

Viscous, friction, windage	6.2 KW
MHD	1.0 KW
I^2R	<u>7.0 KW</u>
Total losses	14.2 KW

For the 100 KW GEC machine the overall calculated machine efficiency was 85.8%. At lower speeds the efficiency rises to a level approaching 94%.

The GaIn liquid metal was purified by an electrolytic regenerative cell during the entire test. The cell performed well during the entire program with no evidence of GaIn contamination. (Fig. 2.3.3).

2.3.3.1 Open-Circuit Test

The machine was installed in the test stand with the output leads open circuited and purged with dry argon for four days prior to the test. The cover gas was maintained at a pressure of 1 cm Hg with a flow of 50 cc/min. A GaIn charge of 80 cc with 380 cc of 3M NaOH was supplied to the purification cell. The moisture of the effluent gas measured approximately 100 ppm at the start of the tests.

The machine was tested at 1800 and 3600 rpm with field excitation currents of 0.0, 1.5, 3.0 and 5.0 amps. During the test, the GaIn pump was switched off to determine losses at zero liquid metal flow.

The test results were evaluated to determine the losses as a function of speed and excitation. The results of open circuit tests are shown in Fig. 2.3.4. As expected the losses increased with machine speed. The effect of excitation on losses was not present until a speed of 3000 rpm was achieved. The losses increased with field at this speed.

Figure 2.3.5 presents the total flux calculated from the generated open circuit volts and speed.

2.3.3.2 Short Circuit Test

The machine leads were short circuited with calibrated shunts to measure the current. The shunt temperature was monitored to provide a thermal correction for shunt temperature. The machine was operated at 1800 and 3600 rpm and the level of excitation was adjusted in order to provide short circuit currents up to 52 kiloamperes. The test data taken is presented in Fig. 2.3.6.

During the short circuit test program a high level of vibration was encountered in the test stand and was determined to be caused by the bearings and the machine support assembly. The vibration was reduced to acceptable levels by making the support assembly more rigid in order to maintain better alignment, and by installing new bearings.

The short circuit performance test showed that a maximum of 52 kiloamperes, is achievable, which is more than three times the rated 16,000 amperes. Above this limiting value the liquid metal could be forced out of the collectors, with consequent loss of output voltage and current.

During the short circuit test program, the GaIn flow was blocked by the formation of black gallium oxide powder. This resulted in overheating of the lower current collector area with consequent reduction in output current. The blockage was removed by reaming the liquid metal drain line, and purging the machine with argon gas. This procedure permitted the short-circuit test program to be satisfactorily completed.

2.3.3.3 Motor Test

For the motor test, the machine was operated at various armature currents, field excitation currents, and machine speeds to determine machine vibration, magnetohydrodynamic losses and machine coastdown time. The data taken during the motor test is presented in Fig. 2.3.7 which shows that input power and accordingly the machine hydrodynamic losses are a strong function of speed.

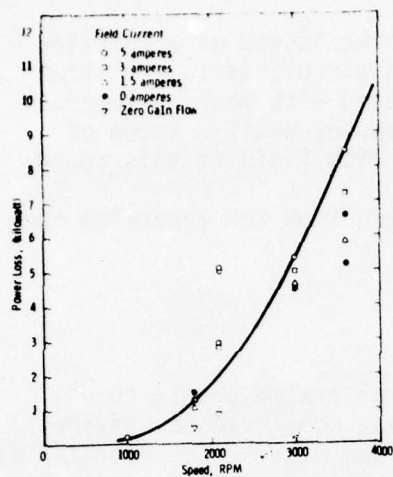


Fig. 2.3.4: GEC open circuit test losses.

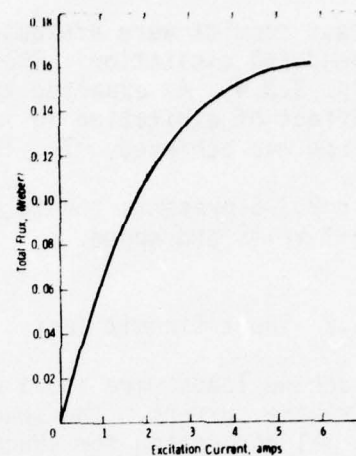


Fig. 2.3.5: GEC total flux calculated from open circuit voltage and speed.

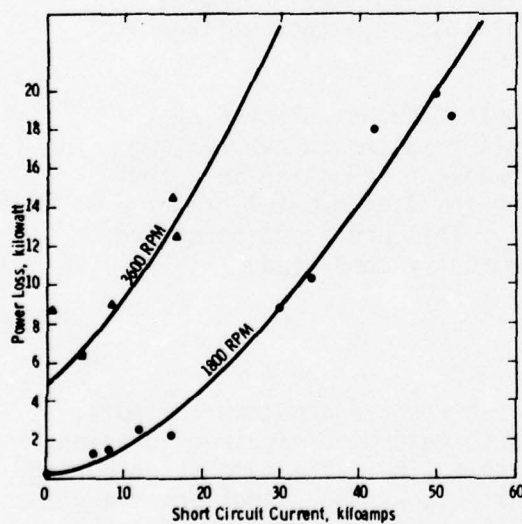


Fig. 2.3.6: GEC short circuit test losses.

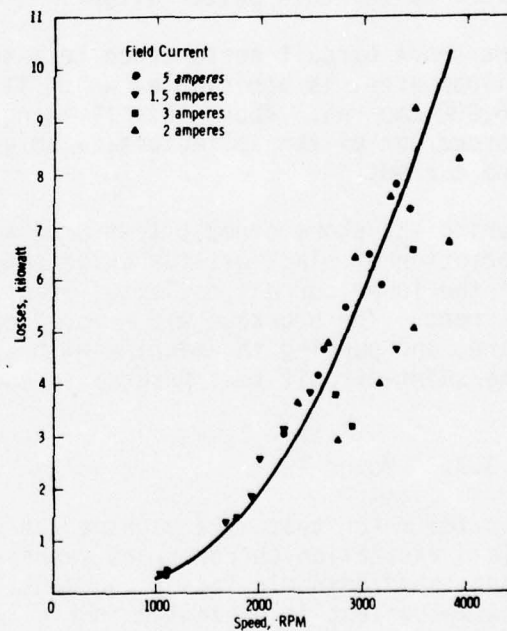


Fig. 2.3.7: GEC motor test losses.

The motor was started from rest by applying a voltage to the output leads after injecting some liquid metal prior to hand rotation. Sufficient GaIn was retained in the collector to carry the current required for machine acceleration.

2.3.3.4 Endurance Test

The endurance test was performed with the machine operating as a motor for two hours at approximately 3000 rpm. All machine temperatures held constant and there was no evidence of abnormal operation.

2.3.3.5 Machine Performance

The viscous, friction and windage losses are shown in Fig. 2.3.8 as a function of speed.

The MHD losses are shown in Fig. 2.3.9 as functions of speed and field excitation.

The I^2R losses are shown in Fig. 2.3.10 as functions of machine current and speed.

For the 100 KW GEC machine the overall calculated machine efficiency was 85.8%. At lower speeds the efficiency rises to a level approaching 94%.

2.3.3.6 GaIn Purification Cell

The gallium indium liquid metal was purified by an electrolytic regeneration cell that is shown schematically in Fig. 2.3.11.

The cell was provided with 3M NaOH as the electrolyte and was operated from a 2A. 5V d.c. supply connected into a terminal block on the side of the frame. It was essential that the polarity be positive for the wire electrode and negative for the liquid metal.

A stirrer was provided to increase the regeneration rate of the cell in the event of an abnormal amount of compound entering the cell (e.g., after storage). The stirrer was not normally used during running as only small quantities of compound were generated.

Precautions were taken to insure a clean, non-reactive cover gas atmosphere inside the machine to minimize the oxidation of Ga. The machine was purged with high purity argon prior to startup. Cover gas pressure was maintained at 1-2 cm Hg and at a flow of 50-100 cc/min. During the prestart degas cycle, the excitation current was turned on to warm the housing and assist in outgassing the machine internals as well as to maintain the GaIn in the liquid state. The effluent purge gas contained a typical level of 100 ppm(v) moisture at the time of machine startup. The GaIn electrolytic purification well functioned

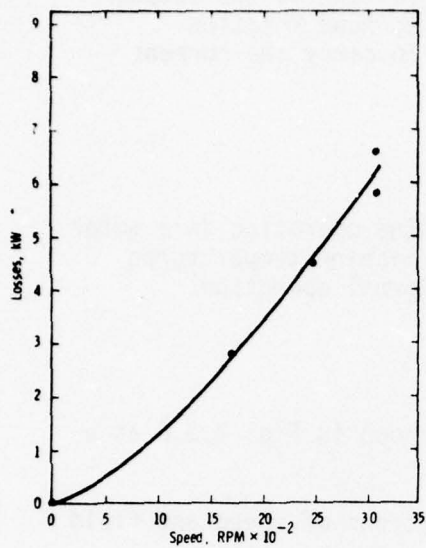


Fig. 2.3.8: GEC calculated losses due to friction windage on liquid metal viscosity.

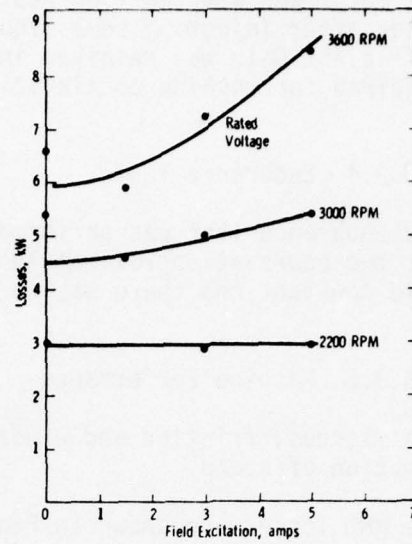


Fig. 2.3.9: GEC calculated MHD losses.

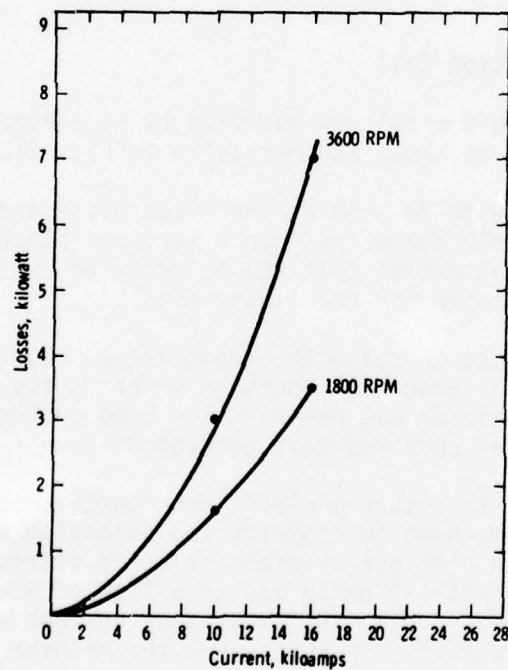


Fig. 2.3.10: GEC calculated I^2R losses.

properly during all the machine tests and only required stirring under the heaviest load conditions. GaIn flow rates were in the 30 cc/min range.

Effluent cover gas impurity levels rose appreciably during machine power tests, but did not cause any problem. For instance, gas chromatograph readings were taken during the endurance test and indicated that oxygen levels in the effluent gas remained below 15 ppm (detection level) throughout the test. However nitrogen and hydrogen levels rose appreciably

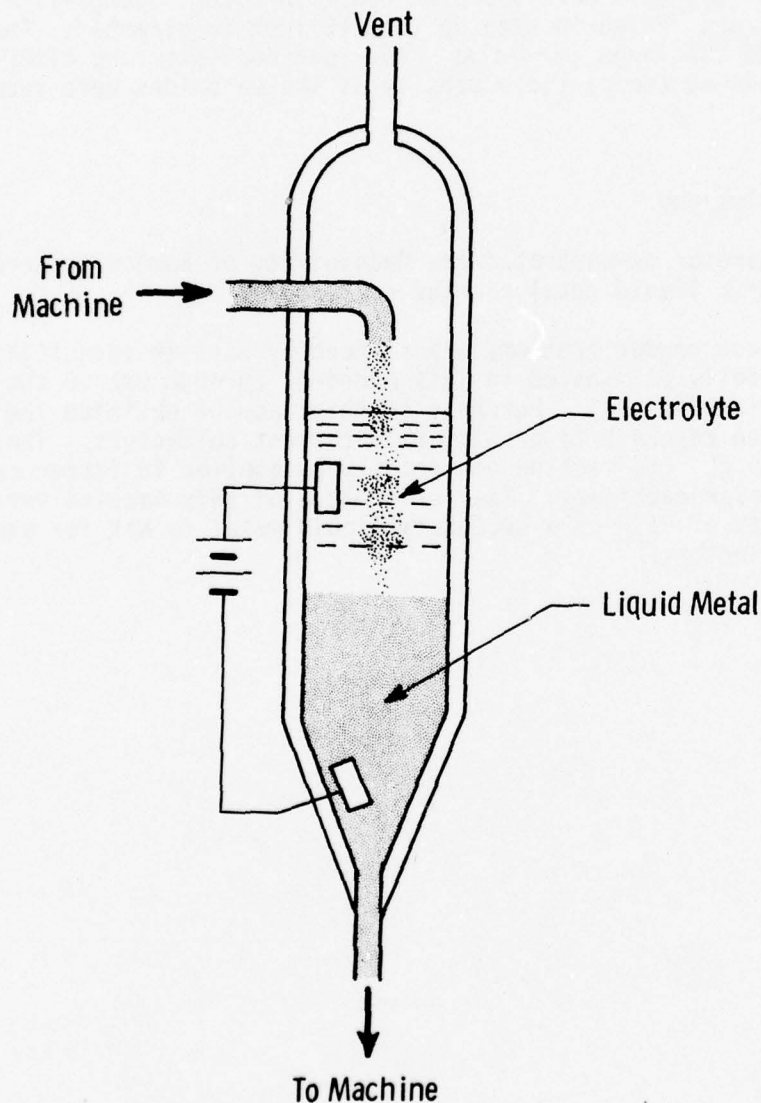


Fig. 2.3.11: GaIn purification cell schematic

at the higher power levels, yet remained below 2000 (.2%) and 8000 (.8%) ppm respectively. These impurities and the high gas moisture content could have been the result of carry over from the 3M NaOH cover fluid in the GaIn purification cell.

The endurance test required high performance from the GaIn purification cell. The white, cloudy sodium hydroxide became grey, and black particulates were observed in the solution. The stirrer was applied, and considerable bubble generation at the GaIn pool surface occurred. The particulates were dark brown to black in color, sponge-like in appearance, and varied in size up to 3/16 inch in diameter. The stirring action broke the large particles and continual stirring after machine shutdown reduced the particle density as the Ga oxides were reconverted to Ga.

2.3.4 Conclusions

The GEC generator demonstrated the feasibility of homopolar machinery utilizing GaIn liquid metal current collectors.

The GaIn black powder problems experienced by earlier investigators, are successfully eliminated in this machine, through use of the electrolytic purification cell. Purchase of this machine obviated the need for extensive research to develop GaIn current collectors. The technology developed in the GEC machine can readily be applied to larger constant speed homopolar machinery. The performance of this machine verifies the applicability of GaIn as a secondary liquid metal to NaK for use in current collectors.

VOLUME II

SECTION 3

APPLICATION STUDIES FOR
SEGMAG MACHINERY WITH CURRENT COLLECTORS

3.1 OBJECTIVES

Review and select promising applications for the segmented magnet homopolar machines and torque converters.

3.2 SUMMARY OF ACCOMPLISHMENTS

3.2.0 General

A number of potential applications were identified for SEGMAG machinery, all of them contingent upon proper solution of the current collection problem.

The use of liquid metal to transmit simultaneously large quantities of electrical current and heat from the rotating armature was resolved in a reliable and safe fashion for unidirectional machines.

Many applications require the collection of current at low speed and in both directions of rotation. Considerable progress on the hydraulic and dynamic aspects of such current collecting system was made during this contract. The potential success of the current collection systems identified in this contract provided encouragement to address the applications study.

Prior studies revealed the advantages and disadvantages of segmented magnet homopolar machines in general and torque converters in particular.

Work on specific applications for SEGMAG and SMHTC was completed regarding:

- 1) Ship Propulsion Systems
- 2) Torpedo Drive
- 3) High Power Pulsing Generators
- 4) Heavy Vehicle Drives
- 5) Variable Speed Input/Constant Speed Output Aviation Drives
- 6) Homopolar Servo Motors
- 7) Tank Propulsion
- 8) Amphibious Vehicles Propulsion Systems

3.2.1 Ship Propulsion

The use of electrical propulsion in ships has long been suggested as a means of reducing a high speed, low torque prime mover to a low speed, higher torque propeller load. Such reduction is necessary to maximize system efficiency. The use of electric drive gave way in the late 1930's to marine reduction gearing, the latter offering an advantage in lighter weight, less required volume, and higher efficiency. The SMHTC is suggested as an alternative to this marine gearing, pending the satisfactory solution of the current collection problem. As a dc machine system, it offers maximum torque to propeller at any speed in reversal and in acceleration. As a self-contained unit, it does not have the problem of high currents circulating in large dc power bus bars that might weigh on the order of 60,000 lb/100 ft for a 30,000 hp system.

The argument may be offered that the SMHTC offers electric propulsion without the advantage of flexibility of machinery location. In essence, the SMHTC uses electrical power as the conversion medium from prime mover to propeller, but is designed as an alternative for marine reduction gearing with the benefit of torque and power control characteristics of dc machinery. The application of SMHTC to propulsion, with typical characteristics, are given below:

- Matches any single prime mover; steam, gas turbine, diesel, In several applications, can combine twin prime movers.
- Reverses by control of low power field excitation rather than reversing turbine required in mechanical gearing systems.
- Delivers full power in reverse versus maximum of 40% reverse power of geared ships with reversing turbines.
- Control of generator and motor field will allow matching variable displacement load condition of ship.
- Efficient utilization of unidirectional prime mover.
- No more geometrically constrained than marine gearing.

The applications in Table 3.1 appear to be technically feasible, but are speculative in the sense that full design and economic analysis of the total propulsion system is required to replace the "existing" or more conventional system normally ordained for such ships.

3.2.2 Torpedo Drive

This application has potential with regard to the possible development of self-contained torque converters or SEGMAG motors for the propulsion

of torpedo or other remote underwater devices. Typical requirements and physical parameters associated with such systems are listed below.

- Power rating approximately 500 hp
- Contrarotating screws, \pm 1800 rpm
- Low specific weight for energy conversion, 1 to 2 lb/hp
- Compatible with either battery or chemical turbine source
- Total system weight fraction 10% of total
- Available volume 20 in. in diameter, 20 in. long
- Possibly short duration of run for torpedo, on the order of 10 minutes
- Possibly expendable machinery for torpedo or remote underwater devices
- Necessarily high efficiency to lower effect upon energy source

TABLE 3.1

Typical Application Parameters

hp	rpm	Prime Mover	Typical Application
5-10,000	150-300	Diesel, gas turbine	Tug or pusher boat
15,000	200	Steam turbine	Submarine
30,000	200	Steam turbine	Advanced submarine
40,000	180	Steam, gas turbine	Single screw naval escort
40,000	180	Steam, gas turbine	Twin screw naval frigate
40,000	180	Steam, gas turbine	Sea control ship
45,000	80	Steam turbine	LNG, tanker

The application of SMHTC to the chemical turbine or to SEGMAg motor for the battery driven case appear to be feasible. Specific weights for the high speed case are on the order of 1.0 lb/hp or less at 800 rpm and decreasing to the order of 0.4 lb/hp for higher speeds of 3600 rpm. The decreasing diameter and the high speed of chemical prime movers are compatible with the SMHTC concept. The nature of design of the integral SEGMAg motor parameters is as follows:

- SEGMAg is a dc machine
- Dc voltages are compatible with existing battery voltages
- Excitation requirements are dc
- Low cost is anticipated for the basic structure
- Rapid response to control of excitation is inherent for non-superconducting homopolars

Solution of the current collection problem will be required to permit compatibility of liquid metal with the drive system and environment of the mobile platform. In the case of the expendable torpedo, it is envisioned that the device could be armed with liquid metal as it is armed with payload, prior to delivery. In this case storage is safe. Liquid metal could be sealed in an internal reservoir until activated. The solution of the current containment would be more of a short-term nature than is the reliability required for propulsion. This is due primarily to the short duration of delivery, on the order of 10 minutes.

3.2.3 High Power Pulsing Generators

This application appears extremely promising in the area of stored energy conversion. In a typical case of energy storage, the rapid rate of pulse and the resilience to undergo a severe frequency of pulses is inherent in the SEGMAG generator. The rapid rate of response to a signal follows from the typically small excitation signal required to generate a high power signal. This will be possible in the non-superconducting SEGMAG homopolar generator. The inductance and high stored magnetic field associated with the superconducting SEGMAG do not appear to be easily overcome by conventional excitation techniques.

Typical pulsing requirements for further conversion are:

- Pulse width of 11 seconds duration
- Power level of 550×10^6 joules
- Rise and fall times of 1 second or less
- Frequency of one pulse per minute

3.2.4 Heavy Vehicle Drive

This application has potential for a wide class of heavy vehicles, including military vehicles of all types. An industrial counterpart of potential benefit is the heavy, earthmoving vehicle, of typical minimum size characteristic ballasted weight 44,000 lb, requiring nominally 300 hp to propel the vehicle at 40 mph.

Recent R&D efforts in the propulsion of vehicles of the sort described above have involved the "electric wheel" concept, utilizing a combination of high speed (39,000 rpm), high frequency (3200 Hz), single shaft gas turbines, ac synchronous generator converted to ac induction motors through solid state cycloconversion equipment. Most systems under development for military equipment utilize ac generators at high rpm, ac motors at high rpm (3,000 to 30,000) for constant horsepower through reduction gearing (typically 140:1) to a vehicular speed of approximately 215 rpm.

The SMHTC and various combinations of SEGMAg generators and motors appear as feasible alternatives to the propulsion system described above. Inverter and/or cycloconverter circuits were utilized to generate the high torques and wide speed range required for a propulsion system. The use of high speed prime movers also precluded conventional dc generation from the viewpoint of excessive weight and volume. These characteristics are feasibly matched by the SEGMAg and SMHTC dc machinery concepts. Although more detailed study is required to determine the competitive status of this application, the high power densities of the SEGMAg units indicate feasible application. The current collection system must be solved, with the added complexity of miniaturization being introduced by the desire to provide high speed generators at power levels in the range less than 1000 horsepower.

The use of electrical transmission in ground vehicles of this type offers the advantage of allowing the evolution of new vehicular forms around the flexibility of location of prime mover from motor connection to the wheel. This has the distinct advantage of placement of components to allow full articulation of the vehicle concept. An advantage to an earth-moving vehicle application follows from the gain in gradability of the vehicle due to smooth and controlled manner of applying tractive effort to ground. The overall system would be attractive from the good utilization of the gas turbine engines and high efficiency of the SEGMAg motor/generator and SMHTC concept over the operating range. Several advantages would be offered to the vehicle class, including remote powering and control capability, accurate steering control, and mechanical isolation of drive components.

Future applications lie in the area of extremely large vehicles, of current size near 645,000 lb under full load. These vehicles employ two 550 hp traction motors operating over the range 0 to 2400 rpm, delivered through 35:1.1 reduction gear to provide vehicular motion at 0 to 70 rpm.

3.2.5 Variable Speed Input/Constant Speed Output Aviation Drives

This application has been utilized to supply fixed frequency electrical power on mobile platforms, i.e., aircraft or ships, from variable speed prime movers. This application takes 4500 to 9000 rpm and delivers a steady output speed of 12,000 rpm, for 400 Hz ac output. Another typical application takes from 2160 to 3700 rpm and delivers a steady speed of 8000 rpm. These devices use a combination of planetary gearing and hydraulics for power conversion. State-of-the-art power range is from 30 to 150 Hp. These power conversion drives are extremely lightweight, on the order of 0.8 to 1.0 lb/hp, involve diameters and lengths from 10 to 18 inches.

This application for the SMHTC involves the difficulty of miniaturization and may not be a competitive alternative in the lower range of horsepower. The high speeds involved will ensure a minimum diameter of SMHTC, with fewer moving parts than the presently used maintenance-troubled mechanical-

hydraulic unit. Present estimates indicate that the basic SMHTC weights will be competitive with the mechanical hydraulic drives. The development of small designs for low values of horsepower will require the systems analyst to estimate auxiliary requirements such as cooling water, bearing oil, and current collection clean-up.

3.2.6 Homopolar Servomotor

Dc machines are often employed in closed loop control systems, particularly for the control of speed and torque where control is normally achieved by varying the field excitation or armature current or both. Dc machines are preferred for intermittent duty or where unusually high starting torque is required. The servomotor is required to produce rapid acceleration from standstill or near standstill conditions. For several reasons, the SEGMAG homopolar motor appears to offer potential for the rapid positioning of large inertia objects, including radar or other antenna arrays where variable directivity is required, rotating gun mounts or missile launchers, and for rotating devices where precision control is essential.

The figures of merit of a servomotor is given by T^2/J , a measure of how speedily the motor is able to respond (T is the value of torque, J the moment of inertia of the motor). A similar measure defined as "goodness" factor is T/J , an exact measure of the motor acceleration without load. Any factor which can increase the torque faster than it increases the square root of inertia can be utilized to improve the figure of merit for a servomotor. The SEGMAG homopolar servomotor is then a promising application. Since the torque is proportional to the armature and the power rate is proportional to the I^2R losses of the armature, the inherent high current characteristics of SEGMAG motors will contribute to the high T^2/J ratio. The increased power density for low weight and low inertia machines suggests that extremely precise control may be obtained in these applications.

Theoretically, the SEGMAG homopolar can be easily controlled to give variable speed and special torque characteristics at high efficiencies. The linear speed-torque relation could be obtained with minimum control equipment in this application.

3.2.7 Tank Propulsion System

Since one of the advantages of the SEGMAG machine is smaller size for a given capacity, an electric propulsion drive for a military tank was investigated. Electric drives for tanks have another advantage in that they provide a readily controlled independent tractive effort to each track over the entire speed range. The present system uses a hydraulic coupling and a gear unit which has the disadvantages of a fixed number of gear ratios and space constraints due to the mechanically interconnected components. The electric drive, on the other hand, permits smooth control of torque over the entire speed range. Historically, however, electric

drives tended to be larger than mechanical drives due primarily to the required motor torque capacity at low speed.

Since the most desired attribute of modern tanks is increased acceleration for more agile mobility, increased horsepower per ton of vehicle weight is obviously the trend to follow. Unfortunately, increasing installed horsepower with present day mechanical drives usually increases the enclosed volume and surface area, thereby requiring more armor weight and more horsepower. Electric drives, although heavy in comparison to mechanical drives, offer one outstanding benefit that breaks this exponentially rising horsepower-weight trend, and that is its freedom in mechanical arrangement. By electrically separating the prime mover and the traction drive, more compact drive systems can be visualized that do not require increasing tank armor weight. Since this separation is accomplished electrically, horsepower increases of the prime mover can be effected by increased speed and thereby increased power density. Utilizing this principle, an improved performance tank drive system was developed. The conceptual system uses modular units of motors, generators and control units. The modularization has distinct advantages for both tracked and wheeled vehicles. It also permits application to many vehicles of varying horsepower requirements utilizing multiples of the modular drive motors with corresponding prime mover sizes.

Tractive effort (TE) basically sets the torque and volume of the drive motors. The maximum TE is specified normally as equal to the vehicle weight. The continuous TE or the point for which the transmission cooling system is rated occurs at a coefficient of friction .5 or 50% of the vehicle weight.

For a 60 Ton tank, the maximum TE is 120,000 lbs and the continuous rating is 60,000 lbs. Above 60,000 lbs the duration of the operation is a function of the thermal time constants of the transmission. On hard surface, the continuous rating point corresponds to operation on about a 50% slope. This, of course, is not a condition that exists for long periods in practice. However, extended periods of operation in clay or mud are encountered which require 1000 lbs of TE per ton of vehicle weight - the same loading condition.

The power of the present generation of tanks is selected on the basis of acceleration capability. This is in contrast to earlier criteria when the measure of performance was speed capability on steep grades. Acceleration is the area of greatest concern. Although present day tanks have maximum TE capabilities of 2000 lbs/ton, during an acceleration from zero speed the torque transferred to the drive sprockets does not exceed about 500 lbs per ton. The accelerating tractive effort is reduced by the ability to accelerate the engine under load and again by the energy required to accelerate the rotating parts of the drive.

Therefore, the WK^2 of an electric transmission is a critical area. The generator WK^2 must be considered at the engine shaft and the motor WK^2 must be viewed at the drive sprocket through the output gear. The other parameter affecting acceleration is the load placed on the engine by the transmission at the time the engine is attempting to accelerate.

The XM-1 is a 58 Ton tank which is basically the M-60 with improved performance. The top design speed is 45 mph which could only be used comfortably on hard surfaces.

Continental is providing a 1500 hp diesel engine which drives through a mechanical-hydraulic transmission. It employs a hydraulic torque converter in conjunction with a four speed gear transmission. A certain speed range is covered by each gear ratio. In the lower portion of each speed range the converter is in operation. At, say, the midpoint of the range the converter is locked-up and the system operates as a mechanical drive.

With this type of drive, the power delivered to the drive sprocket peaks at four points. At other speeds the power is reduced either due to the losses in the converter or because the engine is overloaded or both. The peak power is about 85% of rated even at lock-up because of hydraulic spin losses in the transmission.

Considering that the SEGMAG system could achieve efficiencies between 90-95%, the steady state performance is clearly improved over the entire range of vehicle speed.

Several machines were considered for this drive, the pertinent data being presented in Table 3.2.

Table 3.2: SEGMAG Machines Considered for Tank Drive

	Generator	Motor (2 req'd.)
Rating, hp	1500	750
Speed, rpm	3000	450/2880
Dia., in.	27	36
Length, in.	34	35
Wt., lbs	5000	4000

The size of the machinery evolved in these preliminary designs appears to fit into the available space in the XM-1 vehicle. The mechanical arrangement of components, however would have to be scrutinized more closely. The system weight of approximately 16,000 lbs appears to be a slight handicap and would have to be evaluated on the basis of the increased accelerating capabilities of the vehicle. The feasibility of

this application can only be evaluated after an intensive analysis of the complete system performance over the required mission profiles and a detailed mechanical layout is completed. These tasks would be outside the scope of the present contract.

3.2.8 Amphibious Vehicles Propulsion Systems

Propulsion systems for several amphibious vehicles were investigated. To gather information on the characteristics of these vehicles and their performance requirements, several visits were made. The first was to the U.S. Marine base at Quantico, Virginia to discuss the requirements of an advanced amphibious vehicle drive.

The present vintage of amphibious vehicles are 25 ton tracked vehicles with 8 knot water speed. They utilize engines with mechanical-hydraulic transmission for land operation and water jets at sea. For the advanced LVA under consideration, the most dramatic performance change desired is to raise the speed to the range of 35 to 70 knots. These high speeds indicate a departure from the displacement type vehicle. Candidate systems include planing hulls, surface effects, etc. In these cases, a drastic reduction in vehicle weight is required to bring the propulsion system within an acceptable power range.

Westinghouse presented a review of the various advanced machines under study and development with special emphasis on the SEGMAG machine concept and the ARPA program objectives.

Also performance characteristics for a typical tracked vehicle were presented and comparisons were drawn between mechanical and mechanical-hydraulic and electric torque converters. The electric drive provides ease of control, high maneuverability and high utilization of the prime-mover rating over a wide range of vehicle speeds. Also, electric drive offers superior acceleration capability.

The need to develop reversing current collectors for the drive motors was identified and a program to define specific machines and the control scheme was suggested.

The vehicle is in the very early stages of idea formulation. Therefore, the needs and the drive systems are too uncertain to permit an evaluation of the advantages that would be derived from an electric drive system.

Due to the limited funds, it appears that the USMC program will be restricted to vehicle concepts based on currently available components or development systems sponsored under a broader program.

A visit was made to the Naval Amphibious Warfare Board at Norfolk, Virginia. They were interested in the present state-of-the-art in electric propulsion systems as they might apply to re-power a range of amphibious vehicles that they operate.

A short Presentation was given of Marine Propulsion Systems utilizing the ARPA developed SEGMAG machine concepts and other electric propulsion arrangements. Interest was indicated by the Navy for several potential applications.

Many questions were generated by these Operations Personnel regarding the application of the SEGMAG drive system. The majority of these questions concerned the liquid metal current collectors, and centered on the following particular categories: 1) The effect of pitch and roll on the liquid metal in the collectors. 2) The types and methods of seals used to maintain the liquid metal in the collectors. 3) The seals required to maintain the nitrogen gas in the machine and the amount of nitrogen required for inventory. 4) The amount of liquid metal discharged from the machine normally and under battle conditions. 5) The effect on safety to personnel in event of liquid metal leakage. 6) Due to the close tolerances in the current collectors, what provisions are incorporated into the machine for thrust absorbtion and thermal growth? 7) Due to the relative high mortality of these small vessels what are the economics of this drive system?

All of the above questions were answered positively with experimentally derived data and potential solutions proffered to the contemplated problems.

3.2.9 Miscellaneous Applications

A number of areas exist in which research and development efforts have been conducted and reported upon in the technical community of the USSR. Several of these are listed below. The potential of such concepts appears high and worthy of further evaluation.

- Impact homopolar pulse generator with plasma current removal
- Ac homopolar generator as stable frequency source
- Low frequency ac homopolar generators for induction mixing of liquid metals
- Homopolar acyclic slip clutches and brakes
- Homopolar generator as acceleration sensor

Several areas which appear of extreme industrial interest involve the generation of large currents at low voltage. These applications are of interest to the national defense in many cases, including:

- Electrolysis of magnesium, sodium, aluminum, gold, silver, lead, copper
- Electrolysis of chlor-alki chemicals
- Electrolysis of water for constituent elements
- Electrowelding of large, seamless pipe
- Brushless exciters for large turbogenerators
- Motor applications for high torque attrition mills
- Motor applications for precision control as in steel rolling mills

3.3 CONCLUSIONS

Many potential applications for homopolar machinery concepts were examined under this contract, touching on both DOD and civilian needs. These studies indicate that intensive research in some areas would be very worthwhile.

VOLUME II

PART A

SECTION 4

LIQUID METAL CURRENT COLLECTION SYSTEMS
TECHNOLOGY AND EXPERIMENTAL PROGRAM

4.1 OBJECTIVES

The objectives of this task are to study liquid metal current collection technology and to identify the preferred systems for the segmented magnet homopolar machines.

During Phase I the specific objectives were: 1) to review the state-of-the-art of liquid metal current collection system technology; 2) to identify preferred liquid metals and preferred current collector designs under a variety of operating conditions; 3) to identify the operational problem areas which must be resolved for successful performance; 4) to establish the constraints which the liquid metal handling and purification systems must satisfy; and, 5) to establish an experimental program to resolve the problems associated with liquid metal current collectors.

During Phase II the objective was to evolve a liquid metal current collector suitable for unidirectional, constant speed machines of the SEGMAG type and to verify its effectiveness in the 3000 HP demonstration SEGMAG generator.

In Phase III which is discussed in Part A, Section 5 "Current Collection Systems Collector Designs", the current collector technology was extended to: 1) unidirectional high speed (96 m/s collector speed) generator applications; and, 2) reversible and variable speed applications such as motors and torque converters.

4.2 PRIOR AND RELATED WORK

Exploitation of the advantages which electrical homopolar machines can offer, such as high power output, small physical size and weight, and high efficiency, rests heavily on development of suitable current collectors. Since the high conductivity and potentially good wetting capabilities of liquid metals are desirable properties for such applications, theoretical and experimental studies of liquid metal collectors has received world-wide attention.¹⁻⁵ A review of the technology reveals a number of concerns in regard to the application of liquid metal current collectors in homopolar machines.⁶ Two major concerns are magnitude of collector power loss and ability to confine liquid metal to the collection zones, both of which are adversely influenced by electrical current-magnetic field (MHD) interactions within the conducting fluid during machine operation.

Liquid metals such as mercury and mercury-indium alloys are being employed in experimental homopolar machines in Europe. The main disadvantages of these liquid metals are their toxicity and high mass density characteristics. The gallium-indium eutectic alloy (76 wt % gallium) is being employed in a vertical shaft generator commercially available in England. Although significantly lower in density than mercury, the disadvantage of this alloy is that it is not compatible with metals such as copper, aluminum, and many grades of steel. Homopolar machines of the impulse power type have been built in the United States and in Australia which use the low density eutectic sodium-potassium alloy (78 wt % potassium) current collector fluid. The eutectic NaK alloy is compatible with most structural metals, electrical conductors, and many insulation materials and possesses relatively good electrical and thermal properties.⁷ The chief disadvantage of NaK is that it is very reactive with oxygen, carbon dioxide, and water and, thus, must be prevented from exposure to normal air atmospheres. This protection is obtained by providing a dry pure inert gas atmosphere for the current collectors within the machine enclosure.

Design analyses show that high efficiency is expected from a segmented magnet (SEGMAG) drum-type homopolar generator.⁸ Employing conventional (rather than superconducting) magnetic excitation coils, these machines contain the magnetic flux within iron circuits, with little leakage in the current collection zones. This is an important factor since large leakage magnetic fields lead to increases in power loss and problems with confining or controlling liquid metal in the collector.

The vital function of a liquid metal current collector is to provide good electrical contact between its rotating and stationary parts for purposes of transferring useful machine load current. This paper analyzes high speed collectors developed primarily for SEGMAG-type homopolar generators and presents results of experimental work with collectors evaluated in a glove box facility. The collectors are of the rotating disk-stationary concentric channel design, utilizing the eutectic sodium-potassium alloy NaK-78.

4.3 SUMMARY OF ACCOMPLISHMENTS

4.3.0 General

The feasibility of employing liquid metal current collectors in powerful homopolar machines requires that the liquid metal be confined to thin ring-shaped volumes or annular channels comprising the current transfer or collection zones of the machines. This requirement is based on a necessity to reduce prohibitively high hydrodynamic power losses which otherwise occur in systems wherein the liquid metal completely fills the machine's internal gaps or void spaces. Such reduction in hydrodynamic power loss is directly achieved through significant limitations in "wetted" contact area. Additional reduction in power loss is obtainable by minimizing the ambient magnetic field intensity in the current collection zones.

Power losses in the liquid metal of "unflooded gap" current collectors used in homopolar machines which employ the SEGMAG design concept will be relatively small. Low power loss is achieved because of the small contact area with the liquid metal and because the ambient magnetic fields in the current collection zones are very weak.

Probably the most serious concern in applying an "unflooded gap" liquid metal current collection system is confinement of the liquid to the annular gap of the current collector. The systems are designed so that centrifugal force tends to keep the liquid metal in the annular gap of the current collectors. This constraining force is opposed by several forces which tend to remove liquid metal from the collectors. The significant opposing, or expelling, forces are classified as gravity, acceleration, and magnetic. The balance between the constraining and expelling forces will depend on the type and specific design of the machine. Since a generator will always be running at high speed, its relatively high constraining force will be helpful in obtaining confinement of the liquid metal. Motors must operate at both low and high speeds, even zero speed, and thus the confinement problem is of much greater concern in that case.

An important concern involving the reliability of liquid metal current collection systems over long time operation is if low electrical resistance within the fluid and low contact resistance at the collector member surfaces can be maintained. Both of these concerns appear to be associated with purity or integrity of the liquid metal, especially in the face of viscous working. Of concern, with regard to volume resistivity, is a change of state phenomenon which has been shown with certain liquid metals. Such transfer in the physical state is manifested by the collector fluid changing to a "powder". Unclean collector surfaces, initially or subsequently formed, may seriously inhibit "electrical wetting" and lead to increased contact resistance with the liquid metal.

During Phase I of this ARPA contract, a preferred current collector design was identified for unidirectional homopolar machines, such as the SEGMAG generator. This selection was based on a review study of the complex electromagnetic interactions and forces which will be experienced by functioning collector systems under a variety of operating conditions and liquid metals. The preferred collector design embodies an "unflooded machine gap", with the low density sodium-potassium liquid metal alloy (NaK) confined in narrow circumferential current transfer zones. The liquid metal alloy gallium-indium (GaIn) was selected as an alternative to NaK, especially for homopolar machine applications wherein relatively low speed and high ambient magnetic field operating conditions exist, or in certain situations where liquid metal handling may be considered a problem. The alternative choice of a higher density liquid metal was based on lower calculated power losses when run under the specified operating conditions. Although not as compatible as NaK with most structural and conducting materials, GaIn is quite easy to handle and lends itself to a relatively simple purification process.

Two of the greatest concerns in applying liquid metal current collectors are: a) the magnitude of power losses developed in the fluid; and, b) the confinement of fluid to the current collection zones during all machine operating conditions.

During Phase II a liquid metal current collector test facility was constructed and an experimental test plan was implemented to resolve recognized problem areas in applying liquid metal current collectors. Part of this effort included an evaluation of collector width effects on the magnitude of the ordinary fluid dynamic power loss. The effect of ambient radial magnetic field and collector width variations on the eddy current power loss was also investigated. The remaining work effort consisted of experimentally evaluating the possible adverse effects which rotor rotational speed, radial magnetic induction, and load current have on liquid metal confinement in the collection zone. This effort culminated in the design and fabrication of the current collectors for the prototypic SEGMAG generator. (See Section 2, Vol. II of this report.)

During Phases II and III the current collector design which was developed was evaluated in a SEGMAG demonstration generator, rated 3000 hp. Tests verified the suitability of this collector for use in homopolar machines of constant speed (to 67 m/s). Concerns include the collector solid-liquid contact resistance, and its influence on machine efficiency, and a collector filling - critical temperature characteristic. Work continued to extend the unidirectional collector technology to higher speeds for generator applications. Other work centered on development of reversible and variable speed collectors for torque converters and motor applications. Concepts considered in this development include flooded, unflooded, and hybrid collectors (see Section 5).

4.3.1 Power Losses in Current Collectors

4.3.1.0 General

For homopolar machine designs that restrict the liquid metal to discrete numbers of thin annular rings or current transfer gaps, four main types of power loss can be identified for each collector site:

1. Ordinary ohmic losses due to electrical load current crossing the collector gap.
2. Ordinary fluid dynamic (viscous) losses.
3. MHD losses arising from an axial magnetic field in the collector gap.
4. MHD losses arising from a radial magnetic field in the collector gap.

Based on a simplified model, see Fig. 4.1, expressions for the above power losses have been derived in terms of machine operating conditions, collector geometry, and physical properties of the liquid metal. This study is limited to high speed analysis, characterized by a turbulent flow regime within the liquid metal.

4.3.1.1 Ordinary Ohmic Losses

The ohmic power dissipation due to load current may be expressed as the sum of bulk resistance and surface contact losses:

$$P_{\Omega} = \frac{I^2}{2\pi r w} \left(\frac{d}{\sigma} \right) + \frac{I^2}{2\pi r w} \epsilon \quad (4.1)$$

where: P_{Ω} = total ohmic power loss per collector, W

r = collector rotor radius, m

w = collector electrical contact width, m

d = collector radial gap dimension, m

σ = electrical conductivity of liquid metal, mhos/m

ϵ = solid-liquid-solid specific contact resistance, $\Omega \cdot m^2$

I = collector load current, A

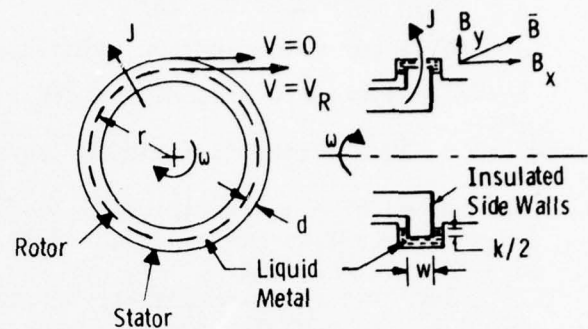


Fig. 4.1: Model of Liquid Metal Current Collector

It is assumed in this expression that (1) the collector's flat side walls are insulated -- thus minimizing MHD rotor-drag losses associated with the axial field, B_x ; and (2) the ohmic loss associated with the solid-liquid interface is dependent upon a specific contact resistance (ϵ) whose value, in turn, depends on the solid and fluid metals which comprise the collector. Reported ϵ values for the copper-NaK-copper contact pair fall in the range 3 to 5 $n\Omega \cdot m^2$.^{9,10} Specific resistance values are reported here in a later section (see Fig. 4.15).

4.3.1.2 Ordinary Fluid Dynamic Losses

These power losses occur due to viscous shear in the liquid metal caused by relative motion of the inner and outer portions of the collectors. In the absence of a magnetic field, and for relatively high speed operation, losses can be shown to be proportional to the density of the liquid, the cube of the rotor surface speed, the wetted area, and a turbulent friction factor which is a weak function of the Reynolds number.^{11,12}

$$P_{fd} = \frac{\pi}{4} f_p v_R^3 r (w+k) \quad (4.2)$$

Where the new symbols are:

P_{fd} = fluid dynamic power loss per collector, W

f = Fanning friction factor (Darcy friction factor/4)

ρ = fluid mass density, kg/m^3

v_R = collector rotor surface velocity, m/s

k = additional fluid contact width along radial sides of collector, m .

4.3.1.3 Axial Magnetic Field MHD Losses

When the machine is electrically loaded, an increase in collector fluid dynamic power loss occurs as a result of the axial magnetic field-radial load current MHD interaction. In the case of a typical generator, circumferential body forces are created in the conducting liquid metal which tend to pump the fluid counter to the rotor's direction of rotation. Resulting changes in the fluid's velocity profile account for the increase in the fluid dynamic power loss. This increased viscous loss, however, is partially offset by an electrodynamic potential ($= \bar{v} \times \bar{B}_x$) which generates useful load power within the gap. Assuming the same friction factor at both collectors walls, a purely axial magnetic field, then, leads to a net (fluid dynamic minus electrodynamic) viscous loss given by:¹¹

$$P_a = \frac{\pi}{4} f \rho v_R^3 r (w+k) (1+3\delta^2), \quad 0 \leq \delta \leq 1 \quad (4.3)$$

where the new symbols are:

P_a = net fluid dynamic loss per collector, W

$$\delta = \frac{2B_x J_y d}{f \rho v_R^2}, \text{ dimensionless}$$

and B_x = axial magnetic field, T

J_y = radial load current density, A/m^2 .

The mean turbulent liquid metal velocity, v , obtained in deriving Eq. (4.3) is given by:

$$v = \frac{v_R}{2} (1-\delta), \quad 0 \leq \delta \leq 1. \quad (4.4)$$

The restriction of $0 \leq \delta \leq 1$, then, is equivalent to $0 \leq v \leq v_R/2$. In the case of low magnetic induction (B_x) and/or low load current density (J_y), perturbations in the ordinary velocity caused by MHD effects will be small and $v \rightarrow v_R/2$. Under the limiting conditions, when $\bar{B}_x \times \bar{J}_y = 0$, the above expression for power loss reduces to Eq. (4.2). Consequently, for low leakage magnetic fields the ordinary viscous loss will not be increased significantly as a result of axial MHD effects.

For large MHD effects where $\delta > 1$ or $v < 0$, fluid flow will be opposite to collector rotation as given by:

$$v = \frac{v_R}{2} (1 - \sqrt{2\delta - 1}), \quad \delta > 1. \quad (4.5)$$

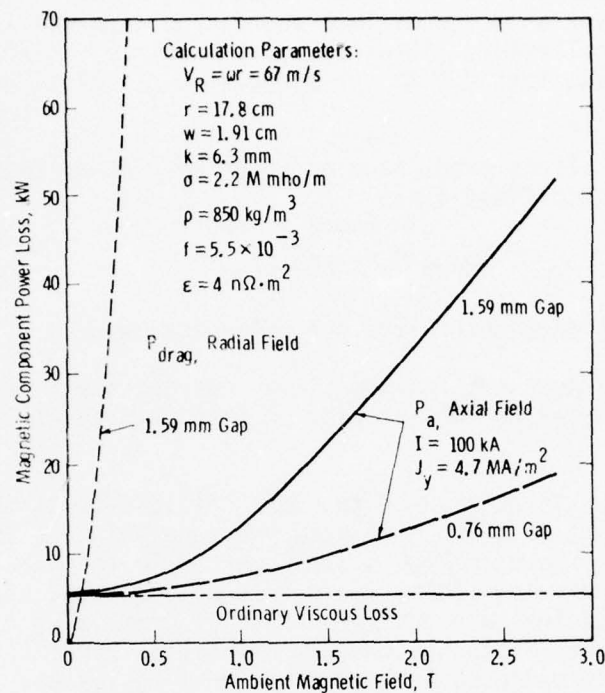


Fig. 4.2: Magnetic field effect on power losses (NaK-78). Axial field effect based upon Eqs. (4.3) and (4.6); radial field effects upon Eq. (4.7).

The corresponding net viscous power loss becomes:¹¹

$$P_a = \frac{\pi}{2} f \rho v_R^3 r (w+k) (1+\delta) \sqrt{2\delta-1}, \quad \delta > 1. \quad (4.6)$$

The two curves in Fig. 4.2 representing axial field effects on net viscous loss are based upon Eqs. (4.3) and (4.6). The two collectors represented by these curves differ only in the extent of the radial gap, d . Power loss is shown to increase directly with the collector radial gap dimension and with the axial magnetic field intensity. In the case of a 1.59 mm stator-rotor gap, the collector power loss is shown to increase 10 times as the magnetic field is increased from zero to 2.8 T.

4.3.1.4 Radial Magnetic Field MHD Losses

Liquid metal current collectors used in homopolar machines will likely be subjected to a radial magnetic field. This field induces a potential gradient ($= \vec{v}_R \times \vec{B}_y$) along the moving collector face, thereby producing current circulation, axially in the moving and stationary solid members and radially through the liquid metal medium. An interaction between

the induced rotor current and the radial magnetic field causes a rotor drag power loss, even under conditions wherein no external load current flows through the collector. Alternately, the $\vec{v}_R \times \vec{B}_y$ interaction may be viewed as an ohmic loss due to the associated circulating current in the liquid metal.

The equation which allows prediction of rotor drag power loss due to a purely radial magnetic field is:¹³

$$P_{\text{drag}} = \frac{\pi \sigma (\omega B_y)^2 (rw)^3}{6(d + \epsilon \sigma)} \quad (4.7)$$

where P_{drag} = rotor drag power loss per collector, W.

Note that Eq. (4.7) does not include a load current term: a radial magnetic field produces no MHD interaction with the radial load current ($\vec{J}_y \times \vec{B}_y = 0$).

Calculated power losses attributed to radial field effects for one of the collector designs (1.59 mm gap) used previously in the axial field evaluation are also shown in Fig. 4.2. Compared to the axial magnetic field case, relatively low radial field intensities cause high power loss. These results indicate the importance of minimizing radial components of magnetic induction within the current collection zone: circulating currents may introduce unacceptably high rotor-drag losses.

Since the radial field loss (Eq. (4.7)) is a cubic function of the collector width, w , significantly large reductions in its value can be made by minimizing the width. Decreasing the collector width by 20%, for example, will decrease this loss by a factor of two. Although the ordinary fluid dynamic loss is also reduced through reductions in collector width, an increase in the ohmic power loss associated with load current transfer occurs as shown by Eq. (4.1). Thus, an optimum width is implied for minimum total power loss.

Equation (4.7) is strictly valid only for the case of a pure radial field (i.e., $B_x=0$). When the field is mixed, as in the general case, and there are components of both B_x and B_y , there is some indication that the net effect* is less than the sum of the individual effects.¹⁴ Thus, Eq. (4.7) overstates the actual radial field effect when $B_x \neq 0$. However, the magnitude of the net reduction is a function of B_x , and for low B_x values the decrease will be small.

*The axial field, B_x , manifests itself in two ways: (1) B_x interacting with the moving fluid produces a net emf that opposes the circulating current density (j_c) thereby reducing the drag loss; (2) B_x interacting with the circulating current increases the velocity gradient at both collector surfaces (through the $\vec{j}_c \times \vec{B}_x$ body forces) thereby increasing the viscous loss. The net result is a tendency toward reduction of total (drag plus viscous) loss.

4.3.1.5 Calculated Total Collector Power Loss

In the case of low axial magnetic fields, total collector loss including load current, viscous, and MHD drag losses is given by the sum of Eqs. (4.1), (4.2), and (4.7). Based on these equations, calculations of collector power loss for a SEGMAG type generator were made, representing wide ranges of collector width and specific contact resistance. Pertinent geometrical parameters, operating conditions, and liquid metal physical properties assumed for the calculations are tabulated below:

$r = 17.8 \text{ cm}$	$I = 100 \text{ kA}$
$d = 1.6 \text{ mm}$	$f = 5.5 \times 10^{-3}$
$k = 6.4 \text{ mm}$	$\sigma = 2.2 \text{ M mho/m}$
$\omega = 377 \text{ rad/s}$	$\rho = 850 \text{ kg/m}^3$
$B_y = 0.03 \text{ T}$	

Results of the power loss calculations are presented in Fig. 4.3. Rather large loss in power are noted to occur as the specific contact resistance, ϵ , is increased, especially for narrow width collectors. Optimum collector widths are indicated by the minimum loss line. If it is assumed that ϵ is near zero, the optimum collector width is 0.6 cm. Reductions in width result in smaller contact areas, higher solid-liquid interface resistance and, consequently higher ohmic loss associated with transferring the machine load current. Consequently, quite high power losses are associated with narrow width collectors, especially with high ϵ values. For a given specific contact resistance, increasing the width will diminish the total power loss until the viscous drag -- due to large wetted areas -- predominates.

An optimum collector width, then, exists for each set of collector parameters. If the specific contact resistance, for example, is $4 \Omega \cdot \text{m}^2$, then with the parameters specified above the optimum collector width is 1.3 cm, as illustrated in Fig. 4.3.

4.3.2 Confinement of Liquid Metal

4.3.2.0 General

The second major concern in the application of liquid metal current collectors is that of maintaining filled collectors and/or confining the

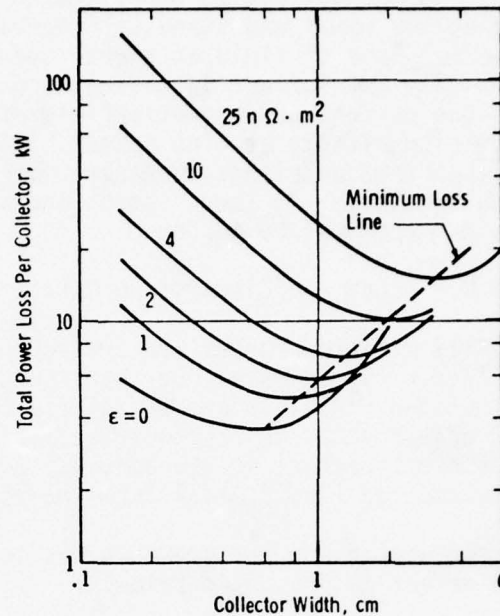


Fig. 4.3: Calculated collector power loss, based upon assumed load current (100 kA), radial magnetic field (0.03T), peripheral velocity (67 m/s), and liquid metal (NaK-78).

fluid to the collection zones. Significant factors are: loss of fluid during low speed and standstill operating conditions because of gravity effects, loss of fluid at higher speed because of inertial-induced turbidity and surface agitation, and loss of fluid at all speeds because of load current and magnetic field effects. To ward against these expulsion effects at high speeds, the collectors are generally designed so that the centrifugal pressure works to keep the liquid metal in the annular gaps.⁶ At lower speeds and standstill, special collectors or fluid seals must be employed.

4.3.2.1 Load and Circulating Current Effects

Axially directed forces are created by pressure variations within the collector liquid metal due to circumferential self-magnetic fields associated with load and radial field induced-circulating currents. This MHD effect tends to fragment the fluid, causing voids and degraded electrical contact in the annulus, disturbances at the free surface, and expulsion of liquid metal from the collector.

An expression for the pressure due to the load and circulating current MHD effect is presented below:¹³

$$p(x) = \frac{\mu_0}{4} \left\{ \left(\frac{\alpha^2 w^2}{2} + \frac{\alpha \beta w^2}{4} \right) \left(\frac{w}{2} + x \right) - \left(-\frac{\alpha^2}{2} + \frac{\alpha \beta w}{2} + \frac{\beta^2 w^2}{4} \right) \left[\left(\frac{w}{2} \right)^2 - x^2 \right] - \alpha \beta \left[\left(\frac{w}{2} \right)^3 + x^3 \right] + \frac{\beta^2}{2} \left[\left(\frac{w}{2} \right)^4 - x^4 \right] \right\} \quad (4.8)$$

Where the new symbols are:

- $p(x)$ = pressure in the liquid, N/m²
- x = axial distance along collector width from center (positive x directed away from load current loop, see Fig. 4.1 and 4.4), m
- μ_0 = permeability of free space, 0.4π μ H/m
- $\alpha = I/(\pi r w)$
- $\beta = \sigma \omega B_y r / (d + \sigma \epsilon)$

This expression assumes a completely filled collector (i.e., the fluid is maintained in the annulus even in the face of the axial forces), and a purely radial magnetic field.

Based on Eq. (4.8), calculations of the axial pressure in the liquid metal for a prototypic collector were made. In addition to the parameters previously tabulated, the present pressure calculations involved a collector width of 1.27 cm and selected values of ϵ . Results of the calculations are presented in Figs. 4.4 and 4.5.

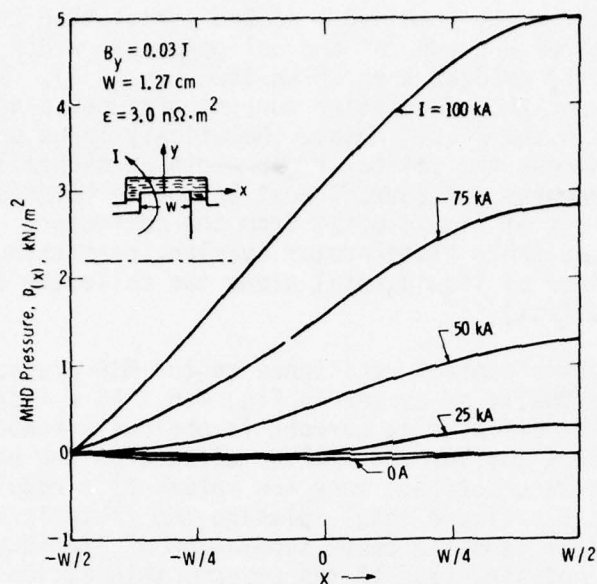


Fig. 4.4: Calculated pressure variation caused by load and circulating currents.

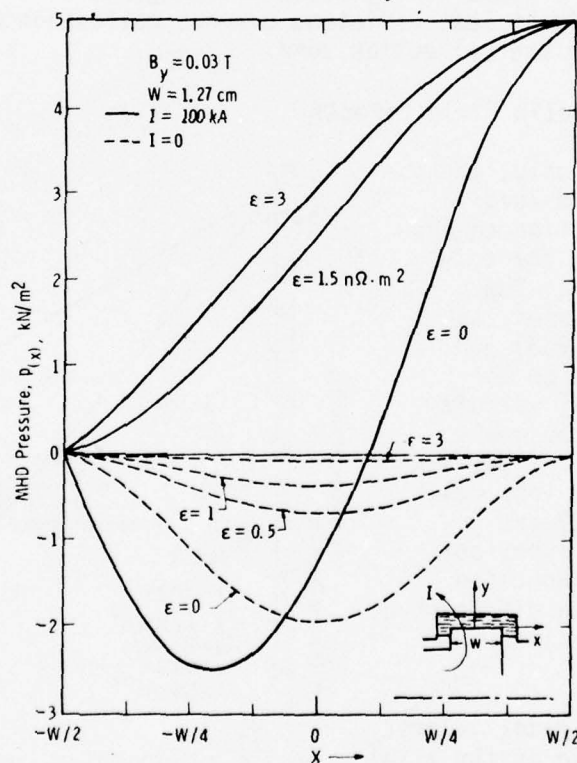


Fig. 4.5: Effect of contact resistance (ϵ) on calculated pressure caused by load and circulating currents.

The pressure caused by the combined load and circulating currents increases axially from one edge of the collector gap width to the other for load currents (I) greater than 25 kA (see Fig. 4.4). With low load current, dominance of the circulating current produces a negative, then positive pressure in the liquid metal. Relatively large unidirectional pressures appear across the collector gap width at higher load current levels. These pressures, of course, must be counterbalanced in order to prevent gross loss of liquid metal from the collector. This may be accomplished with suitable stator-rotor overlap, permitting self-adjusting asymmetric extensions of liquid metal along the collector's radial side walls (manometer effect).

Influence of collector contact resistance on the MHD pressure is indicated by the contrasting family of curves in Fig. 4.5. As ϵ increases from zero to $3 \text{ n}\Omega\cdot\text{m}^2$, the circulating current is obviously reduced to such an extent that it has smaller and smaller effects on the basic load current-self field interaction. Very low values of ϵ result in axially opposing forces in the liquid metal, placing the fluid in a state of tension. This effect tends to cause separation of liquid metal in the annulus, which is undesirable. If too severe, this action would likely cause gross loss of liquid metal from the current transfer zone, leading to high bulk and contact resistance, and high ohmic power loss. If present, a varying ϵ would likely cause sloshing action of the liquid metal leading, again to less efficient current collection and excessive fluid spillage from the collection zone.

4.3.2.2 Axial Magnetic Field Effects

As mentioned previously, the axial magnetic field-load current MHD interaction causes velocity changes in the collector liquid metal. The associated power losses, as expressed by Eqs. (4.3) and (4.6) are dependent on the average liquid metal velocity. Fluid velocities previously determined from Eqs. (4.4) and (4.5) for the power loss calculations (Fig. 4.2) are presented now as a function of axial magnetic induction for the cases of two different collector gap dimensions in Fig. 4.6.

The average liquid metal velocity is shown to decrease as the axial magnetic field intensity increases.

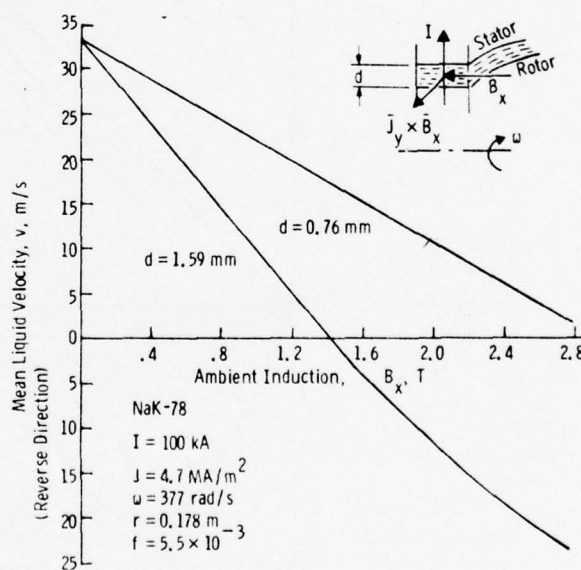


Fig. 4.6: Calculated liquid metal velocity characteristics.

At a certain level of induction, the liquid flow velocity reaches zero, then, with still higher induction levels, reverses in direction. The reverse flow point is reached when the MHD body force, which occurs as a result of the axial magnetic field-load current interaction ($\vec{J}_y \times \vec{B}_x$), and a hydrodynamic viscous force, which arises in the fluid due to rotation of the rotor, are equal. If the axial field becomes sufficiently strong to a point where the MHD and the viscous drag forces become equal, relative to an observer on the stator, the resulting liquid flow velocity will be reduced to zero. As this operating condition is approached, the liquid metal will likely "drop out" of the collector, since the inertial constraining force also approaches zero. Thus, even with high speed homopolar generators, if the ambient axial magnetic field becomes critically high, confinement of liquid metal to the collection zone will be a serious problem. The above is not considered a problem for SEGMAG-type machines, however, where the axial magnetic leakage field in the collection zone will be much too low (i.e., about 0.1 T). Also, as shown in Fig. 4.6, some relief from this problem may be gained through reductions in the radial extent of the rotor-stator gap.

4.3.3 Current Collector Evaluation Program and Test Facilities

4.3.3.0 General

Since many assumptions must be made in any theoretical study of liquid metal current collectors, it is mandatory that many of the results be substantiated or refuted by experimental studies. An experimental program was initiated to investigate the operating characteristics of liquid metal current collectors, with special interest in operating conditions and collector geometries peculiar to SEGMAG-type homopolar generators. A test rig permitting evaluations of prototypic size collectors for a 2.24 MW, 100 kA generator was designed and constructed. Initial test runs were made to assure that each collector would perform in a stable manner without magnetic field effects over the speed range of interest. The degree of annulus filling and the ability to confine liquid metal to the collector during its operation were determined for a range of injection or circulation flow rates. The magnitude of the ordinary hydrodynamic power loss was also determined and related to calculated values obtained from the derived analytical expression. An indication of the influence which viscous working of the liquid metal has on its chemical composition over an extended period of continuous running was also obtained. Later runs were made to determine the specific contact resistance and to qualitatively evaluate the effect of fluid expelling pressures.

Figure 4.7 is an overall view of the current collector test stand; portions are shown of the test rig enclosure, the NaK-78 liquid metal circulation feed loop, the nitrogen cover gas recirculation and purification system, the collector cooling system, and other associated apparatus and equipment

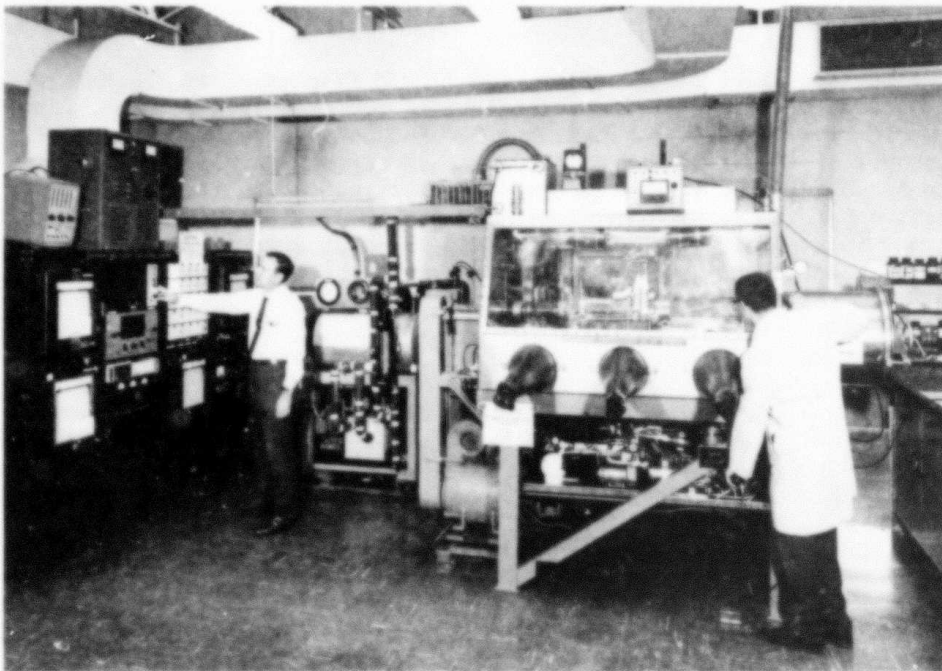


Fig. 4.7: Test stand with auxiliary systems.

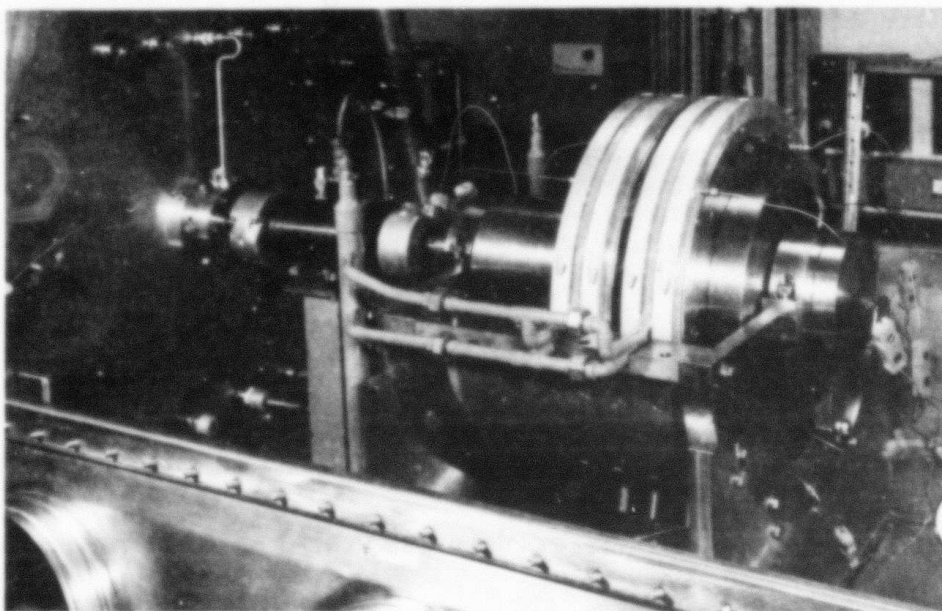


Fig. 4.8: Current collector test rig.

such as the drive motor, the shaft transmission, and the data monitoring and control instrumentation. Figure 4.8 is a view of the test rig itself in the glove box enclosure, but without the magnetic field coil and top iron housing in place. During certain experiments the top housing was not employed to afford better accessibility and to allow good observation of the test collectors. Tip speeds at the rotor edge of about 70 m/s are attainable.

Provisions were made so that controlled levels of radial magnetic field (up to 0.1 T) could be applied to the test collector zone, thereby generating large circulating currents in the liquid metal (see Eq. (4.7)). A 15 hp dc motor was selected to meet the drive power and torque requirements imposed by the circulating current and viscous drag power losses anticipated in the test collectors. A torque sensor mounted in series with the drive shaft measures the collector power losses. A magnetically loaded, nitrogen gas-buffered rotating contact type seal prevents room air leakage into the glove box through the drive shaft penetration.

Stainless steel tubes convey NaK from its supply source to the test current collectors. By choice, either batch amounts or continuous flows of NaK are delivered to the collectors. The liquid metal circulation loop possesses a capability for continuous on-line purification. The fluid loop includes a collector drain sump tank, centrifugal pump, EM flow meter, cold trap filter, and associated control valves and level probes. Copper tubes convey coolant fluid in and out of the collector stators.

4.3.3.1 Glove Box Current Collector Tests

The following test results to be described were obtained using 17.8 cm radius rotor current collectors. Both flat and tapered rotor end shapes were evaluated, with quite similar results. NaK-78 liquid metal was fed tangentially in the direction of rotation into the collector gap annulus and withdrawn at the sides. Multiple groove seals were employed to catch and control any spills of liquid metal from the current transfer gap.

4.3.3.2 Rotor Speed Effects

During the experimental runs, complete filling of the collector annulus with liquid metal was evident from electrical continuity indications (between insulated probes disposed axially and circumferentially around the collector stator), increase of viscous drag torque and collector temperature, and reduced pressure at the NaK inlet location (due to Bernoulli effect or "suction").

The viscous torque-NaK flow characteristics for one of the copper rotating disk collectors are shown in Fig. 4.9. This family of curves reveals that, with increasing NaK inlet flow rate, a limiting maximum torque

level is approached, becoming successively higher as the speed increases. Based on electrical continuity measurements, complete filling of the gap occurs at low inlet flow rates, near the starting knee of the curves. Significantly, the collector operates satisfactory over a wide range of NaK inlet flow rates, from 0.8 to at least 13.3 ml/s. Dynamic flows of liquid metal into the collector were necessary to assure continuous filling against the expelling effects associated with rotor rotation.

Computations of fluid dynamic power loss-speed characteristics were made using the experimental torque data of Fig. 4.9. The expression which relates fluid dynamic power loss and torque is:

$$P_{fd} = \omega \tau \quad (4.9)$$

where the new symbol is:

τ = viscous drag torque, N·m.

Figure 4.10 shows the power losses obtained versus speed (ω) using (4.9) and constant 6.7 ml/s NaK flow rate-torque data. The dashed curve of Fig. 4. shows the same loss predicted by Eq. (4.2). In the latter case, we used the Fanning friction factor for smooth surfaces and fluid overlap $k = 6.4$ mm. The overlap is based on observed radial extent of NaK wetting on the rotor walls following testing. The close agreement between observed and predicted viscous losses supports validity of the turbulent flow assumption implicit in Eq. (4.2).

A continuous 76-hour run was made with the rectangular shaped rotating disk current collector. Operating conditions held constant throughout the period include rotor speed (60 r/s), collector temperature ($88^\circ\text{C} \pm 2^\circ\text{C}$) and NaK inlet flow rate (3.3 ml/s). An analysis of the liquid metal's alloy constituents before and after the run showed no detectable change from its eutectic composition as a result of the viscous working.

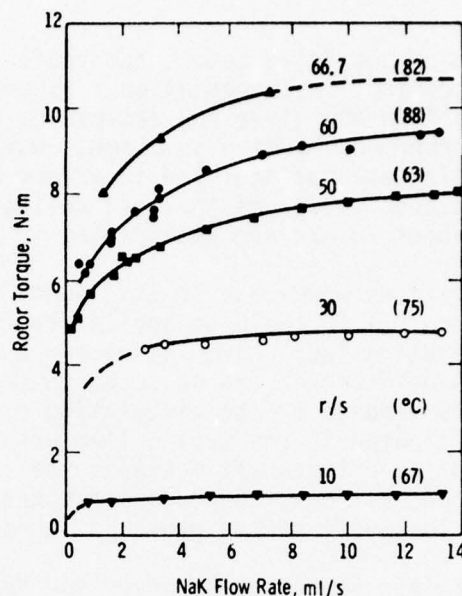


Fig. 4.9: Typical viscous torque-NaK flow characteristics: Collector radius, $r = 17.8$ cm; radial gap, $d = 1.59$ mm; width, $w = 1.91$ cm.

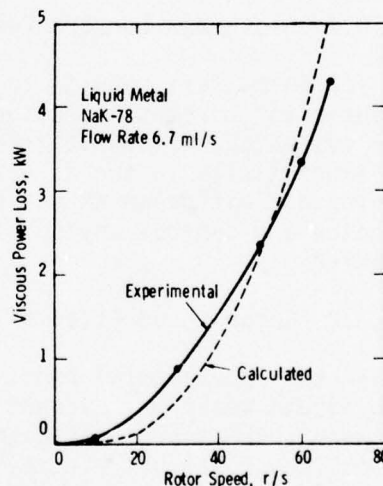


Fig. 4.10: Ordinary fluid dynamic power loss-speed characteristics for collector of Fig. 4.9.

As mathematically implied by Eq. (4-2), the ordinary fluid dynamic power loss is proportional to collector width. To verify this relationship two similar collectors, differing only in rotor width (1.27 and 1.91 cm), were run in the test rig. In both runs, the rotor speed was varied to 60 r/s, while the NaK inlet flow rate was held constant near 5 ml/s. Results of the experiment are shown in Fig. 4.11. The average power loss ratio of the two collectors, representative of the entire speed range, is 0.77. The corresponding wetted fluid width ($w+k$) ratio for the two collectors is $(1.27 + 0.64)/(1.91 + 0.64) = 0.75$. The close agreement between the loss and width ratios is interpreted to confirm validity of the width relationship in the ordinary fluid dynamic power loss predictive expression (Eq. (4.2)).

4.3.3.3 Temperature Effects

During the course of experimental work, filling of the current collector was found to be critically dependent on temperature. This characteristic was observed when collectors were run at rotor speeds greater than about 40 r/s (45 m/s). Sometimes complete filling was noted, and other times not. This phenomenon was found to be correlated with collector temperature. The temperature sensitivity is illustrated for a rotor speed of 60 r/s by the two curves in Fig. 4.12. Below the "critical" temperature, viscous drag torque is relatively low but then increases abruptly when a slight rise in temperature is allowed. When the temperature is now reduced from above to just below the "critical" level, the viscous drag torque drops abruptly to its original low value. This phenomenon was repeated many times.

The temperature dependency for other rotor operating speeds is illustrated in Fig. 4.13. Good performance was observed, in terms of gap filling and confinement of NaK to the collector, if operation occurred at temperatures above the specific critical level for each speed. Operation below the critical temperature line caused an adverse effect on collector performance. Although an experimental solution to the liquid metal filling problem was achieved by operating above the critical temperature, lower temperature operation is desirable so that the machine cooling capacity will not be compromised.

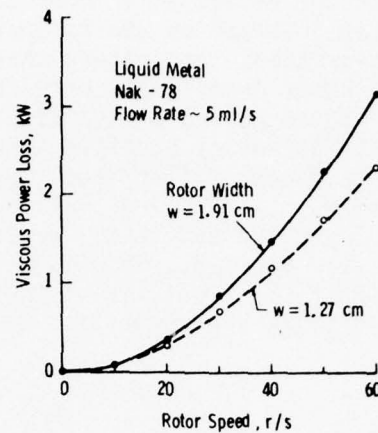


Fig. 4.11: Rotor speed and width effects on ordinary fluid dynamic power loss.

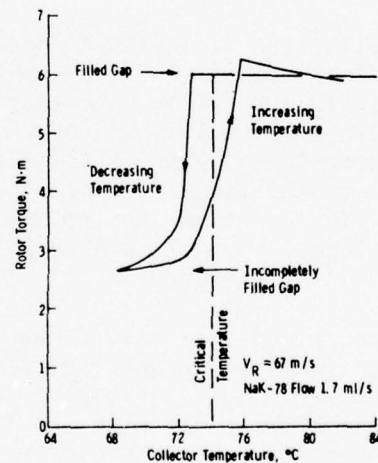


Fig. 4.12: Torque temperature -- characteristics related to collector gap filling.

A number of experiments were run to evaluate the effect of a lower density cover gas (helium) on the collector filling-critical temperature characteristic. Other experiments were run with nickel plated collector surfaces to ascertain potential benefits in regard to easier collector filling and lower contact resistance. In these, as well as in previously described tests, no magnetic fields were applied. Results of collector filling-critical temperature determinations are summarized below:

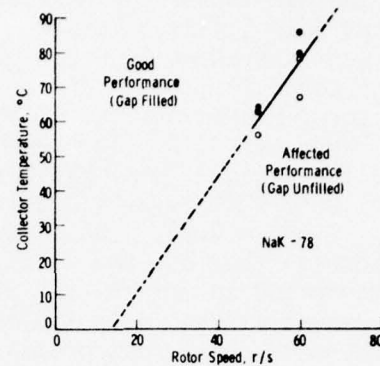


Fig. 4.13: Critical performance dependency on temperature and speed.

Collector Side Walls	Collector Contact Surfaces	Cover Gas	Critical Temperatures @ 60 r/s, (°C)
Uninsulated	Bare Copper	N ₂	78
Insulated	Bare Copper	N ₂	62
Insulated	Bare Copper	He	51
Insulated	Nickel Plated	N ₂	<28

Insulating the flat side walls of the rotor and stator permitted a significant lowering of the operating temperature without sacrificing capability for filling and maintaining a filled collector when operating in nitrogen. Additional lowering of the critical temperature (to 51°C) was demonstrated when the 60 r/s collector ran in a helium environment. Finally, temperature was not found to be critical in regard to liquid metal filling of the collector, down to 28°C, when the contact surfaces were electrolytically plated with nickel and operation was again in a cover gas of nitrogen.

Although beneficial results were shown experimentally for the above noted collector design changes and cover gases, a complete physical understanding of their effects is incomplete at this time. Conjecture as to the mechanisms which explains the improved collector filling ability will likely include gas-liquid flow dynamics as well as surface films and solid-liquid wetting. Additional theoretical and experimental investigations are needed.

4.3.3.4 Radial Magnetic Field Effects

The pressure described by Eq. (4.8) is produced through interaction of collector currents and their associated circumferential magnetic fields.

With no load current this pressure (due entirely to radial-field induced circulating currents) increases symmetrically about the collector's center, tending to expel liquid metal axially, each way, from the gap (see Fig. 4.5). As may be seen by substituting $I=0$, $B_y \neq 0$ in Eq. (4.8), pressure varies as width to the fourth power and radial field squared, suggesting significant disturbances will occur in the liquid metal as either width or radial field increases.

Experiments were conducted to verify the above concern, wherein two similar collectors differing in width (1.27 and 1.91 cm) were exposed to a radial field, but no load current. The results are given in Fig. 4.14 in terms of NaK inlet pressure vs. B_y . As the magnetic field imposed on the collector increased, a less negative pressure (reduction in suction) occurred at the NaK inlet location. We found such pressure changes preceded fragmentation of liquid metal in the gap: gross expulsion of liquid metal from each side of the gap occurred as B_y approaches 0.015 T for the wide (1.91 cm) and 0.075 T for the narrow (1.27 cm) collector. This was accompanied by intermittent electrical contact, as detected by continuity probes located in the gap. The onset of instability (positive pressure region of Fig. 4.14) and visual expulsion occurred at a lower field intensity for the wide collector.

Although a correlation is shown here between the calculated axial pressures and experimentally observed disturbances in the fluid flow, more work is needed to quantify the phenomena.

4.3.3.5 Specific Contact Resistance Determinations

A knowledge of the magnitude of the specific contact resistance, ϵ , is necessary for designing a minimum power loss collector. Experiments were run to determine the contact resistance of collectors with bare and nickel-plated copper surfaces. Such determinations were possible utilizing experimental values of power loss associated with circulating currents induced by radial directed magnetic field in the liquid metal. The difference between drive shaft power with and without controlled levels of magnetic field, less a correction for previously determined stray power loss (measured under the same conditions but with an unfilled collector), is taken as the circulating current power loss, P_{circ} . An expression for that loss in terms of ϵ and the known operating conditions is obtained from Eq. (4.7).

$$P_{\text{circ}} = \frac{\pi \sigma (\omega B_y)^2 (rw)^3}{6(d + \epsilon \sigma)}, \quad (4.10)$$

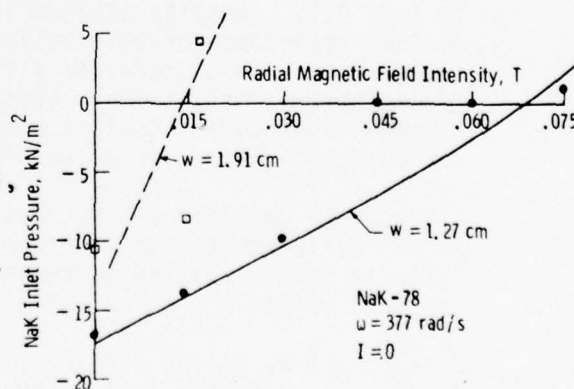


Fig. 4.14: Indication of collector fluid flow instability.

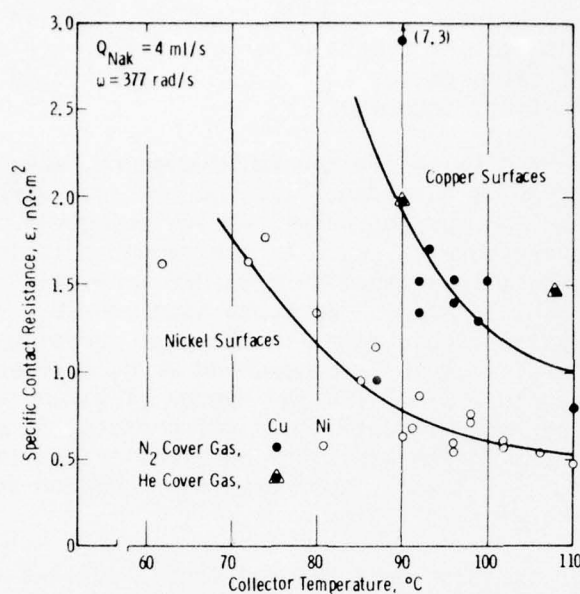


Fig. 4.15: ϵ values determined from radial field experiments with 17.8 cm radius collectors.

or rearranging terms

$$\epsilon = \frac{\pi}{6} \frac{(\omega B_y)^2 (rw)^3}{P_{\text{circ}}} - \frac{d}{\sigma} \quad (4.11)$$

The specific contact resistances determined for collectors with copper and nickel-plated copper surfaces are plotted as a function of temperature in Fig. 4.15. Despite scatter in the data, a tendency is shown for the contact resistance of both collectors to decrease with increasing temperature. This characteristic is possibly related to another experimental observation, namely, an increasing fluid flow stability with rising temperature. Lower resistance is thus attributed to larger solid-liquid contact areas and to improved wetting at higher temperatures.

The average specific contact resistance is reduced nearly 50% when the copper collector contact surfaces are plated with nickel. This characteristic is likely related to thinner and less continuous tarnish films on surfaces of nickel, which leads to lower contact resistance.

Nickel, unlike silver and gold, is essentially insoluble in NaK. Upon disassembly and decontamination of the test collector following eight days of testing and exposure to NaK, the 0.005 mm thick nickel plate was intact and bright.

Specific contact resistances reported here for copper surfaces are one-third lower than the values reported by others.^{9,10} Even lower values were found using a simple electrode-type cell, in which surface preparation significantly influenced the contact resistance. Platings with silver and gold produced the lowest values, suggesting that surface wetting has a strong influence on the effective contact resistance. Maintenance of low contact resistance with silver and/or gold surfaces is questionable, however, since these metals are readily soluble in NaK.

4.4 CONCLUSIONS

While many simplifying assumptions are implicit in the relatively compact analytical expressions presented above, these results, nevertheless, provide a tractable basis for future collector development. The following conclusions apply to NaK-filled collectors subjected to weak magnetic fields:

1. Initial liquid filling of disk-type collectors and subsequent operation in the filled mode is dependent on a "critical" operating temperature, which increases with speed. Nickel plating the current transfer surfaces lowers the critical temperature.
2. Reliable long-term collector operation requires a continuous or dynamic inlet flow of liquid metal.
3. Liquid metal inlet pressure measurement provides a reliable means for monitoring collector filling.
4. Our experiments show that radial magnetic fields disturb the liquid metal annular flow and that wide collectors amplify this effect. The existence of liquid body forces, which increase directly with collector width, is predicted by Eq. (4.8).
5. Our analysis shows that specific contact resistance reduces radial-field (MHD drag) losses, but increases the ordinary ohmic power loss.
6. Specific contact resistance depends upon surface preparation and temperature. Based on our data, nickel-plating lowers contact resistance of the Cu-NaK-Cu combination, and for both plated and unplated surfaces the contact resistance tends to decrease with increasing temperature in the range 70-110°C.
7. Observed ordinary fluid dynamic power loss agrees with a simple turbulent-flow model, Eq. (4.2).
8. For a given set of operating conditions, total collector power loss can be minimized by choosing an optimum width in accordance with Eqs. (4.1), (4.2), and (4.7).

4.5 REFERENCES

- (1) Klaudy, P., "Advances in the Construction of Unipolar Machines by the Use of Liquid Contacts," Elektrotechnik und Maschinenbau, 78 (3), pp. 128-143, 1961.
- (2) Chabrerie, J.P., Fournet, G., Mailfert, A., "Flooded Rotor, Direct Current, Acyclic Motor, with Superconducting Field Winding," Proc. 1972 Applied Superconductivity Conference, pp. 93-7.
- (3) Lewis, D.L., "Practical Homopolar Machines, Use of Liquid-Metal Slip Rings," Journal of Science and Technology, Vol. 38, No. 2, pp. 46-54, 1971.
- (4) Gigot, E.N., "Applying Unipolar Generators," Allis Chalmers Electrical Review, Second Quarter, pp. 14-20, 1962.
- (5) Hibbard, L.U., "The Canberra Homopolar Generator," Atomic Energy Australia, Vol. 5, No. 3, pp. 2-5, July 1962.
- (6) Johnson, J.L., Mole, C.J., Arcella, F.G., "Important Problems in Applying Liquid Metal Current Collectors," Electrical Contacts/1973, IIT, Chicago, IL, pp. 201-210, 1973.
- (7) Witkowski, R.E., Arcella, F.G., Keeton, A.R., "Vital Support Systems for Liquid Metal Collector Homopolar Machines," 1976 IEEE Winter Power Meeting.
- (8) Part II, Section 2 of this report.
- (9) D'Albon, G., Parteni, C., Polytechnic Iassi's Institute Report, 1956, 2, p. 253, Popular Rumanian Academy Issue, p. 458, 1953.
- (10) Poulain, J., "Récents développements des machines acycliques à courant continu," Bull. Soc. Fr. Electr., 2, No. 23, p. 656, 1961.
- (11) Rhodenizer, R.L., "Development of Solid and/or Liquid-Metal Collectors for Acyclic Machines," Final Report for Tasks 1, 2, and 3, Naval Ship Systems Command Report, Contract No. N00024-68-C-5415, Feb. 27, 1970.
- (12) Harris, L.P., "Hydromagnetic Channel Flows," MIT Press, 1960.
- (13) Mole, C.J., "Design and Development of a Segmented Magnet Homopolar Torque Converter," Advanced Research Projects Agency, Contract No. 1, DAHC 15-72-C-0229, Semi-Annual Report for Period Ending May 31, 1975.
- (14) Rhodenizer, R.L., "Development of Solid and/or Liquid-Metal Collectors for Acyclic Machines," Final Report for Tasks 4 and 5, Naval Ship Systems Command Report, Contract No. N00024-68-C-5415, Sept. 30, 1971.

VOLUME II

PART A

SECTION 5

LIQUID METAL CURRENT COLLECTION SYSTEMS COLLECTOR DESIGN STUDIES

5.1 OBJECTIVES

During Phase III current collector technology was extended to: 1) unidirectional high speed (96 m/s collector speed) generator applications; and, 2) reversible and variable speed applications such as motors and torque converters. This is the workscope of this Section of the report.

Work with liquid metal current collectors terminated with Phase III. Phase III-A efforts were redirected to solid brush current collection, as described in Volume II, Part B of this report.

5.2 PRIOR AND RELATED WORK

During Phase I of this contract, a preferred current collector design was identified for unidirectional homopolar machines, such as the SEGMAG generator. This selection was based on a review study of the complex electromagnetic interactions and forces which will be experienced by functioning collector systems under a variety of operating conditions and liquid metals. The preferred collector design embodies an "unflooded machine gap", with the low density sodium-potassium liquid metal alloy (NaK) confined in narrow circumferential current transfer zones. The liquid metal alloy gallium-indium (GaIn) was selected as an alternative to NaK, especially for homopolar machine applications wherein relatively low speed and high ambient magnetic field operating conditions exist, or in certain situations where liquid metal handling may be considered a problem. The alternative choice of a higher density liquid metal was based on lower calculated power losses when run under the specified operating conditions. Although not as compatible as NaK with most structural and conducting materials, GaIn is quite easy to handle and lends itself to a relatively simple purification process.

During Phase II a liquid metal current collector test facility was constructed and an experimental test plan was implemented to resolve recognized problem areas in applying liquid metal current collectors. Part of this effort included an evaluation of collector width effects on the magnitude of the ordinary fluid dynamic power loss. The effect of ambient radial magnetic field and collector width variations on the eddy current power loss was also investigated. The remaining work effort consisted of experimentally evaluating the possible adverse effects which rotor rotational speed, radial magnetic induction, and load current have on liquid metal confinement in the collection zone. This effort culminated in the design and fabrication of the current collectors for the prototypic SEGMAG generator. A complete exposition of this work is contained in Volume II, Part A, Section 4 of this report.

During Phases II and III the current collector design which was developed was evaluated in a SEGMAG demonstration generator, rated 3000 hp. Tests verified the suitability of this collector for use in in homopolar machines of constant speed (to 67 m/s).

As described in this section, work was then begun to extend the unidirectional collector technology to higher speeds for generator applications. Other work centered on development of reversible and variable speed collectors for torque converters and motor applications.

5.3 SUMMARY OF ACCOMPLISHMENTS

5.3.0 General

The problems inherent in containing liquid metal in the annular gap collectors of constant speed generators were discussed in Volume II, Part A, Section 4. Torque converter motor requirements however specify the need for variable and reversible speeds and the problems of liquid metal containment become more difficult. Potential solutions to this problem are explored in the liquid metal current collector designs described below and including the following types of collectors:

- a) High Speed Collectors
- b) Flooded Collectors
- c) Unflooded Collectors
- d) Hybrid Collectors

For collectors of the SEGMAG and high speed type, the theoretical power loss and expulsion pressure expressions were redeveloped to account for the solid-liquid-solid electrical contact resistance. Calculations which illustrate the effects of contact resistance were made. This is reported in Volume II, Part A, Section 4 of this report.

Values of specific contact potential were determined for collectors with copper and nickel plated copper surfaces, using 3000 hp SEGMAG prototype size liquid metal (NaK) current collectors and typical operating conditions. Changes in the collector filling-critical temperature characteristic were also observed as a function of side wall insulation, cover gas density (nitrogen vs. helium), and contact surface treatment (bare copper vs. nickel plate).

Current collector concepts were developed for the reversing unflooded motor application. Specific configurations were defined and these were evaluated, based upon the previously-established list of criteria, to determine feasibility. Three of the collector concepts which passed this screening procedure were recommended for further development.

An analytical study of the hybrid current collector was made during the period. General expressions derived during the study permit

calculation of pertinent collector design parameters and performance characteristics. Incorporating the mathematical expressions in a computer program, quantitative information was obtained for a selected hybrid pad collector. The selected design utilizes circular cross-section pads and they are applied in an axial manner along one flat side wall of the collector rotor.

5.3.1 High Speed Collectors

The current collector test stand was modified to permit higher test speed capability, controlled circulation of load current through the test collectors, and acceptance of narrower width collectors.

A number of experiments were run to evaluate the effect of a lower density cover gas (helium) on the collector filling-critical temperature characteristic. Other experiments were run with nickel plated collector surfaces to ascertain potential benefits in regard to easier collector filling and lower contact resistance. All experiments were made with the glove box test rig, using 3000 hp SEGMAg prototypic size liquid metal (NaK) current collectors. The results of these tests can be found in Volume II, Part A, Section 4 of this report.

5.3.2 Flooded Collectors

Work on flooded collectors is reported in the Machinery Section 2.1 of this report.

5.3.3 Unflooded Collectors

5.3.3.0 General

In a horizontally mounted machine with an unflooded active length, the collector design problem becomes one of confinement of the liquid to the annular collector gap. For a motor, the confinement technique must be independent of rotor speed and direction of rotation. Use of centrifugal forces induced by disk rotation, as in the case of high speed generators, cannot be used as the sole device for achieving containment of the liquid metal. The objective of this study is to develop new concepts for the current collectors in an "unflooded" motor application, to evaluate these, and to select the most promising ones for more detailed investigation.

Collector concepts were developed, using the classification list (Table 5.2) as a guide, and these were evaluated using the list of criteria (Table 5.3) as a feasibility check-list.

5.3.3.1 Reference Unflooded Motor Design-Collector Requirements

The "reference" motor design (Table 5.1) was defined to establish approximate parameters as requirement guides for the current collector design. The axial field through the collector was 0.1 Tesla, a minimum axial clearance requirement of 0.15 cm (0.06 in.) was established, and the radial gap due to machine operation was introduced as 0.11 cm (0.045 in.) minimum.

The radial clearance in a journal bearing of a size adequate to transfer the machine torque, has been estimated to be about 0.030 cm (0.012 in.), which is the amount of additional eccentricity that can occur due to changes in the shaft position with varying speed. An additional change in radial gap will be caused by any differential thermal growth of the rotor and the stator. For example, if the rotor and stator expansion rates are based upon the properties of iron (expansion coefficient $\approx 11.7 \times 10^{-6}$ m/m°C, 6.5×10^{-6} in/in°F) then the differential thermal radial growth will be:

$$\delta = R \alpha \Delta T \quad (5.1)$$

$$\delta = 1.07 \times 10^{-5} \text{ m/}^\circ\text{C} \text{ (} 0.234 \times 10^{-3} \text{ in/}^\circ\text{F) ,}$$

for a radius, $R = 0.914$ m (36 in), and for a 28°C (50°F) temperature difference:

$$\delta \approx 3.05 \times 10^{-4} \text{ m (0.012 in)}$$

TABLE 5.1
Unflooded Motor Reference Design - Collector Requirements

1. Power Rating - 40,000 hp
2. Maximum Speed - 180 rpm (18.9 rad/sec)
3. Collector Diameters: outer - 72 in. (1.83 m), for drum (SEGMAG and disk-type machines (DISKMAG))
inner - 32 in. (0.81 m), for disk-type machines
4. Axial and Radial Dimensions Allocated for Current Collector Cross-section - 1.5 in. (3.81×10^{-2} m)
5. Maximum Permissible Current Density - 16,000 amps/in² (2.48×10^7 A/m²)
6. Maximum Collector Current - 300,000 amps
7. Axial Field through Collector - 1000 gauss (0.1 Tesla)
8. Maximum Radial Field through Collector - 500 gauss (0.05 Tesla)
9. Liquid Metal Leakage from Collector - near zero
10. Maximum Power Loss per Collector Pair - 65 hp (4.85×10^4 w)

The above values were used to establish the following related parameters:

11. Tip Speeds (from 2 and 3): outer - 57 ft/sec (17.2 meter/sec)
inner - 25 ft/sec (7.7 meters/sec), for disk-type machine
12. Bearing Radial Clearance 0.012 in. (3.05×10^{-4} m) (based on 1 mil/in. (1 mm/m) diametral clearance and a 24 in. (0.61 m) shaft dia., necessary for 3 per unit torque at 15,000 psi (1.03×10^8 N/m²) shear design strength)
13. Minimum Width of Liquid Metal Contact: outer - 0.083 in. (2.11×10^{-3} m)
inner - 0.187 in. (4.74×10^{-3} m), for disk-type machine

ADDITIONAL REQUIREMENTS

1. Collector must pass 150% rated current at zero speed for 10 secs.
2. Collector must be operable cold without pre-heating.
3. Collectors for a machine must be supplied from a common liquid metal source.
4. Collector must be capable of deceleration from full speed forward to full speed reverse in several seconds.
5. Collector shall be designed for sudden stops.
6. Collector shall be designed for sudden load changes.
7. Collector shall be designed to provide for axisymmetric current flow.

The following assumptions will be made, but will be re-evaluated, if necessary, when more specific machine and collector designs are available:

1. Relative axial movement between the rotor and stator will be a minimum of 0.06 in. (0.15 cm).
2. Coolant channels or other cooling techniques will not interfere with the current collection design.
3. Joining of any required conductor bars to collector rings will not interfere with collector design.
4. Any mechanical strengthening rings will be outside of the current collector envelope (i.e., the collector will not have to support the loading of other components, due to centrifugal force or relative thermal growth).
5. Changes in radial gap, due to operation, will be assumed to be a minimum of 0.045 in. (0.11 cm).
6. Insulation requirements will not interfere with collector design.

If the thermally-induced dimensional changes are based upon the expansion coefficient of copper ($\alpha = 17.5 \times 10^{-6} \text{ m/m}^\circ\text{C}$, $9.7 \times 10^{-6} \text{ in/in}^\circ\text{F}$), then the change in radial gap would be:

$$\delta_p = 4.3 \times 10^{-4} \text{ m (0.017 in.)}$$

Rotor growth due to rotational stresses, should be negligible at the expected tip speed. Therefore, the cumulative gap change that must be accommodated by the seal, including an additional $3.8 \times 10^{-4} \text{ m (0.015 in)}$ for dimensional tolerances, would be about $11 \times 10^{-4} \text{ m (0.045 in)}$ (for a 28°C , 50°F maximum temperature difference).

TABLE 5.2
Classification of Unflooded Reversing Collector Concepts

A. Sealed Annular Chamber (Seal Types)

1. Rubbing - lip seal, face, radial
2. hydrostatic - face, radial, floating
3. hydrodynamic - face, radial, floating
4. labyrinth - clearance, knife/groove, slinger, transverse gas flow, adjustable
5. buffer fluid - liquid, gas, grease, wax
6. electromagnetic retention - special field/current source
7. absorbent (wick) - labyrinth, slinger/wick
8. low-speed only - centrifugal, electromagnetic
9. magnetic fluid
10. surface tension - wetted/non-wetted surfaces
11. solidification - thermal, chemical

B. Conducting Seal

1. conducting wick - stationary/rotating, fiber, foam
2. hydrodynamic/hydrostatic
3. flooded (alternately) labyrinth

C. Low-Speed Flooding or Low-Speed Brush Contacts

1. pressure-controlled volume
2. pump/control system
3. gas injection

D. Axial Injection (or Radial Ejection)

1. inertial containment
2. venturi effect

E. Zero Pressure (free-fall)

F. Constant-Speed Seal-Rotor

TABLE 5.3
Evaluation Criteria for Current Collectors

1. Containment (Leakage)
 - a) aerosol
 - b) liquid

[free-surface stability, gravity force, acceleration/deceleration (angular/transverse), momentum changes (coriolis)]
2. Power Loss
 - a) viscous
 - b) ohmic (bulk & contact)
 - c) MHD
 - d) friction (rubbing)
3. Circulation System Requirements
 - a) pressure/flow control
 - b) purification/separation
4. Radial/Axial Clearance
 - a) bearing clearances
 - b) dimensional tolerance
 - c) thermal growth
 - d) centrifugal growth
5. Mechanical Adequacy
 - a) thermal stress
 - b) rotational (torque) loading
 - c) hydraulic load (static/dynamic)
 - d) centrifugal loading/stresses
 - e) MHD forces (radial, tangential, axial)
 - f) wear (rubbing, erosion)
 - g) vibration/oscillation stability
 - h) load rate (shock)
6. Temperatures (cooling)
 - a) heat generation (see power loss)
 - b) temperature distribution (collector and rotor conductors)
7. Electrical Adequacy
 - a) voltage drops
 - b) recirculating currents
 - c) asymmetry effects (including variable NaK thickness/area)
8. Material Compatibility
 - a) chemical
 - b) mechanical (e.g., rubbing surfaces)
9. Assembly
10. Fabricability
11. Maintenance

5.3.3.2 Collector Concepts and Evaluation

A. Sealed Annular ChamberA1. Rubbing Seal

The peripheral speed of the "reference" design (17.2 m/s, 3380 ft/min) approaches the upper limit of about 17.8 to 25.4 m/s (3500 to 5000 ft/min) typically recommended for lip-type elastomeric oil seals.^{1,2} Maximum pressure differential capability recommended for this type of seal is about 69,000 N/m² (10 psi). In small quantities, the cost of relatively standard Buna-"N" seals, which generally use garter springs to generate lip pressure, is about \$1 per inch of diameter, or about \$72 for the "reference" machine. Catalog listed seals of this diameter are about 1.91×10^{-2} m (3/4 in) wide and an inch or less in radial thickness. Split seals are available to simplify installation. (Special configurations can be made to order.) Shaft eccentricities greater than 2.36×10^{-3} m (0.093 in) can be accommodated. Standard "Axial Clamp Seals," which provide an axial sealing lip, are also available. These have an axial length of 3.18×10^{-2} m (1-1/4 in) and a radial height of about 1.27×10^{-2} m (1/2 in), with an operating deformation of about 2.39×10^{-3} m (0.094 in).

Figure 5.1 shows an arrangement of lip-seals which provide isolation of adjacent collectors in a multi-turn motor. The chambers formed between collectors may be used to introduce oil droplets to lubricate the seals and to drain any NaK leakage that might occur. Alternatively, they may be filled with oil to balance the gravity-induced pressure drop across the seal, which would otherwise increase from top to bottom. In addition, it may be possible to circulate the oil between the collectors at a rate great enough to cool the collectors.

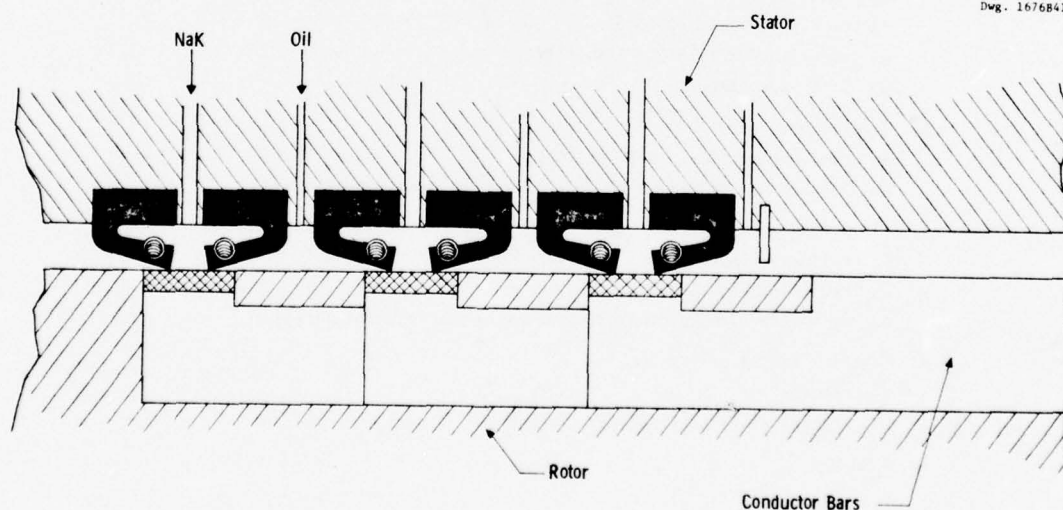


Fig. 5.1: Lip-Seal Collector Configuration

A rubbing seal, which may ride on a very thin ($\sim 2.54 \times 10^{-6}$ m, 1×10^{-4} in) film of oil or liquid metal, should provide excellent containment. Even without pressure balancing techniques, these seals should be adequate for the expected ejection pressure of about $20,700 \text{ N/m}^2$ (3 lb/in^2) in the "reference" machine. Since there is no free surface of the liquid metal, aerosol formation should not be a problem unless there is significant leakage.

The power loss in a rubbing-lip-seal is difficult to estimate, but one supplier provided a rough estimate of radial sealing force at the lip, as 131 N per meter ($3/4 \text{ lb/in}$) of circumference. If this value is used with an effective friction coefficient of 0.125 , then the estimated power loss for the "reference" motor design becomes:

$$P_s = \pi D \mu m V = 1.63 \text{ kW} \quad (5.2)$$

where: D = diameter of seal
 μ = friction coefficient
 m = radial contact force
 V = rubbing velocity of the seal

Another estimate of power loss may be made by calculating the viscous loss in a thin supporting film of oil, using the following expression for power loss:

$$P'_s = (\mu V/h)(\pi DL)V, \quad (5.3)$$

$$P'_s = \pi DL \mu V^2/h$$

where in this case:

P'_s = power loss
 μ = absolute viscosity
 D = diameter
 L = length of seal lip contact film
 V = seal velocity
 h = film thickness

If an oil film $2.54 \times 10^{-6} \text{ m}$ ($1 \times 10^{-4} \text{ in}$) thick¹ is assumed, with a viscosity, $\mu = 8.07 \times 10^{-3} \text{ N sec/m}^2$ ($1.17 \times 10^{-6} \text{ lb sec/in}^2$), the power loss becomes:

$$P_s = 5310 \text{ kW per meter (135 kW per inch) of contact length}$$

If the contact length is assumed to be $7.62 \times 10^{-4} \text{ m}$ (0.030 in.), then the estimated power loss for each seal would be:

$$P_s = 4.05 \text{ kW}$$

The power loss can be reduced by using a lower-viscosity fluid. For example, if NaK is assumed to be the lubricating film ($\mu = 5.2 \times 10^{-4} \text{ N-sec/m}^2$, $7.55 \times 10^{-8} \text{ lb-s/in}^2$), then

$$P_s = 0.261 \text{ kW}$$

In addition to the seal lip loss, there will be the viscous and ohmic losses in the liquid metal annulus ($\sim 6 \text{ kW}$ for a 1 in. collector width). The combination of these losses must not exceed the maximum permissible ($\sim 20 \text{ kW}$ per collector) based on machine efficiency objectives.

Liquid metal circulation requirements are expected to be quite flexible for this concept. Minimum flow rate would be based on purification requirements and replacement of any leakage that might occur. A "batch" loading system may be feasible. An oil separation system may be necessary, but contamination (oil-in-NaK or NaK-in-oil) should be small and simple gravity separation techniques may be applicable.

A smooth rotor with axial insertion into the stator appears feasible with this design. This may greatly simplify assembly, and axial movements should not be a problem. Simple components and perhaps off-the-shelf components can be used for sealing. This would result in minimal fabrication and component costs. No compatibility problems are foreseen, however, "aging" (loss of elasticity) of Buna-"N" or other possible seal materials should be investigated.

Although seal life should be long, once a satisfactory design has been established, it is possible that contaminants (such as oxides) would reduce the operating life of the seals. On-site seal replacement appears to be impractical, unless a scheme is devised for use in conjunction with a split stator. However, seal replacement should be a relatively simple operation, if the motor is taken out of service.

The use of simple lip-type oil seal appears to be feasible for large motor applications where the tip speeds are about 17.8 m/s (3500 f/min) or less. The low cost of these seals makes the experimental evaluation of this concept a relatively simple task. Initial tests, to evaluate tip-speed limits, oxide-induced wear, and "aging" effects, can be run on a simple shaft and smaller diameter seals (at increased rpm). Subsequent evaluation of large-diameter seals would also be inexpensive because the seal cost would add little to the cost of the test set-up required for any full-size concept evaluation.

A2. Hydrostatically-Positioned Seal

A hydrostatically-positioned seal uses gas or liquid pressure differences to control the size of a small gap between the rotor and the stationary seal. An increase in the seal gap tends to increase the leakage flow from a chamber; this reduces the chamber pressure, thus creating a force which brings the seal closer to the rotor and maintains the small gap. The seal may be positioned either axially, against the face of a disk or ring, or radially, in which case the seal ring must be segmented or otherwise flexible enough to permit the changes in diameter required to follow rotor thermal expansion and dimensional tolerance variations.

Two important considerations in the seal design are the selection of fluid used in the seal, and the pressure in the seal chamber. Three fluid types may be considered: the cover gas, an oil, or the liquid metal itself. For the large circumference, even a very small seal clearance would result in a significant leakage into the machine if NaK were used. Therefore, use of NaK requires an added drain chamber; otherwise, it would not satisfy the objective of near-zero leakage into the machine. An added drain chamber is also required with an oil or gas buffer fluid (Figure 5.2) unless the buffer pressure is higher than the collector pressure (Figure 5.3). In that case, however, buffer fluid will enter the collector, and it must be demonstrated that there is no resulting deterioration of collector performance. Another consideration is the possibility that MHD-induced forces will upset the pressure balance if the liquid metal is used for this purpose.

It may be desirable to segment an axial seal (as well as the radial seal) if dimensional controls, such as flatness, become difficult for rings of such large diameter. In this manner, or by making the seal ring very flexible, the seal clearance can be kept small at all points along the circumference. In any event, it will probably be necessary to provide local pockets (chambers) along the seal circumference so that an angular shift of the ring axis would provide a restoring moment. This restoring force might not exist for a complete annular pressure pocket.

Seal clearances of about 2.54×10^{-5} m (1×10^{-3} in) or less should be achievable with hydrostatically-positioned seals. Fluid leakage through such a narrow annular gap would be approximately:³

$$q = \frac{\pi D h^3 \Delta p}{12 \mu L}, \quad (5.4)$$

where: q = leakage flow
 D = seal diameter
 h = seal clearance
 Δp = pressure drop across seal

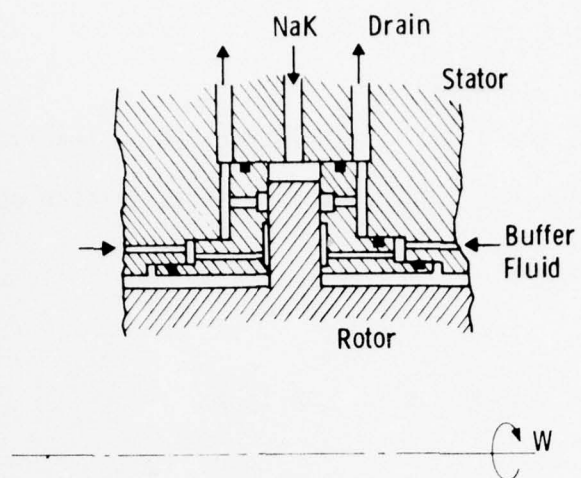


Fig. 5.2: Hydrostatically-Positioned Seal (Sealed Drain)

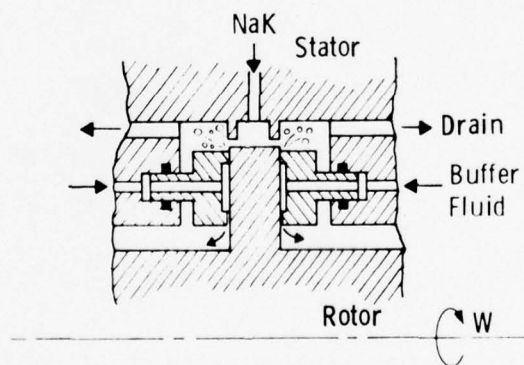


Fig. 5.3: Hydrostatically-Positioned Seal

μ = absolute viscosity

L = width of seal land, in the direction of leakage flow

As in the previous section, viscous power loss associated with this seal land would be:

$$P'_S = \pi D L \mu V^2 / h, \quad (5.5)$$

Equations 5.4 and 5.5 may be combined to find:

$$P'_S q = \frac{\pi^2 D^2 V^2 \Delta p h^2}{12}. \quad (5.6)$$

Based upon estimated liquid-metal ejection pressures of roughly 6,890 N/m² (1 psi) (at the top) to 20,700 N/m² (3 psi) (at the bottom), an average of at least 13,800 N/m² (2 psi) can be assumed to induce leakage from the collector. (The gravity head could possibly be balanced by a buffer liquid.) To provide some margin, a pressure difference of 20,700 N/m² (3 psi) will be used in the leakage calculation.

For the specific case where:

$$D = 1.83\text{m (72 in).}$$

$$V = 17.2 \text{ m/s (57 ft/s)}$$

$$\Delta p = 20,700 \text{ N/m}^2 \text{ (3 psi),}$$

and if the units for " P'_S " are (kW), h (m) and those for " q " are (cc/min), then:

$$P'_S q = 1.01 \times 10^{12} h^2.$$

This relationship (which is independent of μ and L) is plotted in Fig. 5.4 which permits the selection of a seal gap that provides both acceptable power loss and acceptable leakage.

Equations 5.5 and 5.6 may also be combined in a manner which eliminates the variable clearance " h " to find:

Curve 680902-B

μL	L		
N - s/m	NaK (m) (in)	Oil (m) (in)	Nitrogen (m) (in)
1.50×10^{-4}	2.87×10^{-1} 11.3	1.27×10^{-2} 0.500	7.72 304
7.45×10^{-5}	1.43×10^{-1} 5.63	6.35×10^{-3} 0.250	3.86 152
1.32×10^{-5}	2.54×10^{-2} 1.00	1.13×10^{-3} 4.44×10^{-2}	6.85×10^{-1} 27.0
6.62×10^{-6}	1.27×10^{-2} 0.500	5.65×10^{-4} 2.22×10^{-2}	3.43×10^{-1} 13.5
3.31×10^{-6}	6.35×10^{-3} 0.250	2.83×10^{-4} 1.11×10^{-2}	1.71×10^{-1} 6.74
1.32×10^{-6}	2.54×10^{-3} 0.100	1.13×10^{-4} 4.44×10^{-3}	6.85×10^{-2} 2.70
3.97×10^{-7}	7.62×10^{-4} 0.030	3.30×10^{-5} 1.33×10^{-3}	2.05×10^{-2} 0.809

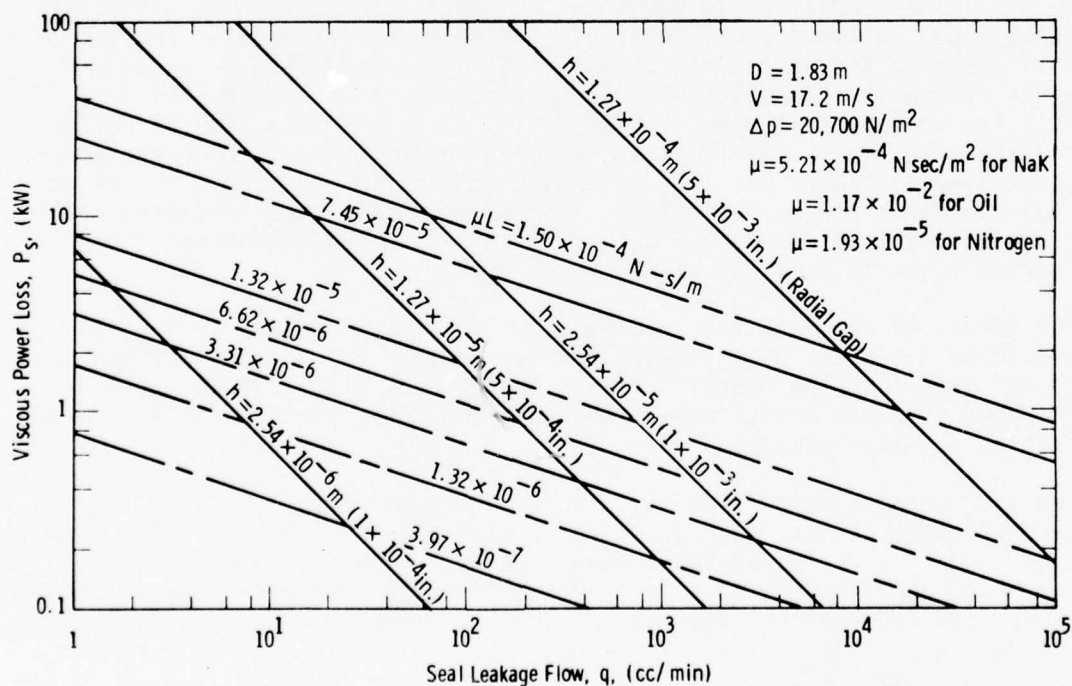


Fig. 5.4: Power-leakage relationship for a single annular seal lip (at $\Delta p = 20,700 \text{ N/m}^2$, 3 psi).

$$(P'_s)^3 q = \frac{\pi D^3 \omega \Delta p}{12} (\mu L)^2. \quad (5.7)$$

With the selected values for D , V , and Δp , this expression is also presented in Fig. 5.4 with the parametric lines of constant (μL) also identified in terms of corresponding values of L for NaK, oil, and nitrogen viscosities. (It should be noted that the equations used for Fig. 5.4 apply only in the laminar regime and should be reviewed when a specific design is selected.)

To avoid the situation where a known leakage of liquid metal is inherent in the design, hydrostatic support of the seals by the liquid metal itself has been ruled-out unless an additional drain is incorporated. This leaves designs such as those shown in Figs. 5.2 and 5.3 where a buffer fluid prevents leakage of the liquid metal, but instead the buffer gas or liquid leaks into the machine space. These designs are expected to provide excellent containment of the liquid metal, provided that a stable operating condition can be maintained.

Leakage flow of the buffer fluid can be estimated from Fig. 5.4 and will depend upon the selected pressure in the position-control pocket. If, for simplicity, a buffer pressure difference of $20,700 \text{ N/m}^2$ (3 psi) is assumed with the configuration of Fig. 5.2, then with $1.27 \times 10^{-5} \text{ m}$ (0.0005 in) as a seal clearance, a seal lip of $1.14 \times 10^{-3} \text{ m}$ (0.045 in) thickness would permit about $4(92) = 368 \text{ cc/min}$ of buffer oil leakage per collector, with half of this entering the machine and the other half entering the seal drain chamber. If a gas buffer (N_2) is used, a wider seal would be desirable. In this case, a seal length of $1.27 \times 10^{-2} \text{ m}$ (0.5 in) would permit about $4(4960) = 19,840 \text{ cc/min}$ (0.7 cfm) of buffer gas leakage. It is difficult to estimate these leakages, however, before a detailed design of the seal is completed and the pressure drop and the seal clearance can be determined. For example, a change in clearance from 1.27 to $1.02 \times 10^{-5} \text{ m}$ (0.0005 to 0.0004 in) would just about cut the leakage rates to half the values shown above.

The effect of acceleration loading (inertial forces on the seal ring) should be evaluated when the application environment and seal design are better defined. The inertial forces on the seal ring must be small compared with the pressure-balance restoring force of the seal to prevent rubbing or seal leakage.

The seal viscous power loss may also be estimated from Fig. 5.4. In a design such as that in Fig. 5.2 with a $1.27 \times 10^{-5} \text{ m}$ (0.0005 in) clearance, the following table shows the power loss for a particular seal configuration. It should be noted that the trade-off between viscous power loss and seal leakage has not been optimized.

<u>Buffer</u>	<u>Buffer Seal Length</u>	<u>Buffer Power Loss</u>	<u>NaK Power Loss (6.37×10^{-3} m, 0.25 in. long seal)</u>	<u>Total Seal Power Loss</u>
oil	1.14×10^{-3} m (0.045 in)	4x1.77 kW	2 x 0.443 kW	7.97 kW
N ₂	1.27×10^{-2} m (0.50 in)	4x0.033 kW	2 x 0.443 kW	1.02 kW

For the configuration shown in Fig. 5.3 the NaK power loss (in the seal) would be eliminated and the losses would become:

<u>Buffer</u>	<u>Buffer Seal Length</u>	<u>Total Seal Power Loss</u>
oil	1.14×10^{-3} m (0.045 in)	7.08 kW
N ₂	1.27×10^{-2} m (0.50 in)	0.13 kW

The viscous and ohmic losses in the liquid metal annulus of the current collector must be added to the above values before comparing them with the permissible total power loss for each collector.

If the design of Fig. 5.2 is used, and if we assume a seal clearance of 1.27×10^{-5} m (0.0005 in), then with the design value of 20,700 N/m² (3 lb/in²) pressure difference the recirculating NaK leakage from the seal would be about 36.2 cc/min per cm of seal length (for each of the two seals), see Fig. 5.4. A seal length of 6.37×10^{-3} m (0.25 in), for example, would permit a total leakage of 736 cc/min for each collector and a recirculation system of at least this capacity must be provided.

Additionally, a system must be provided to circulate the buffer fluid. Coarse estimates of circulation flow rates, based upon the configurations assumed in this evaluation, were given previously as about 368 cc/min of oil or 19,840 cc/min (0.7 cfm) of nitrogen per collector.

Consideration must be given to prevention of plugging of the orifices or capillary inlet lines that are used to establish the clearance-flow-pressure relationships for the hydrostatically-positioned seals. This is another reason to select oil or gas instead of NaK to establish the pressure-balance since NaK oxide formation could alter the restriction characteristics. Even with gas or oil, however, it may be desirable to add inlet screens to filter the fluid before it enters the restriction.

An oil/NaK separation system would be required if an oil buffer fluid is used. A high percentage (~ 33%) of oil may be expected in the mixture, however, simple gravity-separation techniques probably can be used with a large reservoir.

For an axially-applied seal, radial thermal expansion will not affect operation although there must be sufficient clearance in the stator to permit relative radial expansion without creating binding or friction forces that would interfere with axial motion. The $3.05 \times 10^{-4}\text{m}$ (0.012 in) potential radial shift of the rotor due to bearing clearance is negligible compared with the $9.15 \times 10^{-1}\text{m}$ (36 in) collector radius. There also should be no problem in accommodating large relative axial movements 7.62×10^{-4} to $1.52 \times 10^{-3}\text{m}$ (0.030-0.060 in) if the static seal ("O"-ring) friction force is made negligible relative to the hydrostatic restoring force of the seal.

A radially-applied seal, however, would have to be segmented to permit relative thermal expansion and in addition must be designed to make the static seal friction negligible relative to the restoring force to accept movement due to rotor bearing clearance. In this case axial rotor movement would cause no problem.

A detailed examination of thermal gradients in the seal ring will be required to assure that distortion of the sealing surface does not occur. The seal rings will require a key to prevent rotation due to viscous forces. The magnitude of the viscous torque can be determined from the power losses defined earlier:

$$T = P_s / \omega, \quad (5.8)$$

where: P_s = viscous power loss

ω = rotor angular velocity

T = viscous torque

The force on a key or keys at the seal diameter would be:

$$F_k = T/R \quad (5.9)$$

where: F_k = tangential force on key

R = seal radius

For the present case, with:

$$R = 9.15 \times 10^{-1}\text{m} \text{ (3 ft)}$$

$$\omega = 18.9 \text{ rad/s (180 rpm)}$$

$$P = 4 \text{ kW/seal,}$$

$$F_k = 231 \text{ N (52 lb) per seal (max)}$$

Additional areas of concern which should be investigated when a more definite design is established are the stability of the seal in relation to oscillation of the ring (both parallel movement and tilting of the ring) and in response to acceleration loading. The possibility of particulate oxide material reaching the seal/rotor interface and causing abrasive wear should also be considered. The possible "aging" (loss of elasticity) of the static seals should be investigated if a material such as Buna-"N" is used for this application. However, minor leakage at these sealing points should not be critical.

A radial application, which results in a more complex seal, might permit a continuous rotor (free of projections) and therefore a simpler assembly. Axially-positioned seals probably require a horizontally-split stator as well as split seal rings. Additional design effort is required to establish an assembly procedure.

Since very small seal clearances are necessary, machining requirements may be affected. The ability of the seal to follow movements of the rotor will establish permissible run-out tolerances, and this must be determined through further design and perhaps experimentation. Flatness of an axially-applied seal (or circularity of a radially-applied seal) may be a manufacturing problem due to the small clearance ($\sim 0.0127 \text{ mm}$, $\sim 0.0005 \text{ in}$) and large diameter ($\sim 1.83 \text{ m}$, $\sim 72 \text{ in}$), unless the seal ring is made sufficiently flexible so that it conforms to the rotor. Fabrication cost should be investigated when a more definite design is established.

Under ideal operating conditions, no seal wear would be expected since no mechanical contact occurs, unless contaminants seriously block the flow restrictions, forcing the seal against the rotor, or oxide particles result in abrasive wear. Seal replacement or repair would probably be difficult and expensive.

In summary hydrostatically-positioned seals appear to be feasible, although the ability to maintain the small clearances on large diameter rings must be demonstrated. Conformity of a large-diameter ring to the mating rotor surface may be a problem unless the ring is segmented or is flexible. Design and analysis of the pressure-balance system remains to be completed. It has the advantage that the collector annulus may be circumferentially continuous, and it has only one pair of solid-liquid contact surfaces. The seal rings will probably have to be segmented for assembly purposes (for an axial seal) or to accommodate relative thermal expansion.

A3. Hydrodynamically-Positioned Seal

A hydrodynamically-spaced seal has the advantage (over hydrostatics) that a significant chamber pressure is not required. This could reduce the liquid-metal recirculation or leakage from the collector. However, the capability of continuous operation at speeds between zero and ± 17.2 m/s (3380 ft/min), is a severe requirement for a dynamic fluid film lubricated seal.

An estimate of the feasibility of low-speed operation may be based upon semi-dry friction induced power loss.

$$P = F_f V = \mu \Delta p (\pi D L) V, \quad (5.10)$$

where

P = power loss

F_f = circumferential friction force

V = seal velocity

μ = friction coefficient

Δp = average pressure difference across seal

D = seal diameter

L = seal face width

If a friction coefficient of 0.15 is assumed, with a maximum (worst case) pressure difference of $27,600 \text{ N/m}^2$ (4 psi), the full-speed power loss may be calculated as:

$$P = 414 \text{ kW/m (10.5 kW/in.) of seal face width}$$

If about 5 kW maximum loss per seal is permitted, the speed at which the hydrodynamic film becomes effective must be less than:

$$\omega = (5/10.5) 180 \text{ r/min} \approx 86 \text{ r/min},$$

for a $2.54 \times 10^{-2} \text{ m}$ (1 in.) seal face width.

If, for simplicity, a Rayleigh stepped bearing is assumed, the optimum load carrying capacity would be:⁴

$$W = \frac{6\mu V L B^2}{h^2} (0.03438), \quad (5.11)$$

where

- W = load
- μ = absolute viscosity
- V = velocity of rotor
- L = bearing length normal to motion
- B = bearing length in direction of motion
- h = minimum film thickness

The bearing load pressure is defined as:

$$P = W/LB = \frac{6\mu VB}{h^2} (0.03438). \quad (5.12)$$

With $B = 1.27 \times 10^{-2}$ m (0.5 in.) and if an effective support area of 40% is assumed (due to the reversing requirement), to give the required effective load pressure as $27,600 \text{ N/m}^2 \div 0.40 = 69,000 \text{ N/m}^2$ (10 psi), then for a NaK lubricant ($\mu = 5.21 \times 10^{-4}$ N-sec/m², 7.55×10^{-8} lb-sec/in.²) eq. 5.12 gives

$$h = 1.85 \times 10^{-5} \text{ m } (0.730 \times 10^{-3} \text{ in.}), \text{ at full speed (180 r/min).}$$

At 86 r/min:

$$h = 1.85 \times 10^{-5} \text{ m } (86/180)^{1/2}$$

$$h = 1.28 \times 10^{-5} \text{ m } (0.505 \times 10^{-3} \text{ in.})$$

This adequate film thickness indicates that a hydrodynamically-spaced seal is probably feasible, although low-speed losses will probably be high, when compared to a hydrostatically-positioned seal. (Power limits for low-speed operation have not yet been established).

Two configuration alternatives are shown in Fig. 5.5. In configuration (a), the gap of the two independent seals (and therefore the leakage) will increase with increasing speed. In configuration (b), the sum of the two gaps is controlled by machining (or shimming at assembly) the space between two joined seals, and the hydrodynamic forces (and the pressurized NaK) tend to center the seal assembly around the rotor collector. The rotational effect on the fluid film would also tend to prevent leakage in configuration (b). However, it may not be possible

Dwg. 6355A82

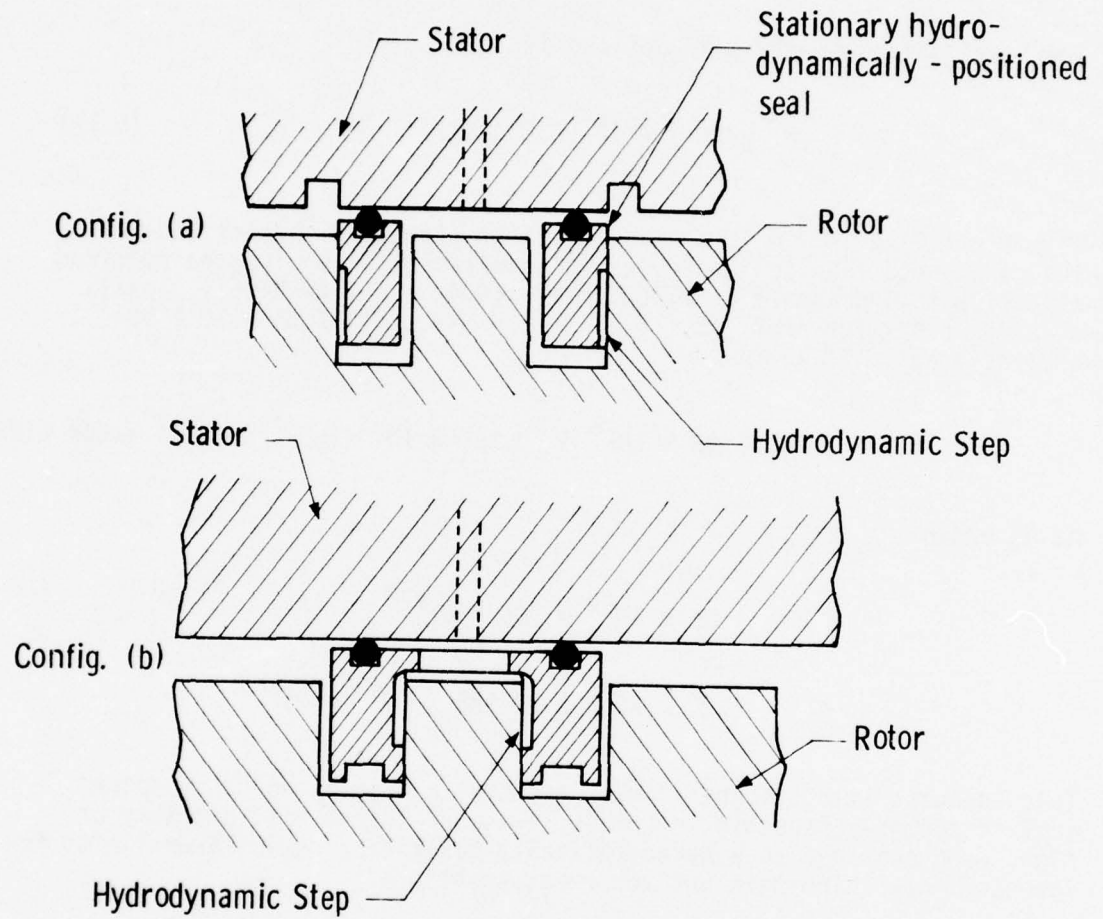


Fig. 5.5: Hydrodynamically-Positioned Seals.

to achieve the very close tolerances necessary for the seal interface, and an externally-pressurized or spring-loaded face may be required.

Since an axial seal is used, radial clearance is a possible problem only for the static seal between the collector seal and the stator housing, which must accommodate relative thermal growth. This seal also must permit relative axial movement due to axial shifts of the rotor. Thermal distortion of the sealing surface could be a problem. Keying of the seal to the housing probably will be necessary to prevent seal rotation. The effect of acceleration loading will have to be determined when a specific application is defined.

Machining tolerances for the large-diameter seal ring will be very tight, to maintain the small gap and to achieve the proper hydrodynamic wedge effect. Possible "aging" (loss of elasticity) of the static seal material should be investigated. It would probably be desirable to have a hard surface or a removable bearing face applied to the rotor so that damage or wear will not destroy the rotor. Rotor face and seal materials must be selected to minimize wear. Circulation system requirements will depend primarily on purification.

The axially-applied seal will probably have to be split and rigidly joined again after assembly on the rotor. Once this is accomplished, it may be possible to install the rotor axially into a smooth stator bore, as shown in Fig. 5.5 thus eliminating the need for a split stator and simplifying the design. If the rotor can be pulled out axially, the sealing system can be easily repaired or replaced, providing that consideration is given to the use of a hardened or removable collector rotor bearing face as noted above.

The use of an Oilite-type porous bearing may be considered, but the path of recirculation of lubricant must be defined for the required face-type bearing, as opposed to the conventional journal bearing application of that material. (A continuous radial seal cannot be used because of the potentially large relative thermal growth which could reduce the radial clearance).

Although this concept appears to be feasible it is probably best considered as part of the hydrostatically-positioned seal.

A4. Deep-Groove Labyrinth

Since the groove depth must be small in comparison with the collector diameter, a deep-groove labyrinth will still have to contain, as a minimum, the gravity-induced pressure head of about $15,170 \text{ N/m}^2$ (2.2 lb/in.^2) for a filled collector annulus. Since the leakage would be large for the required seal clearance of about $1.02\text{--}1.52 \text{ mm}$ ($0.040\text{--}0.060 \text{ in.}$), even for an extensive seal length, the concept might be feasible only if the expulsion pressure is minimized. The major pressure component, due to gravity, may be minimized by establishing a liquid metal flow rate such that the frictional drag at the collector wall is just equal to the gravitational body force.

For a static rotor and a uniform-thickness annular collector groove, and if no leakage of liquid metal occurs, the recirculating liquid metal introduced at the top will be split equally between the two collector paths and will join again at the bottom of the collector. In each path the flow velocity will be constant at:

$$v = Q/2A, \quad (5.13)$$

where:

Q = liquid metal flow rate

A = collector area

Including the frictional drag loss in head, Bernoulli's equation may be written as:

$$P_1/\gamma + v_1^2/2g + Z_1 = P_2/\gamma + v_2^2/2g + Z_2 + h_f, \quad (5.14)$$

where:

P = pressure

γ = density

v = velocity

h_f = head loss due to wall friction drag

Z = height (location) relative to bottom of collector, and the subscripts relate as follows:

1. inlet (at top of machine)
2. variable point between top and bottom.

Since the velocity will be constant:

$$v_1 = v_2, \text{ and}$$

$$h_f = f(\ell/d)v^2/2g, \quad (5.15)$$

where:

f = friction factor

ℓ = length of circumferential path

d = hydraulic diameter.

Then, Bernoulli's equation may be re-written as:

$$(P_2 - P_1)/\gamma = (Z_1 - Z_2) - f(\ell/d)(v^2/2g),$$

$$\Delta P = D\gamma - f(\ell/d)(v^2/2g)\gamma. \quad (5.16)$$

For a rectangular collector channel, the hydraulic diameter is:

$$d = 4(cw)/2(c+w), \quad (5.17)$$

$$d = 2c/(1+c/w)$$

where:

c = radial collector gap

w = collector width

If the radial dimension is small in comparison with the width, the hydraulic diameter is approximately:

$$d = 2c.$$

For a value of $\Delta P = 0$, from top to bottom, equation (5.17) gives

$$f(\pi D/2)(v^2/2g) = D(2c).$$

$$v^2 = 8gc/\pi f. \quad (5.18)$$

The Reynolds number for flow in this annulus is:

$$R_e = \frac{vd}{\nu} = \frac{2vc}{\nu}, \quad (5.19)$$

where:

$$\nu = \text{kinetic viscosity.}$$

If the radial collector gap is selected as 3.18×10^{-3} m (0.125 in.), the above relationships may be combined (for NaK, $\nu = 2.32 \times 10^{-3}$ m²/hr, 6.95×10^{-6} ft²/sec) to find:

$$f = 32gc^3/\pi \nu^2 R_e^2 \quad (5.20)$$

$$f = 7.68 \times 10^6 / R_e^2$$

This expression may be used with the curves of friction factor vs " R_e " for very smooth pipes to find:

$$f \approx 0.027$$

$$R_e \approx 16,900$$

$$\nu \approx 1.72 \text{ m/s (5.64 ft/s)}$$

The corresponding liquid metal flow rate (in two parallel paths), for each cm of collector width would be:

$$Q = 6,530 \text{ cc/min, per cm of width} \\ (16.9 \text{ in.}^3/\text{s, per inch}).$$

The above values seem possible to achieve. Some pressure inequality will exist along the flow path due to the fact that the friction drop is linear along the angular (circumferential) path while the gravity head is linear with vertical height, but this deviation is probably small. More important will be the effect of rotation and surface conditions on the friction factor, and changes of properties with temperature.

In any event, some pressure will probably be necessary to assure low contact resistance, or will be caused by magnetic or acceleration forces. Rotor eccentricity due to bearing clearance is another source of pressure build-up and velocity variation due to the varying gap thickness. Therefore this technique is not recommended for use alone but may be considered for incorporation into another system in order to reduce the expulsion pressure.

A5. Variable Viscosity Buffer Material

This concept would utilize a seal made of a material with a low viscosity in the rotational direction (perhaps at a local radial position) but with sufficient strength to prevent extrusion in the axial direction. It could also consist of a slurry of solids larger than the leakage gap ($\sim 1.52 \times 10^{-3}$ m, 0.060 in.) in an adhering liquid retained by the particles.

Since no material of this nature is presently available, the concept could not be fully evaluated and therefore it was dropped from further consideration.

A6. Electromagnetic Retention

Electromagnetic retention utilizes the forces generated between magnetic fields and electrical current flow in the liquid metal, to counter the various expulsion forces. Although this technique may be used in combination with a small-clearance hydrostatically-positioned seal or collector, it is probably not required for those designs. Therefore, this concept will be evaluated for the case of the relatively large seal clearance required to accommodate thermal expansion, bearing clearance, and dimensional tolerances. The sum of these requirements to prevent seal rubbing, is dependent upon the specific design configuration, materials, and operating procedures, but an estimated minimum clearance of 1.02 to $1.52 \times 10^{-3}\text{m}$ (0.040 to 0.060 in) will be assumed for the present evaluation.

Because of the gravity effect on expulsion pressure, and for other reasons, a uniformly-filled seal gap cannot be assumed. That is, the retention technique must also function with only a locally-filled or partially-filled annulus, and must prevent droplets and aerosol from escaping.

General Relationships

In general, the retention body force on an element of the liquid metal will be:

$$F = J \times B,$$

where: F = retention body force (N/m^3)

B = flux density (T)

J = uniform current density through the element (A/m^2)

and where "B" and "J" are normal to each other and also normal to the resulting force "F". The maximum containment pressure (N/m^2) will be:

$$p = J \times B (\ell), \quad (5.21)$$

where: ℓ = length of element in the direction normal to "B" and "J" (meters).

Neglecting contact resistance, the corresponding ohmic power losses would be:

$$\begin{aligned} P &= I^2 R = I^2 \rho (b/\ell t) = J^2 (\ell t)^2 \rho b/\ell t \\ P &= \rho J^2 (\text{vol}), \end{aligned} \quad (5.22)$$

where: P = ohmic power loss (watts)
 b = length of element in direction of current flow (m)
 t = length of element in direction of magnetic flux (m)
 $(vol) = b \times t$ = volume of element
 ρ = liquid metal resistivity (Ω -m)

As a specific example, to establish the order of magnitude of pressure build-up and power loss that might be obtained, we may select:

$$1/\rho = 2.20 \times 10^6 \text{ mhos/m (NaK)}$$

$$J = 6.20 \times 10^6 \text{ A/m}^2 \text{ (4,000 A/in}^2\text{)}$$

$$B = 1 \text{ T}$$

$$p/\ell = 6.20 \times 10^6 \text{ N/m}^3 \text{ (22.8 lb/in}^3\text{)}$$

$$P/vol = \frac{(6.20 \times 10^6)^2 \text{ A}^2/\text{m}^4}{2.2 \times 10^6 \text{ mhos/m}} = 17.5 \times 10^6 \text{ W/m}^3 \text{ (286 W/in}^3\text{)}.$$

If in addition, we select a radial gap of $1.27 \times 10^{-3} \text{ m}$ (0.05 in), and a $27,600 \text{ N/m}^2$ (4 psi) containment pressure, then for a 1.83 m (72 in) collector diameter:

$$\ell = 27,600 / 6.20 \times 10^6 = 4.45 \times 10^{-3} \text{ m (0.175 in)}.$$

$$P = 17.5 \times 10^6 (1.27 \times 10^{-3}) (4.45 \times 10^{-3}) = 98.8 \text{ W/m (2.50 W/in)} \\ \text{of circumference}$$

$$P = 98.8 \times \pi(1.83) = 568 \text{ W}$$

For a full seal annulus at $27,600 \text{ N/m}^2$ (4 lb/in²) and $4.45 \times 10^{-3} \text{ m}$ (0.175 in) length, the required current and voltage (for radial current flow and circumferential flux) would be:

$$I = 6.20 \times 10^6 \text{ A/m}^2 \times \pi(1.83 \text{ m}) (4.45 \times 10^{-3} \text{ m}) = 159,000 \text{ A}$$

$$V = P/I = 568 / 159,000 = 3.57 \times 10^{-3} \text{ volts}$$

(An additional voltage drop would be introduced due to contact resistance.)

For circumferential current flow and radial flux:

$$I = 6.2 \times 10^6 \text{ A/m}^2 \times 1.27 \times 10^{-3} \text{ m} \times 4.45 \times 10^{-3} \text{ m} = 35 \text{ A}$$

$$V = P/I = 568/35 = 16.2 \text{ volts (neglecting contact drops)}$$

Therefore, the use of a radial flux with annular current flow permits more reasonable values of required voltage and current for containment, if a satisfactory configuration can be defined.

Self-Field Concept

One possible electromagnetic containment technique which would not require an externally imposed magnetic field is shown in Fig. 5.6. This concept uses the ejection pressure resulting from current flow in a separate electrical path provided for containment. As shown in the figure, axial conductor bars are embedded along the stator bore, and these are alternately connected to the positive and negative terminals of the retention system power source. When liquid metal enters the rotor/stator gap and contacts two or more conductors, a current flows through the liquid metal and the self-field provides a body-force which drives the liquid metal back toward the collector. A shoulder is provided on the rotor to eliminate a direct leakage path and assure liquid metal contact with the embedded conductors.

A simplified analysis of this concept shows the following relationship for containment pressure:⁵

$$p = (5/6) \mu \ell^2 J^2, \quad (5.23)$$

where: μ = gap permeability ($\sim 4\pi \times 10^{-7}$ hy/m)

ℓ = axial length of liquid metal extension into the containment system (m) (see Fig. 5.6).

The ohmic power loss was found (as above) to be:

$$P = \rho J^2 (\text{vol}) = \rho J^2 (\pi D \ell t), \quad (5.24)$$

with:

$$J = V/\rho b, \quad (5.25)$$

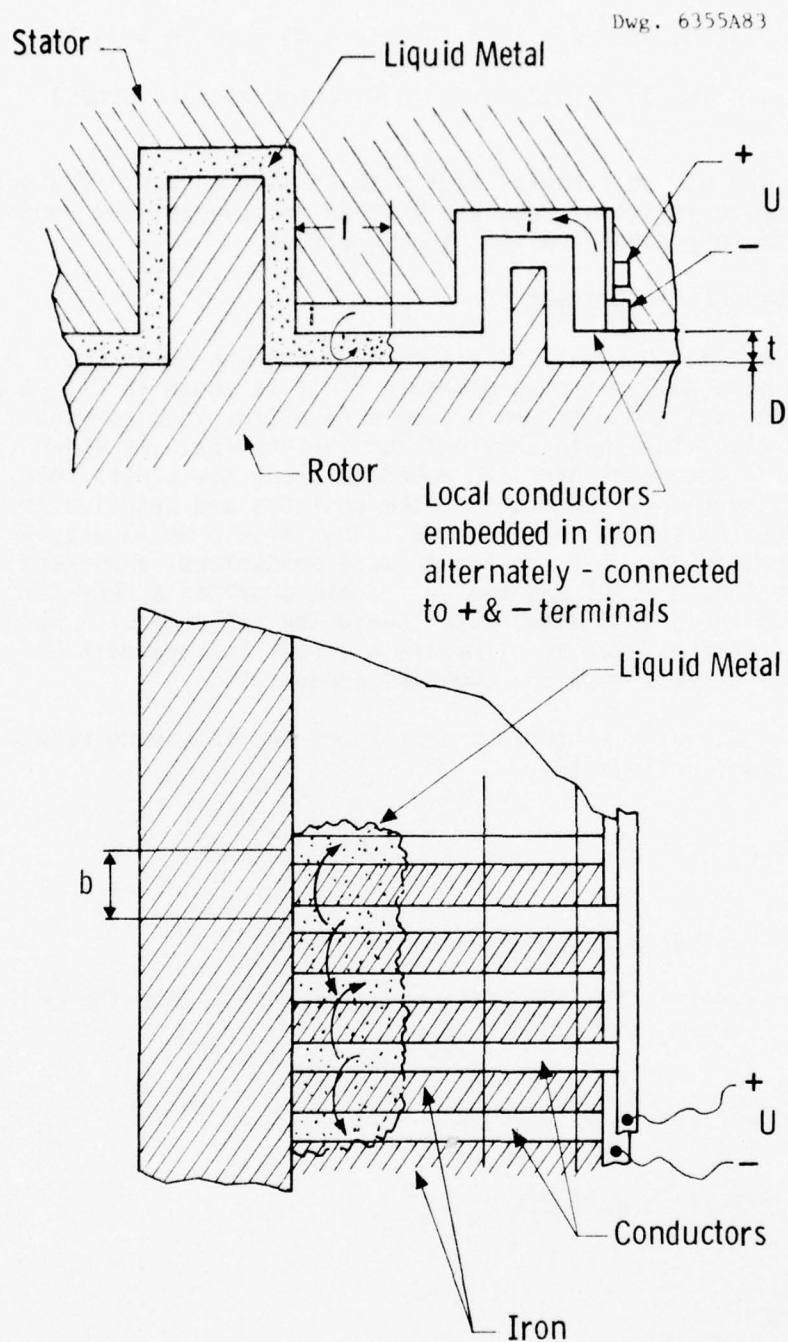


Fig. 5.6: Self-field electromagnetic (E.M.) containment

where: V = applied voltage between conductors
 b = circumferential spacing of conductors
 D = collector diameter (1.83 m)

Equations 5.23 and 5.24, above, may be combined to find:

$$P = 6\pi D t p_0 / 5\mu \ell. \quad (5.26)$$

For a radial gap (t) of 1.27×10^{-3} m (0.05 in) and a pressure of $27,600 \text{ N/m}^2$ (4 psi):

$$P = 87.5 / \ell. \quad (5.27)$$

For an acceptable power loss limit of 5 kW, the minimum length of liquid metal extension into the gap, would be:

$$\ell = 87.5 / 5,000 = 0.0175 \text{ m (0.688 in)}$$

Equations 5.24 and 5.25 may be combined to show:

$$V/b = (P_0 / \pi D \ell t)^{1/2} \quad (5.28)$$

For the 5 kW condition, above, the resulting value becomes:

$$V/b = 4.21 \text{ volts/m (0.107 volts/in).}^* \quad (5.29)$$

It can be seen from Equations (5.27) and (5.28) that the length " ℓ " cannot be reduced without increasing the power loss, and that increasing " ℓ " (and reducing " P ") results in even lower values of (V/b) . Therefore, equation (5.29) shows the maximum acceptable value for (V/b) .

The spacing of conductor bars must be selected to minimize the probability of a droplet escaping without "shorting" of two adjacent bars. If a spacing of 3.18×10^{-3} m (0.125 in), is selected, the supply voltage would be only:

$$V = 4.21 \times 3.18 \times 10^{-3} = 0.0134 \text{ volts,}$$

and the corresponding current (for a full ring) would be:

$$I = 5,000 / 0.0134 = 373,000 \text{ A.}$$

*Contact resistance would increase the required supply voltage, but would also increase the power loss.

where: V = applied voltage between conductors
 b = circumferential spacing of conductors
 D = collector diameter (1.83 m)

Equations 5.23 and 5.24, above, may be combined to find:

$$P = 6\pi D t p_p / 5\mu \ell. \quad (5.26)$$

For a radial gap (t) of 1.27×10^{-3} m (0.05 in) and a pressure of 27,600 N/m² (4 psi):

$$P = 87.5 / \ell. \quad (5.27)$$

For an acceptable power loss limit of 5 kW, the minimum length of liquid metal extension into the gap, would be:

$$\ell = 87.5 / 5,000 = 0.0175 \text{ m (0.688 in)}$$

Equations 5.24 and 5.25 may be combined to show:

$$V/b = (P_p / \pi D \ell t)^{1/2} \quad (5.28)$$

For the 5 kW condition, above, the resulting value becomes:

$$V/b = 4.21 \text{ volts/m (0.107 volts/in).}^* \quad (5.29)$$

It can be seen from Equations (5.27) and (5.28) that the length " ℓ " cannot be reduced without increasing the power loss, and that increasing " ℓ " (and reducing " P ") results in even lower values of (V/b). Therefore, equation (5.29) shows the maximum acceptable value for (V/b).

The spacing of conductor bars must be selected to minimize the probability of a droplet escaping without "shorting" of two adjacent bars. If a spacing of 3.18×10^{-3} m (0.125 in), is selected, the supply voltage would be only:

$$V = 4.21 \times 3.18 \times 10^{-3} = 0.0134 \text{ volts,}$$

and the corresponding current (for a full ring) would be:

$$I = 5,000 / 0.0134 = 373,000 \text{ A.}$$

*Contact resistance would increase the required supply voltage, but would also increase the power loss.

A power source of this type does not appear to be feasible. If a higher-voltage source is used, with the same bar spacing, Equation (5.25) shows that the current density would increase proportionally; Equation (5.23) shows that the axial length of the liquid metal along the bars would decrease in inverse proportion; and Equation (5.26) shows that the power loss would then increase in proportion to the increased voltage. Therefore this concept does not appear feasible for containment of small droplets, which requires close spacing of conductors and an extremely high-current power source.

External-Field Concept

A practical configuration which will provide either a continuous (uni-directional) circumferential current or a continuous circumferential magnetic flux (independent of load current), has not been found. Therefore, a modification of the self-field concept (Fig. 5.6) was considered, with magnetic poles of alternate polarity added between the local conductors. A preliminary review of techniques to provide the localized magnetic field, either electromagnetically or with permanent magnets, indicates that the large radial gap and the required small spacing of opposite magnetic poles make it impractical to achieve a sufficiently high field within the specified geometric constraints.

Rotational Force Concepts

Because of the difficulty in providing either circumferential flux or current in the seal annulus, it may be preferable to produce a circumferential force due to field and current in the other two orthogonal directions. The resultant circumferential motion of the liquid metal can then be converted to an axial pressure gradient by the use of angled vanes, such as a "wind-back" seal, or by using a "manometer effect" due to centrifugal force. These concepts have not yet been fully evaluated, but justify additional analysis.

Considering the many possible configurations, it is recommended that further study be made in this category, although no satisfactory arrangement has been found thus far.

A7. Absorbent Wick

The use of an absorbent wick as a seal has the advantage of improved energy absorption for particles of liquid metal, and it also may be used to directly drain the captured material. However, it is not expected that a wick will reduce leakage from a filled annulus of large radial thickness, other than by perhaps improving the wetting action. It may prove advantageous, however, if a flexible material can be found which will fill the radial gap and still permit relative expansion and movement of the rotor. The material then becomes, in essence, a rubbing seal and should be considered as an alternative to the lip-seal or hydrodynamic seal discussed in (A1) and (A3) above. Materials such as "Foametal" or "Feltmetal", elastomer sponge, or other fibrous configurations could be considered. Since experimentation would be necessary to establish flexibility, wear characteristics, and containment adequacy, feasibility cannot be established at this time.

A8. Low-Speed Seal

This concept would include a seal that could be applied when the centrifugal effects could no longer retain the liquid metal against the force of gravity. Neglecting MHD expulsion effects, this "dropout" speed is expected to be about 60 rpm for the rotor.

The power loss for this type of seal will probably be acceptable if the seal area is made small. The complication and added cost of the retraction mechanism suggests that this concept be considered only if simpler rubbing seals (A1 and A3 above) are not acceptable.

A9. Magnetic Fluid

The technology involved in the suspension of a solid electromagnetic filler in a liquid for use as a seal, has been under development by Ferrofluidics Corp. and has resulted in their "Ferrometic" rotary seal. A cartridge seal of this type is presently being tested at the Westinghouse Research Labs. The peripheral velocity limit for this sample is about 7.11 m/s (1400 ft/min), 3.81×10^{-2} m (1.5 in) dia. at 3600 r/min due to temperature rise from the viscous power loss, without cooling. The supplier's literature gives a temperature limit of 107°C (225°F) for continuous operation, probably based on fluid vapor loss. The sales literature gives rpm limits for various shaft diameters which indicate a similar maximum peripheral speed for modular seals. With cooling and fluid replenishment, peripheral speeds as high as 56 m/s (11,000 ft/min) are claimed.

The radial gap in the commercial units, is typically 5.08×10^{-5} to 1.27×10^{-4} m (0.002 to 0.005 in), but the company states that this value can be much larger if required, apparently by increasing the mmf of the magnet and by scaling up the geometry and fluid volume. (The viscous shear area and power loss also would be scaled up.) The pressure capability per seal land, for this radial gap, is about 20,700 N/m² (3 lb/in²). If the present pitch (between lands) of about 1.57×10^{-3} m (0.062 in) is scaled up to a desired radial gap of 1.02×10^{-3} m, it would become:

$$L = (1.02 \times 10^{-3} / 1.27 \times 10^{-4}) 1.57 \times 10^{-3} = 1.26 \times 10^{-2} \text{ m } (\sim 0.5 \text{ in})$$

This might be reduced with a modified configuration, so that two of these seals could be fit within the collector space allocation.

Present cost of a 3.81×10^{-2} m (1.5 in) dia. cartridge seal is about \$750, but the components are relatively simple and the cost of some of the presently used fluids is only about 10 cents per cc. (probably less than \$10/seal point). Present fluids have a very high start-up torque (viscosity) at low temperature and may not be compatible with the liquid metal, and a search for a better fluid such as a silicone oil may be necessary. The use of a mineral oil carrier is presently being considered in a Navy program, which utilizes liquid metal current collectors.

A visit to the Ferrofluidics Corporation was made in November of 1972 by \odot personnel primarily to evaluate the feasibility of developing a metallic (liquid metal) magnetic-fluid shaft-seal for large turbine-generators. It was concluded that the magnetic liquid metal, necessary to improve thermal conduction for the high-speed (~ 10.2 m/s, 20,000 ft/min) shaft application, would require a research and development effort, and a program of that nature is under consideration. (Design with a conductive magnetic fluid must also consider the possibility of circulating current losses due to radial field.)

Both of the above approaches, magnetic fluid seal and magnetic fluid conductor, require two steps in the development program; materials (fluid) development, and configuration development. Fluid properties (including magnetic characteristics) are necessary to complete a design study. Presently, it appears that magnetic saturation due to the high circumferential flux of the load current could greatly reduce if not eliminate the effectiveness of a magnetic seal within the current loop. Therefore, although some additional study would be required to verify that the problem cannot be overcome, it appears that these concepts have low probability of success for a short-range program, and have been eliminated from consideration as primary contenders.

A10. Surface Tension/Wetting

The feasibility of retaining the liquid metal in the current collector through the use of surface tension, is strongly related to gap width (rotor/stator) and shear energy input at the surface. The maximum retention capacity can be determined by examining the case of perfect wetting in the sealing zone, and complete non-wetting external to that zone, along an annular gap. For this configuration, the surface tension angle will be zero or parallel to the gap surface.

The annular gap configuration may be approximated by that between two parallel plates, and the retention force would be:

$$F = 2\sigma, \quad (5.30)$$

where " σ " is the surface tension of the sealing fluid. The maximum pressure that can be retained will then be:

$$\Delta P_{\max} = 2\sigma/h, \quad (5.31)$$

where h is the radial (or axial) gap width.

For NaK, the surface tension would be about 1.05×10^{-1} N/m (6.00×10^{-4} lb/in), and the maximum pressure capability for a radial gap of 1.02×10^{-3} m (0.040 in) would be:

$$\Delta P_{\max} = 206 \text{ N/m}^2 \text{ (} 3.0 \times 10^{-2} \text{ lb/in}^2 \text{)}$$

The surface tension of NaK is high. By comparison, oils have values of only 2.0 to 6.5×10^{-2} N/m, and water has a value of 7.5×10^{-2} . Mercury has a surface tension of almost 5×10^{-1} N/m, but even this would retain only 980 N/m^2 (1.42×10^{-1} psi) pressure difference. To contain $27,600 \text{ N/m}^2$ (4 psi), the gap width would have to be reduced to 3.62×10^{-5} m (1.4×10^{-3} in) for mercury or 7.61×10^{-6} m (3×10^{-4} in) for NaK. In addition, even these gaps would not be adequate during rotation, with shear energy disruption of the surface.

It is apparent that surface tension cannot sustain any significant pressure difference and therefore cannot be utilized as a primary seal. It is probably possible, although not easy, to place a number of these interfaces in series, with another fluid between them, to increase the pressure capacity. However, the large number required and the shear effect of rotation makes this alternative infeasible. Therefore this concept has been dropped from further consideration.

All. Solidification

The concept which involves sealing with a locally solidified region of the liquid metal would require a complex thermal or chemical control system. Additionally, the shear area of the seal would have to be made very small because of the increase in viscosity (by a factor of 2 or 3) as the liquid metal approaches the solidification point. Also, the seal could freeze when the rotor is stationary and no viscous heat is generated, greatly increasing start-up torque. Since no simple configuration has been found which would eliminate these problems, no further effort is recommended for this concept.

B. CONDUCTING SEALB1. Conducting Wick

In the use of a conducting wick as a current collector, the large gap and the need to wet both rotor and stator elements to assure good electrical contact eliminates any improvement in liquid metal retention. Improvement in retention can result only if the effective gap is made smaller or is eliminated. This may be possible by providing a wick which is flexible and will deform as the rotor expands or shifts. As in the case of the wick-type seal, the possible materials would be "Foametal", "Feltmetal", elastomer sponge, or other fibrous materials.

The wick could be divided into a central feed zone and two adjacent drain zones, all made up of the same material, with a small radial gap to prevent aerosol generation. Gas flow may be used to assist drainage and to improve containment.

Since the lip-seal and the hydrodynamic seal (A1 and A3 above) were found to be marginally feasible, the conducting wick applied in a similar manner may also prove to be adequate. However, since material properties such as flexibility, wear rate, and permeability are not established, a complete evaluation of feasibility cannot be made at this time. An experimental program to evaluate various candidate materials is planned. An important consideration to be evaluated during a test program, is the tendency of the wick material to be wiped over the pores at the rubbing interface and possibly interfering with the flow of liquid metal.

B2. Hydrostatically-Positioned Collector

The hydrostatic positioning technique described for the seals (above) can also be applied to the complete collector/seal assembly. The collector may be positioned either axially or radially. If radially applied, the collector ring must be segmented or otherwise flexible enough to permit the changes in diameter required to follow rotor thermal expansion and dimensional tolerance variations. In comparison to the separate seals, this configuration has only one floating member instead of two, but introduces two NaK/copper contact-resistance interfaces in place of one. (It might be feasible to join the two seals to form one floating assembly, and to provide a conducting flexible bellows or spring support of the collector to eliminate a second liquid-metal contact-resistance interface, but this would complicate the designs.)

Many design configurations are possible. Some of the alternatives are listed below:

- 1) Use of liquid metal, oil, or gas as the positioning fluid.
- 2) Either annular channels or localized pockets for the liquid metal, for the second fluid, and for the drain chambers.
- 3) Pressure of a buffer fluid less than, equal to or greater than that of the liquid metal.

Local pockets are expected to improve the stability of the collector ring by providing a restoring moment (or centering force) when the ring is tilted (or radially displaced). An annular ring would permit circumferential flow to equalize the pressures and thereby reduce the restoring force. A configuration containing local pockets, adapted from the "hybrid" pad design, is shown in Fig. 5.7.

The alternative of an annular groove has the advantage (over pockets) that an increase in the relative motion (angular velocity) of the rotor would probably not increase the liquid metal recirculation requirement, although detailed concepts of both would be required for an adequate comparison. The required collector width to produce $2.48 \times 10^7 \text{ A/m}^2$ ($16,000 \text{ A/in}^2$) would be less than $2.11 \times 10^{-3} \text{ m}$ (0.083 in) for an annular groove at 1.83 m (72 in) diameter.

The use of oil or a gas to provide the collector positioning force would make this independent of magnetic forces that might otherwise alter the operation if the conducting liquid metal is used for this purpose. Gas is probably preferable to oil because of the much lower viscous power loss, although an evaluation of damping requirements should be made, and because separation from the liquid metal does not appear to be a problem with gas. However, the design sealing requirements may be more complicated if a separate system is required for the gas. The permissible pressure of a gas pocket, relative to that of the liquid metal, would be related to the pocket size and geometry.

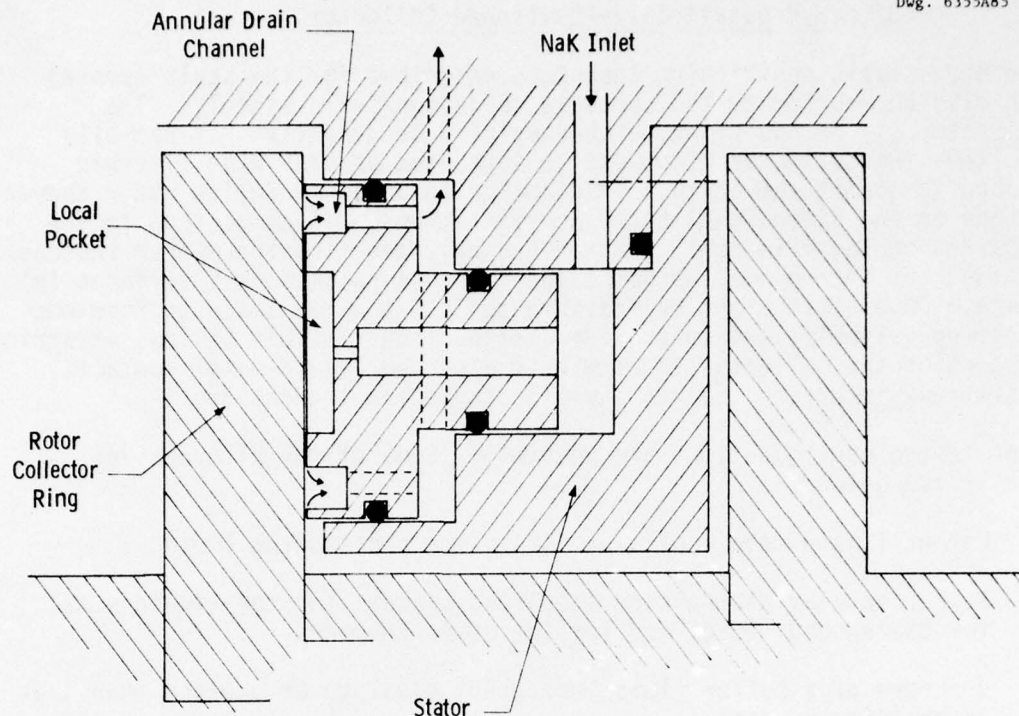


Fig. 5.7: Adaptation of pad design to annular collector ring

For the present evaluation, a configuration will be assumed, which uses the liquid metal to provide positioning force, and which has dimensions similar to those now being considered for the "hybrid" pad.

Good containment of liquid metal within the collector ring pocket is expected. This is due to the small seal gap, and the gas flow into the annular drain chambers from the machine gap. (The required gas flow velocity and corresponding pressure drop must be determined.) Since the drain grooves are annular, a step or projection could be provided so that the gas seal lips would overlap the rotor and not be directly in-line with the liquid metal seal gap.

The drain channels should be evaluated to assure that they can adequately handle the liquid metal flow without filling or significant accumulation at the bottom of the annular channel. Assembly requirements will probably necessitate a split seal ring, and two or more segments may be preferable to a rotationally symmetric design to prevent leakage at the split. (Sealing of the stator split may still be required.)

For power loss calculations, it will be assumed that the collector ring is insulated to prevent current flow except in the area of the local

pressure pockets. This reduces the MHD-induced viscous power loss, and also reduces the recirculating (eddy) current which produces a power loss and an ejection pressure.

Since the MHD force occurs only in the pocket, where the tangential flow is blocked, the viscous losses will be primarily in the narrow seal gap. This can be estimated from Fig. 5.4 of concept A2, as less than 1.5 kW for a radial length of $2.1 \times 10^{-2}\text{m}$ (0.825 in) and a liquid metal gap of $1.27 \times 10^{-5}\text{m}$ (0.0005 in).

The load current ohmic loss due to bulk resistivity of the liquid metal in a cylindrical volume was previously defined as

$$P_B = J^2(\text{vol})/\sigma,$$

where: σ = conductivity of the liquid metal (2.20×10^6 mhos/m for NaK).

For $2.48 \times 10^7 \text{ A/m}^2$ ($16,000 \text{ A/in}^2$) current density and a pocket cross-sectional area of $1.73 \times 10^{-4}\text{m}^2$ (0.268 in^2), the power loss becomes

$$P_B = 48.4 \text{ kW per meter (1.23 kW/in) of pocket depth (for each pocket).}$$

For 70 pockets with a depth of $1.52 \times 10^{-3}\text{m}$ (0.06 in), the total power loss due to bulk resistivity would be:

$$P_B = 5.16 \text{ kW.}$$

It will probably be necessary to add dams or otherwise design to prevent MHD-induced viscous losses in the liquid-metal supply annulus behind the collector ring. The load current ohmic loss in this annulus will depend on final dimensions, but a rough estimate will be made based on the assumptions that the radial width is the same as the pocket diameter, $1.48 \times 10^{-2}\text{m}$ (0.583 in), the depth is $3.18 \times 10^{-3}\text{m}$ (0.125 in), and that the full area is uninsulated. The conduction area and current density are

$$A = 1.83\pi(1.48 \times 10^{-2}) = 8.5 \times 10^{-2}\text{m}^2 (132 \text{ in}^2)$$

$$J = 300,000/8.5 \times 10^{-2} = 3.53 \times 10^6 \text{ A/m}^2 (2,270 \text{ A/in}^2)$$

The power loss becomes:

$$P_B = (3.53 \times 10^6)^2(8.5 \times 10^{-2})(3.18 \times 10^{-3})/2.2 \times 10^6$$

$$P_B = 1.53 \text{ kW.}$$

The contact resistance loss for each interface pair due to load current will be:

$$P_C = \epsilon_k JI, \quad (5.32)$$

where: ϵ_k = specific contact potential ($4.1 \times 10^{-9} \text{ Vm}^2/\text{A}$). The total for the pockets and the annular supply ring would be

$$P_C = 4.1 \times 10^{-9} (300,000)(2.48 \times 10^7 + 3.53 \times 10^6)$$

$$P_C = 30.5 \text{ kW} + 4.33 \text{ kW} = 34.8 \text{ kW}.$$

Due to the larger area, it is seen that only about 15% of the contact loss is associated with the annular supply channel.

The eddy-current ohmic power loss per unit area, without laminations and assuming $\epsilon_k = 0$, would be

$$P = \frac{B^2 V^2 L^2 \sigma}{12 d} = 79.6 \text{ kW/m}^2 \text{ (51.4 W/in}^2\text{)} \quad (5.33)$$

where: B = flux density normal to collector (0.1 T)

V = linear velocity of collector (17.3 m/s)

L = collector width ($1.48 \times 10^{-2} \text{ m}$, max)

σ = liquid metal conductivity ($2.2 \times 10^6 \text{ mhos/m}$)

d = conducting gap thickness ($1.52 \times 10^{-3} \text{ m}$)

The power loss would be less than that shown above, since the conduction pocket area is circular rather than rectangular. The total eddy-current power loss for the 70 pockets would be less than

$$P = 79.6(70)(1.73 \times 10^{-4}) = 0.964 \text{ kW}$$

The following table summarizes the power loss approximations. These are meant only to establish the relative significance of each type of loss, since the values may change greatly as a collector design is developed.

Type of Loss	Power Loss (kW)
Viscous	Less than 1.5
Bulk Resistance	
Pockets	5.16
Supply Ring	1.52
Contact Resistance	
Pockets	30.5
Supply Ring	4.33
Eddy Current	<u>0.96</u>
Total	44.0

Review of the table leads to the conclusion that a reduction in current density to reduce contact losses, should be made by increasing the number of pockets or by increasing the pocket area.

The leakage of a circular pad (hybrid design, Eq. (5.6) would be:

$$Q_p = \frac{\pi c^3 P_1}{6\mu \ln(D_2/D_1)} \quad (5.34)$$

where: Q_p = leakage flow
 c = seal clearance
 μ = absolute viscosity
 D_2 = outer diameter of seal
 D_1 = inner diameter of seal
 P_1 = pocket pressure

For the pad presently under consideration, the following values may be assumed:

$$\begin{aligned} c &= 1.27 \times 10^{-5} \text{ m } (5 \times 10^{-4} \text{ in}) \\ \mu &= 5.2 \times 10^{-4} \text{ N-s/m}^2 (7.55 \times 10^{-8} \text{ lb-s/in}^2) \\ D_2 &= 2.1 \times 10^{-2} \text{ m } (0.825 \text{ in}) \\ D_1 &= 1.48 \times 10^{-2} \text{ m } (0.583 \text{ in}) \\ P_1 &= 137,900 \text{ N/m}^2 (20 \text{ lb/in}^2) \\ A_c &= 1.73 \times 10^{-4} \text{ m}^2 (0.268 \text{ in}^2) (\text{conduction area}) \end{aligned}$$

This results in a leakage flow of:

$$Q_p = 50 \text{ cc/min } (0.051 \text{ in}^3/\text{s}).$$

For 300,000 amperes and $2.48 \times 10^7 \text{ A/m}^2$ ($16,000 \text{ A/in}^2$), the required area for all the pads on a single collector is 1.21 m^2 (18.75 in^2), and therefore 70 pads will be required (this would give about $8.13 \times 10^{-2} \text{ m}$ (3.2 in) of circumference per pad), and the total leakage would be:

$$Q_p = 3,500 \text{ cc/min } (0.356 \text{ in}^3/\text{s}).$$

For comparison, from Eq. (5.4), an annular gap would have a leakage flow (inward and outward) of approximately:

$$Q = 2 \times \frac{\pi c^3 p_0}{12\mu L/D}, \quad (5.35)$$

where: D = collector diameter

L = seal length

If the seal length is taken to be the same as that for the pad $(\frac{D_2 - D_1}{2})$, the flow may be calculated as:

$$Q = 10,100 \text{ cc/min } (10.3 \text{ in}^3/\text{s}).$$

This is almost three times as great as that for the pads.

It is possible, however, to machine local pockets in a collector ring, in which case the leakage will be less than or equal to that for the pads. (The viscous power loss would be greater if the seal area is greater than that for the pads.)

The effect of gravity head (about $15,170 \text{ N/m}^2$, 2.2 lb/in^2 , for an annular ring) is relatively small, but should be considered when a firm design is established.

Ejection pressure built-up by rotational forces may be evaluated (approximately) on the basis of a model consisting of a thin annular liquid-metal ring of radial thickness " L ". If the rotational velocity of the liquid ring is assumed to be half that of the rotor, the pressure at the outside diameter, required to constrain this fluid, would be:

p = rotational force/area

$$p = \frac{(2\pi R w L \rho) R (\omega/2)^2}{2\pi R w} = L \rho R \omega^2 / 4, \quad (5.36)$$

where: w = ring width

L = radial thickness

ρ = mass density of liquid metal

R = radius of thin ring

ω = angular velocity of rotor.

The pressure may be evaluated with the following values used in the above equation

$$L = 2.54 \times 10^{-2} \text{ m (1.0 in)}$$

$$\rho = 865 \text{ N-s}^2/\text{m}^4 \text{ (1.68 lb-s}^2/\text{ft}^4)$$

$$R = 9.15 \times 10^{-1} \text{ m (36 in)}$$

$$\omega = 18.8 \text{ rad/s (180 r/min)}$$

The result is the small pressure:

$$p = 1790 \text{ N/m}^2 \text{ (0.259 psi), for } 2.54 \times 10^{-2} \text{ m (1.0 in) radial thickness.}$$

The ejection pressure resulting from load-current, assuming a single-turn module, would be:

$$P_L = 6.28 \times 10^{-7} I_p^2, \quad (5.37)$$

where: I_p = load current per unit circumference (A/m)

P_L = ejection pressure (N/m^2).

For the assumed current density of $2.48 \times 10^7 \text{ A/m}^2$ ($16,000 \text{ A/in}^2$), and an effective pad diameter of $1.48 \times 10^{-2} \text{ m}$ (0.583 in), the current per unit of collector circumference would vary from zero at each end to a peak at the central line (of maximum radial height) of $I_p = 367,000 \text{ A/m}$ ($9,330 \text{ A/in}$). This is equivalent to a peak pressure of:

$$P_{L_{\max}} = 84,600 \text{ N/m}^2 \text{ (12.3 lb/in}^2\text{)}.$$

This value is sufficiently large, that a more detailed analysis of the load-current influence on positioning (gap) and flow rate is required.

The interaction of radial field "B" and axial current density "J" (for an axially-applied collector ring) results in a circumferential body force which is similar to a gravitationally-induced pressure head. The peak pressure, at one circumferential point, will be:

$$P_{\max} = (J \times B)d, \quad (5.38)$$

where: $d = 14.8 \times 10^{-3} \text{ m}$ (0.583 in. pocket diameter)

$$J = 2.48 \times 10^7 \text{ A/m}^2 \text{ (16,000 A/in}^2\text{)}$$

$$B = 0.05 \text{ T}$$

$$P_{\text{max}} = 18,300 \text{ N/m}^2 \text{ (2.66 lb/in}^2\text{)}.$$

For a radially-applied collector the result would be similar except that an axial field would be used in the computation. For an axial field of 0.1 Tesla, the maximum pressure would be:

$$P_{\text{max}} = 36,600 \text{ N/m}^2 \text{ (5.32 lb/in}^2\text{)}.$$

For an axially-applied collector ring, radial thermal expansion relative to the rotor, and the rotor shift due to the 0.012 in. radial bearing clearance, should not affect operation. However, expansion of the collector ring relative to the stator could cause binding or increased friction and prevent axial movement. Sufficient clearance must be allowed to accommodate this relative growth, or the ring should be segmented. A radially-applied collector would also have to be segmented to permit relative thermal expansion. In both cases, static seal friction must be made negligible relative to the restoring force which positions the collector ring.

The force required to oppose the torque and prevent rotation due to viscous drag would be small (unless a rub occurs). From Eqs. (4.2.4.8) and the previously determined viscous drag power loss of less than 1.5 kW, this force will not exceed:

$$F_K = 87.2 \text{ N (19.6 lb)}$$

A detailed examination of thermal gradients in the collector ring will be required to assure that distortion of the sealing surface does not occur. Additional areas of concern which should be investigated when a more definite design is established are the stability of the seal, in relation to oscillation of the ring or segments (both parallel movement and tilting of the ring) and in response to acceleration loading. The possibility of oxide material reaching the seal/rotor interface and causing abrasive wear should also be considered.

Heat transfer to remove the viscous and electrically-induced losses from the collector ring will depend on the cooling techniques used in the rotor and stator. The temperature does influence the seal gap and flow rate of the liquid metal, but if the operating temperature is held below about 93°C (200°F), the variation is expected to be less than 15%. This effect should be reviewed again when a more-definite design is selected.

The acceptability, from an electromagnetic point of view, of local conduction paths at each pocket, as opposed to a rotationally symmetric collector, should be verified. The pocket width used in this sample analysis subtends an angle of 0.927° with a spacing (pitch) of 5.15° , and covers 18% of the circumference. For a multiple-turn machine, the possible effect of this lack of rotational symmetry on the magnetic forces in the liquid metal should also be investigated.

The possible "aging" (loss of elasticity) of the static seals should be investigated if a material such as Buna-"N" is used for this application. However, minor leakage at these sealing points should not be critical.

A radial application of the collector segments might permit a smooth cylindrical rotor and therefore a simpler assembly. An axially-applied collector would probably also be split at least on the horizontal centerline, for assembly purposes. The collector ring can be pushed back to increase the clearance for assembly. Additional design effort is required before an assembly procedure is established.

The ability of the collector to follow movements of the rotor will establish permissible run-out tolerances, and this must be determined through further design and perhaps experimentation. Flatness of an axially-applied collector (or circularity of a radially-applied seal) may be a manufacturing problem due to the small clearance ($\sim 1.27 \times 10^{-5}\text{m}$, $5 \times 10^{-4}\text{in}$) and large diameter ($\sim 1.83\text{m}$, 72 in), unless the collector is segmented or made sufficiently flexible so that it conforms to the rotor. Fabrication cost should be investigated when a more definite design is established.

Under ideal operating conditions, no collector wear would be expected since no mechanical contact occurs, unless contaminants block the restrictions or oxide particles result in abrasive wear. Seal replacement or repair would probably be difficult and expensive.

In summary, the hydrostatically-positioned collector ring is very similar to the hybrid pad design. It has the advantage, however, that collector rotation does not tend to drag liquid metal from the sealed area. Also, more design flexibility is provided since gas-pressured positioning pockets may be interspersed along the circumference. This is particularly important if contact resistance is a significant factor, since the number of contact pairs can be reduced from two to one. (The hybrid pad can probably be extended circumferentially to provide an intermediate configuration with similar advantages.) Conformity of a large-diameter ring to the mating rotor may be a problem unless the ring is segmented or flexible. The concept appears to be feasible but its success is dependent upon the maintenance of a very small clearance without rubbing.

B3. Flooded Labyrinth

A (semi-) flooded labyrinth will not be effective with the large radial clearance necessary to prevent rubbing and the low leakage velocity for reasonable recirculation rates. It may be used as a retractable or hydrostatic/hydrodynamically-positioned device, but these are covered in other sections of this report. Another alternative is the addition of solid material particles between labyrinth seal strips. If the particles are sized or shaped such that they cannot escape through the seal gap, and if the material is selected so that the liquid metal readily wets the particles, then it may be possible to retain the liquid metal within the conducting seal. This concept then becomes similar to the Variable-Viscosity Buffer Material (A5 above), which has more flexibility in material selection since either the liquid metal or another fluid may be used. Therefore the Flooded-Labyrinth concept should not be considered further.

B4. Conducting Bearing

A roller or ball bearing may be used to maintain concentricity between the stator (outer race) and the rotor (inner race), to improve the performance of a lip-type seal. A sealed bearing might be used, eliminating the need for a separate sealing device. If the sealed bearing is filled with liquid metal, then the rolling elements will be lubricated by the liquid metal and an electrical conduction path would be provided between the rotating and stationary parts. (Provisions must be made for relative expansion in the radial and axial directions). A preliminary survey shows no bearings available which are intended for operation as high as 180 rpm for diameters of about 1.83 m (72 in.). Therefore this concept should not be considered further.

C. LOW-SPEED FLOODING OR LOW-SPEED BRUSH CONTACTS

C1. Pressure-Controlled Liquid Volume

If the machine is initially flooded with liquid metal, then as the rotor is brought up to speed, projecting collector rings will act as viscous pumps tending to increase the fluid pressure in the collector region. If the liquid metal supply system is designed to maintain a constant pressure in the collector, and if this pressure corresponds to a semi-filled collector (the outermost, conducting region of the collector would be completely filled) at full speed, then the fluid in the machine gap will flow toward the collector as the speed is increased and will be drained into the recirculation system until the proper fluid level is reached in the collector. As the speed is reduced and the centrifugal pressure reduced, the fluid will be pumped back into the collector and eventually into the gap, flooding the machine at standstill. In this manner, an acceptable viscous power loss may be achieved.

The part-speed power loss of this system would have to be evaluated and the effect of MHD pumping of the liquid metal must be included. However, since the machine insulation would have to be designed for flooded operation, and since the objective of this study is to develop collectors for an unflooded machine, this concept should not be carried further.

C2. Low-Speed Brush/High-Speed Liquid

The use of solid brushes at low speed which are retracted at high speed after injection of liquid metal permits the use of liquid metal only at the high speeds where brush wear and power loss would be high and where centrifugal containment of the liquid is effective. However, the cost of a dual system will be large, periodic replacement of brushes will be required (and this requires removal of the liquid metal and decontamination of the machine), the brush material would probably have to be compatible with the liquid metal, and the brush wear debris must be contained. Total size of the dual system may also be a problem.

Although this concept appears to be technically feasible, it does not seem to be a practical solution to the collector problem and should not be considered further.

C3. Gas Injection

An alternative way to reduce viscous power loss in a flooded machine is the injection of cover gas to displace the liquid metal at the rotating or stationary surfaces (or both). Injection of gas may be local or through porous walls, and may be continuous or only at high speeds. However, as in concept C1 above, the machine insulation must be designed for flooded operation. Also, since the objective of this study is the development of unflooded machine collectors, this concept should not be evaluated further.

D. Axial Injection (or Radial Ejection)

D1. Inertial Containment

Inertial containment would utilize the kinetic energy of the liquid metal, as it enters the collector, to contain or rotate the fluid within the collector annulus. Probably the most effective configuration would be tangential inlet ports at both sides of the collector, causing unidirectional rotation of the liquid metal annulus, with tangential exit ports near the center of the collector width. Wind-back type grooves between the inlet and exit ports may assist in preventing leakage flow out of the collector region. Analysis of the velocity distribution in such an annulus would be difficult when the viscous drag at the collector surfaces are considered. At present, it is felt that the probability of developing a feasible configuration of this concept is small, and therefore a detailed analysis is not justified.

D2. Venturi Effect

Proper orientation of the liquid metal inlet flow and the shaping of the annular passage to minimize disturbance and to guide the liquid directly toward the exit, would reduce the tendency for aerosol formation and leakage from the collector. The liquid metal inlet could be either in the rotor or the stator, but rotation of the rotor should be designed to encourage flow along the normal path rather than oppose it. However, due to the large annular gap area, the flow rate in the axial or radial direction would have to be very large to provide sufficiently high velocity to create a venturi effect for containment. Therefore, this concept should not be pursued further.

E. Zero-Pressure (Free Fall)E1. Variable-Area Annulus

This technique is similar to the "Deep-Groove Labyrinth" system (A4) described above, except that the cross-sectional area of the collector annulus is varied to permit a matching of inertial head with gravitation head to prevent a pressure rise from the liquid metal inlet at the top, to the exit at the bottom of the annulus. The area variation could be obtained either by tapering the radial gap thickness from the top to a smaller value at the bottom, or by varying the width in a similar manner. The possible advantage of this technique is a lower liquid metal recirculation flow rate, since the wall friction drag is not required (and will be assumed equal to zero for the initial computation). Bernoulli's equation, for constant pressure and negligible friction factor, becomes:

$$v_1^2/2g + Z_1 = v_2^2/2g + Z_2 \quad (5.39)$$

Examining this expression from inlet to exit gives:

$$\Delta(v^2) = 2g\Delta Z = 2gD = 35.9 \text{ m}^2/\text{s}^2 \text{ (386 ft}^2/\text{s}^2\text{)}$$

For example, if $v_1 \approx 0$, then $v_2 \approx 5.99 \text{ m/s (19.7 ft/s)}$, or:

$$v_1 = 1.52 \text{ m/s (5 ft/s)}; v_2 = 7.10 \text{ m/s (20.4 ft/s)}$$

$$v_1 = 3.05 \text{ m/s (10 ft/s)}; v_2 = 7.66 \text{ m/s (22.0 ft/s)}$$

Since the inlet and exit flow rates must be equal, the annulus cross-sectional area must vary inversely with the velocity. If the channel at the exit is $3.18 \times 10^{-3} \text{ m (0.125 in.)}$ radially and $6.35 \times 10^{-3} \text{ m (0.25 in.)}$ wide, since the exit velocity is relatively constant at $\sim 6.10 \text{ m/s (20 ft/s)}$, the flow rate through two parallel paths would be:

$$Q = Av \approx 14,750 \text{ cc/min (15.0 in.}^3/\text{s)}$$

The inlet width could be varied depending on the selected velocity. For an inlet velocity of $1.52 \text{ m/s (5 ft/s)}$, the width of a $3.18 \times 10^{-3} \text{ m (0.125 in.)}$ radial gap would be:

$$w = (6.10/1.52) 6.35 \times 10^{-3} = 2.54 \times 10^{-2} \text{ m (1.00 in.)}$$

The calculated velocities were not negligible in terms of wall-friction pressure drop (even for a zero inlet value), and therefore this approach, at best, must be a combination with that of concept A4. For simplicity, then the concept of concept A4 should be preferred, since the annulus is then of uniform cross-section. The variable-area concept should therefore be dropped from further consideration.

F. Constant-Speed Seal Rotor

Rotation of liquid metal in the collector annulus may be achieved by electromagnetic or injection inertial forces as described above, or through mechanical or viscous shear forces induced by a separately rotating ring. In one possible form, this ring could be the collector well itself, as a rotating "U"-shaped channel with both a rotor and stator collector ring projecting into the liquid-metal filled well. The ring (well) could be hydrostatically floated on its outside diameter to provide the bearing function, and if cover gas were used as the hydrostatic fluid, it might also be allowed to escape in a tangential direction to provide a rotational reaction force. In addition to machining complexity, assembly and liquid metal supply and drainage would be difficult. Therefore, a detailed analysis of this design was not made.

5.3.3.3 Summary of Results

Of the 25 to 30 concepts that were studied, three have been selected for continued development. Two of these are hydrostatically-positioned (the seal A1, and the collector ring B2) and have similar advantages. The ability to maintain a very small clearance gap, between the large-diameter rings and their mating rotor surfaces, is the primary area of concern. The rings will probably be segmented or made flexible to improve conformity to the rotor surface.

The third selected concept uses a simple, inexpensive lip-type oil seal for the large-motor applications with tip speeds of about 3500 fpm or less. Experimental evaluation of this concept should be relatively simple.

Further study of concepts utilizing electromagnetic retention forces will be pursued in order to achieve a practical configuration. Analysis shows that adequate forces can be achieved with reasonable current and flux densities, and acceptable size and power loss.

A number of concepts are dependent upon the development of new materials, and further effort in this area is expected to be productive; in particular, the characterization and evaluation of presently available felt-, foam-, and wick-type materials for sealing or impregnation with liquid metal.

5.3.4 Hybrid Collectors

The hybrid collector is in general a cross between a solid brush and a liquid metal annulus current collector. Specifically the hybrid collector consists of hydrostatically positioned pads which utilize liquid metal for hydrostatic support as well as current transfer. Each hybrid pad is designed such that the liquid metal is confined to sealed flow paths.

The present objectives are: 1) to establish collector geometry for a typical application, 2) to define problem areas for future study, and 3) to establish collector feasibility.

Table 5.4 is a list of general requirements that are used to evaluate operational feasibility for the hybrid collector. These general requirements apply to any homopolar machine that would use a hybrid current collector. Table 5.5 is a list of specific requirements for a hybrid current collector when applied to a chosen application, which in this case is an 8000 horsepower, 500 rpm motor.

A schematic of the hybrid current collector is shown in Figure 5.8. The stator, represented by the shaded portion, houses and provides support for the hybrid pads. By design, movement of the pads is restricted to reciprocating motions along their axial centerlines. Current is transferred from the rotor to the stator or vice versa through the pads. Liquid metal flows into and out of the pad through holes in the stator. The confinement buffer gas flows toward the pad from the inside of the machine (i.e., the inside of the machine is pressurized with buffer gas). Figure

5.9 shows a typical hybrid pad, revealing current transfer and supporting fluid flow paths. A detailed description and analysis of the current transfer and fluid flow for the hybrid pad will be covered in a later section on theory.

Figures 5.8 and 5.9 show axially mounted hybrid pads. Location of the pads on one of the rotating ring's flat sides, rather than on its curved circumference (radially mounted pad), was selected here because:

- 1) The machining costs associated with matching flat surfaces are expected to be less than the costs associated with matching curved surfaces.
- 2) The general theory for the flat surface type collector is applicable to the rounded surface. If a distinct advantage is found for the radially mounted over the axially mounted collector, the analysis would remain valid.

Table 5.4 - General Requirements for Reversing Collectors

1. Horizontally mounted machine.
2. Variable speed with reversing capability.
3. Max. current = 300,000 A.
4. Max. collector current density = $2.48 \times 10^7 \text{ A/m}^2$ (16000 A/in²).
5. Max. collector cross-sectional space 0.038 m axially by
0.038 m radially (1.5 in x 1.5 in).
6. Max. allowable collector loss = 2% total power.
7. Liquid metal leakage to be near zero.
8. Collector must pass 150% rated current at zero speed for
10 secs.
9. Collector must be operable cold without pre-heating.
10. Collectors for a machine must be supplied from a common liquid
metal source.
11. Collector must be capable of deceleration from full speed
forward to full speed reverse in several seconds.
12. Collector shall be designed for sudden stops.
13. Collector shall be designed for sudden load changes.

Table 5.5 - Specific Requirements for Typical Application

1. Type machine = motor for a torque converter.
2. Power = 5966 kw (8000 hp).
3. Speed = 8.3 r/s (500 rpm).
4. Collector dia. = 0.864 m (34 in).
5. Current = 250,000 A.
6. Collector radial flux = 0.05 T.
7. Collector axial flux = 0.1 T.
8. Number of collectors = 8.
9. Number of turns = 2.

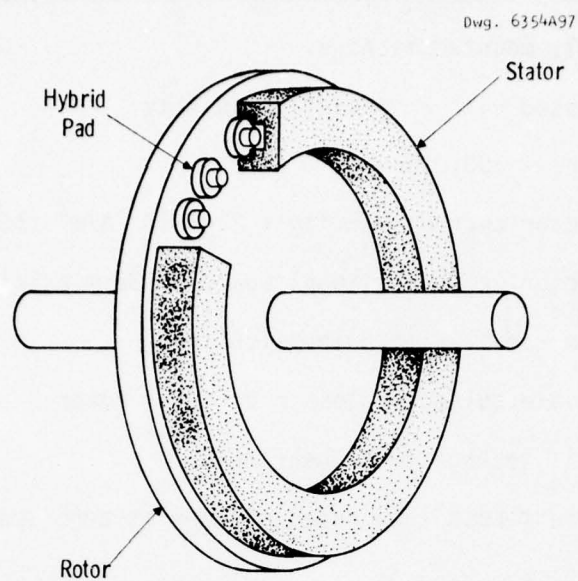


Fig. 5.8: Hybrid pad current collector schematic

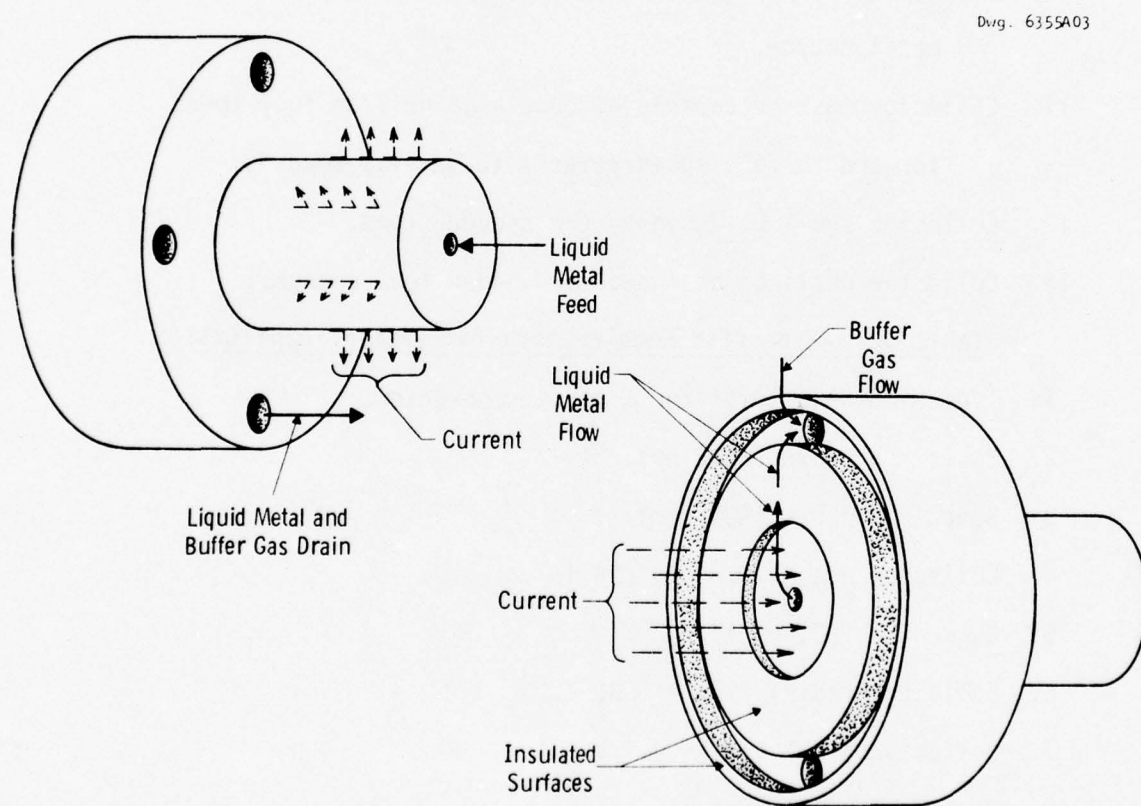


Fig. 5.9: Typical hybrid pad

- 3) For some or all of the radially mounted collectors, the MHD force is always in the direction of rotation which tends to encourage leakage. The axially mounted collector can be applied such that the MHD force is either with or against the direction of rotation.

Typical current collectors are illustrated schematically in Figure 5.10. In all cases, the current (I) is the useful load current being transmitted out of the rotor and the magnetic field (B) is a stray field from the excitation coil. For the axially mounted collector the MHD force due to the interaction of the load current and the magnetic field can be directed either in the same direction (Figure 5.10 a) or opposite direction (Figure 5.10 b) to the rotor viscous drag force. These forces act on the liquid metal which is contained between the hybrid pad and the rotor.

The direction of the MHD force for the radially mounted collector can likewise be in either direction as shown in Figure 5.10 c and 5.10 d. A similar analysis can be made regarding the load current loop ejection force direction for both axial and radial pad placements. Because of construction and assembly complications, the design depicted by Figure 5.10 c is not considered to be practically feasible.

Figure 5.11 is a schematic of the homopolar motor which is being used as a typical application for the hybrid collector. The collectors are distributed in four regions of the motor with the current and flux directions defined for each region. For convenience, the current collectors are assumed to be placed on the rings such that the MHD force opposes the viscous drag force. Such force opposition will likely aid in confining the liquid metal, but this must be proven. With axial pad placement, as assumed, the load current loop ejection force is always directed radially outward. Figure 5.12 depicts the four machine collector regions, each complete with directions of the load current, ambient magnetic field, and associated pressure forces acting on the liquid metal. Power loss and confinement pressure relationships based on the forces displayed in Figure 5.12 are derived in the following section on theory.

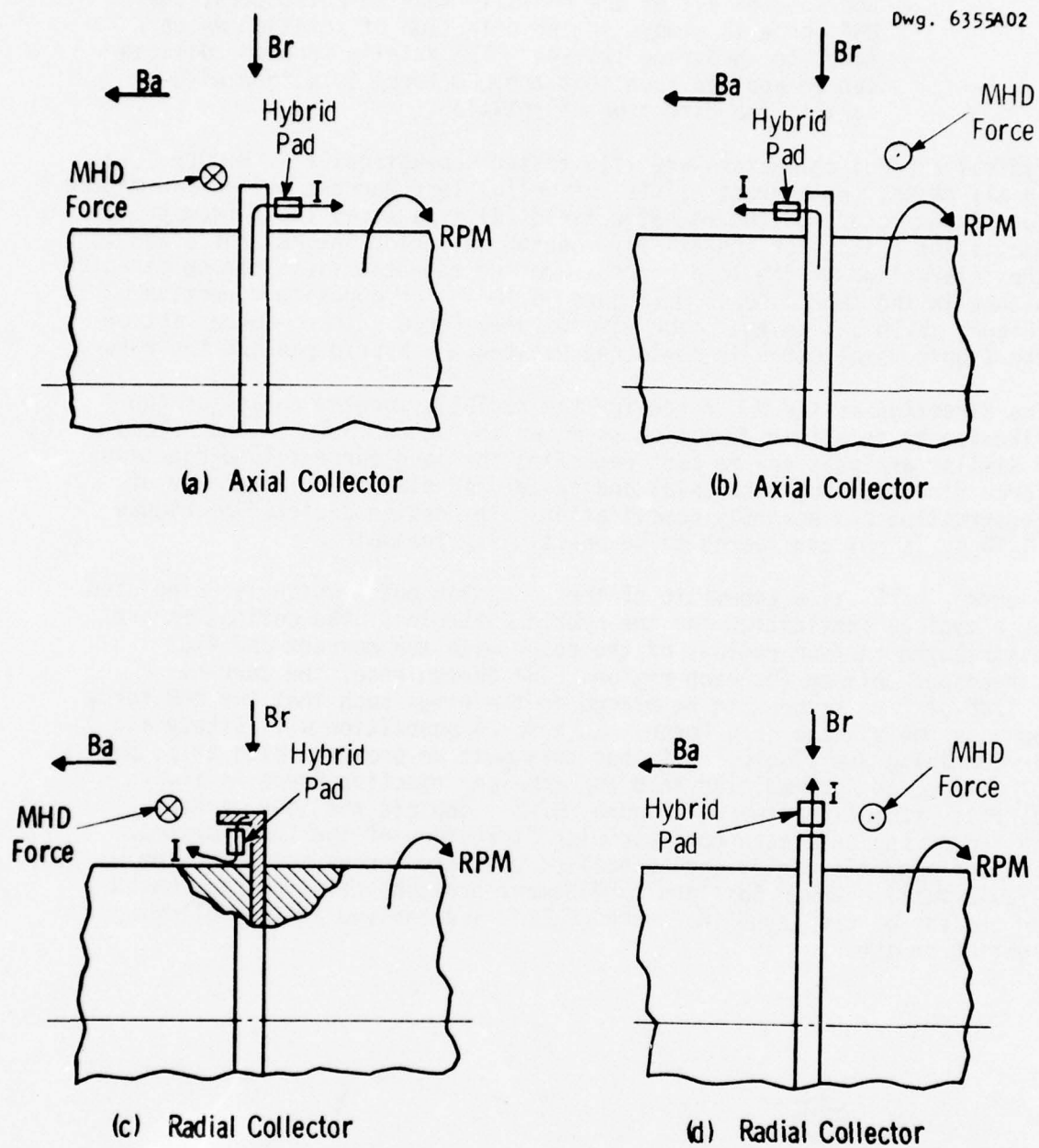
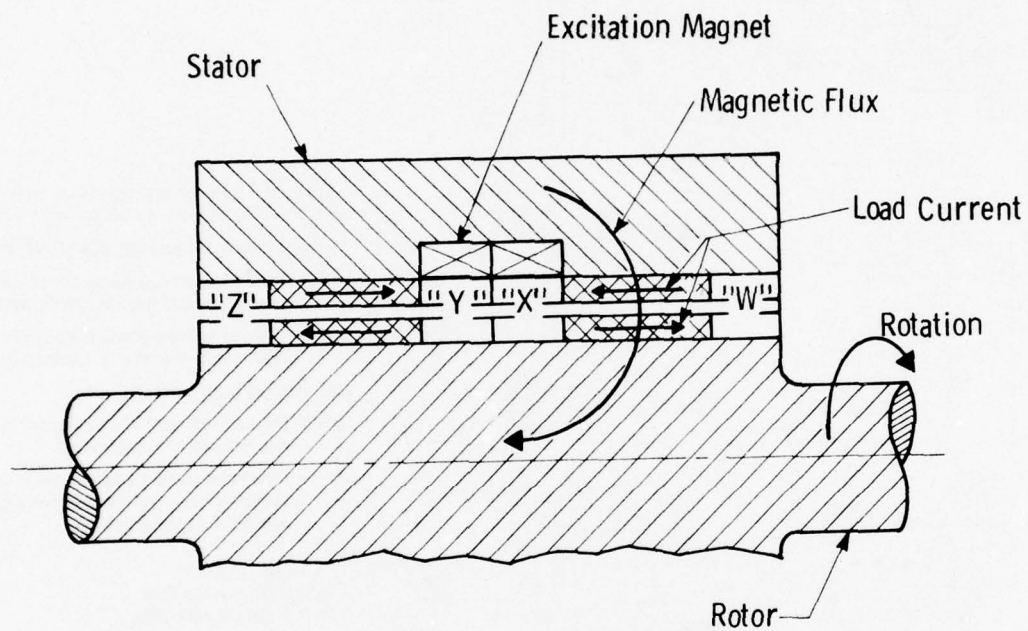


Fig. 5.10: Axial and radial current collector schematic

Dwg. 6354A98



Collector Region	Rotor Current	Axial Flux	Radial Flux
W	Out of Rotor	←	↓
X	Into Rotor	←	↓
Y	Into Rotor	←	↑
Z	Out of Rotor	←	↑

Fig. 5.11: Homopolar motor schematic

Dwg. 257C272

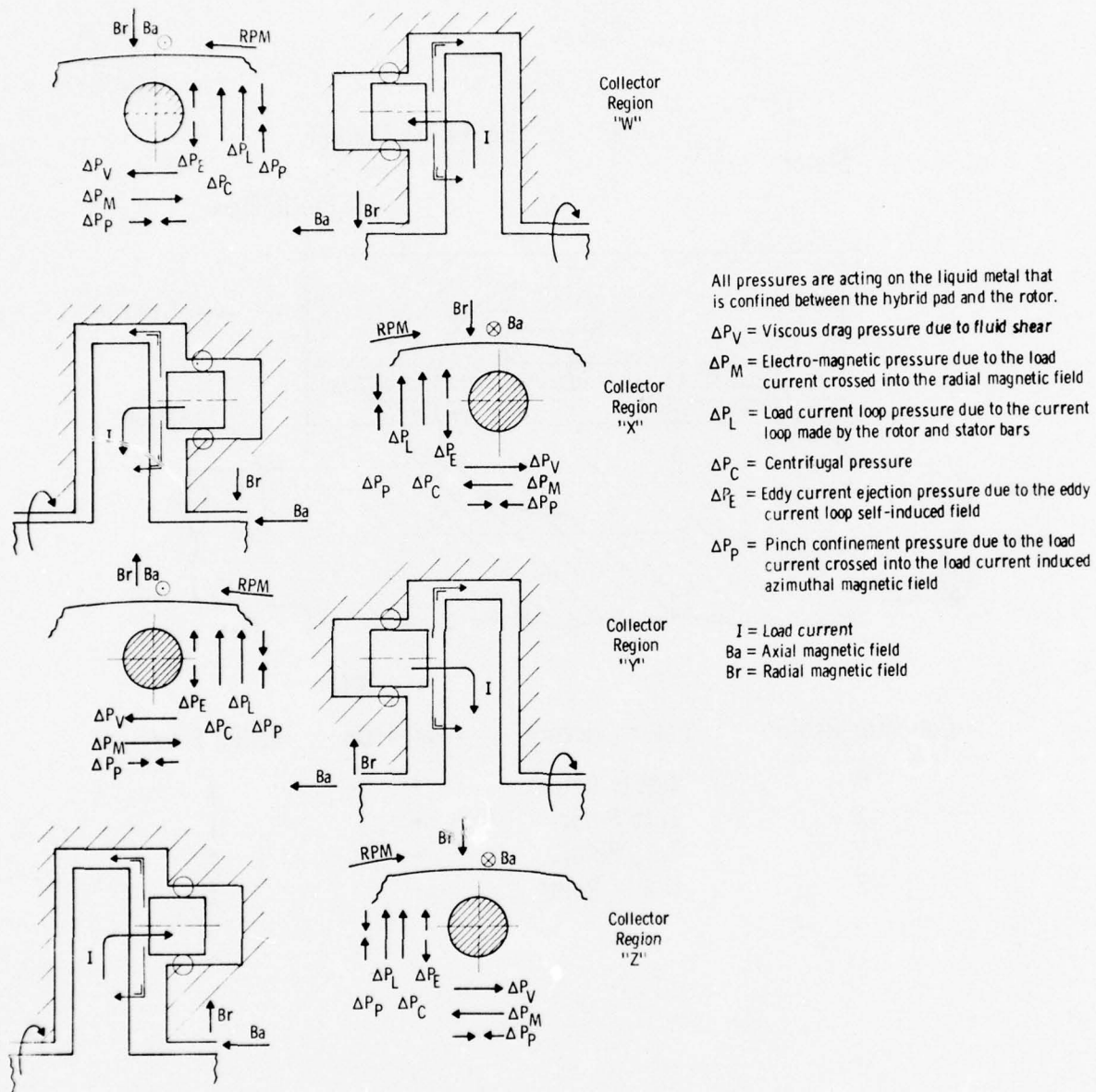


Fig. 5.12: Schematic of collector regions for the homopolar motor

5.3.4.1 Theory of the Hybrid Collector

5.3.4.1.1 Hydrostatics and Liquid Metal Flow

Consider the hydrostatically positioned pad in Figure 5.13. The liquid metal flows axially toward the rotor through the center of the pad and then, when it reaches the rotor, radially outward over the pad face. The liquid metal is then collected in the pad's circumferential annulus, and drained to a sump. The buffer gas flows radially inward over an outer circumferential containment labyrinth and is collected in the circumferential annulus with the liquid metal. The buffer gas is then drained to the sump with the liquid metal.

Assume:

- 1) Lift due to containment labyrinth is negligible, i.e., $p_3 \ll p_1$.
- 2) p_2 is approximately equal to atmospheric pressure and can be assumed equal to zero when all other pressures are gage pressures.
- 3) Pad face liquid metal flow velocity is greater than the rotor collector velocity.
- 4) The hybrid pad cross section is circular.

The lift force due to the pressure profile over the pad face is:⁶

$$F_L = \frac{p_1 A_L}{K_p}, \text{ N.} \quad (5.40)$$

where:

p_1 = pocket pressure, N/m^2 .

A_L = projected land area. For the case of the circular pad displayed in Figures 5.13 and 5.14,

$$A_L = \pi(D_2)^2/4, \text{ m}^2.$$

K_p = pressure factor. The pressure factor is a function of geometry, and for the circular pad

$$K_p = \frac{2 \ln(D_2/D_1)}{1 - (D_1/D_2)^2}, \text{ dimensionless.}$$

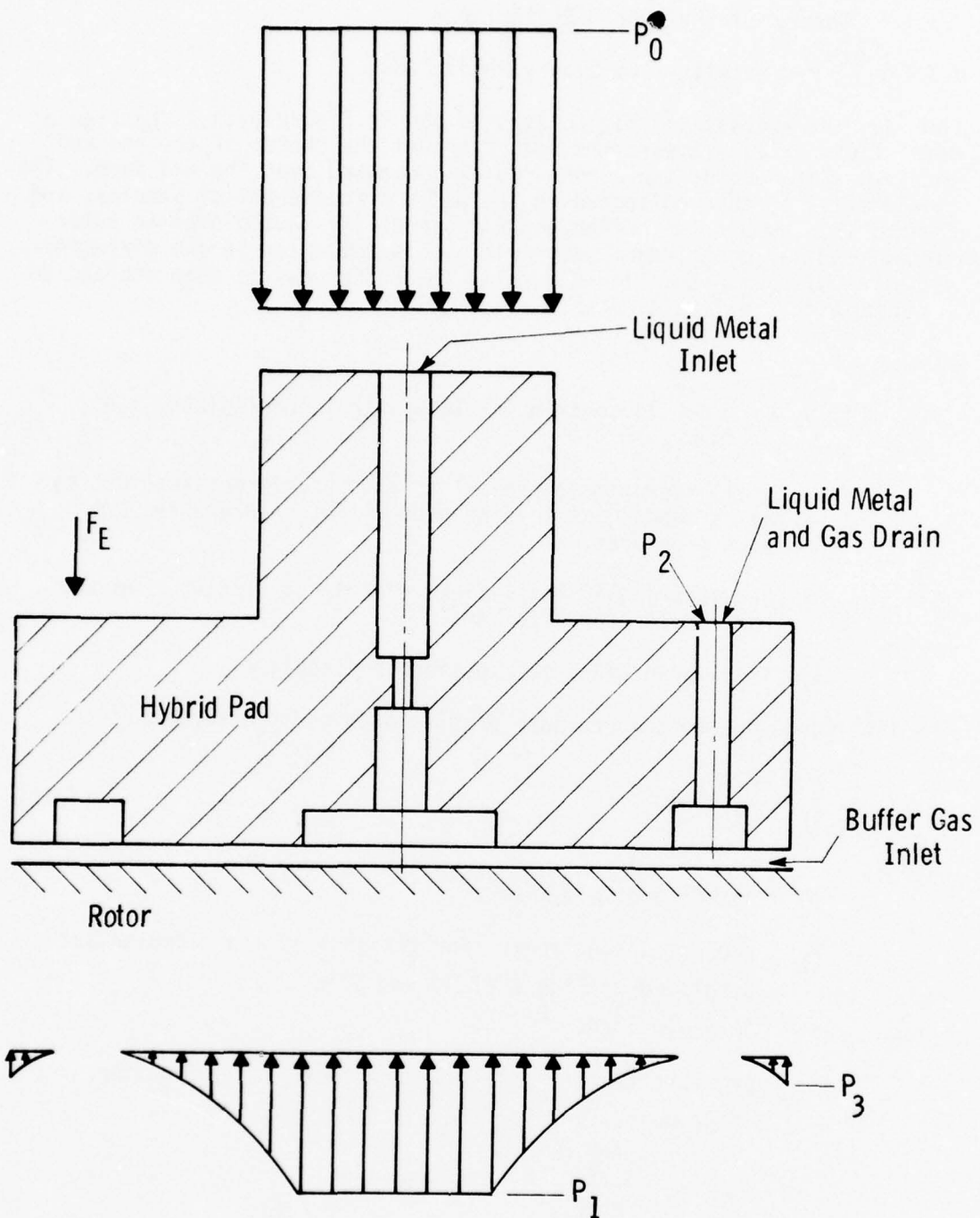


Fig. 5.13: Hydrostatically positioned pad

An outer stem force opposes the lift force. The outer stem force is given by the following expression.

$$F_o = P_o A_o, \text{ N} \quad (5.41)$$

where:

P_o = liquid metal supply pressure, N/m^2 .

A_o = pad stem area. For the circular pad

$$A_o = \pi(D_o)^2/4, \text{ m}^2.$$

Summation of the axial directed forces yields

$$F_E + P_o A_o = \frac{P_1 A_L}{K_p} \quad (5.42)$$

where:

F_E = remaining extraneous pad forces parallel to the pad center line, N.

The flow rate of liquid metal through the hydrostatic pad is a function of the method of compensation and the pad face geometry. The most common methods of compensation are orifice, capillary and flow control valve. For the present discussion, the orifice method of compensation is considered. The effects of other methods of compensation can be found in ref. 7.

The flow through the orifice is

$$Q_o = 0.661 d_1^2 \left(\frac{P_o - P_1}{\rho} \right)^{1/2}, \text{ m}^3/\text{s} \quad (5.43)$$

where:

ρ = mass density of liquid metal, kg/m^3 .

d_1 = orifice diameter, m.

The flow over the pad land is⁶

$$Q_L = \frac{q_f}{12 K_p} \frac{c^3 P_1}{\mu_L}, \text{ m}^3/\text{s} \quad (5.44)$$

where:

q_f = flow factor. The flow factor is a function of geometry and for the circular pad

$$q_f = \frac{4\pi}{1 - (D_1/D_2)^2}, \text{ dimensionless.}$$

c = clearance, m.

μ_L = absolute viscosity, $\frac{N \cdot s}{m^2}$.

Setting $Q_0 = Q_L$, equations 5.43 and 5.54, solving for P_1 , and then substituting this expression for P_1 in equation 5.42 yields the following expression for clearance as a function of supply pressure.

$$c = \left[\frac{63 \mu_L^2 d_1^4 A_L}{\rho q_f^2 (A_o^2 P_o^2 + 2A_o P_o F_E + F_E^2)} (P_o A_L - K_p A_o P_o - K_p F_E) \right]^{1/6}, \text{ m.} \quad (5.45)$$

Solving equations 5.45 and 5.44 for P_1 , equating them to each other to eliminate P_1 , and making $Q_0 = Q_L = Q$, yields the following expression for flow as a function of supply pressure and clearance.

$$Q = \frac{2.625 N_p M d_1^4}{\rho} \left\{ \left[\frac{6.35 \times 10^{-2} \rho P_o}{d_1^4} \right] + \left(\frac{\mu_L K_p}{c^3 q_f} \right)^2 \right\}^{1/2} - \left[\frac{\mu_L K_p}{c^3 q_f} \right], \text{ m}^3/\text{s}/\text{machine} \quad (5.46)$$

where:

N_p = number of pads per collector.

M = number of collectors per machine.

Thus, for a given geometry, fluid physical properties, and extraneous force, the clearance and flow can be found for various supply pressures.

The buffer gas flow equation is derived from the relationships presented in reference 8. Since the lift effect due to the buffer gas is small relative to the liquid metal lift, the clearance is determined by the liquid metal hydrostatic relationship in equation 5.45. For gas pressure drops across the confinement labyrinth of 6895 to 68,950 N/m² (1 to 10 psi), the buffer flow can be approximated by the expression:

$$Q_B = \left[\frac{(\Delta P)^{1/2} + 3.63}{1.086} \right] N_p M c L, \text{ m}^3/\text{sec} \quad (5.47)$$

where:

ΔP = differential gas pressure across labyrinth, N/m^2 .

c = clearance calculated by equation 5.45, m.

L = length of labyrinth tooth perpendicular to the flow per pad, (πD_4) , m.

5.3.4.1.2 Power Losses

The power losses associated with the hybrid collector are:

P_Ω = Ohmic

P_V = Viscous on pad face

P_C = MHD and viscous core loss

P_E = Eddy current loss

P_P = Pumping power for hydrostatic fluid

P_B = Pumping power for buffer gas

Ohmic Loss

$$P_\Omega = I_p^2 R M N_p, \text{ watts/machine} \quad (5.48)$$

where:

I_p = load current per pad, amps.

R = pad resistance including contact potential resistance, ohms.

Viscous Loss on Pad Face

Assume: 1) $\delta \ll 1$, where δ is a dimensionless ratio of the Lorentz body force to the viscous drag force.⁹

- 2) Flow regime is turbulent.⁹
- 3) Viscous loss due to buffer gas is negligible.

$$P_V = \frac{\rho f_L (V)^3 A_L}{8} N_p \text{ M, watts/machine} \quad (5.49)$$

where:

f_L = friction factor based on pad-to-rotor clearance, dimensionless.

V = collector rotor tangential velocity, m/s.

A_L = pad projected area, m².

Core Viscous and MHD Loss

The core MHD loss is based on an induced current due to the fluid velocity in the presence of a magnetic field.

$$P_C = (\pi/4) M N_p \left[(2f_c \rho V_c^3 d_3 H_4) + (\sigma_L B_r^2 V_c^2 d_3^2 H_4) \right], \text{ watts/machine} \quad (5.50)$$

where:

f_c = friction factor based on core diameter.

V_c = fluid velocity through core, m/s.

d_3 = core diameter, m.

H_4 = core length, m.

σ_L = electrical conductivity of liquid metal, mhos/m.

B_r = radial component of collector magnetic field, T.

Eddy Current Loss¹⁰

Assume: 1) No load current.

- 2) No transverse current, i.e., no circulating current within the liquid metal.

$$P_E = M N_p A_p \left(\frac{\sigma V_B^2 W^2}{12 c'} \right) \left(\frac{c'^2}{W^2} + 1 \right), \text{ watts/machine} \quad (5.51)$$

where:

A_p = current transfer area per pad, m^2 .

B_a = axial component of collector magnetic field, T.

W = collector width normal to B_a , m.

c' = effective clearance, m.

$c' = (c + \sigma \epsilon_k + h_2)$, m.

ϵ_k = specific contact potential for each contact pair, Vm^2/A .

h_2 = current transfer pocket depth, m.

Hydrostatic Fluid Pumping Power

$$P_P = \frac{Q P_0}{\eta_L}, \text{ watts/machine} \quad (5.52)$$

where: η_L = liquid metal pump efficiency, %/100.

Buffer Gas Pumping Power

$$P_B = \frac{\gamma Q_B R(T+273)}{\eta_B} \left(\frac{k}{k-1} \right) \left[(r_p)^{\frac{k-1}{k}} - 1 \right], \text{ watts/machine.} \quad (5.53)$$

where:

γ = mass density of buffer gas at drain, kg/m^3 .

R = gas constant of buffer gas, $\frac{\text{watt-s}}{kg \text{ } ^\circ C}$

T = buffer gas temperature at pad drain, $^\circ C$.

η_B = buffer gas pump adiabatic efficiency, %/100.

k = Specific heat ratio of cover gas, dimensionless.

r_P = ratio of buffer gas supply pressure to drain pressure, absolute pressures.

The total collector loss is found by:

$$P_{tot} = P_{\Omega} + P_V + P_C + P_E + P_P + P_B, \text{ watts/machine} \quad (5.54)$$

The relative loss is found by calculating the percent of machine power attributed to the total collector loss. The percent collector loss is found by the relationship:

$$LOSS = \frac{P_{tot}}{(POWER)} \times 100, \% \quad (5.55)$$

where: POWER = total machine power, watts.

5.3.4.1.3 Expulsion Pressures

Pressures are developed in the liquid metal due to the MHD body forces. These MHD pressures are considered in order to determine if they are significantly large with respect to the hydrostatic control pressures. Figure 5.12 shows the direction of selected forces which upon integration yield eddy current ejection pressure, load current ejection pressure, pinch pressure and the pad face MHD pressure. The MHD pressure drop in the core is not shown on this figure, but it always works to retard the liquid metal flow.

Eddy Current Ejection Pressure

As reported in previous Semi-Annual Technical Report,

$$\Delta P_E = \frac{\mu\pi}{32} \left[\frac{\sigma_L R_C B_a \omega}{c^2} \right]^2 W^4, \text{ N/m}^2, \quad (5.56)$$

where:

μ = permeability of free space (10^{-7} , mks units)

ω = angular velocity, rad/s

R_c = average collector radius, m

Load Current Ejection Pressure

$$\Delta P_L = (2n-1)\mu\pi J^2 R_1^2 \left[(R_2/R_1)^2 - 2\ln(R_2/R_1) - 1 \right], \text{ N/m}^2 \quad (5.57)$$

where:

n = number of series load circuits

J = collector average current density, A/m^2

R_1 = inner radius of current collector, m

R_2 = outer radius of current collector, m

Pad Pinch Pressure

$$\Delta P_p = \mu J I_p, \text{ N/m}^2 \quad (5.58)$$

Pad Face MHD Pressure

$$\Delta P_m = J B_r L_c, \text{ N/m}^2 \quad (5.59)$$

where: L_c = length of current transfer area in direction of rotor circumference, m.

Core MHD and Viscous Pressure

The core MHD pressure is based on the induced current due to the fluid velocity in the presence of a magnetic field.

$$\Delta P_c = \sigma_L V_c (B_r)^2 H_4 + 2\rho f_c V_c^2 \left(\frac{H_4}{d_3} \right), \text{ N/m}^2 \quad (5.60)$$

5.3.4.2 Discussion of the Hybrid Collector

A computer program was developed to evaluate different pad configurations. The program calculates pad performance based on the relationships presented in the previous section on theory. The following assumptions are inherent in the computer program:

1. The pad lift force at zero liquid metal flow equals the pad drive force at infinite flow. (That is, the hydrostatic force developed by the pad to move away from the rotor equals the hydrostatic force developed by the pad to move toward the rotor.)
2. The minimum allowable supply pressure is that value which, when integrated over the pad stem area, provides a force equal to the extraneous force. If the rotor moves away from the pad, the minimum supply (control) pressure corresponds to the minimum pressure required to force the pad to follow the rotor.
3. The electrical load current is transferred between the rotor and pad solely through the center pocket portion of the pad, with no transfer through the pad land portion.
4. The load current is transferred between the pad and stator through the circumferential area of the pad stem.
5. The hydrostatic flow velocity at any point on the hydrostatic land must be equal to or greater than the mean collector rotor tangential velocity.
6. The liquid metal and the buffer gas are constrained by seals such that no flow is allowed to bypass the pad. For convenience the bypass seals are assumed to be sliding O-rings.

Table 5.6 contains general information required to calculate the performance characteristics of a hybrid pad design collector and, with these results, permits assessment of how well it meets the restrictions or requirements outlined in Tables 5.4 and 5.5. The values shown in Table 5.6, although representative, are not intended to be taken as optimum values, but are merely to provide a reference frame for discussion.

Based on a total flow of $0.0314 \text{ m}^3/\text{s}$ (500 gpm), see Table 5.6, the liquid metal flow per collector pad is $5.6 \times 10^{-5} \text{ m}^3/\text{s}$ (0.89 gpm). This flow appears to be excessive and should be reduced if possible. For the given pressure, the flow can be reduced by making the pad orifice and/or pocket diameter smaller. This, however, will reduce the hydrostatic flow velocity below the collector rotor tangential velocity. The result is that the pad lift force is impaired. In this situation, the fluid film

TABLE 5.6
TYPICAL DESIGN INFORMATION
(Also see Table 5.5)

<u>General Collector Data</u>		<u>Value</u>
1) Number of pads		90 (N)
2) Buffer gas flow per machine	.294 m ³ /sec (624 ft ³ /min)	(Q _B)
3) Liquid metal flow per machine	.0314 m ³ /sec (500 gal/min)	(Q)
4) Buffer gas pump efficiency	50%	(η_B)
5) Liquid metal pump efficiency	30%	(η_L)
6) Extraneous force	39.14 N (8.8 lb)	(F _E)
7) Pad spring constant with respect to rotor	2.92 x 10 ⁶ N/m (16700 lb/in.)	(K _S)
8) Hydrostatic fluid — Eutectic NaK 78		
a) Viscosity	540 Ns/m ² (.783 x 10 ⁻⁷ lb-sec/in ²)	(μ_L)
b) Mass density	858 kg/m ³ (.031 lb/in ³)	(ρ)
c) Electrical conductivity	.22 x 10 ⁷ mhos/m	(σ_L)
d) Specific contact potential	.18 x 10 ⁻⁸ Vm ² /A	(ϵ_K)
9) Pad material — Copper		
a) Electrical conductivity	.448 x 10 ⁸ mhos/m	
10) Buffer gas — Nitrogen		
11) Liquid metal supply pressure	345000 N/m ² gage (50 psig)	(P ₀)
12) Liquid metal pocket pressure	172000 N/m ² gage (25 psig)	(P ₁)
13) Buffer gas supply pressure	13800 N/m ² gage (2 psig)	(P ₃)
14) Liquid metal and buffer gas combined drain pressure	0.0 N/m ²	(P ₂)
15) Collector temperature	94°C (200°F)	(T)

TABLE 5.6 (Continued)

<u>General Collector Data</u>	<u>Value</u>
16) Minimum allowable hydrostatic control pressure	245000 N/m ² gage (35.5 psig)
17) Flow factor	87.04 (q _f)
18) Pressure factor	1.08 (K _p)

Collector Geometry (Refer to Fig. 5.14.

$R_C = .442 \text{ m}$ (17.4 in)	$\delta_1 = 2.03 \times 10^{-5} \text{ m}$ (.0008 in)
$D_0 = .0143 \text{ m}$ (.562 in)	$\delta_2 = 2.03 \times 10^{-5} \text{ m}$ (.0008 in)
$D_1 = .0194 \text{ m}$ (.763 in)	$H_1 = 3.05 \times 10^{-3} \text{ m}$ (.12 in)
$D_2 = .0210 \text{ m}$ (.825 in)	$H_2 = .0102 \text{ m}$ (.40 in)
$D_3 = .0290 \text{ m}$ (1.14 in)	$H_3 = .0297 \text{ m}$ (1.17 in)
$D_4 = .0305 \text{ m}$ (1.20 in)	$H_4 = .0282 \text{ m}$ (1.11 in)
$d_1 = 2.16 \times 10^{-3} \text{ m}$ (.085 in)	$H_7 = .0130 \text{ m}$ (.51 in)
$d_2 = 4.06 \times 10^{-3} \text{ m}$ @ 12 holes (.16 in)	$h_1 = 3.94 \times 10^{-3} \text{ m}$ (.155 in)
$d_3 = 6.10 \times 10^{-3} \text{ m}$ (.24 in)	$h_2 = 1.52 \times 10^{-4} \text{ m}$ (.006 in)
$d_4 = .0140 \text{ m}$ (.55 in)	$C = 2.72 \times 10^{-5} \text{ m}$ @ $F_E = 0$ (.00107 in)

on the pad land cannot cover the full hydrostatic area because it is drawn away too fast by the rotor.¹¹⁻¹² In regard to the sample operating conditions presented here, the pad land hydrostatic liquid flow velocity is equal to the mean collector rotor velocity.

A method for reducing the flow with only partial impairment of the lift force is to utilize pad geometries other than the circular cross section.⁷ Future effort should be directed to find low-flow geometric configurations which impose minimal hydrostatic life impairment.

The extraneous force (F_E) listed in Table 5.6 is equal to 39.1 N (8.8 lbf). This force should be reduced so that a lower minimum allowable hydrostatic control pressure can be used. The major portion of the extraneous force is attributed to O-ring friction. The O-rings could be replaced by controlled leakage seals which would offer essentially zero friction. Future effort in this area would be placed on finding the optimum bypass seal with respect to leakage and friction.

The pad spring constant, see Table 5.6 is a measure of stiffness with respect to the rotor. It is numerically equal to the change in extraneous force (from positive to negative) divided by the corresponding change in pad-rotor clearance. The spring constant is useful when making a mechanical response analysis of the rotor-pad-stator system. Future effort would determine the mechanical response of the pad with respect to the rotor and derive the current collector design relationships with respect to resonance.

The power loss associated with the hybrid current collector is given in Table 5.7 as 2.4% of the total machine output power. This is 0.4% greater than the design requirements (see Table 5.4, item 6). The major component of the collector loss is the ohmic loss, which is caused by the solid-liquid-solid interface contact resistances and the pad pocket liquid metal bulk resistance.

TABLE 5.7
SUMMARY OF CURRENT COLLECTOR COMPONENT POWER LOSSES

Component	Power Loss	
	kW	%
1) Ohmic loss, P_Ω	69.5	49
2) Eddy current loss, P_E	22.9	16
3) Core loss, P_C	0.9	1
4) Viscous loss, P_V	6.6	5
5) Liquid metal pump loss, P_p	36.3	25
6) Buffer gas pump loss, P_B	5.4	4
7) Total collector loss, P_{tot}	141.6	100
8) Percent of total machine power		2.4% (LOSS)

One method considered for reducing the ohmic power loss is to reduce the current per pad by adding more pads. However, the present 90 pads employed per collector is the maximum that can be accommodated. Another possible method for reducing the ohmic loss is to increase the pad face area (i.e., effectively reducing the contact resistance). This event, however, also reduces the hydrostatic flow resistance which, in turn, results in an undesirable increase in fluid flow. By employing non-circular cross section pads, where lower flow velocities may be feasible, greater current transfer areas may be achieved.

Counter to the original design philosophy, a reduction in contact resistance may also be obtained by permitting the load current to be transferred between rotor and pad through the pad land area in addition to the pad pocket. Initially, current transfer was allowed only through the pocket area in order to avoid excessive eddy current power loss and ejection pressure. Although the eddy current induced loss will be increased as a result of the above suggested changes, it will likely be offset by reduced load current ohmic and liquid metal pumping power losses. Future effort should be placed on determining the optimum current transfer geometry with respect to losses.

Calculated MHD pressures for the sample pad collector design are summarized in Table 5.8. The liquid metal-load current ejection pressure reported here is of a significant magnitude, $6 \times 10^4 \text{ N/m}^2$, when compared with the higher pocket pressure, $17 \times 10^4 \text{ N/m}^2$ (see Table 5.6, item 12). The pressure profile through the liquid metal due to load current-self field effects is not known at this time, since pressure calculations using the derived expression only yield maximum values at one end of the collector. Future work is suggested to ascertain the disturbing effects of load current on liquid metal confinement, if any, through laboratory experimentation.

The pad face MHD pressure does not appear to be excessively large for the present hybrid pad collector design. If the pad geometry is changed from the circular shape, however, elongating the area of current transfer circumferentially would cause an increase in the pad face MHD pressure.

TABLE 5.8
SUMMARY OF CALCULATED CURRENT COLLECTOR MHD PRESSURES

Source of Pressure	Pressure	
	N/m^2	(lbf/in^2)
1) Eddy current ejection pressure, ΔP_E	2100	(0.30)
2) Load current loop ejection pressure, ΔP_L	60200	(8.7)
3) Pinch pressure, ΔP_p	2580	(0.37)
4) Pad face MHD pressure, ΔP_m	9020	(1.3)
5) Core MHD and viscous pressure, ΔP_C	380	(0.06)

At present no quantitative method has been developed to evaluate the collector's ability to confine liquid metal to the current transfer zone. Confinement of liquid metal is defined as the ability of the hybrid pad to transport liquid metal in and out of the current collection area in the presence of a moving rotor surface without liquid metal leakage beyond the outer confinement labyrinth. In general, the following qualitative statements may be made concerning confinement:

1. A reduction in the liquid metal supply flow will improve confinement ability.
2. An increase in the buffer gas flow will work to reduce leakage of liquid metal at the labyrinth location.
3. Certain MHD pressures may be utilized to aid confinement. In other cases, through design, the MHD expelling pressures can be reduced.

The above actions are intuitive and the degree to which confinement will be affected can only be determined through experimentation. This, again, is an area for future work in the development of a hybrid pad current collector.

Because of potential mechanical force couples, the circular geometry hybrid pad is undesirably susceptible to tilting. It appears that force couple compensation can be achieved by employing parallel flow restrictions.⁷ This technique must be theoretically and experimentally studied in more detail.

5.4 CONCLUSIONS

Liquid Metal Current Collectors were demonstrated in the SEGMAG generator to be reliable in unidirectional speed homopolar machines. The results of Section 5 indicate that it is feasible to extend the technology to the more complex requirements of variable and reversing speed machinery such as torque converters and motors.

5.5 REFERENCES

1. Warring, R. H., Seals and Packings, Trade and Technical Press Ltd., Morden, Surrey, England, 1967.
2. Chicago Rawhide Catalog No. 457013, Large Diameter Oil Seals.
3. Fuller, D. D., Theory and Practice of Lubrication for Engineers, John Wiley and Sons, 1956.
4. Shaw, M. C. and Macks, E. F., Analysis and Lubrication of Bearings, McGraw-Hill, New York, 1949.
5. Private communication with Dr. G. T. Hummert, Westinghouse Research Laboratories, April 29, 1975.
6. Loeb, A. M. and Rippel, H. C., Determination of Optimum Proportions for Hydrostatic Pads, ASLE Trans., Vol. 1, No. 2, p. 241, 1958.
7. Malanoski, S. B. and Loeb, A. M., The Effect of the Method of Compensation on Hydrostatic Bearing Stiffness, Journal of Basic Engineering, Trans. ASME, Series D, Vol. 83, No. 2, p. 179, June 1961.
8. Egli, A., The Leakage of Steam through Labyrinth Seals, ASME Paper No. FSP-57-5, 1935.
9. Rhodenizer, R. L., Development of Solid and/or Liquid Metal Collectors for Acyclic Machines, Final Report for Tasks 1, 2 and 3, Navy Ship Systems Command, Contract No. N00024-68-C-5414, February 27, 1970.
10. Hummert, G. T., Calculation of Eddy Losses in Liquid Metal Current Collectors, Westinghouse Memo 73-8G1-LIQMT-M1, November 20, 1973.
11. Boyd, J., Raimondi, A. A., and Kaufman, H. N., A Manual on Bearing Analysis, Westinghouse Research Laboratories, 1310 Beulah Road, Pittsburgh, Pennsylvania 15235, 1966.
12. Boyd, J., Kaufman, H. N., and Raimondi, A. A., Basic Hydrostatic Pad Design, Lubrication Engineering, Vol. 21, 1965 (Westinghouse Report 63-117-517R2).

VOLUME II
PART A
SECTION 6
LIQUID METAL SUPPORT SYSTEMS

6.1 OBJECTIVES

The objectives of this task during Phase II are: (1) to investigate the compatibility of candidate machine materials with NaK and GaIn, as well as with potential decontamination solutions; (2) to perform literature, analytical, and experimental studies for the purpose of identifying suitable materials and suggesting alternate choices where necessary; (3) to design, fabricate, and test the liquid metal loop and cover gas systems that will be required in the SEGMAG generator; and (4) to establish the operating parameters and interactive responses of these systems.

6.2 PRIOR AND RELATED WORK

Scientific study of those liquid metals which are of greatest concern to homopolar machines, namely NaK and GaIn, has largely concentrated on their usefulness as high temperature heat transfer media, as in fast breeder reactor technology. Consequently, much of the chemical and materials methodology which has been built up with these liquid metals involves information which is not directly applicable to the operating conditions of homopolar machines. Some extrapolation was, therefore, required, as well as some technique development, to produce a homopolar machine capable of sustained long term operation.

6.3 SUMMARY OF ACCOMPLISHMENTS

6.3.0 General

The compatibility of machine materials, both organic and inorganic, with the liquid metal current collection fluid and cover gas were reviewed in the literature and analyzed by chemical composition. Consideration was also given to the reaction products which would be generated during machine cleanup and decontamination. In the event that total materials compatibility could not be achieved, alternate methods were studied such as the canning or encapsulation of those component materials which may be reactive with the liquid metal or the decontamination products. In addition, the canning or encapsulation had to prevent insulation outgassing products from reaching the liquid metal.

Proposed methods of liquid metal handling and purification, as well as the required on-line instrumentation to monitor the chemistry of the liquid metal were reviewed. This included the liquid metal loop system and the requirements necessary to interface the liquid metal/cover gas system with the machine current collector. In addition, the requirements for machine cleanup, routine operation, and safety were analyzed.

The liquid metals proposed for use as current collection fluids in advanced design homopolar machines are sodium potassium alloys (NaK) and gallium-indium alloys (GaIn). These methods, depending on their composition, may be liquids at room temperature (25°C). For this particular application, NaK₇₈ (eutectic) is the prime candidate current collection fluid. GaIn has been considered, but due to the higher power losses associated with it and to its strong corrosive action on structural metals, it is only secondary as a candidate fluid. Because NaK is so reactive, an inert cover gas is necessary to prevent oxidation of the liquid metal alloy. High purity nitrogen may be used in this application although other gases such as argon or helium may be considered.

Once the current collection fluid and cover gas were defined, the machine was studied from a total materials compatibility point of view, since many components were expected to be in contact with both the liquid metal alloy and also the cover gas. Materials compatibility problems may result from many areas. A few of those considered are listed below:

- (1) Liquid metals reacting with materials,
- (2) Materials outgassing and contaminating the liquid metal,
- (3) Local machine hot spots,
- (4) Impurities in the cover gas contaminating the liquid metal.

Assurance of continuous on-line operation of a liquid metal current collection system required investigation from the standpoint of maintenance of liquid metal purity. Of the various methods of preventing liquid metal contamination, the following were selected as most reasonable for machine application: (1) Fabricate the machine from the standpoint of high vacuum technology to prevent serious outgassing of oxygen and moisture to the liquid metal current collector region; (2) Utilize a positive pressure gradient inert cover gas inside the machine housing to prevent the entrance of atmospheric contaminants (oxygen, moisture); (3) Continuously recirculate the cover gas through a purification cycle; (4) Continuously recirculate liquid metal from the current collector region through a purification loop. Total system contamination control can be expected through currently available technologies.

Integral gas purification/machine/liquid metal loop system variables were considered with respect to system interacting, startup, operation,

and shutdown problems, safety, decontamination practices, and instrumentation. As a result of these considerations, no potential problems were viewed as insurmountable.

A number of homopolar machines are now in operation which utilize both NaK and GaIn as current collection fluids. The cleanup and decontamination procedures which are currently being utilized are adequate for most situations which are now encountered. In general, more problems are encountered with NaK than with GaIn but the procedures to handle these problems were reviewed and were found to be fairly well defined. Methods which are now employed utilize alcohol, alcohol/water, and live steam to safely react and decontaminate NaK systems. In utilizing these procedures a number of hazards are involved. These include liquid metal exposure to personnel, the evolution of hydrogen as one of the reaction products and the caustic liquids which result from the cleanup procedures. From visiting a number of homopolar machine sites which employ NaK as the current collection fluid, the most hazardous problem appears to be that of hydrogen generation and the possibility of explosions which exist under decontamination conditions.

NaK was selected as the reference liquid metal, with GaIn as the alternate choice.

An extensive materials compatibility program was conducted, and the selection of materials for use in SEGMAG was based on their ability to withstand NaK exposure in a simulated machine environment.

Investigation was made of the chemical problems associated with wetting between NaK and copper or copper-based alloys.

Procedures were established for the disassembly and decontamination of machines using NaK and GaIn. Liquid metal recirculation and purification loops were designed, fabricated, tested, and employed in SEGMAG performance tests to maintain NaK in the current collectors. Cover gas recirculation, purification, and pressure maintenance systems were designed and constructed for SEGMAG performance tests. Full scale prototype current collectors were developed, tested, and characterized prior to their employment in SEGMAG. The SEGMAG test bed, instrumentation, coolant system, and performance readout networks were developed and constructed for the machine evaluation tests.

During the design stage of the 3000 hp SEGMAG demonstration machine, great emphasis was placed upon developing the machine support systems since these were recognized to be necessary to successful, long-term machine operation. An integrated design approach was employed, since many components were to be in contact with the liquid metal alloy (NaK) and also with the protective cover gas, nitrogen. To insure system compatibility many parameters and subsystem interactions were evaluated, including the following:

1. Effect of liquid metals on machine materials.
2. Contamination of liquid metal by out-gassing of machine materials.
3. Contamination of liquid metal by impurities in the cover gas or through atmospheric in-leakage.
4. Interference of NaK aerosols and oxides on current collector performance.

6.3.1 Machine Materials Selection

NaK is an alloy of sodium and potassium and is prepared by mixing these two elements in liquid form. Potassium and sodium are miscible in all portions, and the alloy in concentrations of 40 to 90 weight percent potassium is liquid at room temperature. The phase diagram for this system is given in Figure 6.1.³ Eutectic NaK is usually characterized by its low density (0.867 g/cm^3 at 20°C), high electrical and thermal conductivity and low vapor pressure. It also reacts rapidly with oxygen to form Na_2O preferentially, and with water or water vapor to form the hydroxides of sodium and potassium. Thus, NaK systems must be protected by inert cover gas systems.

NaK may be incompatible with materials due to a number of factors. NaK is usually compatible with transition metals, but may show incompatibility with organic insulation materials because of its chemical reactivity.¹ Additionally, material incompatibility may result from materials out-gassing and contaminating the liquid metal. Outgassing problems may arise from structural, but more likely from organic insulation, materials. Outgassing may be due to either (1) adsorbed gases on surfaces and in pores, or (2) reaction products from the polymerized organic insulating materials or solvents. In addition, local machine hot spots may be generated during machine operation which may cause thermal decomposition of organic materials.

A literature survey has indicated that most work dealing with liquid metals has involved their employment at elevated temperatures as heat transfer agents. In applications of this type, the liquid metal does not contact organic electrical insulation materials. A supplier's brochure² states that NaK is more reactive than either sodium or potassium at low temperatures, and that in reactions with organic materials, the potassium derivative is usually formed preferentially. NaK is particularly reactive with organic halides, and the use of halogen-containing polymers (PTFE or PVC for instance) for insulation applications in the homopolar machine appears to be precluded.³ NaK reacts readily at low temperatures with all reactive hydrogens such as those in carboxyl, hydroxyl, and amines. It also cleaves some ether linkages. Although these considerations might appear to eliminate essentially all

Curve 64963 +A

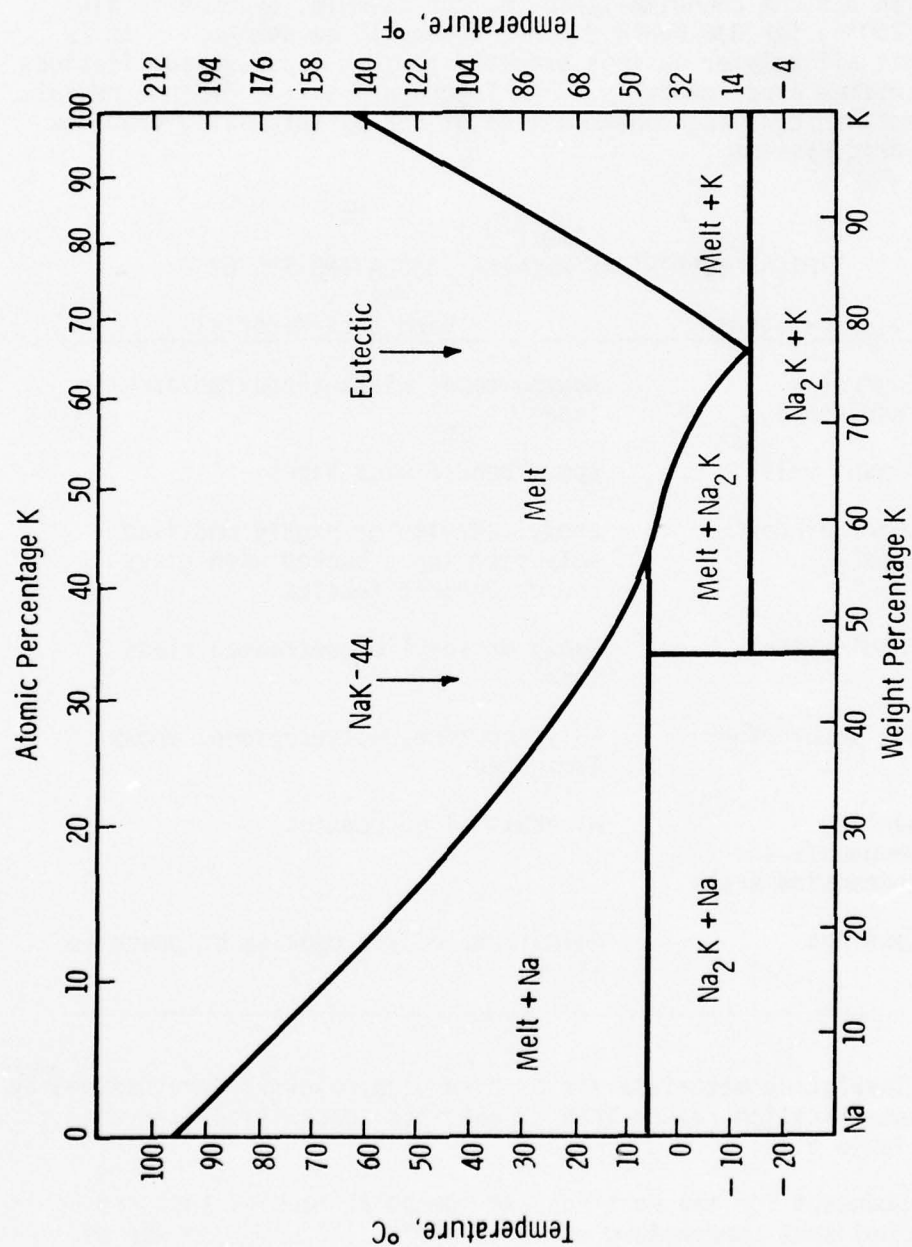


Fig. 6.1 Phase diagram for the NaK binary system.

polymer systems from consideration except those of strictly hydrocarbon nature, other information⁴ which tabulates data for exposure of certain polymer systems to NaK indicates that the lowered reactivities of these groups in large molecules may permit use of many polymer systems in contact with NaK. A phenolic laminate, for example, exposed to NaK at 384°K (250°F) for 336 hours did not appear to be damaged. It is evident that all polymer systems proposed for NaK exposure applications must be verified experimentally. The literature survey did not reveal any information regarding contamination of NaK by outgassing products from polymeric systems.

TABLE 6.1
TYPICAL ELECTRICAL MACHINE INSULATING SYSTEMS

Service Category	Candidate Materials
1. Conductor insulation	Kapton tape; glass-supported acrylic tape
2. Ground wall	Epoxy bonded mica tapes
3. Outer binder tape	Epoxy, acrylic or highly modified polyester tapes backed with glass and/or organic fabrics
4. Banding tape	Epoxy or acrylic pretreated glass tape
5. Collector ring	Polypropylene, polyethylene, epoxy laminated
6. Sealing compounds and connection seals	Mineral-filled epoxies
7. Coatings	Aminoformaldehyde epoxies or phenolic alkyds

Candidate insulating materials for each service category were defined by generic classification rather than by specific composition, and are listed in Table 6.1.

The design concept for the Westinghouse homopolar machine included an insulation hot spot temperature of about 403°K (130°C). The use of Class F (428°K, 155°C) insulation was, therefore, indicated in all service categories identified above except for the collector ring where Class A (378°K, 105°C) insulation was considered adequate.

Reaction of low molecular weight organic by-products with NaK constitutes a major problem area. Such compounds as water, carbon dioxide, carbon monoxide, and monomers which would contaminate the liquid metal can be given off by the insulation, either as a result of continuing cure during the operation of the machine or as a result of thermal pyrolysis.

Periodic cleaning of the machine is expected to involve exposure of the insulation to alcohol-water mixtures, and this necessarily will result in some absorption of both. Exposure of insulation to any sort of humid environment while the machine is not in operation must also result in some water absorption. Failure to properly outgas the insulation prior to returning the machine to operation would result in exposure of the liquid metal to both compounds.

Formation of an aerosol suspension of NaK in the confinement area during operation of the machine is believed to be unavoidable. In consequence, deposition of discrete droplets or possible films of NaK on insulating surfaces is expected to occur. Since cleaning of these surfaces is anticipated not oftener than once every six months, the insulation must remain substantially unaffected by this environment.

Plastics and elastomers are usually considered for gasketing materials at low temperatures or for total containment of NaK. There is scarce, if any, room temperature data as to the compatibility of plastics and elastomers in NaK. However, a number of tests were conducted at 394°K-450°K (250°F to 350°F).⁴ These data eliminate some of the low melting plastics, and some of these can be ruled out due to their chemical composition. It is known that room temperature NaK will react with Teflon; tests have also been made with Viton, a fluorinated material, with unsatisfactory results.

The Liquid Metals Handbook⁵ discusses the compatibility of plastics with alkali metals based on work performed at NASA. In part it concludes that, from the standpoint of weight loss of the plastic and contamination of the metal, the materials that demonstrated the most acceptable behavior were Kel-F3700 and Buna-N in 394°K (250°F) sodium for 9 days and neoprene and Buna-N in 450°K (350°F) sodium for 7 days.⁵ Neoprene and Kel-F are halogenated, and therefore it is recommended that these not be used with alkali metals because of the potential of an explosion hazard associated with their use. Polyethylene has been tested at room temperature in NaK for 3-1/2 years with no visible change.⁴

With the definition of candidate homopolar machine materials, experimental verification of NaK compatibility was initiated. More than 1000 hours of cumulative NaK exposure time has been attained on more than 120 individual samples. These include: (1) rotor banding materials, (2) rotor bar insulation, (3) laminate composites, (4) potting compounds, (5) silastic elastomers, (6) coatings and paints, (7) seal materials, (8) cooling fluids, (9) braze alloys, and (10) structural metals. The evaluation of candidate materials proceeded through a defined test plan which was so

designed as to incorporate the material exposure sequence which was to be followed during actual machine start-up, operation, machine decontamination, and requalification of components after decontamination and subsequent reassembly. Proposed materials were exposed to commercial grade NaK in test canisters heated isothermally in a constant temperature oil bath. Figure 6.2 illustrates the glove box facilities which were utilized to prepare and handle candidate materials and to charge them into test canisters with NaK.

All compatibility studies were performed at 140°C for defined time intervals. This temperature was selected because, in all instances, it represented the most severe condition that any one machine component was expected to encounter (machine hot spot temperatures were calculated to be 130°C max). Therefore, it was assumed that materials which survived this condition in liquid NaK would be prime candidates for the demonstration machine. In addition, materials were evaluated at NaK exposure intervals of 100, 500, and 1000 hours by defined physical measurements. Water was employed as the NaK decontamination fluid. The antechamber of the sample preparation glove box served as a sample baking chamber, simulating machine pre-start up conditions of roughing pump vacuum at 100°C for a fixed time interval of 24 hours.

Physical testing for materials evaluation included: weight changes, dimensional changes, hardness, electrical resistivity, flexural properties, tensile properties, infrared spectroscopy, and scanning electron microscopy (SEM).

Figure 6.3 illustrates the flow sequence of selected materials during the NaK compatibility studies. This program provided quantitative information on the compatibility of materials with eutectic NaK.

6.3.1.1 Rotor Banding Material

An epoxy Novolac/glass fiber tape was selected as the rotor banding material. Since this material was expected to serve as both insulation and a NaK barrier to the rotor bar system in the Westinghouse design, it was important that NaK compatibility be established. Selected material specimens were exposed to NaK and material compatibility established by tensile testing and scanning electron microscope (SEM) examination. Table 6.2 lists the tensile test data for this material.

Since the ultimate strength remained essentially unchanged after more than 1000 hours of NaK exposure, as compared with air aged specimens, and no material degradation had occurred, as shown by SEM examination, this banding material was selected as a prime candidate for use in the demonstration machine.



Fig. 6.2: Glove box facilities utilized for the preparation and handling of materials being evaluated for NaK compatibility.

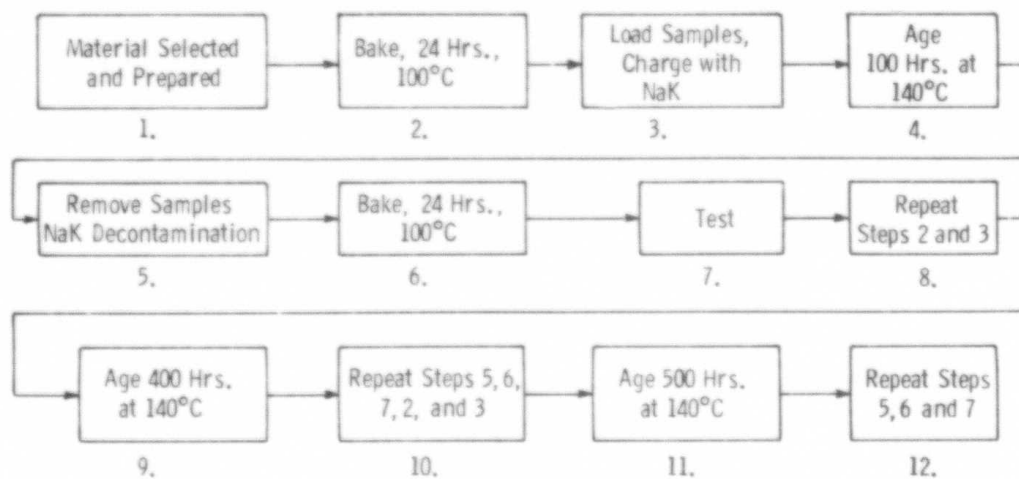


Fig. 6.3: Simplified flow chart of materials compatibility test plan.

TABLE 6.2
 ROTOR BANDING MATERIAL 431-S-2 (EPOXY NOVOLAC
 RESIN/GLASS FIBERS) TENSILE TEST DATA

Specimen I.D.	Specimen No.	Ultimate Strength (ksi)
Archives - as prepared	1	122.9
	2	116.9
Air aged (180°C) 250 hours	3	150.1
	21	157.8
Air aged (180°C) 998 hours	5	163.5
	17	154.3
NaK Exposed (140°C) 99.5 hours	7	142.8
	9	139.3
NaK Exposed (140°C) 507.5 hours	8	132.2
	10	132.2
NaK Exposed (140°C) 1009.5 hours	11	150.9
	12	149.2

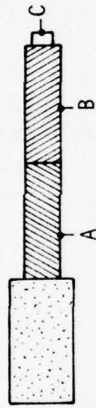
6.3.1.2 Electrical and/or Rotor Bar Insulation

Electrical insulation systems were evaluated for NaK compatibility. Since no reported literature values could be found for NaK compatibility of materials of this type, insulation materials were defined from the known reactivity of NaK with organic compounds. Test specimens were prepared and exposed to liquid and vapor eutectic NaK at 140°C. Surface and volume resistivity measurements for these insulation systems have shown that these selected materials qualify as NaK compatible, see Figure 6.4. Since these specimens were also decontaminated prior to electrical measurements, they also qualified as being compatible with the anticipated machine decontamination scheme.

6.3.1.3 Silastic Elastomers

Early in this study Silastic elastomers, 116 RTV and RTV 732, were selected as probable sealing materials for use in the demonstration machine. Compatibility studies have shown that, although these materials are compatible with NaK at room temperature, severe degradation occurs at elevated temperatures (140°C). As a result of this study, Silastic elastomers have been found to be incompatible with the NaK environment and are not recommended for machine applications in which NaK exposure may occur.

**MATERIALS COMPATIBILITY STUDY
ELECTRICAL INSULATION SYSTEMS**



Insulation System	Electrodes	Archives	Resistivity, Megohms				
			Heat, 112 Hrs.	Heat, 1156 Hrs.	NaK 112 Hrs.	NaK, 449 Hrs.	NaK, 1156 Hrs.
1. Kapton Film 1/2 Lapped, Mica Bonded to Kapton Tape, Polyester on Dacron	A-C (Vol) B-C (Vol) A-B (Surface)	∞ - ∞	∞ - 5×10^5	∞ - ∞	5×10^5 5×10^5 5×10^5	∞ ∞ ∞	∞ ∞ ∞
2. Kapton Film 1/2 Lapped, Mica Bonded to Kapton Tape, Epoxy on Dacron and Glass	A-C (Vol) B-C (Vol) A-B (Surface)	∞ - ∞	10×10^5 - ∞	∞ - ∞	5×10^5 5×10^5 10×10^5	∞ ∞ ∞	∞ ∞ ∞
3. Kapton Film 1/2 Lapped, Mica Bonded to Glass Tape, Polyester on Dacron	A-C (Vol) B-C (Vol) A-B (Surface)	∞ - ∞	10×10^5 - ∞	∞ - ∞	9×10^3 22×10^3 1×10^5	37×10^3 ∞ ∞	4×10^5 ∞ ∞
4. Kapton Film 1/2 Lapped, Mica Bonded to Glass Tape, Epoxy on Dacron and Glass	A-C (Vol) B-C (Vol) A-B (Surface)	∞ - ∞	∞ - 10×10^5	∞ - ∞	∞ ∞ 10×10^5	∞ ∞ ∞	∞ ∞ ∞

Note: $\infty > 10^6$ Megohms

Ageing Temperature = 140°C

Fig. 6.4: Surface and volume resistivity values obtained on heat aged and NaK exposed electrical insulation systems.

6.3.1.4 Machine Laminates

A number of laminate composite materials have been evaluated for NaK compatibility. In addition to noting weight and dimensional changes, flexural properties were also determined. From these measurements, trends were established for the ultimate stress and elastic modulus of these materials as a result of NaK exposure. Figures 6.5 and 6.6 note the changes in maximum stress and elastic modulus respectively of selected candidate laminate materials as a result of NaK exposure at 140°C.

6.3.1.5 Braze Alloys

It has been known for some time that microbrazed alloys are compatible with NaK. On the other hand, soft solders of tin/lead composition are incompatible even for very short periods of time.¹ Silver solders may be employed, but little quantitative information is available concerning the compatibility of these braze alloys with NaK. This study determined whether or not selected silver braze alloys could be employed in the segmented magnet (SEGMAG) demonstration machine.⁶ Since all the braze joints were to be protected from the NaK environment by the rotor banding material in the Westinghouse design, total braze alloy compatibility was not essential. However, in the event that NaK did penetrate the protective barrier of the rotor banding material, the most compatible alloy had to be selected. Five silver braze alloys were evaluated for eutectic NaK compatibility at 140°C to a maximum exposure time of >500 hours. Table 6.3 summarizes the various alloys studied and the weight changes which were observed at exposure times of 112 and 592.8 hours.

TABLE 6.3

BRAZE ALLOYS EVALUATED FOR NaK COMPATIBILITY AT 140°C

Sample I.D.	Composition	% Weight Change		Visual Observation
		112 Hrs	593 Hrs	
BAG-8	72% Ag, 28% Cu	-1.5	-4.03	OK
BAG-18	60% Ag, 30% Cu, 10% Sn	-0.6	-0.44	OK
BT-Li	71.8% Ag, 28% Cu, 0.2% Li	-0.4	-0.69	OK
BCuP-5	15% Ag, 80% Cu, 5% P	+2.1	-4.25	Severe Attack
BAu-4	81% Au, 18.5% Ni	-71.0	--	Sample Dissolved

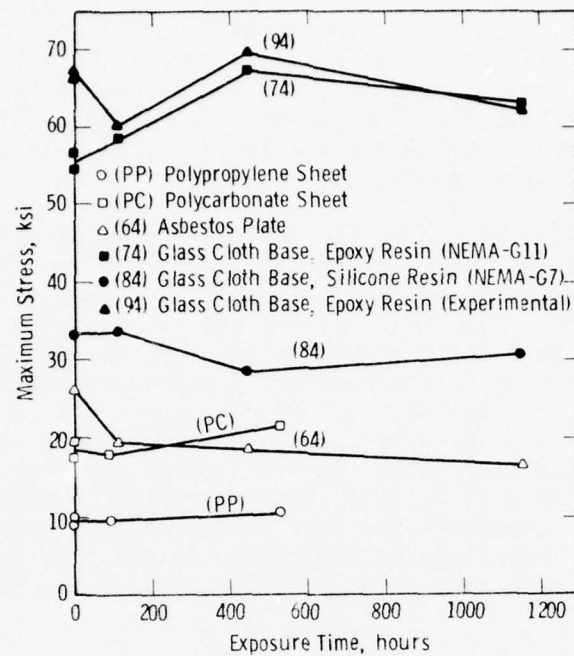


Fig. 6.5: The change in maximum stress of candidate laminate materials as a result of NaK exposure at 140°C.

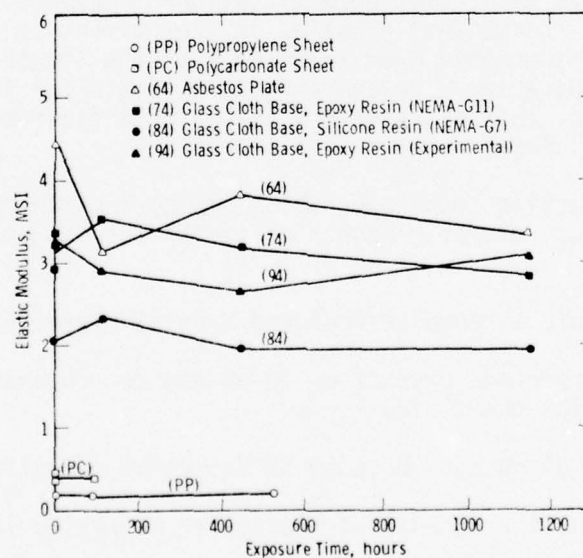


Fig. 6.6: The change in elastic modulus of candidate laminate materials as a result of NaK exposure at 140°C.

Note that two (BCuP-5 and BAu-4) of the five braze alloys completely failed in 112 hours. SEM studies performed on these materials have indicated that the failure mechanism is by way of the selective leaching of precious metals (silver or gold) from the alloy matrix. The three remaining materials have also lost weight due to the removal of silver from the alloy matrix, but these small losses occur only under the most severe NaK exposure conditions.

A summary of the materials compatibility program is presented in Table 6.4. This table lists the generic classification of all the candidate materials which were evaluated for NaK compatibility at a temperature of 140°C. This table also lists the quantitative physical measurements which were carried out for each of the materials specified and indicates whether or not each material may be employed for use in the SEGMAG machine. In general, as noted in Table 6.4, almost all of the candidate materials were found to be acceptable for the machine environment, thus indicating that our initial assumptions concerning the chemical reactivity of NaK with various organic systems were valid. In addition, Table 6.4 also shows that reported NaK incompatible seal materials (graphite base) may be employed provided that a protective supporting matrix, such as a polyimide, is employed when formulating seal materials.

6.3.2 Liquid Metal Systems

Successful operation of a homopolar machine employing a liquid metal as the electrical current transfer media requires intimate and continuous contact of the fluid with rotating and stationary members. Ideally, this fluid would be hermetically sealed in the current collector zone, thus preventing contaminants from reacting with the liquid metal and the liquid metal from escaping. However, rotating seals for large diameter high speed machines, that are also compatible with candidate fluids, are not technically feasible at this time.

Other current collection techniques which employ a batch process without adequate sealing must overcome severe obstacles for long-term operation. These include:

- Loss of fluid through aerosol and droplet migration.
- Oxide and reaction product build-up due to contaminants reacting with the fluid.
- Compositional changes because of selective oxidation.
- Flow instability because of inadequate supply during some operating conditions.

TABLE 6.4 - MATERIALS COMPATIBILITY SUMMARY

CANDIDATE SEGMAG ORGANIC BASE MATERIALS
EVALUATED FOR NaK COMPATIBILITY (140°C)

Material	Type	NaK Compatibility	Preliminary Screening Experiments	Weight Changes	Dimensional Changes	Hardness	Electrical Resistivity	Elastic Modulus	Maximum Stress	Tensile Properties	Mass Spectrometry	Infrared Spectroscopy	Scanning Electron Microscopy	Friction and Wear Studies
Banding Tapes	1. polyester on glass	A	✓	✓	✓	✓								
	2. acrylic modified epoxy on glass	A	✓	✓	✓	✓								
	3. polyester on experimental fibers	A	✓	✓	✓	✓								
	4. epoxy Novolac resin on glass	A	✓	✓	✓	✓								
Banding Pads	1. epoxy on glass	A	✓	✓	✓	✓								
Laminates	1. glass cloth base, silicone resin	A	✓	✓	✓	✓		✓	✓					
	2. glass cloth base, epoxy resin	A	✓	✓	✓	✓		✓	✓					
	3. asbestos plate	A	✓	✓	✓	✓		✓	✓					
Rotor Bar Insulation	1. Kapton film 1/2 lapped, mica bonded to Kapton tape, polyester on dactron	A	✓				✓	✓						
	2. Kapton film 1/2 lapped, mica bonded to Kapton tape, epoxy on dactron and glass	A	✓				✓	✓						
	3. Kapton film 1/2 lapped, mica bonded to glass tape, polyester on dactron	Q	✓				✓	X						
	4. Kapton film 1/2 lapped, mica bonded to glass tape, epoxy on dactron and glass	A	✓				✓	✓						
	5. Kapton film, type H (2-3 mil)	U	X	X	X									
Coatings	1. epoxy enamel	A	✓	✓										
	2. electrostatically deposited epoxy coatings	A	✓	✓										
Silastic Sealants	1. 116 RTV	Q	✓	X	X									
	2. 732 RTV	U	X	X	X									
	3. 892 RTV	U	X	X	X									
Miscellaneous	1. cooling fluid - Wemco C	A	✓										✓	
	2. adhesive - (Eastman 910 MBT)	U	X											
	3. potting compound - silica filled epoxy	A	✓	✓	✓	✓								
	4. polyethylene sheet	U	✓	✓	X									
	5. polypropylene sheet	A	✓	✓	✓	✓								
	6. polycarbonate sheet	A	✓	✓	✓	✓								
CANDIDATE SEGMAG INORGANIC BASE MATERIALS EVALUATED FOR NaK COMPATIBILITY (140°C)														
Seals (125°C)	1. 99.9% graphite	U	X											
	2. carbon-graphite + MoS ₂	U	X											
	3. carbon-graphite + MoS ₂ (>SK-235)	U	X											
	4. similar to above with phenolic impregnation	U	X											
	5. straight carbon-graphite	U	X											
	6. bronze matrix + carbon	A	✓											
	7. polyimide matrix + 15% graphite + 10% Teflon	A	✓											✓
	8. polyimide matrix + 15% MoS ₂	A	✓											
	9. 80% tungsten diselenide - 20% gallium-indium	U	X											✓
	10. WGI + oxide coating	U	X											
	11. 90% WGI - 5% Ag - 5% CaF ₂	U	X											
	12. tungsten diselenide	U	X											
	13. carbon-graphite, density = 1.8 gms/cc	U	X											
	14. carbon-graphite, density = 1.9 gms/cc	U	X											
	15. pyrographite	U	X											
	16. impervious pyroimpregnated graphite	U	X											
	17. boron nitride + 3 w/o boric oxide	A	✓											
Structural Metals	1. copper PDL35 (rotor)	A	✓											
	2. copper OFHC (stator)	A	✓											
	3. rotor steel	A	✓											
Brazing Alloys	1. microbrazing	A	✓											
	2. precious metal	U	X											X
	3. soft solder	U	X											X

A = acceptable for use in both NaK liquid and vapor.

Q = questionable NaK compatibility - may be used at lower temperatures (50-100°C).

U = unacceptable - adequate protection from NaK must be provided.

✓ = passed test.

X = failed test.

The most practical method for overcoming these obstacles is through the use of a recirculating system. Such a system was selected to service the Westinghouse 3000 Horsepower Prototype Homopolar Generator (SEGMAG). Figure 6.7 schematically presents a loop design to service each of the six SEGMAG current collectors. Eutectic NaK, the SEGMAG current transfer fluid, is circulated by a centrifugal pump through a high resolution electromagnetic flowmeter, through a water cooled cold trap, and into the current collector annulus. Drain channels collect NaK overflow from the current collector and return it to the sump tank and back to the pump inlet. Gravity drainage of the NaK to the sump tank is assisted by a recirculating gas system. Original design plans considered one large NaK loop with six parallel feed-drain legs for current collection fluid circulation. Problems were apparent when the I^2R losses were considered for common NaK current collection lines. Losses of over 40 kW were predicted. A technique of breaking the NaK flow through insulated connections and utilizing the NaK loop demonstrated that electrical isolation of the current collectors could be maintained. However, verification of this novel NaK recirculation technique for extended, unmanned operation was considered too time consuming for contract schedules, and the more secure, individual loop approach was followed.

Each NaK loop was designed to service one current collector and was completely isolated electrically from other loops and ground. The sump tank contains approximately two liters of eutectic NaK, which is sufficient to maintain long-term compositional stability and replace that which may be lost by aerosol formation and fling-out. Level probes in the sump tank indicate whether NaK levels are becoming unacceptably high or low. The sump tank also provides the first stage of NaK purification whereby insoluble or precipitating oxides and impurities float to the surface of the NaK pool.

In the loop, the NaK flows from the flowmeter up through a cold trap, which removes soluble impurities and oxides by a precipitation process and particulates by a filtering process, before returning NaK to the current collector. Figure 6.8 presents one of the SEGMAG NaK loops; components can be identified from Figure 6.7. The loops are of type 304 stainless steel, and consist of all welded, dye-penetrant and helium mass spectrograph leak checked construction, employing liquid metal bellows seal valves. Loop capabilities are presented in Table 6.5. As presented in Table 6.5 and demonstrated in Figure 6.9, the six NaK loops are placed beneath the SEGMAG unit.

The NaK pump was selected after evaluating EM, gear, bellows, and centrifugal pumps. It is a canned rotor, inductively coupled, centrifugal pump and was qualified for over 1,000 hours in NaK prior to its selection. The flowmeter is electromagnetic, and was designed by Westinghouse for low temperature, low flowrate NaK service. A calibration curve presented in Figure 6.10 demonstrates the meter's accuracy to ± 5 cc/min in the 0-800 cc/min range. The NaK system proved to be entirely satisfactory for SEGMAG operation. Each of the six loops operated for hundreds of hours without major problems, and a prototype loop has operated for more than 9,000 hours continuous operation.

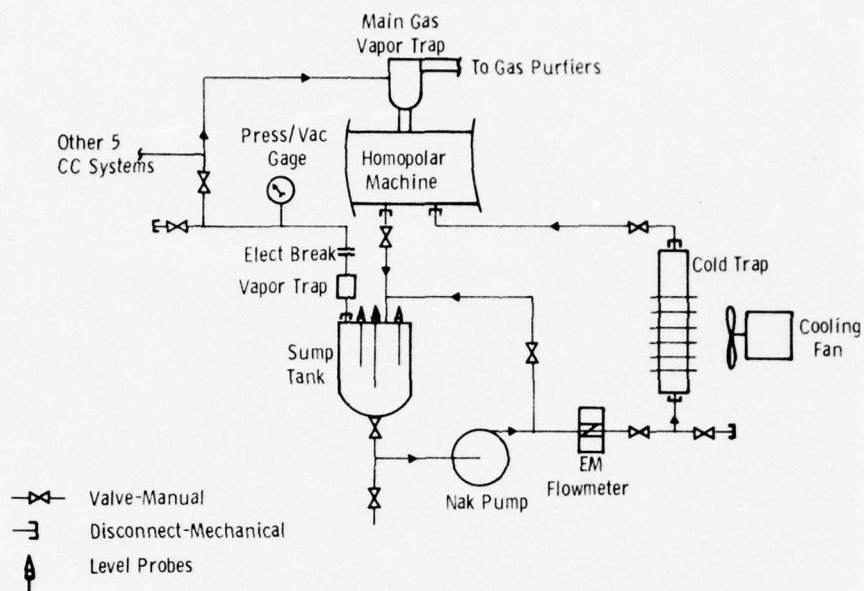


Fig. 6.7: Small NaK loop concept for servicing each current collector independently.

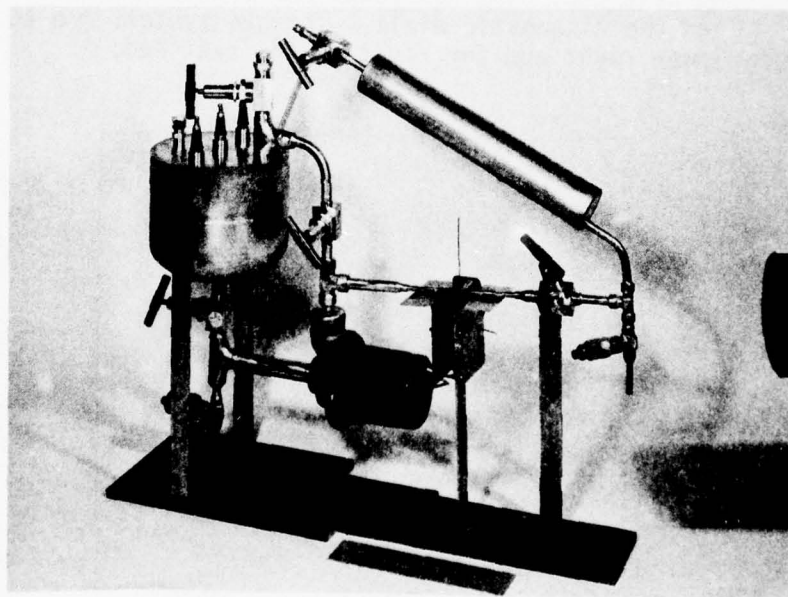


Fig. 6.8: Assembled NaK loop of a current collector service in prototype SEGMAG machine.

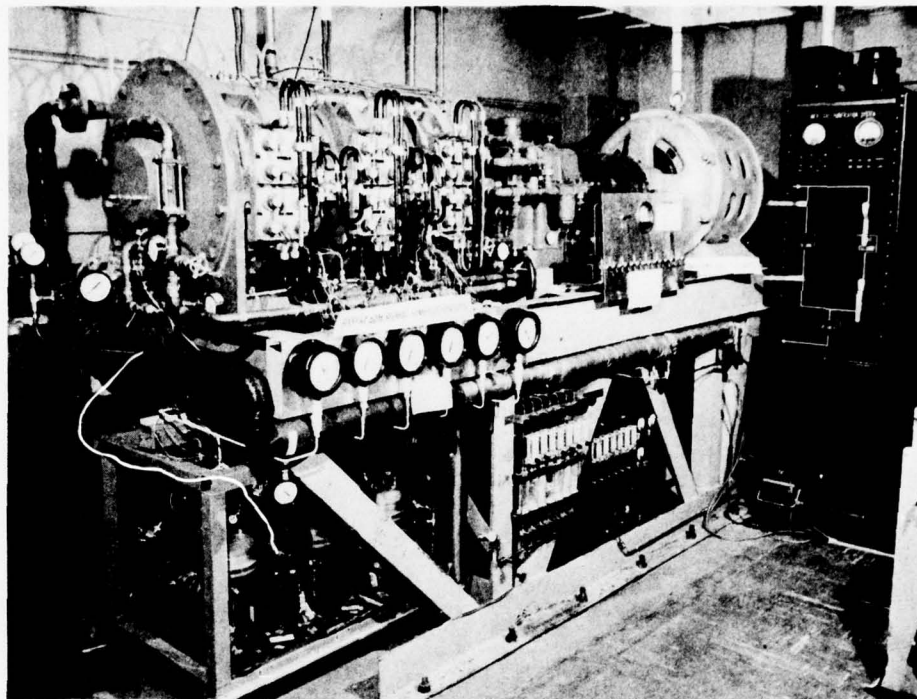


Fig. 6.9: 3000 HP segmented magnet homopolar generator (SEGMAG) on test bed. The NaK loops are located below the SEGMAG and the diagnostic dials. The gas systems are to the lower right and far right of the test bed.

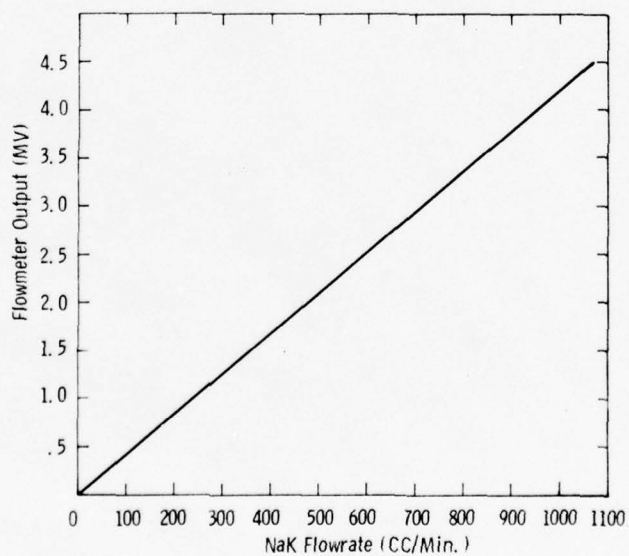


Fig. 6.10: Calibration of NaK flowmeter.

TABLE 6.5
NaK LOOP CAPABILITIES

1. Temperature:	Max. 250°C loop, 150°C pump Min. 0°C loop and pump
2. Flowrate:	0-800 cc/min
3. Inventory:	Sump tank volume - 2700 cc NaK charge in system - 2000 cc Total working NaK - 850 cc
4. Physical size:	Each loop 2' x 2' x 7" wide Six loops fit into 2' x 2' x 3½' enclosure
5. Pressure:	Max. 50 psig loop, 15 psig pump Min. high vacuum loop, 0 psig pump
6. Material:	All 304 s/s or 316 s/s Valves - Metal bellows seal welded All welded, inspected construction
7. Purity control:	Two stages First stage - sump tank, oxides float Second stage - cold trap, filter
8. Level control:	Sump tank - three electrical con- tinuity probes

6.3.3 Cover Gas Systems

An automated cover gas handling system was fabricated for the demonstration SEGMAG machine. The gas system consisted of three subsystems: 1) main gas recirculation and purification unit; 2) gas pump and supply for tandem gas circumferential seals; and 3) intercollector gas system. These are illustrated in the schematic in Figure 6.11.

The main gas recirculation and purification system consists of a commercial unit which Westinghouse designed and contains tandem (parallel) towers of Dow resin and molecular sieve materials. Dry nitrogen is thus circulated through the machine, and through one tower at a time. The tower removes oxygen and moisture to levels of 1 ppm and below. Refrigerant-cooled heat exchangers were added to remove condensable vapors (NaK vapor, organic compounds) that could leave the machine and affect the active resins. One tower may be automatically regenerated while the other is on-line. Flowmeters and control valves balance the flow and circulation of dry nitrogen through the machine housing. The pressure is maintained at 4 psig and high and low pressure alarm interlocks are provided. A continuous sample of gas is drawn and sampled for oxygen and moisture purity, and a trace recorder is employed to indicate oxygen levels. An alarm interlock is provided for the detection of oxygen levels above 10 ppm (V). Cover gas

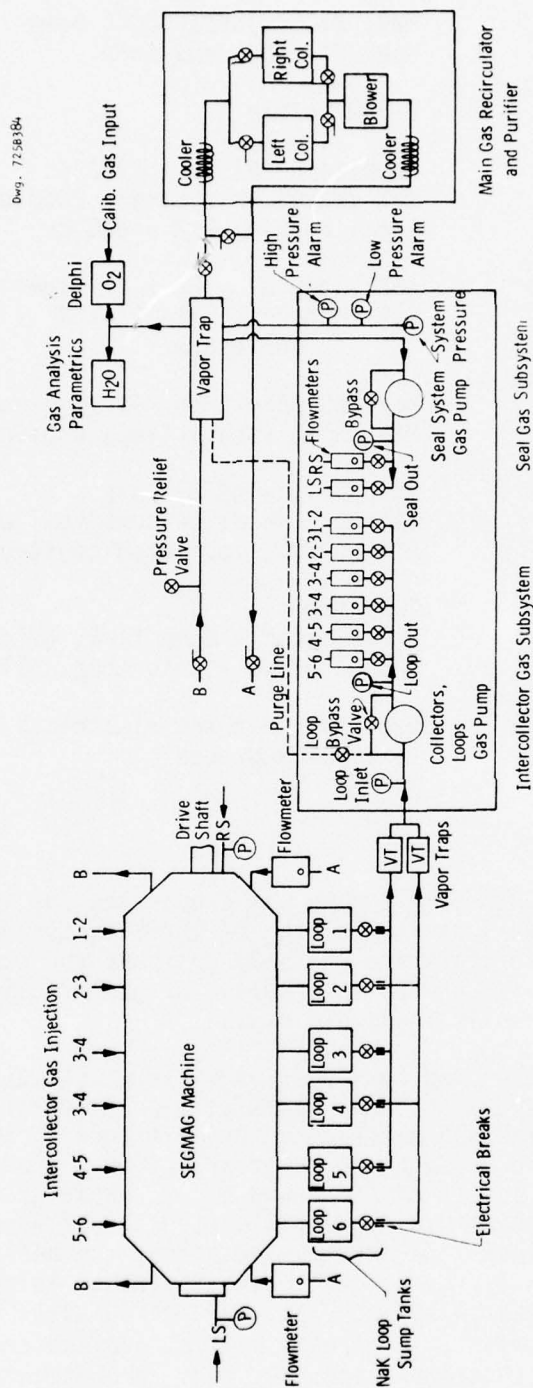


Fig. 6.11: SEGMA cover gas systems

can be circulated through the system at 0 to 35 SCFM. Experimental operation of this unit with the SEGMAG showed it to perform better than expected, and to maintain machine cover gas purities at 1 ppm (V) for oxygen and even better for moisture during machine temperature excursions reaching 90-115°C. Thus the NaK inside the machine was not subject to oxidation and oxide formation problems.

A second gas system operated from the main gas system to distribute the nitrogen. A mechanical, bellows pump is employed to extract gas from the main gas system recirculation lines and to raise the pressure to 5-7 psig for insertion into the tandem circumferential shaft seals. Dry nitrogen is thus supplied to the seals at 1-2 SCFH. Half of the gas is lost to the environment, half returns to the machine housing for recirculation and purification. A gas pressure controller automatically supplied cover gas makeup for losses, as well as maintaining system pressure.

A third gas system, also illustrated in Figure 6.11, called the inter-collector gas system, is employed. A mechanical, bellows gas pump is employed to pull cover gas down the NaK drains of each current collector (gravity drains to a sump tank) and thus assist drainage. This gas is removed from each loop at the sump tank (the void space above the NaK level), drawn through a vapor trap, and then forced by the gas pump through six flowmeters, and reinjected into the intercollector gas gaps between the rotor and stator. Once in the gas gap, the gas divides and flows into the adjacent current collectors, sweeping aerosol and NaK vapor. The gas then exits via the NaK drains and repeats the cycle. Contaminants which enter the gas are removed by reaction with the NaK; the reaction products float on the NaK surface in the sump tank.

Trial operation of the cover gas system, first with the glove box (100 CF), and subsequently with the SEGMAG machine (less than 1 CF), have confirmed its operation. For the initial startup, a roughing pump vacuum was applied to the machine while it was heated to 70-80°C. Following removal of the volatiles, moisture, etc., in this fashion, a dry nitrogen gas purge was initiated. Monitoring of the effluent purge gas for oxygen and moisture showed both to be below 100 ppm (V), and the main cover gas recirculation system was started. This system operated continuously once the machine was clean of oxygen and moisture. The shaft seal system was activated only prior to and during rotation. The intercollector gas network was only active during NaK circulation through the machine. The on-line oxygen and moisture monitors operated continuously.

A fourth cover gas system, not illustrated in Figure 6.11, provided an auxiliary blow-down network for NaK which collected between current collectors. This network provided a good indication of collector performance (i.e., NaK retention) during machine transient conditions. NaK lost to the intercollector gaps was removed from the machine and collected in graduated catch basins (one for each intercollector zone). Continuous or intermittent operation of this blowdown network could be selected, and a bellows gas pump was provided to assist lost NaK removal.

6.3.4 Support System Summary

As can be envisioned, all three subsystems were vital to successful machine performance. All machine materials employed were compatible with NaK and NaK decontamination products and processes. The materials, NaK loops, and cover gas systems all interacted in a viable fashion to ensure long term operation of the machine. The NaK and cover gas systems were sufficiently flexible to allow fine tuning the machine operation through a wide range of performance testing.

6.4 CONCLUSIONS

Long term homopolar machine operation will require a design incorporating: (1) selection of proven NaK compatible materials; (2) a liquid metal recirculation and purification system; (3) a cover gas network which can remove degas as well as inleakage contaminants to provide for clean NaK environments. The materials selected by this study have exhibited NaK compatibility, and show trends for continued long term compatibility. The NaK recirculation and purification loop (prototype) has over 9,000 hours continuous operation with various contamination levels of cover gas. The cover gas purification system is a modified commercial unit which has typically operated many months without maintenance.

6.5 REFERENCES

1. O. J. Foust, Ed., *Sodium-NaK Engineering Handbook*, Gordon and Breach, Science Publishers, Inc., New York, 1972.
2. MSA Research Corporation Technical Bulletin, NaK and Potassium, Bull. No. MD-70-1, MSA Research Corporation, Evans City, PA 16033.
3. C. G. Allan and J. L. Drummond, The Reaction of PTFE with Liquid Sodium, Potassium, and NaK Alloy, TRG Report 2104(D), National Technical Information Service, Springfield, VA 22151, 1970.
4. MSA Research Corporation Publication, Introduction to NaK and BZ Alloys, MSA Research Corporation, Evans City, PA 16033.
5. C. B. Jackson, Ed., *Liquid Metals Handbook*, Sodium (NaK) Supplement, July, 1955.
6. C. J. Mole, "Design and Development of a Segmented Magnet Homopolar Torque Converter," Semi-Annual Technical Report, EM 4648, February, 1975.

VOLUME II
PART A
SECTION 7
SEAL STUDY

7.1 OBJECTIVES

The seal study associated with this program had two primary objectives: 1) to review the current state-of-the-art of seal technology and identify those locations in homopolar machines requiring seals; and, 2) design a test apparatus capable of evaluating the performance of various seal concepts under operating conditions anticipated in homopolar machine applications.

There are two subtasks to the seal study:

- 1) Confinement of liquid metal to the current collection zone. This work is reported in Sections 4 and 5, "Current Collection Systems".
- 2) Development of the seal systems for the primary rotor shafts of the homopolar machines. This work is reported in this section.

During Phase I of this program, our objectives were: 1) to review the state-of-the-art of seal technology as applicable to homopolar machines, 2) design a test apparatus capable of evaluating the performance of various seal concepts under operating conditions anticipated in homopolar machine applications.

During Phase II our objective was to develop a shaft seal system for homopolar generator applications, where the mode of operation is both unidirectional and continuous. In particular, the goal was a shaft seal for the SEGMAG generator.

In Phase III, consideration was given to extending the seal technology to: 1) torque converter and motor applications where reversible and variable speeds are encountered; and, 2) unidirectional high speed (96 m/s collector speed) generators.

7.2 PRIOR AND RELATED WORK

Continuing demands for higher efficiency and higher performance of modern machinery; such as, gas turbines, compressors, and other types of rotary gas-handling equipment, have generated increased attention to the problems of seal performance in these applications. Clearance seals, by their very nature, yield leakages that are unacceptable in many of these installations. For this reason, considerable effort has been devoted to

the development of high performance, low leakage, contact-type seals for use in critical applications. A circumferential seal is one such design that exhibits the ability to not only withstand high-velocity rubbing at their primary sealing surfaces, but also to provide a high degree of sealing ability. In addition, it allows for considerable relative axial motion between the rotating and stationary members of the machine. The general configuration of a typical circumferential seal consists of relatively stationary segmented rings which mate with a rotating member on their bore. The rings are loosely keyed to the stationary member by rotation locks. Circumferential garter springs are used to maintain contact under static conditions. Under dynamic conditions, incorporation of appropriate seal life configurations results in the separation of the sealing surfaces from the rotating member by hydrostatic means. The amount of separation is in the order of 100 to 500 micro-inches. Seals of this type have provided 4,000 to 5,000 hours of operation at surface velocities of about 450 ft/sec. Gas leakage rates fall in the range of 0.1 to 0.3 SCFM.*

The second major category of contact seals is the face-type, or mechanical seal. Complementing the circumferential seal, the face seal is designed for applications requiring a high order of sealing effectiveness where axial motion between shaft and casing is limited. Unlike the circumferential seal, the face seal can be made to accommodate fluids with practically no regard to their viscosities. The conventional type of face seal is composed of a seal ring that is keyed by a rotation lock to a stationary housing. This seal ring contacts a shoulder that is constrained to rotate with the shaft. Primary sealing occurs in the radial plane of relative motion between the shoulder and a projecting dam on the seal ring. A secondary seal - in many cases an elastomeric, O-ring type seal - is located between the seal ring and the housing to which it is keyed. To maintain contact between the primary sealing members, an axial driving force is required to move the seal ring. The use of axial springs to supply this driving force is most common. Current practice employs this type of seal for confining both gases and liquids. For example, high-speed, industrial, face-type air seals have demonstrated their ability to provide several years of operation at surface velocities of nearly 300 ft/sec. The seals have demonstrated their ability to accommodate pressure differentials ranging from 10 psi to 135 psi without either excessive wear or high leakage. Dynamic air leakage at 30 psig, for example, is well below 0.3 SCFM.

High-speed industrial oil seals have provided successful operation for years in oil refinery compressor operation at surface velocities of 180 fps. Oil leakage in the order of 30 to 400 cc/hr (depending on speed) are easily accommodated by appropriately designing wind-back seals and drainage ports.

* Standard Cubic Feet Per Minute

7.3 SUMMARY OF ACCOMPLISHMENTS

7.3.0 General

Studies performed during Phase I indicated that a tandem circumferential seal,^{1,2} or bore seal, was the prime candidate for satisfying the requirements imposed on the primary rotor shaft. The circumferential seal not only exhibits the ability to withstand high velocity rubbing at its primary sealing surfaces, but also the ability to provide a high degree of sealing effectiveness. Its design conserves weight and space, provides virtually unlimited shaft travel, and is easily assembled. Figure 7.1 is a schematic of this seal type.

With regard to material selection for use in these seals, care was exercised to insure that the self-lubricating composite employed retained its lubricating ability in a no-moisture, inert gas environment. Standard grades of carbon-graphite seal materials exhibit extremely poor friction-wear characteristics in dry argon.³ Face seal screening tests on candidate seal materials for use in the primary rotor shaft seals of homopolar machines indicated that two polyimide matrix composites exhibit satisfactory friction-wear characteristics in the inert, no-moisture environment required for these machines. The composites contain solid lubricants, such as molybdenum disulphide, Teflon, and graphite, as fillers. Both materials were also found to be compatible with NaK at a temperature of 108°C. Seal segments suitable for use in tandem circumferential seals were fabricated from these materials.

A seal test stand was designed and constructed (Fig. 7.2). Through the use of a 2:1 pulley ratio, the test stand is capable of performing experiments on various seal configurations over a 7000 rpm speed range in inert, bone-dry environments. Leakage rates, operating speed, and seal and bearing temperatures are continuously monitored. The test stand is capable of evaluating seals for shafts ranging in diameters from 2 to 6 inches.

Tandem circumferential seals were purchased for functional testing purposes as well as for use on the SEGMAG machine. Testing results on these units indicated that seal leak rates can be held to 0.02 cfm or less and that the use of carbon-graphite seal materials in these units is unsatisfactory when they are applied in dry, inert gas environments.

The test program for functional seal testing consisted of three phases:

- 1) Candidate seal materials were evaluated with regard to their ability to operate effectively in an inert, no-moisture environment.
- 2) Concurrently, these materials were evaluated with respect to their compatibility with NaK at room temperature and, where appropriate, at elevated temperature.

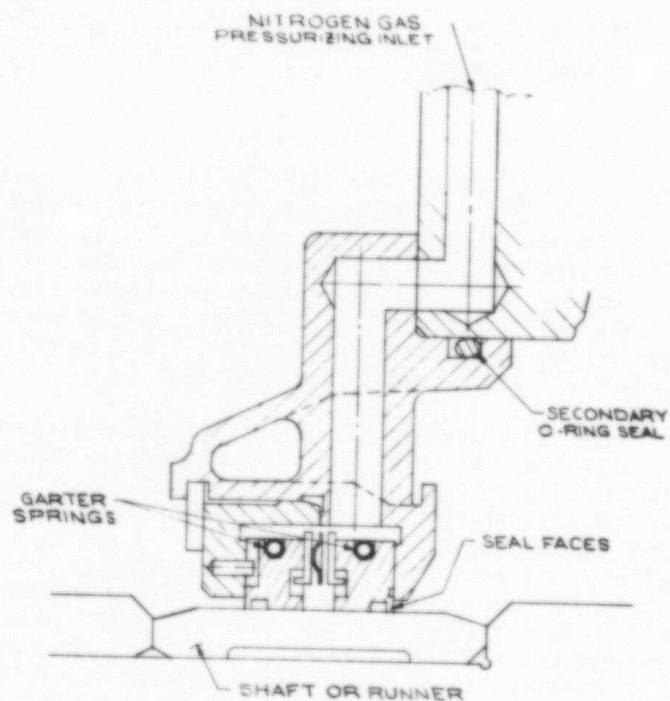


Fig. 7.1: Schematic of typical tandem circumferential seal

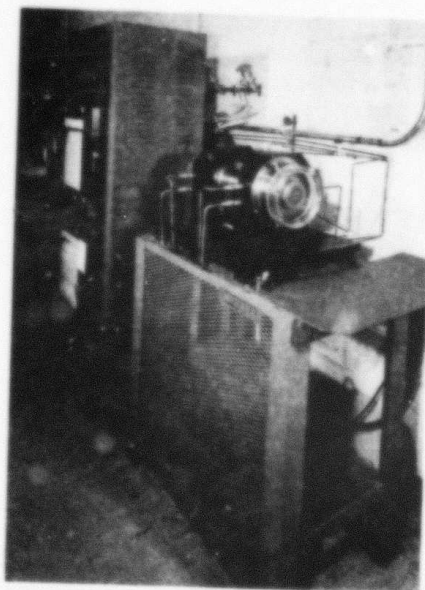


Fig. 7.2: Tandem circumferential seal test rig

- 3) Finally, the most promising materials were fabricated into actual seals and tested extensively with respect to operating speed, runner design and material, and load pressure. The results were compared against those obtained on units employing standard carbon-graphite materials. Parameters monitored during these tests included seal wear, leakage, and operating temperature.

7.3.1 Test Stand Construction

Based on the decision to utilize the tandem circumferential seal as the rotor shaft seal, a seal test stand was designed during the Phase I effort of this program. Figure 7.3 is a schematic of the device and provides an overall view of the drive motor, support frame, and the seal test stand itself. Figure 7.4 is a more detailed view of the test stand, illustrating slave bearing preload techniques and test seal mounting and locking arrangement. The drive motor is a 10 hp, 3 phase, 230 volt adjustable speed drive with a static dc thyristor drive control. Maximum operating speed of the motor is 3600 rpm, regulated to within $\pm 1\%$ by means of a separate tachometer unit. The motor is equipped with jogging and reversing capabilities as well as dynamic braking. Figure 7.5 is a photograph of this test rig.

The hardened, tool steel (#21) shaft is 3 inches in diameter at the test seal site. Precision bearings employed as slave bearings are grease packed and equipped with riveted phenolic retainers. Maximum speed rating for these bearings is 8400 rpm when grease is used as the lubricant. A sealed, plexiglas housing is located around the test seal and provides for not only visual observation of the test seal while in operation but also a means for monitoring gas leakage past the seal face. The flow rate of gas feeding the seal faces is continuously monitored. Seal temperature and both spindle bearing temperatures are also continuously monitored and recorded. A temperature excursion at any of these locations will automatically terminate the test by interrupting power to the motor.

7.3.2 Material Studies of Candidate Seal Composites

In considering carbon-graphite base materials as potential candidates for seal applications in NaK, or NaK-containing environments, material compatibilities must be determined. Compatibility studies performed under the Phase II effort of this program illustrated that many of the conventional carbon-graphites employed as seal materials undergo rapid chemical reactions with NaK at room temperature. Table 7.1 lists and identifies the various seal materials procured for compatibility studies.

As indicated in the compatibility studies, the rapid reaction of graphite with potassium presents a serious problem in respect to considering graphite composites as seal materials for NaK. In addition, the potassium

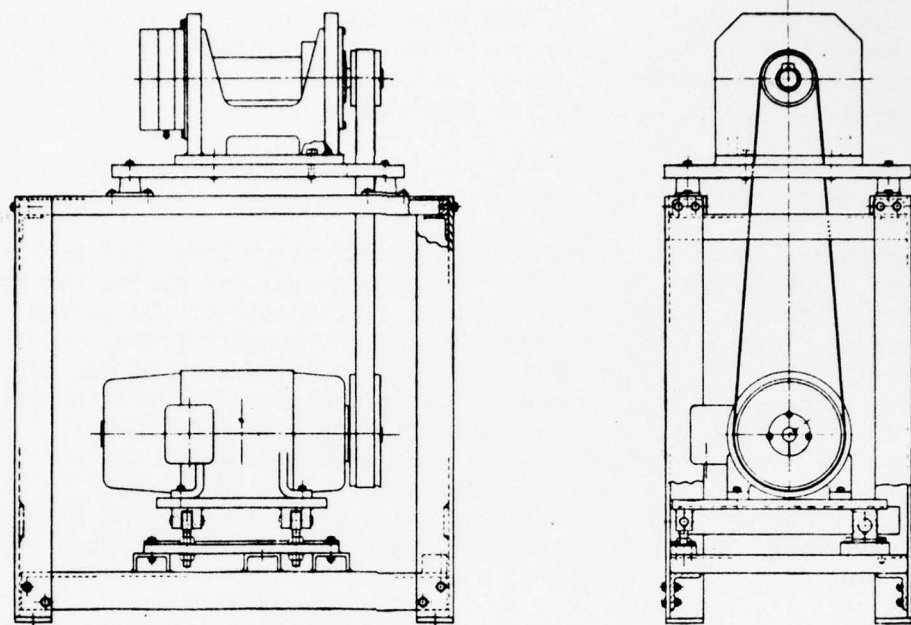


Fig. 7.3: Shaft/Containment Seal Test Stand

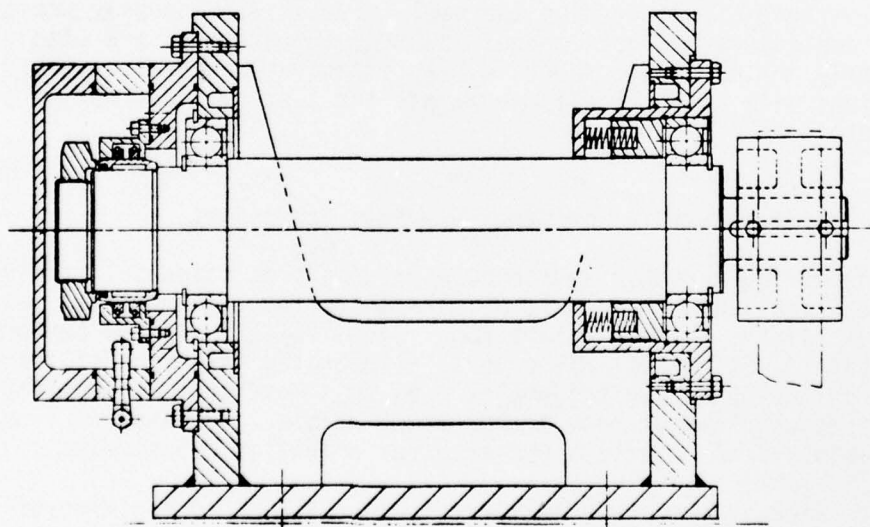


Fig. 7.4: Details of Seal Test Device

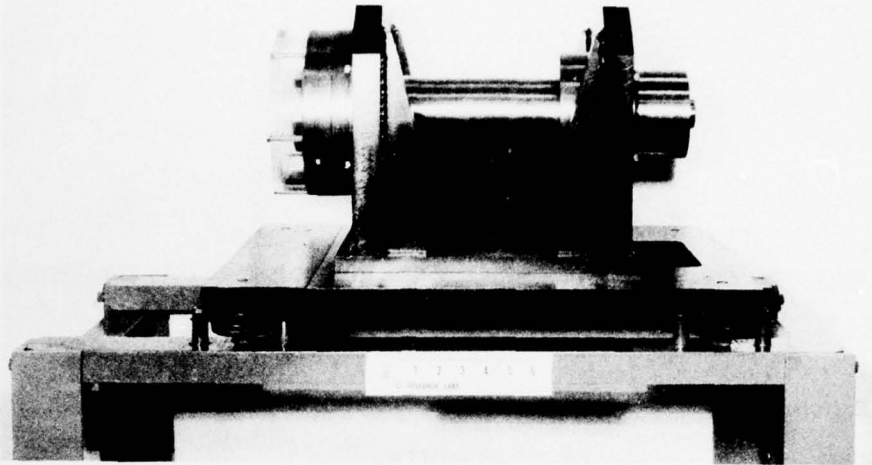


Fig. 7.5: Seal Test Stand

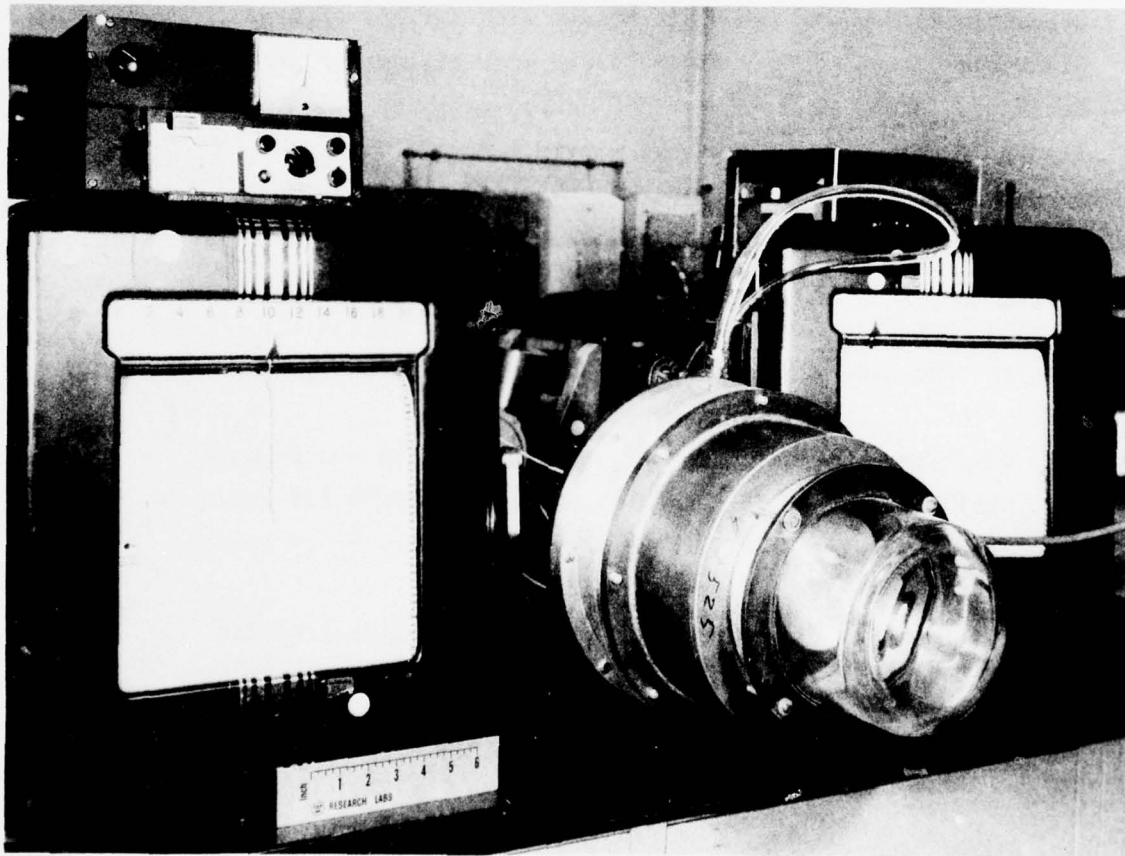


Fig. 7.6: Face Seal Test Stand

TABLE 7.1
SEAL MATERIAL PROCURED FOR FRICTION-WEAR AND COMPATIBILITY STUDIES

Grade Number	Supplier	Identification
EVC	U.S. Graphite	99.9% graphite
Sk-235	Stackpole Carbon Co.	Carbon-graphite + MoS ₂
Sk-278	Stackpole Carbon Co.	Carbon-graphite + MoS ₂ (>Sk-235)
Sk-218	Stackpole Carbon Co.	Similar to Sk-278 with Phenolic impregnation
CR-218	Stackpole Carbon Co.	Resin bonded with fillers of graphite and Teflon
CR-219	Stackpole Carbon Co.	Resin bonded with fillers of graphite and Teflon
1257	Stackpole Carbon Co.	Straight carbon-graphite
MF-343	Stackpole Carbon Co.	Bronze matrix + carbon
SP-3	Dupont	Polyimide matrix + 15% graphite + 10% Teflon
SP-211	Dupont	Polyimide matrix + 15% MoS ₂
WGI	Westinghouse Electric	80% tungsten diselenide - 20% gallium-indium
WGI-O	Westinghouse Electric	WGI + oxide coating
WGI-A	Westinghouse Electric	90% WGI - 5% Ag - 5% CaF ₂
WSe ₂	Cerac, Inc.	Tungsten diselenide
AXZ	Poco Graphite	Carbon-graphite; density = 1.5 gms/cc
AXM	Poco Graphite	Carbon-graphite; density = 1.8 gms/cc
AXF	Poco Graphite	Carbon-graphite; density = 1.9 gms/cc
LEM-1	Raytheon	Pyrographite
LEM-2	Raytheon	Impervious pyroimpregnated graphite
BN-0	Raytheon	Boron nitride + 3 w/o boric oxide

may act as a "spacer" for opening the lattice for reaction with sodium. Since the reactions take place between the layer planes of graphite, the less structured carbon-graphite or carbon materials should be less reactive and may represent potential materials for "carbon" type base composite seal materials where direct exposure to NaK is involved. Composite matrices could be comprised of NaK-resistance metals or polymers, such as iron, beryllium copper, polyimide, polypropylene and polyethylene. Throughout these matrices would be distributed potentially NaK compatible solid lubricants such as boron nitride, carbon, or inorganic fluorides.

In addition to NaK compatibility studies, it is also necessary to evaluate the friction-wear characteristics of candidate seal materials to determine their ability to retain their self-lubricating properties in a no-moisture, inert environment. It is a well-known fact in the lubrication field that the solid lubricating characteristics of graphite and carbon-graphite composites are lost when moisture is removed from their environment. The rotor shaft seals of the prototype SEGMAG machine must operate effectively in the dry, inert cover gas of the machine's containment vessel. For this reason, the ability of the seal material to lubricate satisfactorily in such an environment is of major concern.

7.3.3 Face Seal Screening Tests

Preliminary NaK exposure studies on conventional and filled carbon-graphite seal materials quickly illustrated their total lack of compatibility with the liquid metal. As a result, the number of candidate seal materials suitable for this application was severely limited. Table 7.2 lists those materials selected on the basis of (a) their potential compatibility with NaK, and, (b) their ability to retain acceptable self-lubricating characteristics in an inert, no-moisture environment.

TABLE 7.2
CANDIDATE SEAL MATERIALS FOR USE IN SEGMAG
PRIMARY ROTOR SHAFT SEALS

Material	Composition	Supplier
Delrin "AF"	Acetal matrix + PTFE fibers	Dupont
WGI	Tungsten Diselenide + Gallium-Indium	Westinghouse
Meldin P-30	Polyimide matrix + PTFE	Dixon
SP-3	Polyimide matrix + MoS ₂	Dupont
SP-211	Polyimide matrix + PTFE + Graphite	Dupont

Prior to fabricating these materials into actual circumferential seals, each composition was evaluated on a face seal test apparatus with respect to its dynamic friction coefficient, wear rate, and ability to retain self-lubricating characteristics in an inert, no-moisture environment. Figure 7.6 is a photograph of the rig used to perform these tests and Fig. 7.7 is a schematic of the test apparatus. Operation of this unit at PV (pressure + velocity) ratios up to 100,000 and temperatures up to 450°F is possible.

The candidate seal material is fabricated into a face seal having a 2-7/8" diameter sealing dam and is dead-weight loaded against a Kennametal WC801 tungsten carbide runner mounted in a KOVAR housing. The runner is driven at a constant speed of 3600 rpm. Through the use of a metal extension and glass bell cover, a sealed test chamber is provided in which the type of environment (air, nitrogen, helium, etc.) and its moisture content can be carefully controlled. Test parameters monitored during each experiment include the dynamic friction coefficient of the seal material with respect to the rotating runner, seal face wear, and operating temperature. Tests on the candidate materials were conducted at ambient temperature and a surface velocity of 41 fps in a nitrogen gas environment having a dew point < -45°C. It will be noted that high dynamic friction coefficients actually caused melting of the Delrin "AF" composite under a unit loading of 30 psi. Both the WGI and Meldin P-30 self-lubricating composites demonstrated excellent friction and wear characteristics over continuous 140 and 200 hour runs, respectively. Unfortunately, later studies with regard to the compatibility of these materials with NaK eliminated them from further consideration at this time. It will be noted from data in Table 7.3 that both polyimide matrix materials (SP-3 and SP-211) exhibited quite high dynamic friction coefficients when operated under unit pressures of 15 psig. Upon reducing this loading to 2.6 psig, however, that material containing PTFE and graphite as fillers (SP-211) performed well with respect to both friction coefficient and wear rate. NaK compatibility studies complementing this seal material development effort (see Volume II, Part A, Section 6) also indicated that the material was indeed compatible with the liquid metal at temperatures up to at least 108°C.

Table 7.4 presents friction-wear data on these composites prior to and after exposure to NaK vapor and liquid. No significant, deleterious effect on these parameters was noted after such exposures. Based on the above experimental results, SP-211 was selected as the primary seal candidate material, with SP-3 considered its back-up. At this point in the program, therefore, fabrication of circumferential seal segments from these composites was initiated. Figures 7.8 through 7.11 are curves presenting friction-coefficient and operating temperature data versus running time for the various materials screened during this task.

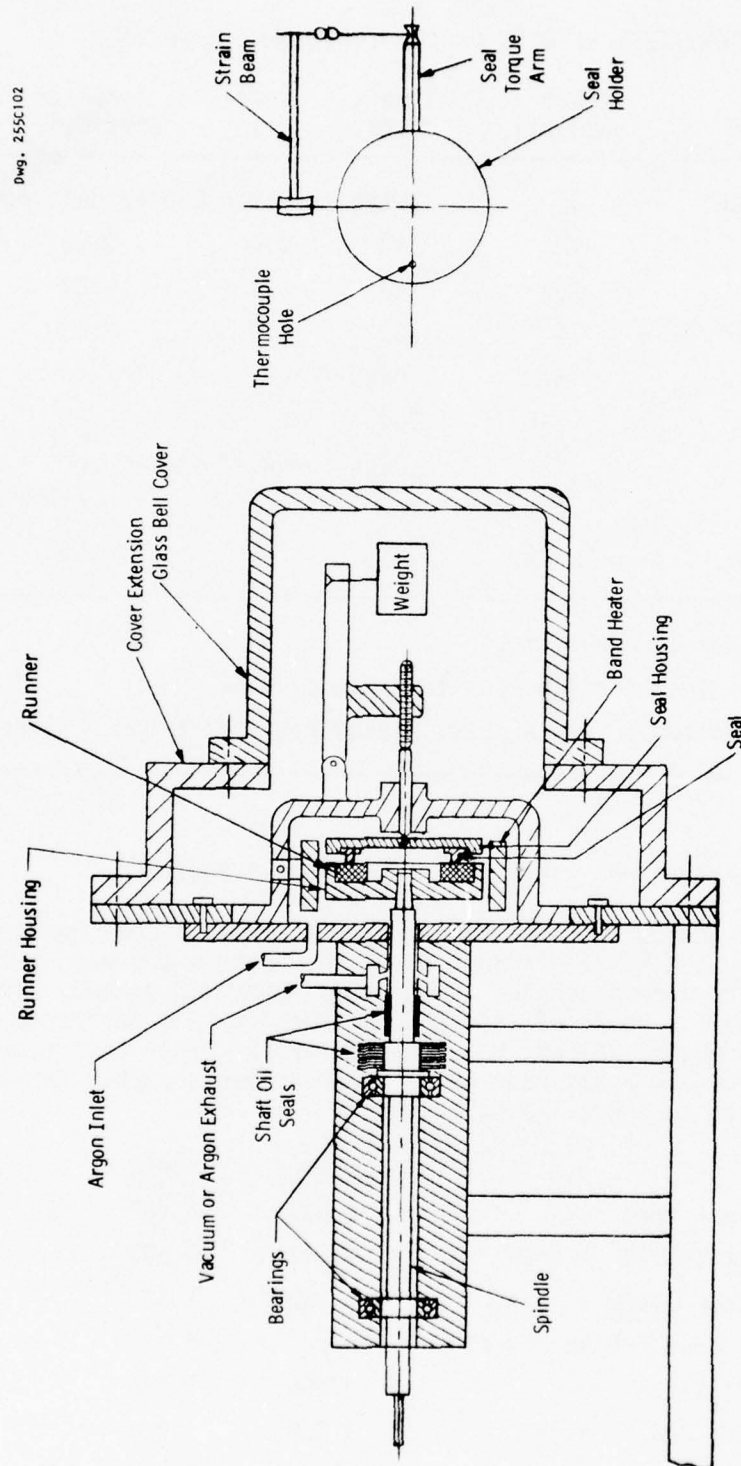


Fig. 7.7: Face seal screening test apparatus.

TABLE 7.3
FACE SEAL TEST RESULTS ON CANDIDATE SEAL MATERIALS

Seal Material	Face Load-psi	Time Hours	Wear Mils	Friction Coefficient
Delrin "AF"	30	High Friction Caused Melting		
WGI	15	140	0.4	0.03
WGI	30	140	0.4	0.02
Meldin	15	200	1.0	0.035
SP-3	15	High Torque-Test Stopped		
SP-3	2.6	164	15	0.33
SP-211	15	High Torque-Test Stopped		
SP-211	2.6	140	1.5	0.09
SP-211*	2.6	102	1.0	0.05

* Runner chrome-plated

All other tests versus tungsten carbide

Conditions: dry N₂ atm. - 3600 rpm - 2450 fpm - 41 fps

7.3.4 Functional Testing: Tandem Circumferential Seal

Figure 7.12 is a photograph of a tandem circumferential seal designed and fabricated by the Metals Product Division, Koppers Company, Inc. Two of these units were purchased during this reporting period. In addition, two similar units of heavier construction were purchased from the Stein Seal Company, Philadelphia, Pennsylvania. Each unit consists of two circumferential seals made up of three segments each. Pertinent parameters of each seal are listed below:

	<u>Koppers</u>	<u>Stein</u>
Bore - inch	3.937	3.437
Outside Dia. - inch	5.697	5.697
Runner Width - inch	1.500	1.530
Gas Feed Pressure - psi	5	5
Seal Width	0.750	1.125
Shaft Dia. - inch	3.000	3.000
Runner Surface	Chrome plate	Tungsten carbide

TABLE 7.4
FRICTION-WEAR CHARACTERISTICS OF CANDIDATE SEAL MATERIALS
PRE- AND POST NaK EXPOSURE

Room Temp - 3 lb Face Load on 1/4" Face Line Contact

Material	Friction Coefficient			Wear Rate in mm		
	Before Exposure	After NaK Liquid	After NaK Vapor	Before Exposure	After NaK Liquid	After NaK Vapor
SP-211	0.27	0.17	0.30	2.7	2.6	2.6
SP-211	0.29	0.24	0.29	2.6	2.0	2.4
SP-3	0.35	0.35	0.35	3.7	3.9	3.9
SP-3	0.36	0.32	0.34	3.9	3.5	3.1

Note: Surface Velocity - 1250 fpm
NaK Exposure - 112-1/2 hours at 108°C

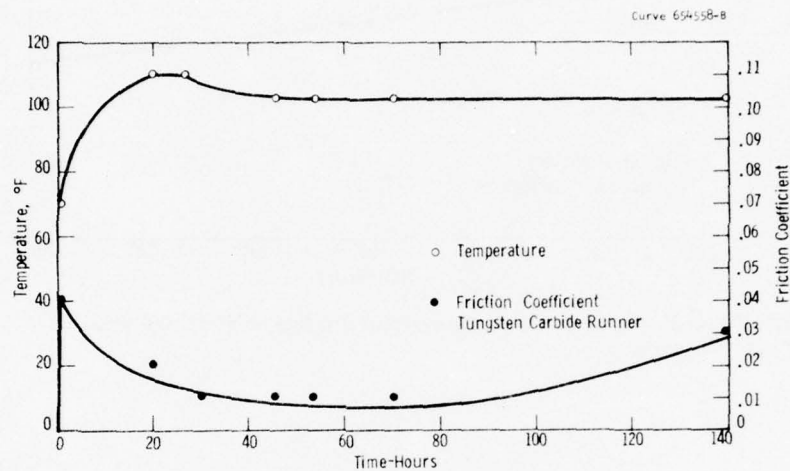


Fig. 7.8 -Operating temperature and friction coefficient vs time for WSe₂/GaIn seal material - 15 psi-2360 fpm-N₂

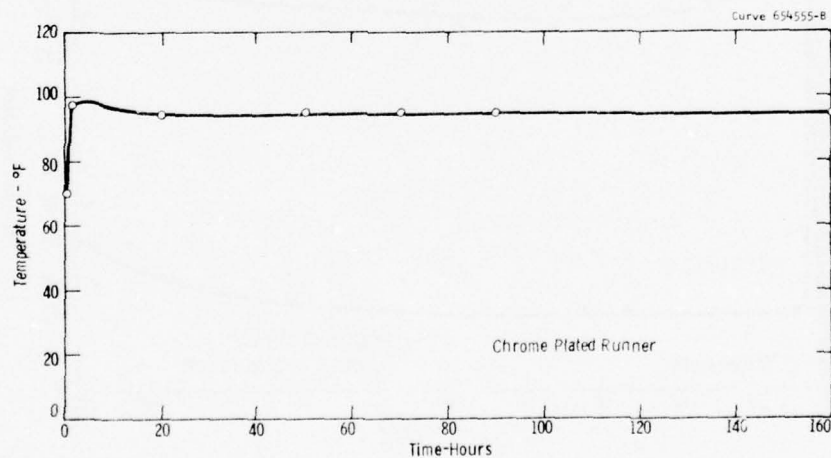


Fig. 7.9-Operating temperature vs time for SP-3 seal material - 2.6 psi-2360 fpm-He

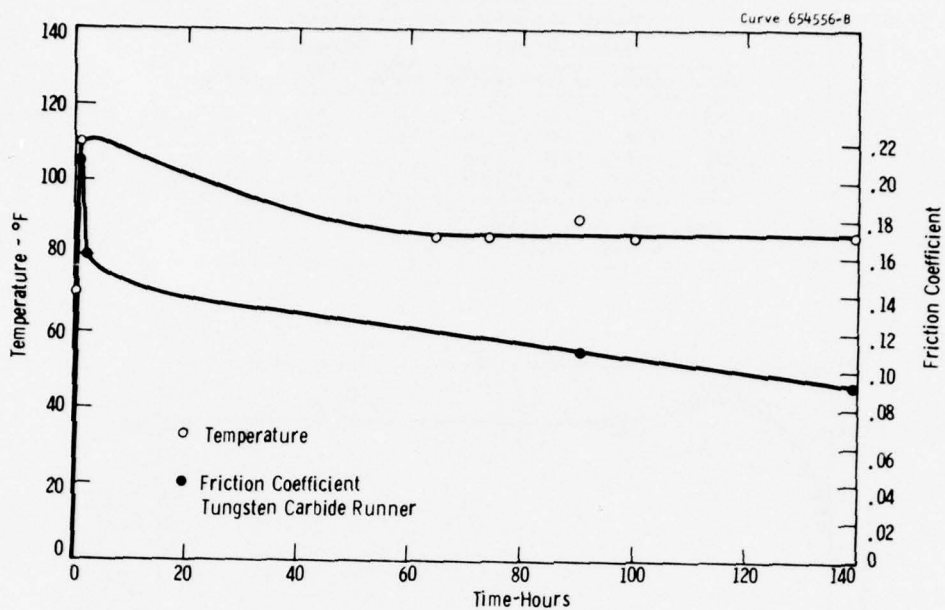


Fig. 7.10-Operating temperature and friction coefficient vs time for SP-211 seal material - 2.6 psi-2360 fpm- N_2

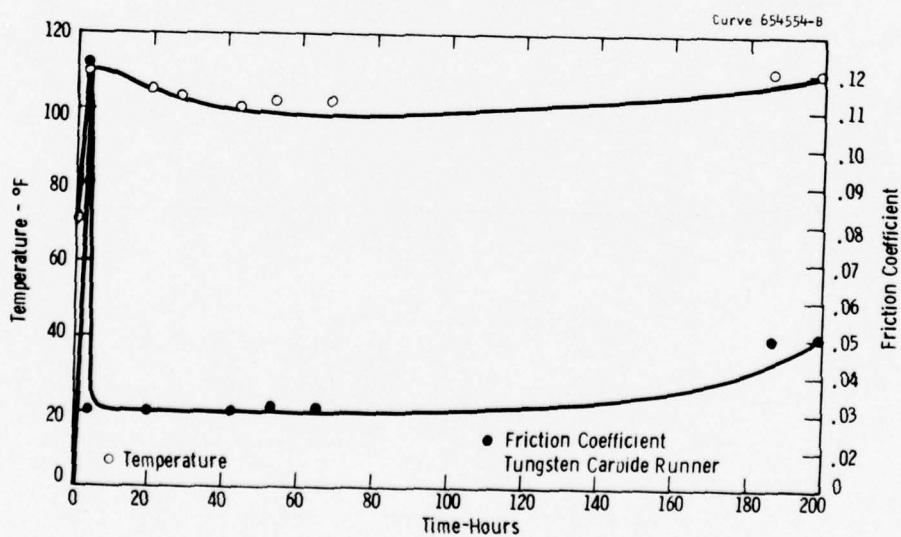


Fig. 7.11-Operating temperature and friction coefficient vs time for Meldin PI-30 seal material - 15 psi-2360 fpm- N_2

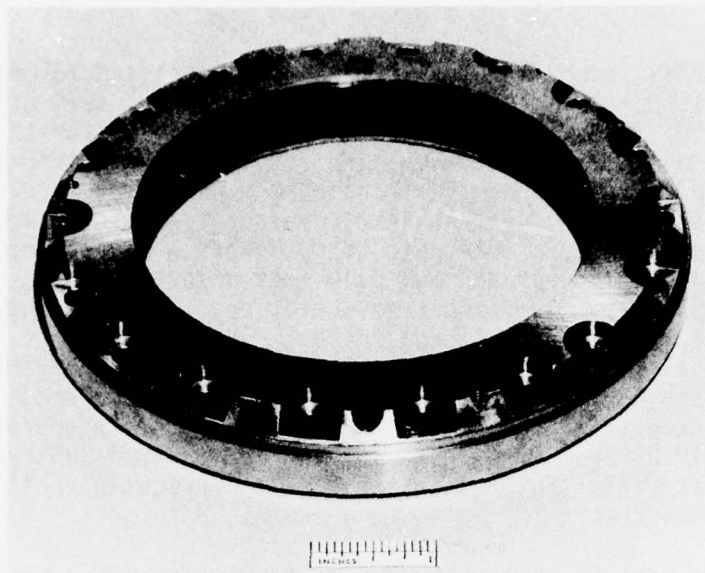


Fig. 7.12: Photograph of tandem circumferential seal; bore 3.97" diameter.

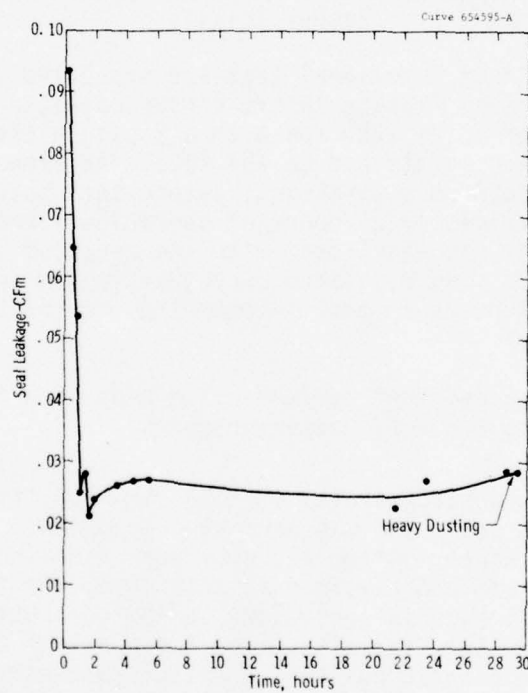


Fig. 7.13: Leak rate vs. running time for Tandem Circumferential Seal operating in dry N_2 2100 rpm - 5 psig feed gas.

In order to obtain bench mark performance data on standard seal designs, the first seals purchased were equipped with standard seal grades of carbon-graphite; namely, USG Grade 84 and USG Grade 67 for the Koppers and the Stein seals, respectively. The results of the first functional test performed on the Koppers seal design are presented in Figure 7.13 as a curve plotting seal leakage in cfm versus operating time. It will be noted that initially a leak rate of 0.095 cfm was observed with the seal operating at 2100 rpm and a 5 psig feed pressure of dry nitrogen gas. After approximately 2 hours of operation, this leak rate had decreased sharply to 0.025 cfm due to seal run-in and runner filming, and remained at this level for approximately 28 hours. At this point, however, abrupt and rapid wear of the seal material occurred, indicating carbon-graphite dusting, due to lack of moisture in its operating environment, and seal failure. The test result graphically illustrates the need to use seal materials that retain their self-lubricating ability in a no-moisture environment.

Three functional tests were performed on tandem circumferential seals designed by the Stein Seal Company. The first two experiments were performed on seals equipped with USG-67 carbon-graphite segments in order to obtain bench mark performance data on standard seal designs. The third experiment was performed on a seal of identical design but equipped with segments fabricated from Vespel SP-211.

The results of the first functional test are presented in Fig. 7.14 as a curve plotting seal leakage in cfm versus operating time. The experiment was performed at 3600 rpm with a 5 psig nitrogen gas ($< -45^{\circ}\text{C}$ dew pt) feed maintained to the seal. As expected with carbon-graphite in such an environment, severe seal material wear occurred after approximately 25 hours of operation. Performance of the seal up to that point was excellent, with the measured leak rate holding steadily at 0.005 cfm. As discussed above, a similar result was observed upon operating the Koppers Company tandem circumferential seal under identical conditions.

The results of the second test performed are presented in Fig. 7.15. Seal material was again USG-67 carbon-graphite.

The test was performed successfully at 3600 rpm with five psig nitrogen gas being fed to the seal, and was permitted to operate continuously for a period of 500 hours. After a 3 hour run-in period, seal leak-rate stabilized at 0.021 cfm and remained at this level for the duration of the experiment. This rate is equivalent to the consumption of one standard gas cylinder per five day period for a set of two tandem seals. It should be pointed out that the test parameters incorporated in this experiment-including seal material-are identical to those used in test #1, which failed due to carbon dusting after 25 hours operation. The only difference between the two experiments was that the nitrogen gas feed in this endurance run was first passed through a water bubbler to raise its dew point to 0°C . At this level, sufficient moisture

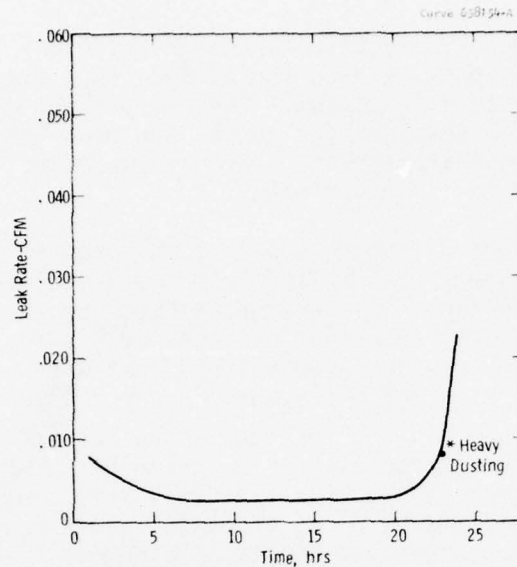


Fig. 7.14: Leak rate versus running time for tandem circumferential Stein Seal; carbon-graphite USG67 3600 RPM- N_2 gas feed < -45°C Dew pt.

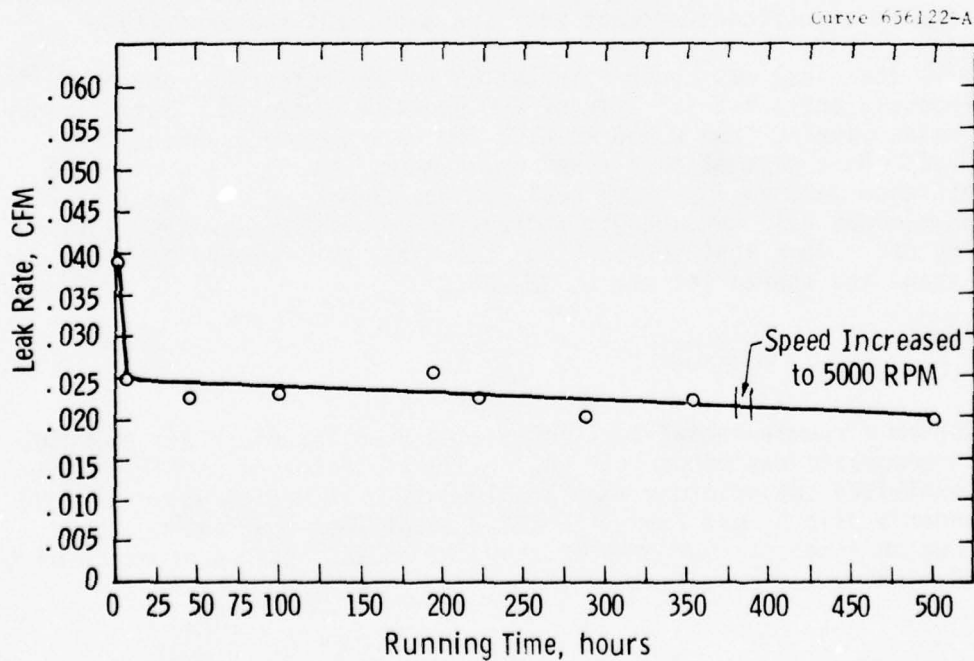


Fig. 7.15: Leak rate versus running time for tandem circumferential Stein seal; carbon-graphite USG67 3600 RPM - N_2 Gas Feed < -45°C Dew pt.

is added to the nitrogen to sustain carbon-graphite dry lubrication. While this technique cannot be used for SEGMAG, this experiment clearly demonstrates, a) the long-life capabilities and sealing efficiency of the tandem, circumferential seal design, and b) the need for a seal material whose self-lubricating characteristics are not dependent on the presence of moisture or oxygen in its environment.

The final test performed during this period utilized a Stein circumferential seal equipped with segments fabricated from the Vespel SP-211 polyimide-matrix composite. The seal was operated at 3600 rpm while being fed dry nitrogen (dew pt < -45°C) at a feed pressure of 5 psig. A total, accumulated life of 800 hours was achieved on this seal with no segment dusting or significant wear. Figure 7.16 presents a curve summarizing the results of this test in the form of seal leakage versus running time. The seal was initially permitted to operate for a period of 100 hours prior to test shutdown for segment inspection. After a period of 10 hours, the seal's leak rate stabilized at 0.015 cfm. Post-test inspection of seal and runner surfaces revealed highly polished sealing surfaces and an excellent film established on the runner surface. Subsequent to this experiment, the seal was again installed in the tester and subjected to a continuous endurance run of 300 hours at 3600 rpm and the same 5 psig dry nitrogen feed as in the previous run. At test shutdown, seal leak-rate was holding steadily at 0.01 cfm. Examination of seal surfaces revealed no significant segment wear and excellent runner filming.

Finally, the seal was again reinstalled in the tester and operated continuously until a total life of 800 hours was reached. Satisfactory leak rates ranging from 0.005 to 0.01 cfm were measured during this interval. As a part of this final experiment, the oxygen content of the nitrogen leaking past the seal dam was monitored. A level of 2 ppm oxygen was held throughout, indicating no air diffusion past the sealing dam. Upon test termination, this seal was removed from the test stand and stored for use on SEGMAG.

7.4 CONCLUSIONS

The tandem circumferential seal fabricated from Vespel SP-211 polyimide matrix composite was chosen for use in SEGMAG prototype machine. This seal exhibited satisfactory wear and leak rate at design speed of 3600 rpm under 5 psig N₂ gas feed with a dew point less than -45°C. Tests were run on this seal for greater than 700 hours. Its performance on the SEGMAG machine was excellent.

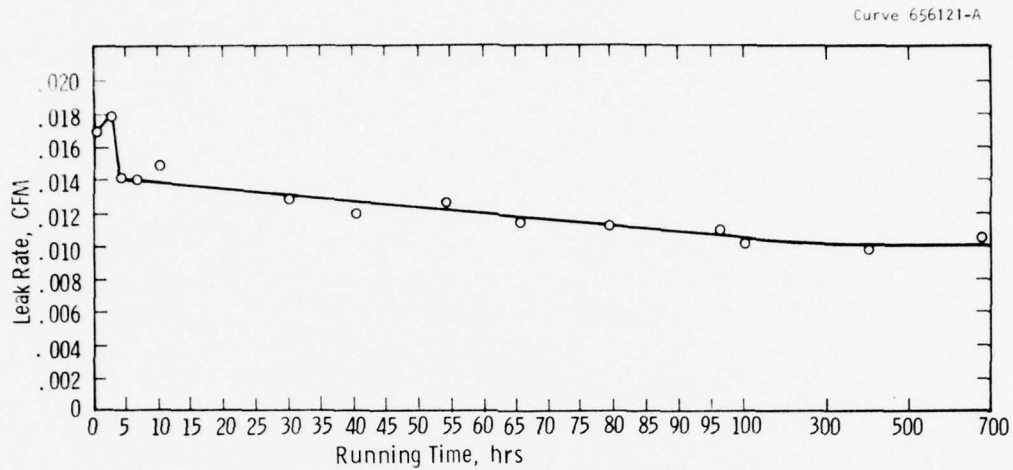


Fig. 7.16: Leak rate vs. running time for tandem circumferential Stein seal - Vespel SP-211 3600 RPM - 5 psig N_2 Gas Feed
 $\sim 45^\circ C$ Dew pt.

7.5 REFERENCES

1. "Dynamic Sealing: Theory and Practice," Koppers Company, Inc., Baltimore, Maryland.
2. "Mechanical Seals," Mayer, E., London 1L1FFE Books LTD, 1969.
3. Bowen, P.H., "Cover Gas Seal Materials for a Liquid Metal Pump," Westinghouse Research Report 73-1B6-PUMAT-R1.

E.M. 4883

VOLUME II

PART B

SOLID BRUSH SEGMAG DEVELOPMENTS

VOLUME II

PART B

SECTION 8

SOLID BRUSH CURRENT COLLECTOR TEST RIGS

8.1 OBJECTIVES

The objectives of this task are to provide two types of solid brush current collector test rigs:

- (1) Laboratory Brush Testers.
- (2) Machine-Environment Brush Tester (MEB).

The objective of the laboratory test rigs is to screen potential brush and slipring material combinations for performance over the desired current and speed range in a controlled environment. The parameters of particular importance are brush friction, current density, double voltage drop, and wear rate. The test rigs are required to provide accurate experimental data on individual sub-size brushes in a controlled environment.

The objective of the MEB is to evaluate solid brush current collection systems for high current density, low losses, and long operation life in an actual machine environment. MEB will subject the current collectors to current densities, leakage flux and other conditions associated with a SEGMAG machine. In addition, the purpose of the unit is to provide for long-term testing of current collectors, their attendant support systems, and to develop operational data for solid brush machines.

8.2 PRIOR AND RELATED WORK

No brush testers were previously available to satisfy the precise needs of this program. However, because of Westinghouse's long involvement in the development of electrical sliding contacts, certain facilities were available for adaptation to this program. These are the Laboratory Environment Brush Testers.

The MEB machine design concept was proven by the successful development of the liquid metal SEGMAG discussed previously in Volume II, Part A, Sections 1-7.

The use of solid brush systems results in a reliable reversing collector for motor applications. This concept removes the complications associated with liquid metal current collectors and simplifies the overall system.

The result of various studies indicates that the minimum current density for a solid brush homopolar with equal volume to a liquid metal collector homopolar is 1000 A/in² (apsi). Since the initial solid brush-gas-vapor testing indicates solid brush current densities up to 2000 apsi, the solid brush SEGMAG machine will have a volume that is equal to or less than the equivalent liquid metal SEGMAG.

8.3 SUMMARY OF ACCOMPLISHMENTS

8.3.0 General

Testing of brush-slipping combinations with the laboratory environment brush testers was initiated, and modifications are presently being made to improve their versatility. Four laboratory brush testers provided for various testing conditions, two with low speed (5000 ft/min) capability and two with high speed (10,000 ft/min) capability. The variable parameters associated with these rigs include brush loading pressure, applied current density, brush-holder temperature and gaseous environment composition and moisture content. These are discussed in subsequent sections in more detail. A large number of materials were evaluated and some of these will be further tested in the MEB, which was assembled and installed on its test stand. Testing of the MEB will be accomplished under a related program (ONR/ARPA Contract N00014-76-C-0683).

The development of solid brush SEGMAG machines required extensive experimental facilities to evaluate two principal areas:

- Brush Material Selection
- Current Collection System Evaluation

The brush material selection requires test rigs to evaluate individual brushes to determine coefficient of friction, double voltage drop, brush pressure and wear rate in specified environments. These test rigs are normally of reduced size and provide an initial screening of brush-slipping material performance.

Evaluation of current collection system performance requires test rigs to study current sharing in multiple parallel connected brushes in flux leakage fields anticipated in machine applications. Concepts in brush restraint, brush shunts and brush cooling must be studied.

The test rigs required for these areas are summarized as follows:

- B1 = Brush Tester #1
- B2 = Brush Tester #2
- HS1 = High Speed Brush Tester #1

HS2 = High Speed Brush Tester #2

MEB = Machine-Environment Brush Tester

B1 and B2 are duplicate testers for initial screening of protoypic materials in small (sub-size) brush configurations. During this contract both B1 and B2 were operational.

MEB will expose the brush and slipring materials and systems to an actual machine environment including high currents, multi-brush systems, and ambient magnetic fields. MEB is a model solid brush SEGMAG system. The MEB is completed and is operational.

8.3.1 Brush Testers B1 and B2 -- For Testing Sub-Size Brushes

Brush Testers B1 and B2 are existing Westinghouse facilities that were adapted to the needs of this contract.

Figure 8.1 shows an idealized section of the B1 test chamber in which sub-size brushes are tested. The slipring is turned from a silver-copper alloy bar and, although the figure does not show this detail, its curved surface is helically grooved with a pitch of 1/4 inch and a width of 1/32 inch. The ring is 3.25 inches in diameter and is fitted with a tapered hole and bolted onto the end of an overhung shaft which enters through a small clearance hole in the steel plate that makes up one wall of the chamber. The 0.5 hp dc drive motor, not shown, drives the ring at infinitely controlled speeds to 6000 rev/min (5000 ft/min). Corresponding measurements of electrical power input to the drive motor and selected brake mechanical loads applied to the slipring surface provide calibration data for subsequent brush friction determinations.

The brushes are fashioned to close dimensional tolerances out of selected materials. The shunts are attached very simply. Gold-plated screws, to which the shunt wires have been soldered, are screwed firmly into holes which have been tapped in the brush. Such a contact to a brush will pass high currents indefinitely and is equivalent in every way to commercial shunting devices, excepting the ability to resist vibration. The normal trailing-type brushholders were modified slightly to accept a larger number of shunts per brush. Each of two brushholders, located 180° apart, supports brushes 5/16 inch thick x 1/2 inch wide. The brushes, one positive and one negative polarity, are constrained to slide in a common track on the ring. Load current is transferred from the positive polarity brush into the slipring, and then out again through the negative polarity brush. With this arrangement current flows in both directions through the slipring film, since both brushes ride in a common track. Cutting back portions of the brush face permits higher current density loading. Brush mechanical load is applied by clock type springs, using screw-locked adjustable pivot pins and calibrated weights.

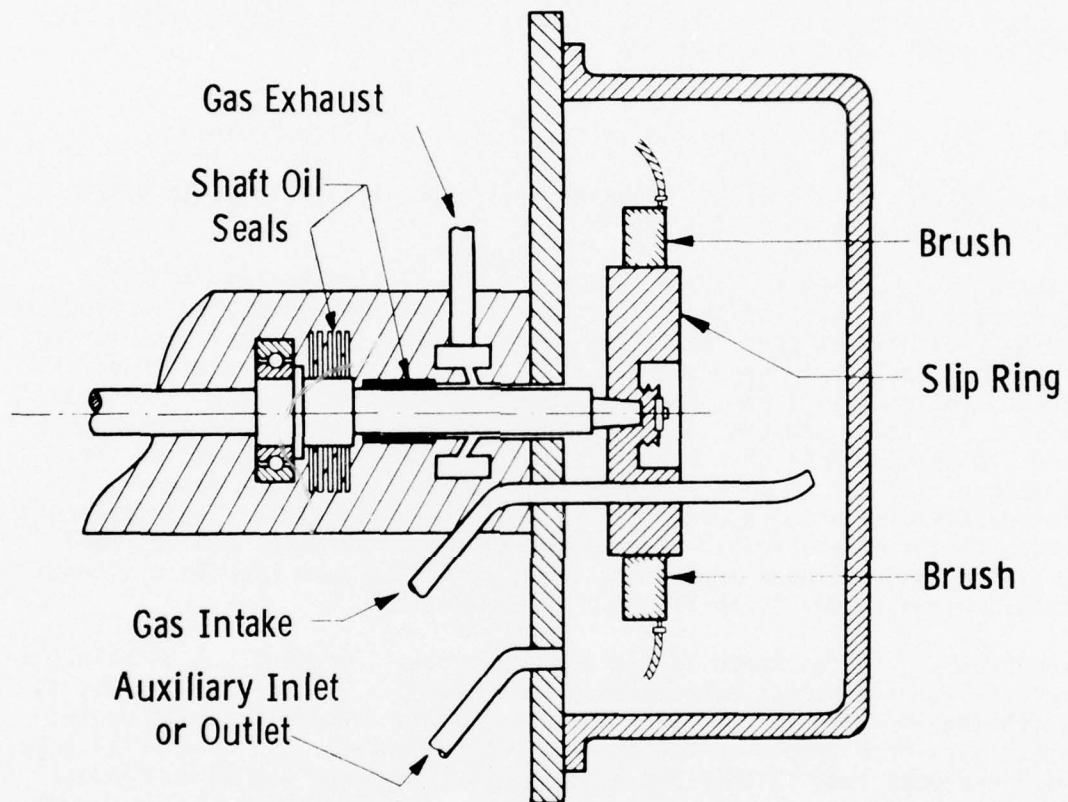


Fig. 8.1: Test chamber of Type B1 brush tester.

Except on one side, the chamber is made up of a flanged glass vessel which is clamped to the steel side plate. The resulting inside ambient gas volume is about 0.07 cubic foot. The purified gas enters through one copper tube and leaves through a second which is let into the side of the cylinder which surrounds the rotating shaft on which the ring is mounted. The gas leaves the chamber at a pressure slightly above atmospheric and any traces of gases, which may get by the elaborate shaft seal and try to enter the chamber, are sucked out through the gas-exit tube along with the very much larger volume of gas which is deliberately passed through the chamber. Gas flow into and out of the test enclosure is at a rate of 2 ft³/h, subjecting the brushes and ring to about one gas change every two minutes.

Prior to entering the test chamber, the gas is saturated with water by flowing through a bubble tower held at either 0° or 20°C. In the first case, the water content will be 2.1 grains per cubic foot (6000 ppm_v) and in the later 7.5 grains (23,000 ppm_v). The end of the entering gas tube of the bubbler is closed by a fritted glass filter which breaks the gas into extremely fine bubbles and this increases the speed with which it is wetted to the desired extent. From time to time the dewpoint of gas samples taken from the chamber is checked to make certain that the humidity is at the desired level. The gas is finally exhausted to the laboratory ventilation system.

Figure 8.2 shows an overall view of the B1 test rig and associated apparatus. A water bubbler packed in ice is centrally located on the bench and a constant current supply, infinitely variable to 80A, and recording meters are located on the shelf above the tester. Electrical equipment for controlling the drive motor and measuring its power input is located on the bench to the right of the tester. Copper cooling-water feed and drain lines to and from the faceplate and an air cooling fan are located near the test chamber.

8.3.2 High Speed Brush Testers HS1 and HS2 -- For Testing Full-size Brushes

Figure 8.3 shows the physical arrangement of components comprising the full-size brush tester used to obtain brush performance data under controlled gas atmosphere and high current test conditions.

The slipring is driven by a long slender shaft which extends about six inches above the drive motor housing. The copper or zirconium-copper alloy ring is six inches in diameter, and the surface on which brushes slide is helically grooved, as previously described. Ring speeds up to 6500 rev/min (10,000 ft/min) may be obtained by varying the frequency of the electrical power supplied to the three phase 0.75 hp drive motor. The drive motor is calibrated by the prony brake method for brush test friction drag determinations, as previously described for the sub-size brush tester (B1).



Fig. 8.2: Type B1 Brush Test System

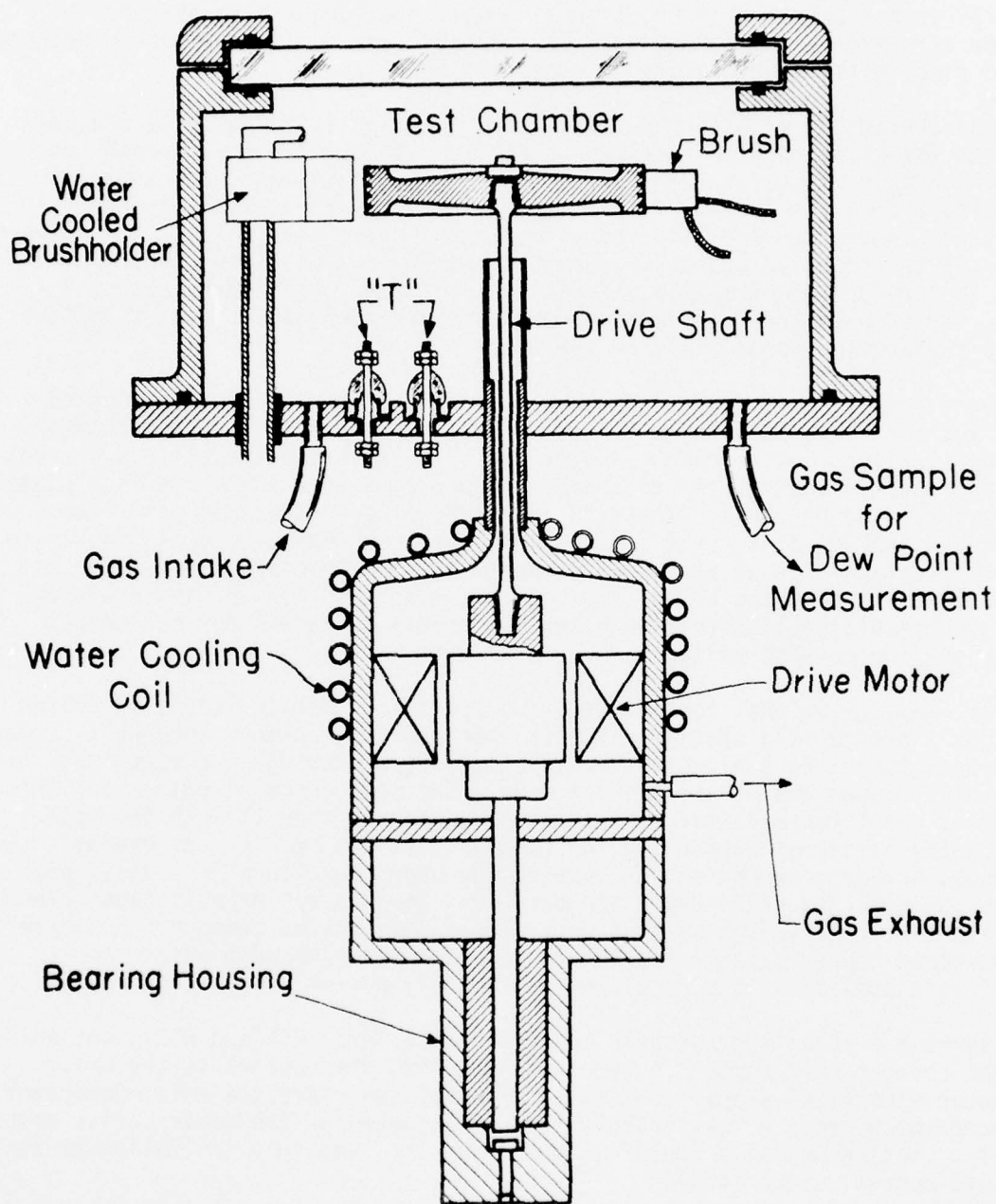


Fig. 8.3: Physical Arrangement of Components of Type HS1 and HS2 High Speed Brush Testers.

Four brushes, two of each polarity, comprise a test set and they are held in a radial mode against the slipring. Each flat-top brush is 5/16 inch x 5/8 inch in cross-section with the longer side aligned in the circumferential direction. The brushes are confined by their holders to ride in two separate tracks according to polarity.

Load current is transferred from two parallel positive-polarity brushes into the slipring along a common track, and then out again through two similarly connected but negative brushes along a common track that differs from the first. With this arrangement current flows in one direction through the slipring film, inward under the positive and outward under the negative brushes. Current distribution is ascertained from direct recording of millivolt drops developed across shunts connected in series with the individual brushes. Brush mechanical load is applied by flat-coiled constant-force springs.

The oil-lubricated guide and thrust bearings of the vertically mounted drive motor are located in the lower housing away from the test chamber. The air-tight motor frame is water cooled. Brush electrical load current is brought into the chamber through copper tubes sealed to the face plate by insulated bushings. These tubes also serve to transmit water for forced cooling of the radial type brushholders. Pairs of glass insulated compensated "T" bushings serve to carry thermocouple signals outside the tester for measuring brush, brushholder, ring, and ambient temperatures. Other insulated leads extend potential points to meters for measuring brush-ring contact voltages.

Test atmosphere gas, conditioned to a specific humidity level, is forced from a pressurized storage cylinder into the test chamber through a copper tube soldered to the tester face plate. After flowing in a turbulent manner around the slipring and brushes, the test gas must pass along the drive shaft for a distance of about four inches, then through the motor housing before exhausting to the room exhaust system. Any extraneous gases or vapors which may diffuse to the upper portion of the stand pipe surrounding the drive shaft are drawn out through the exhaust tube, along with the large volume of test gas deliberately passed through the chamber. A second copper tube is located in the face plate through which samples of test atmosphere may be drawn for humidity and/or composition analysis.

Figure 8.4 shows the two high-speed brush testers (HS1 and HS2), one with the chamber bell removed. Immediately behind the testers is the drive motor electrical supply control panel. Not shown are the motor-generator sets which produce the variable frequency power for the tester drive motor. Also not shown is a rectifier which supplies smoothly controlled brush load current up to 1000A.

8.3.3 Machine Environment Brush Tester (MEB)

The Machine-Environment Brush Tester (MEB) consists of a single module SEGMAG configuration incorporating solid brushes in the current collection

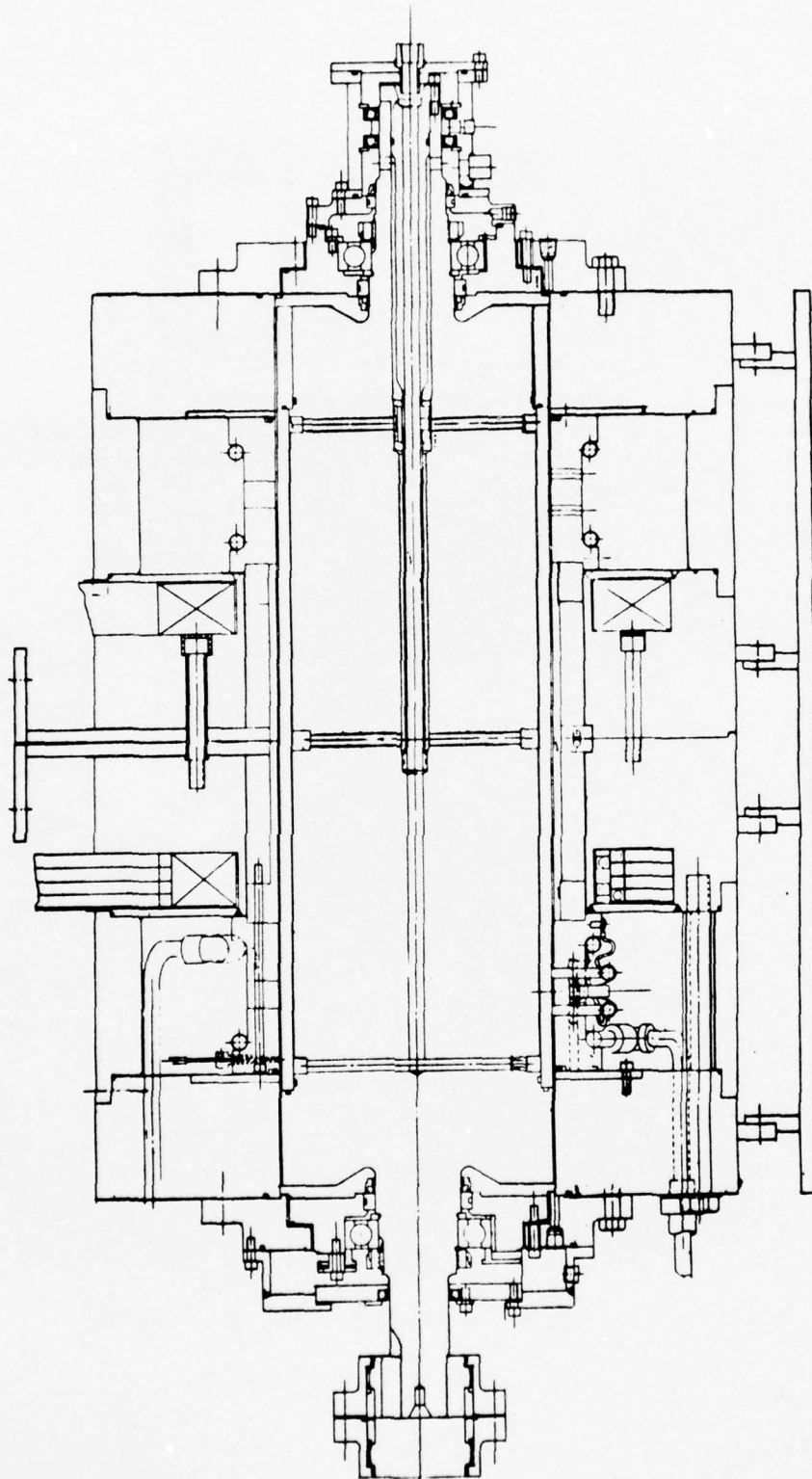


Fig. 8.5: Machine-Environment Brush Tester (MEB).

areas as shown in Fig. 8.5. The primary objective of MEB is to provide a test vehicle for the evaluation of solid brush current collection systems in a machine environment.

The mechanical design of the MEB considered the same factors as those for the design of conventional rotating electrical machinery. In addition to the current collection system, the design of the MEB incorporated simplicity and maximum flexibility of its components to minimize the down time between test sequences.

The following factors were considered:

- 1) Mechanical conductor support
- 2) Rotor to stator alignment
- 3) Removal of losses
- 4) Machine environment
- 5) Erosion of cooling system components
- 6) Electrical insulation
- 7) Instrumentation.

The rotor conductor drum was restrained to withstand both centrifugal forces due to rotation and torsional forces due to the machine torque reaction. The torsional forces (8,000 in-lb) were restrained by shrinking the copper conductor drum onto the iron rotor in the MEB. Since the rotor conductor drum and rotor iron have the same electrical potential, no insulation was required.

The support of the stator conductor was somewhat simpler since there were no rotational forces. The conductor drum was restrained by an interference fit between it and the ferromagnetic stator iron. This concept provides adequate support to meet the 3/unit torque design criterion. Each stator conductor was insulated from the iron as well as from each other.

The alignment of the rotor in the stator is accomplished by four (4) positioning blocks, two (2) at each end of the test stand. These blocks provide vertical and horizontal adjustment capability. To measure the alignment, four (4) viewing ports are provided at each end of the machine at 3, 6, 9 and 12 o'clock positions. Measurements can be made of the rotor to stator gap at these locations and the proper adjustment can be made with the blocks. This arrangement provides maximum positioning flexibility for the systems including the possibility of testing brush operation with the rotor deliberately misaligned.

This test capability is very important since the run out of the slipring surface can adversely affect brush performance. Such run outs result in radial acceleration of the brush known as "brush bounce". This condition must be accommodated in the brush actuation gear to ensure proper contact pressure on the slipring for optimum life with minimum losses.

Rotor alignment is a function of the stator alignment, provided by the rotor support structure, and dynamic deflection during operation. The MEB incorporates rolling element bearings which are adequate for the design loads and speed. Since the total flux of the machine must be carried by the ferromagnetic iron in the rotor, there is a substantial structural member in the active length and flux return path, thus resulting in a high critical speed for the machine. Because of high rotor stiffness, the dynamic deflection of the rotor is small.

Water cooling was adopted for the MEB to provide cooling in the brush bearing area, machine leads and the rotor conductor drum.

The major losses requiring removal from the MEB include:

- Armature joule heating
- Brush friction
- Brush joule heating
- Friction and windage losses

The cooling system was designed to remove 80% of the machine losses through the rotor and 20% through the stator. The losses generated in the brush account for the majority of the total machine losses, and must be removed through a sliding surface.

In the rotor the coolant is passed immediately below the rotor conductor drum in small channels (.38"W x .03"D) which provide parallel cooling paths for the two collector areas. In this way the slipring temperature can be regulated to give optimal brush performance.

To control the environment within the MEB, shaft seals were used. The shaft seals were mounted inboard to the bearings to prevent contamination from the bearing lubricants. Since the environment will be adjusted for low brush friction, it is anticipated that the conventional rubbing face seals will perform adequately.

The design provides for measurement of the important parameters. Temperature measurements of the rotor conductor, ferromagnetic iron, as well as the slipring surface will be accomplished by thermocouples placed inside the rotor and brought out through sliprings. Brush temperature and potential drops from brush to brush will be measured by instruments imbedded in specified brushes. The machine torque will be measured by a torque meter installed between the MEB and the prime mover. Associated instrumentation of the stator, gas system, and the cooling water system was also provided.

The MEB is completed and was installed on the same test bed which supported the liquid metal SEGMAG. More detail on this stand and photograph are contained in Volume II, Part A, Section 2 of this report.

VOLUME II

PART B

SECTION 9

CURRENT COLLECTOR CONTACT MATERIAL/PERFORMANCE

9.1 OBJECTIVES

The objective of this task is to develop sliding contact system materials for use in advanced electromechanical machines, including the brushes, collector rings, environment gas, and vapor additives. Important requirements of the contact system of advanced machines are high current density, low power loss, and long life.

9.2 PRIOR AND RELATED WORK

Early experimental studies at Westinghouse showed that a marked increase in lifetime could be achieved when carbon and metal-graphite solid brushes were operated in inert gas atmospheres rather than in air.¹ The original work along these lines was undertaken prior to World War II and has continued to date.² Until recently, conventional current densities have been employed. Commercial verification is provided by the use of conventional brushes in synchronous condensers, where brush lifetimes of more than 100,000 h/in (>10 y/in) have been achieved.

No attempt was made until recently to extend the current density capability beyond the conventional level, (60 A/in²), since no requirement for such brushes existed. However, within the last year this situation has changed. Brush tests were conducted in 1974, with the objective of achieving current densities of 300 to 500 A/in² and a long life. These tests, which were run at a relatively low speed of 2500 ft/min typical of motor applications, were extremely successful.

The low voltage drop and friction factor and long brush life observed during these tests were unexpected and led to a decision to conduct tests at even higher current densities, to permit the possibility of utilization in SEGMAG machines to be assessed. These tests were conducted at up to the current collector test stand limit of 2000 A/in² (i.e., more than 30 times the conventional brush current density), again with excellent results.

These encouraging results forced a reassessment of the role of solid brushes for homopolar dc machines, since even independent analyses³ have shown that solid brushes become attractive for these machines at current densities >1000 A/in².

9.3 SUMMARY OF ACCOMPLISHMENTS

9.3.0 General

Test procedures were established and existing test rigs were modified for evaluating contact system materials. Screening tests were initiated with an objective of looking sequentially at candidate brush, ring, additive, and gas materials.

A number of brush materials were evaluated for high (to 500 A/in²) and ultrahigh (to 2500 A/in²) current density application. Scaled-down electrographitic brushes performed with long life and reasonably low energy losses in the high current density range. Metal graphite brushes showed best overall feasibility for the ultra high current density application. In general, brush performance appeared to be affected by the base graphite material, percentage metal content, and applied mechanical load.

Additional testing is required to evaluate the effect of greater numbers of brushes, larger load currents, higher ring speeds, and the presence of ambient magnetic fields such as will be imposed by actual electro-mechanical machines. A test rig (MEB) is being readied for such investigations. In addition to the test features mentioned, provision for forced cooling of the contact system is also included in the MEB design. This additional testing will be performed in a related program (ONR/ARPA Contract N00014-76-C-0683).

9.3.1 Testing Procedure

Original test work completed in this area was exploratory in nature. In the main, screening type tests were conducted with selected available brush stock materials, to evaluate their feasibility for high (2000 A/in²) and medium-high (500 A/in²) current density applications. Copper and silver-graphite materials are considered prime candidates for the high current density and electrographite and metal graphite materials for medium-high density usage.

Prior to each run the slipring surface was cleaned by abraiding with 240 grit alundum cloth. This technique permits repeated generation of fresh metal surfaces with roughness values in the range 15-18 micro-inches. Total indicated run-out of the sliprings is less than 0.0005 in.

Prior to starting each run the brush faces were run-in to achieve good conformity with the slipring surface curvature. Linear brush wear was determined from pre- and post-test brush length measurements made with a special micrometer-jig fixture.

Nominally, each test run was 24 h in duration, unless terminated earlier due to unusual circumstances such as accelerated brush wear. Where life

was very long, a few 70-h tests were run in order to obtain a more accurate determination of brush wear rate. Although the brush mechanical load force was an independent variable, a minimum value was required to achieve arcless current transfer. The threshold value varied for each material, but depended mainly and directly upon the electrical load level. Experiments were started after thoroughly purging air from the chamber enclosure with the conditioned test gas.

The brush-ring interface temperature is recognized as an important test condition. Low temperature is necessary to achievement of the high current density brush performance goals. Limited control of the interface temperature was achieved by gas convection cooling in both laboratory testers, with additional conduction cooling provided by circulating chilled water through the brushholders in the full-size brush tester. The MEB tester, described previously, is being fabricated and will incorporate forced water cooling of the sliprings as well as the brushholders. Other test capabilities of this tester include ambient magnetic field, large numbers (50) of parallel-connected brushes, and load currents and ring speeds to 20,000 A and 14,000 ft/min, respectively.

Regarding results of work reported on here, the following brush-ring test conditions or factors are considered independent variables: mechanical load, electrical load, ring speed, environment gas, brush size, brush shape, and brush physical support. These variables were set prior to each run.

Measurements of the dependent response variables permit either direct or indirect determination of contact voltage drop, friction coefficient, brush face power loss density, brush life, and current distribution. Average results of the above determinations provide the data for comparison of brush materials.

Brush face power loss, W_B , is composed of mechanical and electrical components. In the absence of magnetic fields, terms of the following expression represent the mechanical and electrical power loss density components, respectively.

$$W_B = 0.0226 \mu p v + J V_{SCD}, W/in^2 \quad (9.1)$$

where: μ = brush-ring friction coefficient

p = brush apparent mechanical load, lb_f/in^2

v = slipring speed, ft/min

J = brush current density, A/in^2

V_{SCD} = single brush contact drop, V

Brush life, L , may be defined as the distance traversed along the slipring per unit of time divided by the volume of brush worn away during the same time period.

$$L = \frac{60 v}{tw(\Delta l)}, \text{ ft/in}^3 \quad (9.2)$$

where: v = slipring speed, ft/min

t = brush thickness, in.

w = brush width, in.

Δl = change in brush length, in/h

Modified versions of equations (9.1) and (9.2) were used in Volume I, Section 3 of this report to expedite comparisons of candidate brush materials.

9.3.2 High Current Density (500-2500 A/in²) Brush Material Test Results

Initial exploratory high current density brush material test results are presented here. Two silver graphite materials (SG212), SG216), and three copper graphite materials (W933, CMO, CMIS) are included. All materials were tested in an inert gas atmosphere.

Experiments with B1 Brush Tester

Performance comparisons of silver graphite material grades SG212 and SG216 (1), operating at 2000 A/in² brush current density, may be made from the data in Table 9.1. Brushes of grade SG216 (1) were fabricated from a small lot of material and they allegedly contain a higher percent silver than grade SG212.

Although both positive and negative polarity brushes are involved here, an average brush-ring interface voltage drop is given. Additionally, these reported values exclude the brush body and flexible shunt lead voltage drops. Nonconventional shunts are being designed wherein the goal is to achieve a combined brush body and shunt voltage drop less than 0.02 volt.

Based on the test results, data in Table 9.1 reveal that grade SG216(1) brushes perform with lower contact voltage than SG212. This result (lower contact resistance) is consistent with higher silver content in the former material. Grade SG216 (1) brushes, however, function with higher friction coefficients than grade SG212. This, too, is consistent with the material compositions. Higher graphite content in the latter material will provide a greater potential for formation and maintenance of lubricating films at the brush-ring interface, resulting in lower friction. The importance of mechanical pressure to both silver-graphite grades is evident by the reductions in contact drop in the 15-20 lbf/in² range.

Table 9.1
Silver-Graphite Material Brush Test Results
(2000 A/in²)
Ring Speed 2500 ft/min

Brush Material	Mech. Pressure lb _f /in ²	Single Brush Drop, V	Friction Coef., μ	Density, W/in ²	Brush-Holder Temp., °C
SG216(1)	15	.25	.15	627	101
SG216(1)	20	.055	.16	291	68
SG212	15	.38	.11	853	109
SG212	20	.33	.10	773	111
SG212	25	.38	.12	930	113

Despite ensuing higher mechanical friction losses when the pressure is increased to 20 lb_f/in², the net power loss (mechanical plus electrical) is reduced. With 25 lb_f/in² pressure, however, the contact drop and friction coefficient of grade SG212 increased. Thus, an optimum load pressure is required to achieve minimum power loss conditions. Considering all runs, a direct correlation tends to exist between the power loss density and total brushholder temperature. Brush life of grade SG216(1) is quite good. In contrast, brush life of grade SG212 brushes is relatively poor. Thus, differences in metal content and/or processing of silver graphite brush materials are important in achieving low power loss and long life.

A more complete characterization of SG216 (1) grade brushes throughout a wide current density range is presented in Table 9.2.

Experiments with HSI High-Speed Brush Tester

Performance comparisons of silver graphite grade SG216 (2) and copper graphite grades W933, CMO, and SM1S may be made from recorded data in Table 9.3. Grade SG216 (2) material was reported by the supplier to contain the same percent silver as grade SG216 (1), but it was processed somewhat differently. Metal content of the copper-graphite materials is claimed to higher than that of the silver-graphite material.

Figures 9.1 and 9.2 illustrate the contrasts in contact voltage and friction coefficient between the material grades. Copper graphite grade W933 performs with very low contact voltage, but with higher friction drag. Much higher mechanical load pressure is required of silver graphite

Curve 683617-A

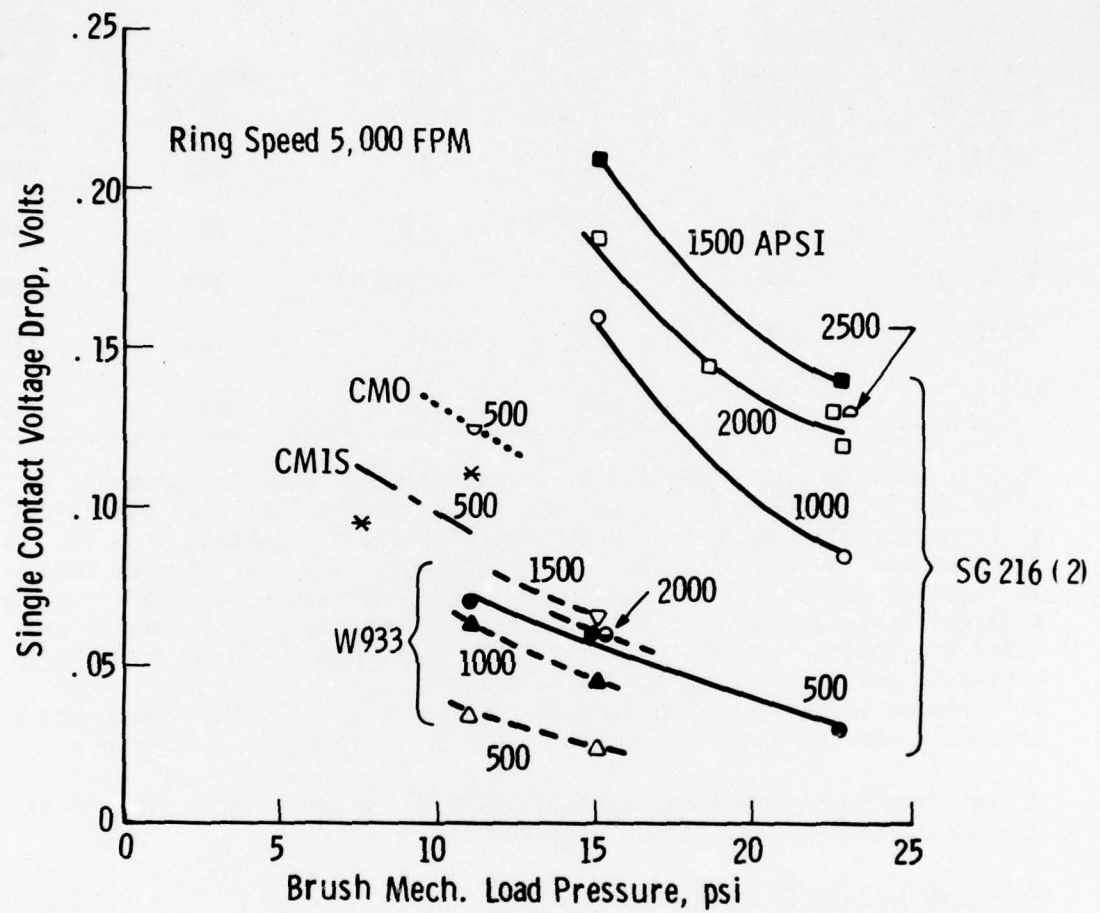


Fig. 9.1: Contact Voltage Drop vs Load Pressure for Various Brush Materials.

Curve 683618-A

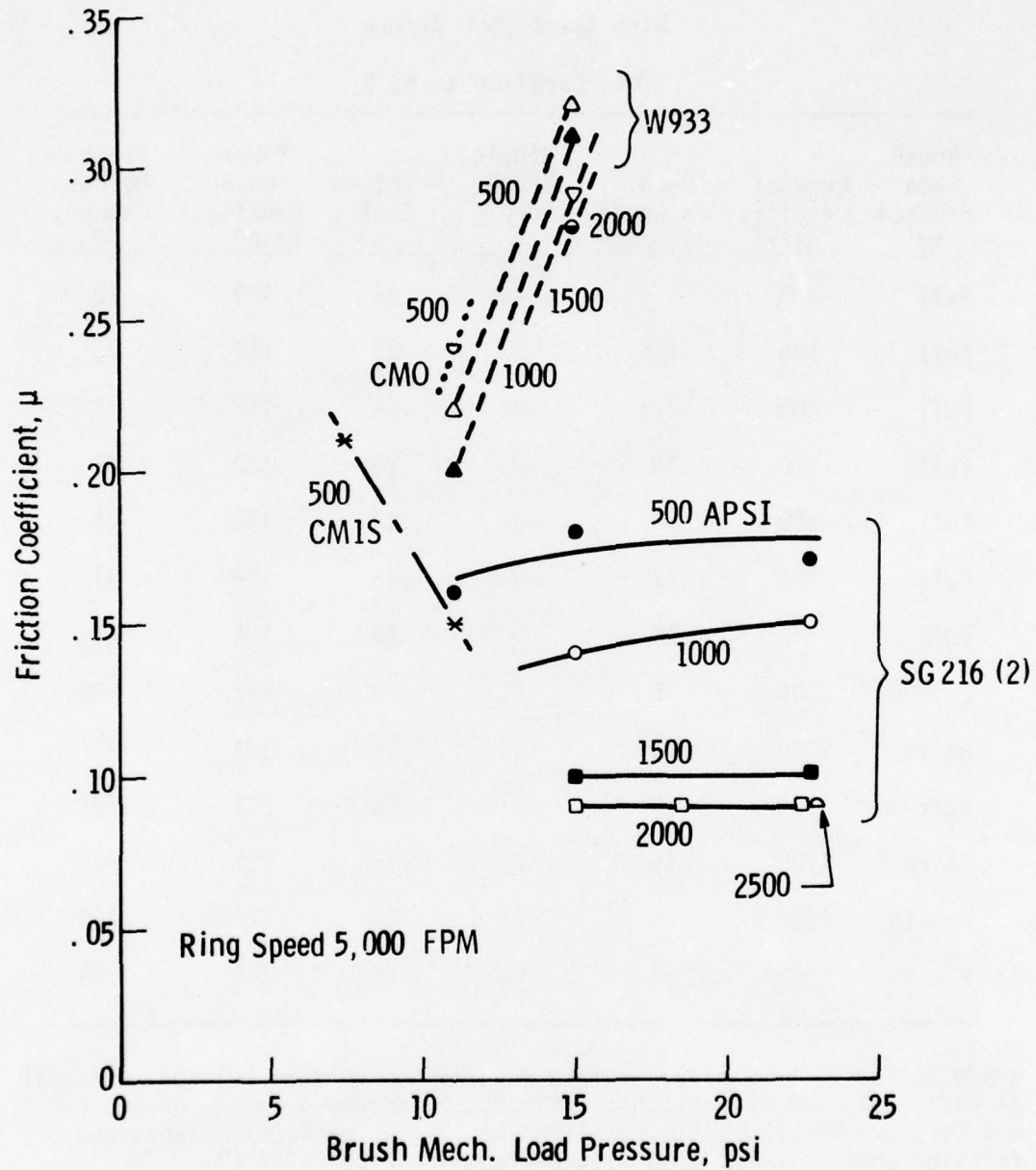


Fig. 9.2: Friction Coefficient vs Load Pressure For Various Brush Materials.

Table 9.2
Performance Characteristics of SG216(1) Material Brushes

Ring Speed 2500 ft/min

Test Duration to 60 h

Brush Face Reduced to	Current Density, A/in ²	Mech. Pressure, lbf/in ²	Single Brush Drop, V	Friction Coef., μ	Power Loss Density, W/in ²	Brush-Holder Temp., °C
Full	500	5	.12	.21	119	72
Full	500	7.5	.03	.24	117	73
Full	500	7.5	.02	.24	112	71
Full	500	10	~0	.23	130	71
Full	500	10	~0	.28	158	81
Full	500	12	0	.26	176	81
Full	500	15	0	.22	186	87
Half	1000	5	.33	.15	372	103
Half	1000	10	.14	.21	259	77
Half	1000	15	.015	.22	201	67
Third	1500	15	.055	.17	227	67
Fourth	2000	15	.25	.15	627	100
Fourth	2000	20	.055	.16	291	68

grade SG216 (2) brushes to achieve equally low contact voltage, but with significantly lower friction coefficients. Copper-graphite grades CMO and CMIS brushes appear to function with higher contact voltages and friction coefficients, than silver-graphite grade SG216 (2).

Brush life was relatively low for the copper graphite grades listed in Table 9.3. This is not too surprising, since they possess very high metal content and, thus, lack lubricating capability.

Table 9.3

Performance Characteristics of Selected Metal-Graphite Material Brushes
Ring Speed 5000 ft/min

Brush Grade	Current Density, A/in ²	Mech. Pressure, lb _f /in ²	Single Brush Drop, V	Friction Coef., μ	Power Loss Density, W/in ²	Brush Temp., °C
SG216(2)	500	11.0	.07	.16	233	57
"	500	15.2	.06	.18	338	69
"	500	22.7	.03	.17	451	77
"	1000	15.2	.16	.14	400	89
"	1000	22.7	.09	.15	470	83
"	1500	15.2	.21	.10	486	105
"	1500	22.7	.14	.10	467	97
"	2000	15.2	.19	.09	524	109
"	2000	18.5	.15	.09	478	107
"	2000	22.7	.12	.09	471	104
"	2000	22.7	.13	.09	491	102
"	2500	22.7	.14	.09	581	114
W933	500	11.0	.035	.22	290	68
"	500	15.2	.025	.32	561	105
"	1000	11.0	.065	.20	313	70
"	1000	15.2	.045	.31	576	108
"	1500	15.2	.065	.29	594	112
"	2000	15.2	.060	.28	600	120
CM1S	500	7.6	.10	.21	227	67
"	500	11.0	.11	.15	241	70
CMO	500	11.0	.13	.24	360	83

9.3.3 Medium-High Current Density (to 500 A/in²) Brush Material Test Results

Results of exploratory brush material tests involving medium-high current densities are presented here. Three silver graphite materials (SG212, SG216 (1), SG216 (2)), one copper graphite material (CM3B), and two electrographitic materials (W417, W457) are included.

Experiments with B1 Brush Tester

Performance comparisons of silver graphite grades SG212, SG216 (1), and SG216 (2), copper graphite grade CM3B, and electrographitic grades W417 and W457 may be made from the data in Table 9.4. Certain data from Table 9.2 are represented here for convenience. Although the metal content of all silver and copper-graphite materials is comparable, the SG216 grades possess somewhat higher amounts. The electrographite materials, of course, contain no additions of metal in their structure.

Perhaps the most notable information in Table 9.4 is the extraordinary long life associated with the electrographitic brush grades, especially grade W417. This characteristic is attributed to maximum availability of graphite at the sliding contact interface.

It seems very likely that the overall performance of electrographitic brushes will be improved with an increase in load pressure. Here, a reduction in brush life is an acceptable compromise in light of an anticipated decrease in the total power loss.

Based on these preliminary tests, electrographitic materials appear to be prime candidates for use as brushes in medium-high current density applications. This must be verified in machine environment tests, involving large numbers of brushes, typical load currents, and ambient magnetic fields.

9.3.4 Brush Power Loss and Wear Characteristics

Based on test results, power loss (mechanical and electrical components) and wear characteristic values were calculated for 26 metal-graphite brush materials. These values are plotted for each material as a function of its metal content in Figs. 9.3 and 9.4. Average curves are drawn through the points to show trends in performance as a function of brush metal content.

The next generation of experimental brush materials are currently being fabricated for use in related program (ONR/ARPA Contract N00014-76-C-0683). The objective, of course, is to develop brushes with improved performance capability for high current density application.

Table 9.4

Performance Characteristics of Brush Materials (500 A/in²)
(Medium-High Current Density Applications)

Ring Speed 2500 ft/min					
Brush Material	Mech. Pressure lbf/in ²	Single Brush Drop, V	Friction Coef., μ	Power Loss Density, W/in ²	Brush- Holder Temp., °C
W417	10	.14	.15	155	111
W417	10	.24	.11	182	115
W457	10	.41	.05	233	185
SG216(1)	5	.12	.21	119	72
SG216(1)	7.5	.025	.24	115	72
SG216(1)	10	~0	.26	144	76
SG216(1)	12	0	.26	176	81
SG216(1)	15	0	.22	186	87
SG216(2)	10	.085	.21	161	80
SG216(2)	10	.085	.20	156	80
SG212	10	.06	.16	120	76
SG212	12	.015	.19	137	80
SG212	15	0	.18	153	82
CM3B	10	.32	.08	205	111

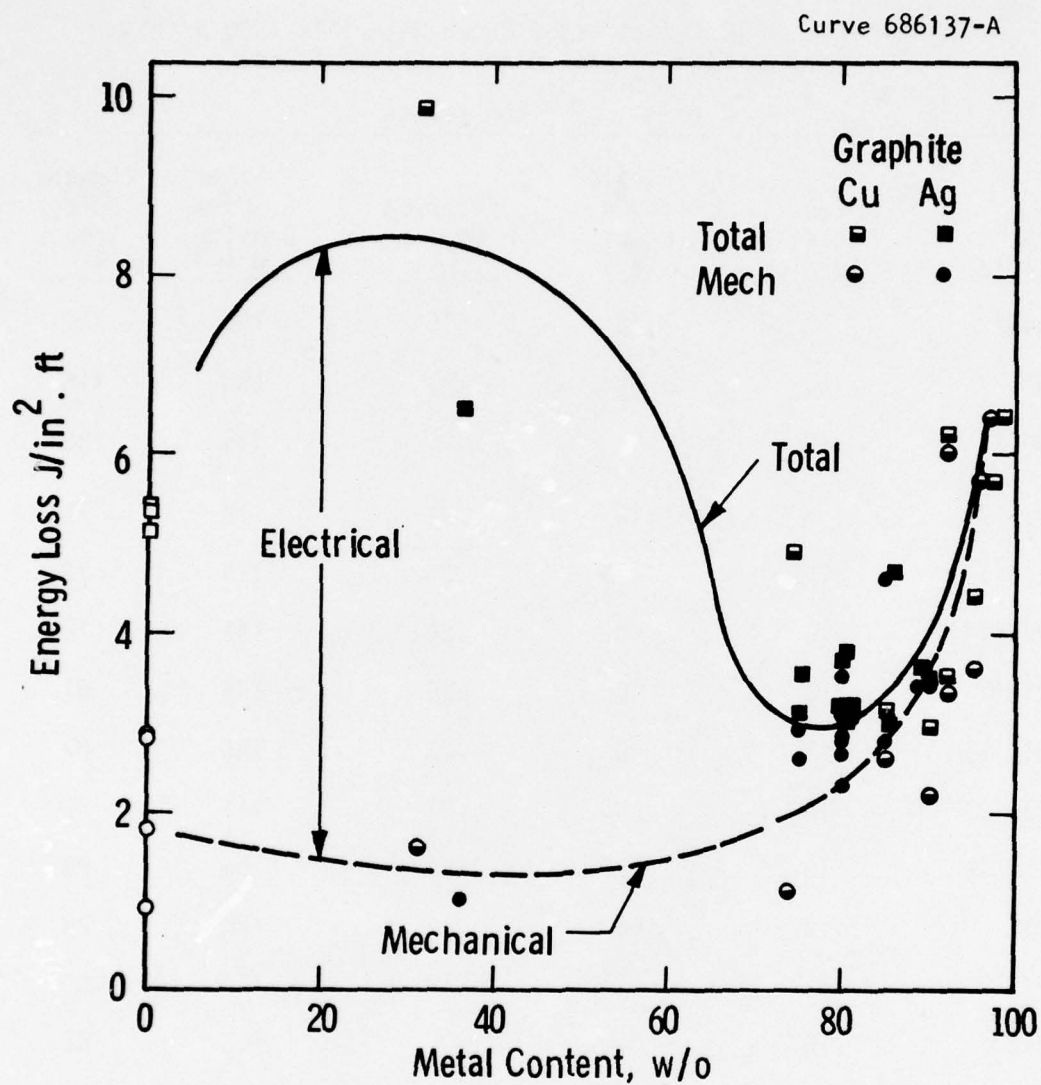


Fig. 9.3: Metal Graphite Brush-Copper Ring Contact Loss Characteristics 500 A/in², 10-12 lb_f/in², 42-83 ft/s, inert gas ambient.

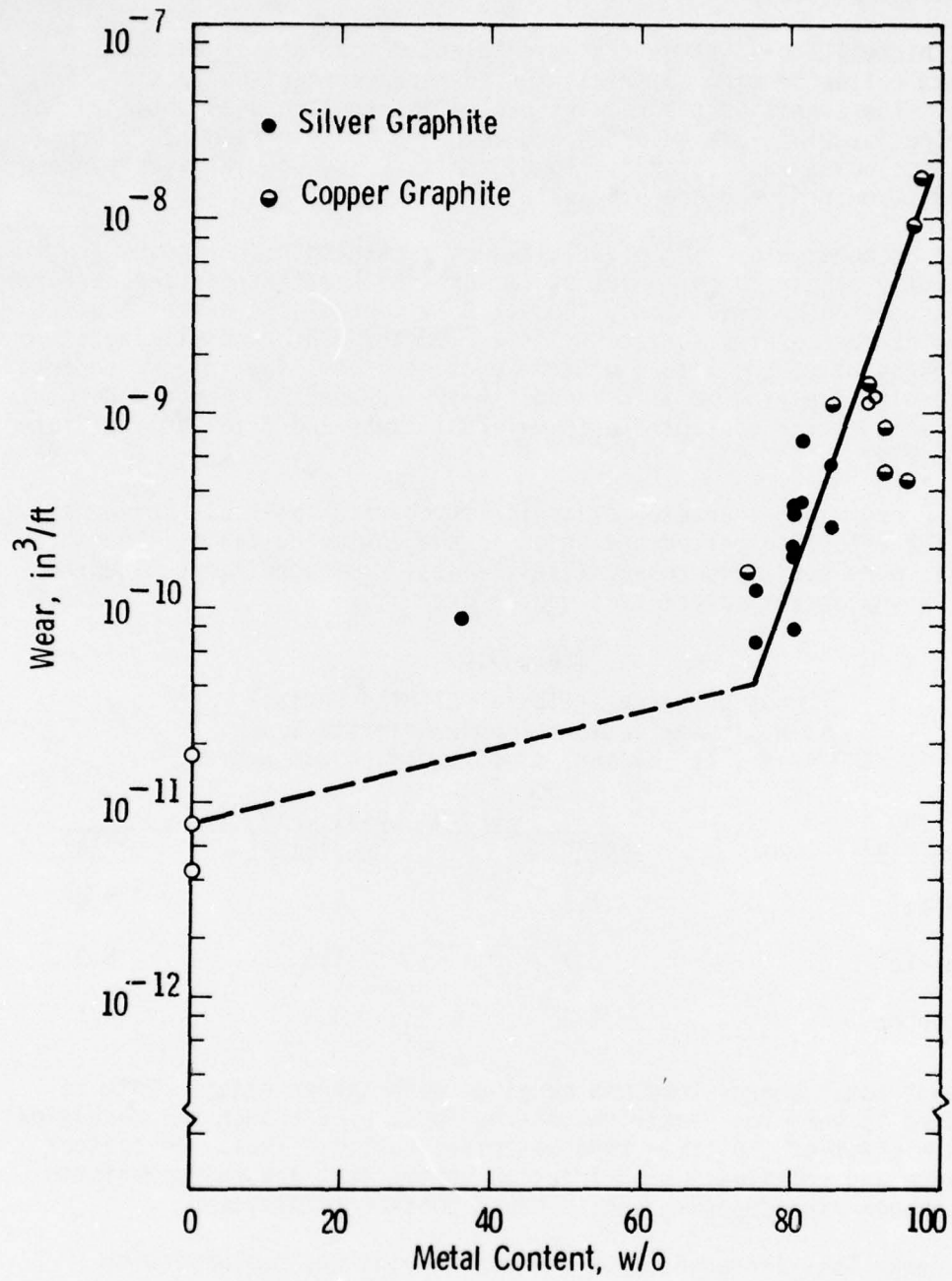


Fig. 9.4: Metal Graphite Brush Wear Characteristics. Copper Ring, 500 A/in², 10-12 lbf/in², 42-83 ft/s, inert gas ambient.

9.3.5 Ring Materials

Copper, nickel, and steel metals were selected for initial evaluation as candidate collector ring materials for advanced current collection systems. The significant screening evaluation test results obtained for these ring materials are reported and compared in this report. Other metals, including super copper alloys, brasses, and special steels, were selected, machined, and are available for testing.

Physical properties of ring materials such as strength, hardness, and conductivity appear to be important factors which affect contact performance. For given operating conditions, these likely control the extent and adhesion of the complex surface films formed through brush sliding action and, consequently, the actual or true contact area. The integrated area, combined with the ring metal's conductivity and specific shear strength, then determines the contact electrical resistance and friction coefficient, respectively.

Contact energy loss characteristics for three ring materials screened during the reporting period are shown in the following table. The three materials were subjected to relatively modest test conditions, and the mating brush contact material is copper-graphite.

Table 9.5
Loss Characteristics of Sliding Contact
Material Combinations Copper-Graphite Brush,
500 A/in², 12 lbf/in², 51 ft/s, inert gas ambient

Ring Material	Energy Loss, J/in ² -ft		
	Electrical	Mechanical	Total
Steel	7.3	2.3	9.6
Nickel	3.7	1.6	5.3
Copper	0.8	3.3	4.1

The lowest total energy loss was obtained with copper rings. This is attributed to very low electrical energy loss, even though the mechanical loss is highest of the three ring materials tested. Thus, low contact resistance and relatively high friction coefficient are characteristic of the copper ring/copper-graphite brush contact combination.

Total energy loss increased when the copper ring was replaced with nickel, then steel. This is attributed to high electrical energy losses associated with the latter materials, especially with steel. The mechanical component losses for nickel and steel rings are significantly

lower than that of copper. Thus, relatively high contact resistances and low friction coefficients are characteristic of the nickel and steel ring/copper-graphite brush contact combinations.

Long brush life was obtained for each of the three ring materials evaluated. The longest and shortest brush life was found for copper and steel rings, respectively.

9.3.6 Additive Materials

In a related program (ONR/ARPA Contract N00014-76-C-0683), additive vapor source materials were selected for further evaluation and will be reported as part of that contract.

9.4 CONCLUSIONS

Based on the data shown above, the following conclusions are made:

- The performance characteristics of copper and silver-graphite brushes of comparable metal content are similar. Thus, economies in brushes can be realized by employing copper rather than silver.
- Total contact energy loss (mechanical plus electrical) is minimal when the metal content of graphite brushes is near 75 w/o.
- Total contact energy loss is dominated by the electrical component when the metal content of brushes is less than about 70 w/o, but by the mechanical component at larger percentages.
- Brush wear is very low for small additions of metal, increasing at a modest rate up to about 75 w/o. At higher metal percentages brush wear increases sharply.
- Based on the screening test data, it appears that commercially available graphite brushes containing 65 to 75 w/o copper are reasonable candidates for more extensive testing and evaluation on larger, more sophisticated test machines.
- Copper graphite brushes riding on a copper ring provide a better contact combination than like brushes on steel or nickel rings. This is based on both loss and wear rate considerations.

9.5 REFERENCES

1. Baker, R.M. and Hewitt, G.W., Contact Drop and Wear of Sliding Contacts, AIEE Trans., Vol. 56, pp. 123-28, Jan. 1937.

9.5 REFERENCES (Cont'd.)

2. Johnson, J.L. and Moberly, L.E., Brush Life and Commutation in Atmospheres of Air, SF₆, and CO₂, Proc. Electrical Contacts, (1967), pp. 109-16.
3. Rhodenizer, R.L., Development of Solid and/or Liquid Metal Collectors for Acyclic Machines, Final Report for Tasks 1, 2, and 3, Navy Ship Systems Command Report, Contract No. N00024-68-C-5415, February 27, 1970.

VOLUME II
PART B
SECTION 10
CURRENT COLLECTOR MECHANICAL LOAD SYSTEMS

10.0 OBJECTIVES

The objective of the mechanical load system program is to develop a system capable of controlling the brush loads to acceptable values. The acceptable values are specified by the Current Collection Contact Material/Performance program that was discussed in Volume II, Part B, Section 9. The contact material performance program will determine what is required of the brush system for efficient current transfer and the mechanical load system will determine how to achieve these requirements.

10.1 PRIOR AND RELATED WORK

The basic function of a current collection system is to transfer electrical power between stationary and rotating contact members efficiently, reliably, and with long life. Much experience in the application of solid brush current collectors for this purpose has been accumulated over the years at Westinghouse and elsewhere, for brush systems operating at conventional current densities (93 KA/m^2 , 60 A/in^2) in ambient air environments. This work has been used as a foundation with the present effort utilized to extend the technology to the high current densities ($3.1 \times 10^6 \text{ A/m}^2$, 2000 A/in^2).

10.2 SUMMARY OF ACCOMPLISHMENTS

10.2.0 General

High current density brush holders were designed and built for the (HS1 and HS2) High Speed Test rigs. These brush holders were the result of efforts to obtain an immediate test vehicle. The design configuration consisted of a water cooled holder surrounding a rectangular shaped solid brush, constant force springs and conventional (pigtail) electrical shunts to provide a low resistance current path.

Brush holders were designed and built for the Machine Environment Brush Tester (MEB). The design philosophy was similar to that used for the High Speed Testers.

In the area of cooling however the design configurations differ. Both machines exhibit water cooled brush holders, but only the MEB has a water cooled rotor.

The ability of fiber brush shunts to transfer high density current through the solid brush and into the stator conductor was proved.

10.2.1 Brush Holding System

The first task was to design a brush holding system suitable for testing high current density brushes. These brush holders were designed for the full-size brush test rigs (HS1 and HS2) described in Volume II, Part B, Section 8 of this report. The basic design philosophy was to utilize existing technology as much as possible in an effort to obtain an immediate test vehicle.

The high power density in the brush holders required water cooling. The cooling water was piped in and out of the brush holders via nominal 3/8 inch copper tubing that also carried the electrical current to and from the brush holders. Before building the test stand a section of copper tubing was subjected to typical testing conditions. The test apparatus consisted of a 3 foot section of nominal 3/8 inch copper tubing with copper blocks attached to each end. One end of the tubing was attached through the use of a nominal 3/8 inch brass "Swagelok" fitting and the other end was attached with soft solder. The conclusions of the test were as follows:

- 1) The tubing, tube fitting and solder joint passed current and cooling water acceptably.
- 2) The nominal design current (400 amps) could be doubled without failure of the circuit in case a current sharing problem would exist in the full size brush test rig.

Figure 10.1 is a photograph of the brush holder arrangement used in the HS1 High-Speed Brush Tester. The copper tubing shown at the right transports cooling water as well as current between the brush holder and ground. The main body of the brush holder is machined from two pieces of copper stock. The two pieces are bolted together at the vertical joint that borders the left side of the brush. The test brushes are nominally 5/16 x 5/8 inch cross-section and 1.56 long. The brush is fitted into a rectangular hole (1.0 inch long) that passes through the brush holder and meets the rotor in radial fashion. A nominal 0.06 inch gap exists between the holder and the rotor. The side clearance between the brush and holder averages 0.0025 inch for all four sides. Current is transported between the brush and holder through three flexible shunts made from braided copper cable. Located directly above the brush is the spring holder assembly. The spring loading mechanism consists of a constant force spring attached to an "L" shaped holder. The mechanical load imposed on the brush by the constant force spring can be changed through the use of different springs and/or multiple springs rolled together in an assembly.

The brush holders were utilized in brush screening tests for several months and have presented no apparent problems. Thermocouples were imbedded throughout the holder for a thermal analysis which is discussed in Volume II, Part B, Section 11 of this report.

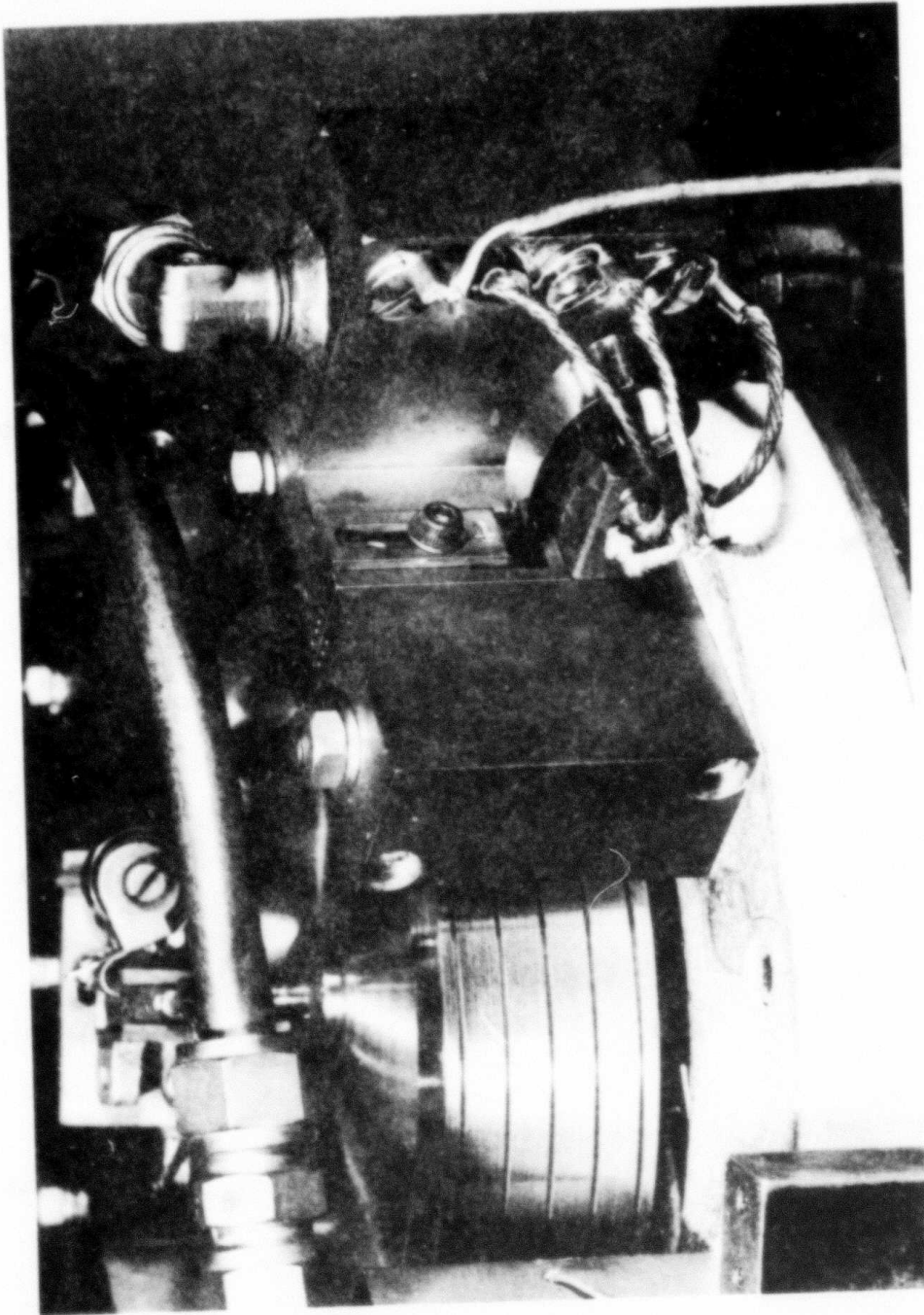


Fig. 10.1: Brush Holder used in HSI brush test rig.

Since the brush holders for the HSI brush test rig worked favorably, a similar system was designed for the Machine Environment Brush Tester (MEB) described in Volume II, Part B, Section 8 of this report. The basic design philosophy was to design the brush holding system utilizing parts from the HSI brush test rig. Figure 10.2 shows an isometric view of the brush holder arrangement for the Machine Environment Brush Tester (MEB). The view shows the machine brush holder area with the brush housing cover removed.

The brush holder consists of three copper rings sandwiched together with bolts that tie the holder assembly to the stator conductor drum. The brush holder has been divided into three rings for ease of machining the brush holes accurately. Good electrical contact is maintained between the brush holder and the stator drum when disassembled and reassembled due to silver plating of the contact faces. Also the flange bolt loading for this electrical contact is on the order of 1000 lb/in^2 .

The electrical shunts from the brushes are connected to the holder ring that makes contact with the stator conductor drum. The shunts are of equal length and cross-section in order to provide uniform electrical resistance. The shunts are instrumented at typical locations in an effort to investigate current sharing between brushes operating in parallel.

The brushes are fit into rectangular holes in a manner identical to that of the HSI Brush Tester. The brushes are held in place with constant force springs. The spring holder assembly consists of a metal cross with springs riveted on two opposing sides as shown in Fig. 10.2. Spare sets of spring holder assemblies utilizing various spring combinations are available for changing brush mechanical loading.

The brush holder is cooled by two circumferential water carrying copper tubes soldered into the brush holder assembly as shown in Fig. 10.2.

10.2.2 Electrical Shunts

The purpose of the electrical shunt is to transfer current from the solid brush to the stator conductor with low loss, and with free radial motion.

Conventional pig tail shunts were analyzed and were found to impose excessive mechanical load on the brush when designed for low electrical loss. The size of these conventional shunts becomes excessive for high current density brushes.

Another disadvantage of the pig tail shunt is the substantial electrical resistance (I^2R) loss in the solid brush. These losses are inherent in this configuration since pig tail shunts cannot be fastened near the brush slip ring interface. Ideally current should be transferred from immediately

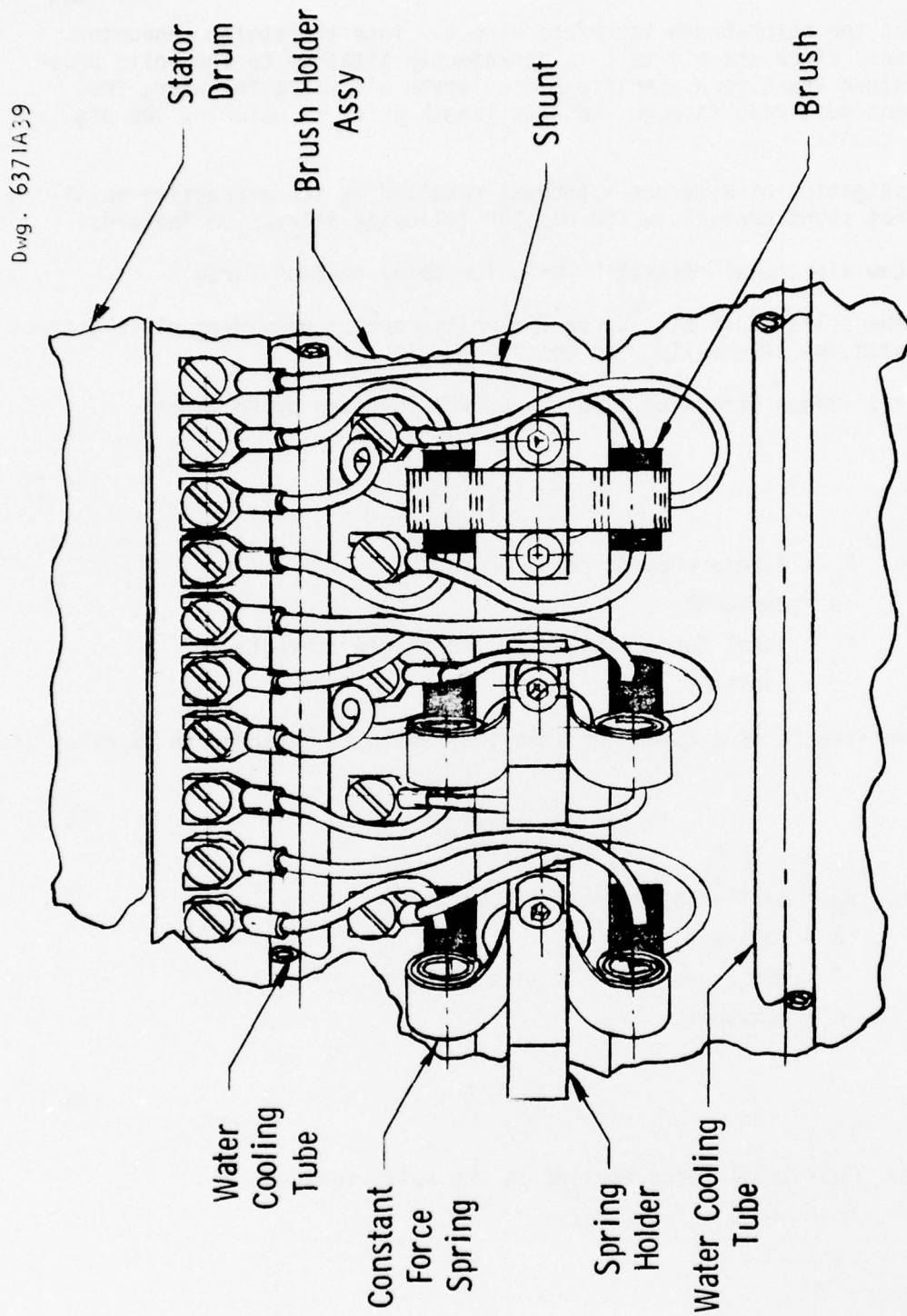


Fig. 10.2: Brushholder Arrangement for the Machine-Environment Brush Tester (MEB)

behind the rotor-brush interface directly into the stator conductor. However, since the pig tail is permanently attached to the solid brush and since there is a specific brush length allowance for wear, the current must pass through the wear length prior to entering the pig tail shunt.

Investigation of alternate concepts resulted in the attractive multi-contact shunt concept, which has the following attractive features:

- 1) Low electrical resistance at a low total contact force.
- 2) The solid brush sliding on the multi-contact providing close contact with the brush-slip ring interface.

The resistance of a single point contact is given by Holm¹ as:

$$R_s = \frac{a}{(F_s)^m} \quad (10.1)$$

where: R_s = single contact resistance,
 a = constant,
 F_s = total force applied to the single contact,
 m = constant.

The resistance of a number of identical contacts arranged in parallel is:

$$R_M = \frac{a}{n(f)^m} \quad (10.2)$$

where: R_M = multi-contact resistance,
 a = constant,
 f = force per multi-contact point,
 m = constant,

$$F_M = n f \quad (10.3)$$

where: F_M = total force applied to the multi-contact,
 n = number of contacts.

$$R_M = \frac{a}{n^{(1-m)} (F_M)^m}$$

$$\text{Setting: } R_S = R_M$$

$$\text{Yields: } F_S/F_M = n^{(1-m/m)} \quad (10.4)$$

Equation (10.4) reveals that for a given electrical resistance the total force required for a multi-contact is less than the total force required for a single contact when $m < 1$. For $m = 0.33$ which corresponds to non-oxidized, lightly loaded, copper on copper contacts:¹

$$F_M = \frac{F_S}{(n)^{2.03}} \quad (10.5)$$

For $n = 10$ contacts the total multi-contact force required is approximately 100 times less than a single contact force (at equal electrical resistance).

The presence of alien films on the contacts reduces the advantages of multi-contacts over single contacts. These films are usually oxides and tend to cause not only higher resistance but also a higher constant, m . For oxidized, lightly loaded and copper-on-copper contacts, $m = .65$,¹

$$F_M = \frac{F_S}{(n)^{.54}} \quad (10.6)$$

For $n = 10$ contacts the total multi-contact force required is approximately four times less than a single contact force (at equal electrical resistance). The advantage of multi-contacts, although still present, has been reduced 25 times due to the oxidized surfaces.

Several metal fiber shunts were made in order to investigate manufacturing techniques and to obtain test data for multi-contacts. The metal fiber shunts were made of brass tufts drawn into a brass base with a brass tie wire. The electrical connection between the fiber tuft and the base was found to be inadequate. The use of soft solder provided an acceptable electrical junction. Figure 10.3 is a photograph of a typical metal fiber shunt with the tufts angled into the base. This particular shunt was also silver plated.

Figure 10.4 is a photograph of the experimental set up for static testing of the metal fiber shunt. The fiber shunt is attached to a large metal heat sink. The mating part of the shunt is a long metal bar suspended from the ceiling. The long length of the suspension cable results in practically perpendicular motion of the bar to the fiber shunt base. The suspended bar completes the electrical circuit with the fiber shunt. The load to the multi-contact was applied through a cantilevered beam and strain gauge assembly. Mechanical loading is provided by adjusting a screw threaded through the end of the cantilever.

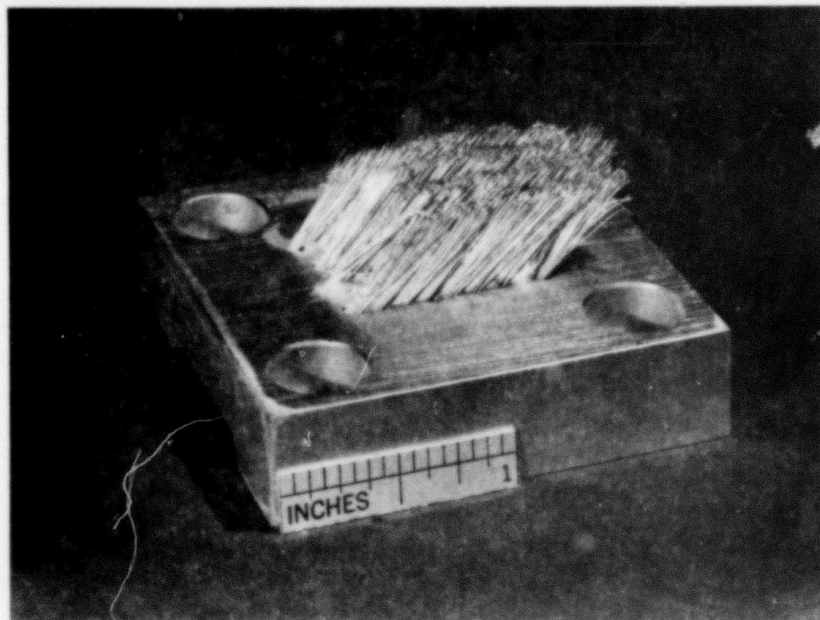


Fig. 10.3: Experimental shunt using silver plated metal fibers.

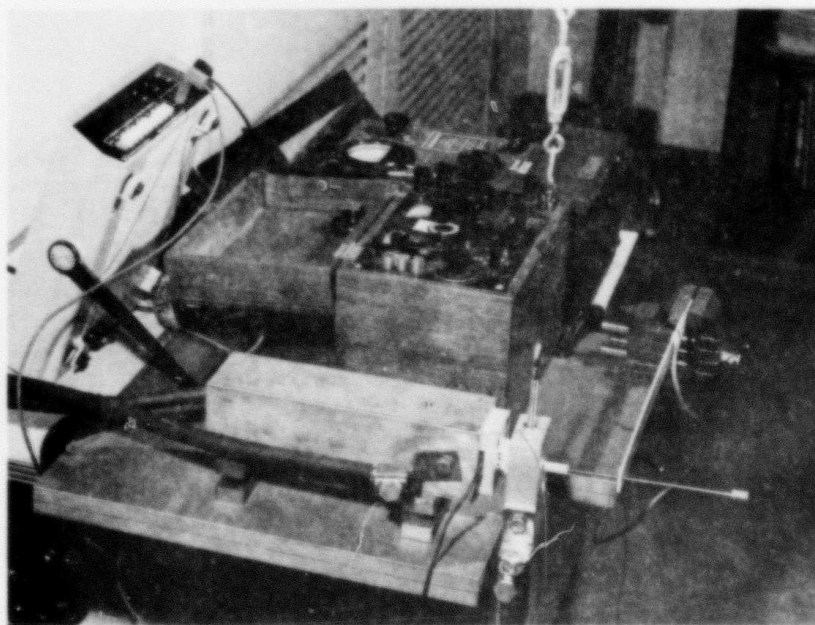


Fig. 10.4: Metal fiber shunt electrical test site; current path in foreground shows shunt test block mounted to heat sink and shunt mating piece suspended from ceiling. Mating piece is pressed against shunt by cantilevered strain gauge assembly.

The static tests were initiated in order to establish the empirical constants in the resistance-force relationship.

Following the static tests, the design of the metal fiber shunts will be reviewed and updated. The redesigned fiber shunt will be utilized in a related program (ONR/ARPA Contract N00014-76-C-0683 in one of the solid brush test rigs. The test data from the dynamic rigs should yield information valuable in the design of full-size SEGMAG machines.

10.2.3 Actuation System

The actuation system is that part of the brush holder system which mechanically loads or lifts the brushes. The brush is loaded; that is pressed against the rotor slip ring, through the use of constant force springs. The mechanism which lifts the solid brush is a cable attached to the solid brush and spring assembly. The cable is pneumatically actuated by a cylinder located outside the brush area. A full-size model of this solid brush holder actuation system was constructed for use in evaluating potential brush holder problems.

10.3 CONCLUSIONS

Solid brush holders for medium high current density applications are within existing technology. To accommodate high current density however, the number of pig tail shunts necessary to maintain minimum electrical loss in the holder becomes unwieldy. Excessive spring mechanical loads are exerted on the solid brush by these shunts. Fiber shunts are the logical alternative to pig tail shunts because they offer the following comparative advantages:

- 1) Less mechanical force is exerted on a solid brush by a multiple contact fiber bustle shunt than by a single contact pig tail shunt, given that both exhibit the same total electrical resistance.
- 2) The current path through the solid brush is shortened by metal fiber shunts since these can be situated closer to the solid brush-slip ring interface than pig tail shunts, thus reducing I^2R losses generated in the solid brush matrix.

Possibilities also exist to apply multiple fiber techniques in construction of fiber brushes. Geometric and dynamic operational characteristics of such brushes require further investigation.

10.4 REFERENCES

- ¹Holm, Ragnar; Electric Contacts - Theory and Application; Springer-Verlag; 1967; Germany.

VOLUME II
PART B
SECTION 11
CURRENT COLLECTOR INTERFACE COOLING SYSTEMS

11.1 OBJECTIVES

The objectives of the Interface Cooling System program is to determine the heat transfer characteristics of the high current density brush-holders. These heat transfer characteristics will be correlated with the solid brush objectives in order to determine high current density brush holder heat transfer design requirements and procedures.

11.2 PRIOR AND RELATED WORK

Westinghouse has accumulated much experience over the years in the application of solid brush current collectors. This experience has been with conventional current densities (93 KA/m^2 , 60 A/in^2) where transferring the heat from the brush holder was not considered a problem area. The high current densities ($3.1 \times 10^6 \text{ A/m}^2$, 2000 A/in^2) increase the power density in the brush holder area to a point where heat transfer has become an area of concern. The intent of the on-going work is to utilize the Westinghouse experience to support the evaluation of the heat transfer in the brush holder area for high current density brushes.

11.3 SUMMARY OF ACCOMPLISHMENTS

11.3.0 General

The brush holder heat transfer characteristics of the HSI Brush Tester and the Machine-Environment Brush Tester (MEB) were analyzed. It was found that the thermal resistance between the brush and the holder was the major thermal barrier of the system. This thermal resistance is complicated and can vary significantly depending on brush position in the holder, clearance, brush loading, geometry, surface finish, material properties and atmospheric properties of the brush holder environment. The brush holders and brushes were instrumented in an effort to determine the thermal resistance. The experimental data was then correlated with theory in an effort to understand the heat transfer mechanism between the brush and holder.

The HSI Brush Tester was instrumented with thermocouples so that one could determine:

- The heat transfer from the brush in each direction.

- The heat generated in the brush.
- The thermal resistance between the brush and the holder.

This brush holder is described in detail in Volume II, Part B, Section 10 of this report, and shown in Figure 11.1.

The heat generated in the brush is due to the mechanical friction at the brush slip ring interface and the electrical joule heating from the brush, the shunts and the brush-slip ring interface. Heat is transferred primarily from the brush via the shunts, the rotor and the brush-to-brush holder contact. An energy balance yields the heat transferred from the brush to the brush holder, which, with the temperature difference between the brush and brush holder, yields the needed thermal resistance.

The thermal data from the HSI test was evaluated. The results indicate the present HSI brush holder meets the program thermal objectives. The brush holder is capable of extracting 30% of the heat generated as a result of brush losses. The remaining heat is extracted through the rotor cooling system.

The losses used for the calculation were based on the present brush testing status. This basic brush holder thermal information will be utilized as a guideline for the evaluation of future brush holder concepts in a related program (ONR/ARPA Contract N00014-76-C-0683).

Similar thermal instrumentation is designed into the Machine Environment Brush Tester (MEB), which is described in detail in Volume II, Part B, Section 10 and shown in Fig. 10-2. The major differences with respect to heat transfer between the MEB and the HSI brush testers are as follows:

- The brush holders in the Machine Environment Tester (MEB) support 48 brushes in two rows (24 in each row). The HSI tester has one brush for each holder. The multiple brush holder must contend with thermal gradients through the holder yielding variations in temperature between different brushes whereas the single brush holder does not.
- The heat transfer from the brush to the rotor in the HSI Brush Tester is approximately 1/3 that for the MEB Tester. An increase in heat removed through the rotor reduces the importance of the thermal resistance between the brush and the holder.

The Machine Environment Brush Tester (MEB) is designed to determine the effects of the thermal gradients and the rotor heat transfer. This fully instrumented test rig will provide valuable information for the heat transfer analysis.

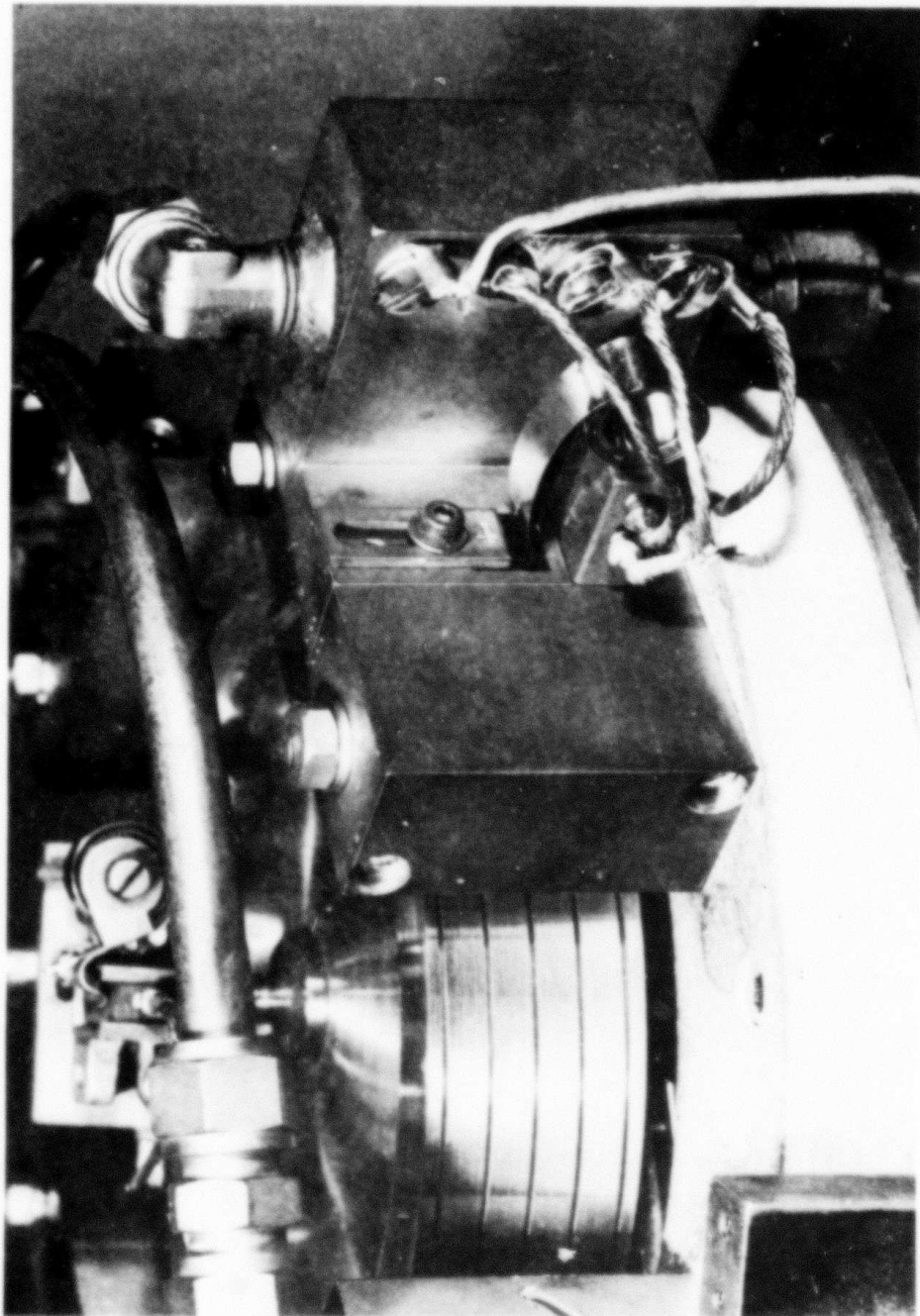


Fig. 11.1: Brush holder used in HSI brush test rig.

VOLUME II

PART B

SECTION 12

CURRENT COLLECTOR GASEOUS ENVIRONMENT/CONTROL

12.1 OBJECTIVES

The objective of this effort is to provide a controlled gaseous environment in the machine current collector area. Internal pressure, gas purity and moisture content must be controlled.

12.2 PRIOR AND RELATED WORK

Work at the Westinghouse Research Laboratories, among others, has indicated the necessity of providing a controlled gaseous environment in the current collector area to prolong brush life.

12.3 SUMMARY OF ACCOMPLISHMENTS

12.3.0 General

A gas recirculating system was designed and constructed for the purpose of controlling the internal ambient atmosphere of a Machine Environment Brush Test (MEB) being used in the development of advanced solid current collection brushes. Capabilities of the gas system include: operation with a variety of non-oxidizing gases over a wide range of flow rates and preset moisture concentrations; removal of particulate debris from brush wear and vapor product contaminants from test facility outgassing; and maintenance of a predetermined positive pressure level. Descriptions of the gas system and of the general operating procedures for its use are presented below.

12.3.1 Gaseous Environment Control System

The MEB environment gas control and purification system was designed and assembled. It is a compact (17" x 22" x 69"), lightweight, and readily portable unit. Once moved into position, only three standard tube connections are required prior to placing it into operation.

The front panel of the gas control system is shown in Fig. 12.1. Here, most control valves, pressure gauges, flowmeters, and the humidity indicator are readily available to the operator. Many of the internal components, such as filters, traps, probes, and the water bubbler may be seen in Fig. 12.2, which is a rear view of the control system. The



Fig. 12.1: Front panel view of gas control system.

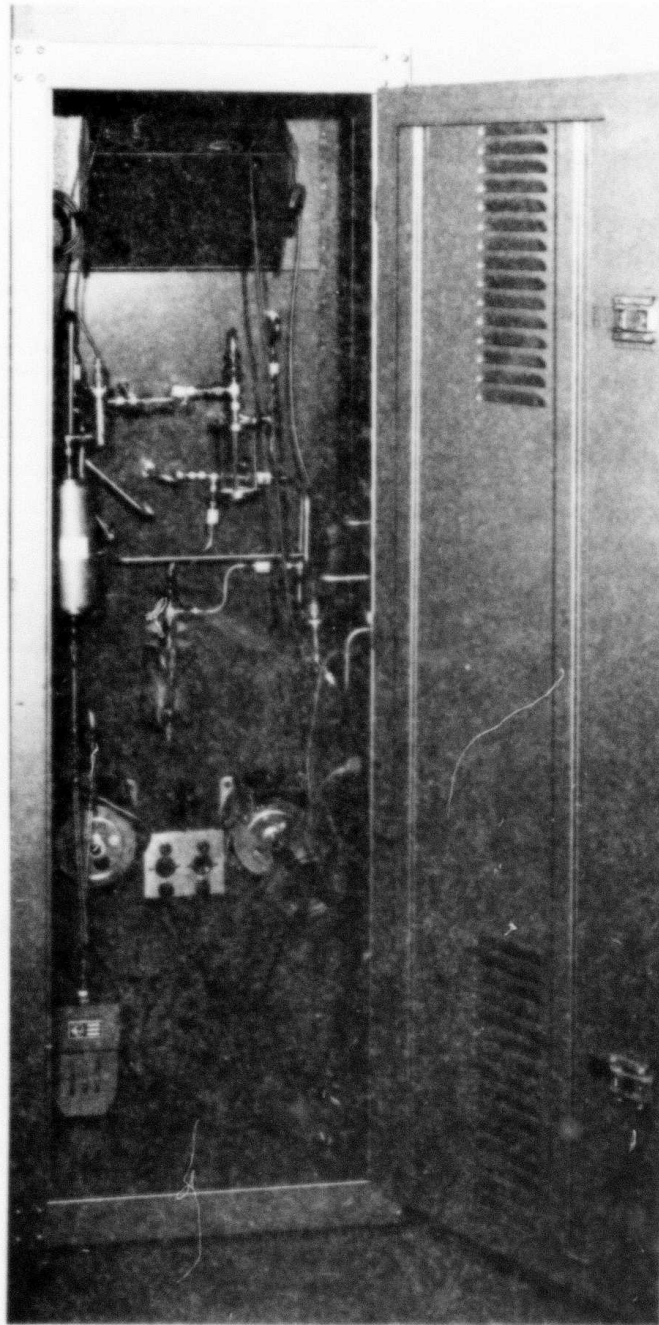


Fig. 12.2: Rear view of gas control system.

design utilizes a closed recirculation loop wherein potential, but undesired, reaction and outgassing products from the MEB test rig are removed from the gas stream, while maintaining the desired internal pressure, dew point, and gas flow rate.

A schematic flow diagram representative of the gas flow system is shown in Fig. 12.3. Starting at the gas inlet port, gas flows through a dust trap (2) with a transparent cover, where large dust particles are removed and can be observed. Then gas flows through a 60 micron-size filter (4) for removing smaller particles. The trap and the filter serve primarily to remove particulate brush-ring wear debris from the gas stream. Pressure gauges (3) and (5) are provided on either side of the filter. A significant change in pressure across the filter is an indication of impending plugging, and filter replacement should be made at the earliest convenience.

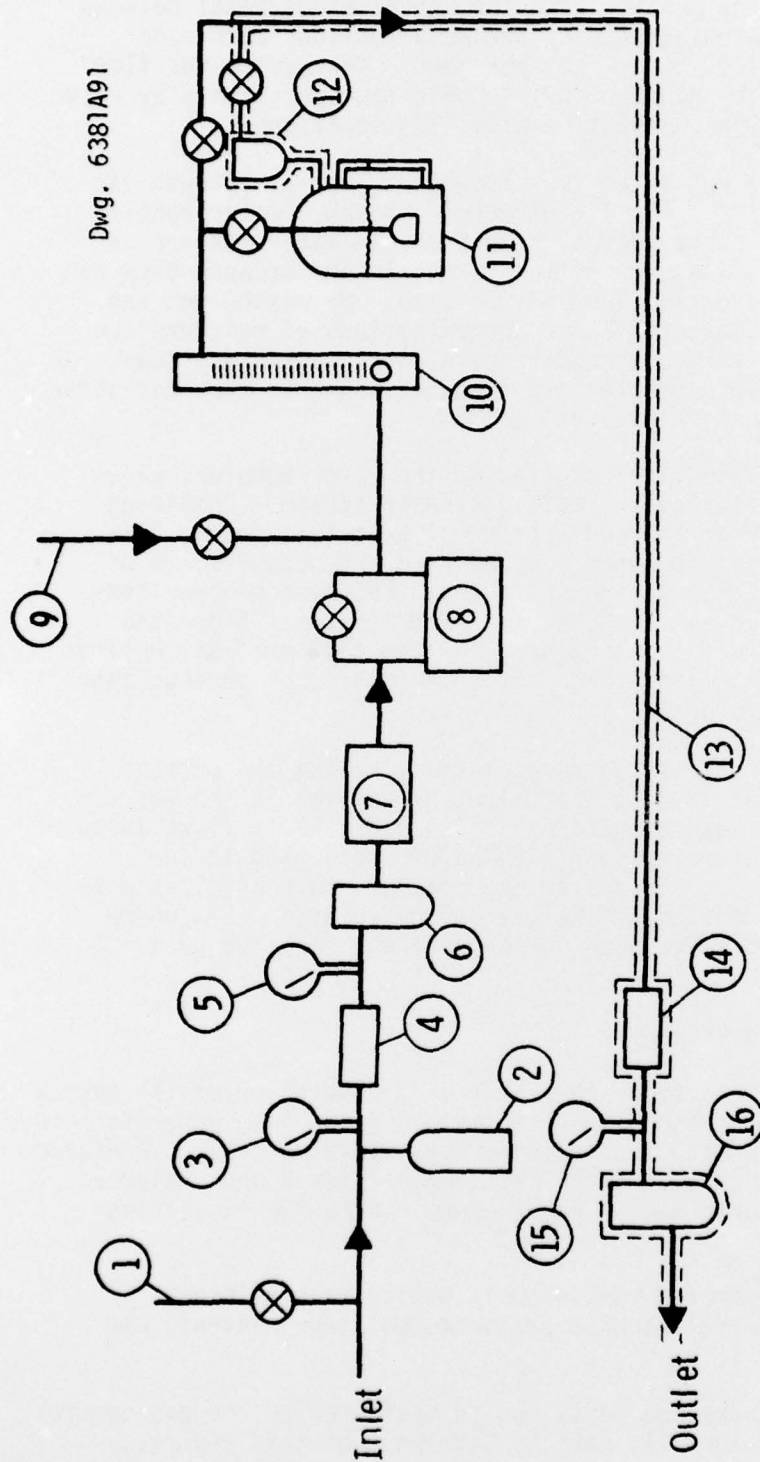
The next element of the flow loop is an electronic moisture probe (6), where moisture content of the machine exit gas is monitored. Here, a Panametrics Electronic Hygrometer (Model 1000) is used to obtain the gas humidity in parts per million by volume. A check on the calibration of the instrument may be made by drawing a sample of gas from the gas sample valve (1) through a simple dew point cup.

Excessive amounts of most organic vapors cause brush performance to be adversely affected. This is manifested by high, unstable contact voltage. To ward against such effects, outgassing products from the material's insulation, seals, etc., must be removed from the gas stream to maintain predetermined optimum gas water vapor content. Following the first moisture probe (6), the gas is passed through an adsorbing bed (7) to remove vaporous outgassing impurities.

During initial machine-brush studies,* when it is planned to use carbon dioxide and water vapor for the gas atmosphere and vapor additive, the adsorbing column will be packed with activated coconut shell carbon. Such activated carbon has a low capacity for adsorbing carbon dioxide and water but a high capacity for adsorbing most acids, solvents, expected decomposition products, and ozone. During subsequent brush-gas tests, where deliberate additions of vapors other than water will be desired, different adsorbing beds may be required. Such bed systems may include molecular sieve, silica gel, or other selective adsorber media.

The present system does not effectively remove oxygen. Consequently, careful initial purging of the machine-gas system will be required if more than trace oxygen concentrations are considered a problem.

*To be performed under a related program (ONR/ARPA Contract N00014-76-C-0683).



- | | |
|---------------------------|-------------------------------------|
| 1. Sample Port | 9. Make Up Gas |
| 2. Dust Trap | 10. Flow Meter |
| 3. Pressure Before Filter | 11. Water Bubblers |
| 4. 60 μ Filter | 12. Aerosol Trap |
| 5. Pressure After Filter | 13. Return Gas Line With Trace Heat |
| 6. Moisture Probe | 14. 15 μ Filter |
| 7. Charcoal Filter | 15. System Pressure |
| 8. Bellows Pump | 16. Moisture Probe |

Fig. 12.3: Current collection gaseous environment control system for use with the Machine Environment Brush Tester (MEB).

Following the adsorber, the gas is drawn through a welded metal bellows pump (8). This pump is manufactured by the Metal Bellows Corp. and has a pumping capacity of 80 cubic feet per hour. The system gas flow rate is controllable in the range of 0-1.4 cubic feet per minute by valve adjustments at the pump bypass and flowmeter (10) locations.

After passing through the rotameter-type flowmeter, the gas stream is split and may be partially or totally directed through a water bubbler (11), which is generally surrounded by either an ice-water mixture or air at room temperature. These conditions are selected because they can be easily held constant over long periods of time. By mixing wet and dry gas streams, intermediate and lower concentrations of moisture are achievable, which otherwise would require more costly auxiliary means for maintaining intermediate bubbler temperatures, such as the incorporation of a trap held at temperatures below 0°C.

A trap (12) is provided immediately following the water bubbler, which prevents aerosols from entering the main gas-vapor stream. Combining the action of this trap with the application of heat (13) to the flow lines assures against possible water condensation and accumulation of fluid. To avoid condensation during operation, the water bubbler temperature must be at the lowest temperature in the system. Since the highest moisture concentration anticipated for the test program requires the bubbler to be held no higher than room temperature, no serious condensation problem is anticipated.

A 15 micron filter (14) follows the aerosol trap, having the purpose of removing solid material or dust that might be carried in the gas stream from the charcoal adsorbing column. The gas finally flows through a second Panametrics moisture monitor (16) before returning to the test machine (outlet port). The system gas pressure is controllable to 15 psi gauge (15) by regulation at the gas source location (9), where gas is continuously added to make up for any leakage from the system.

12.3.2 General Operating Procedure

After the initial tube connections have been made, operation of the system can begin with evaluating the MEB test facility and the gas system to remove the air, then backfilling with the selected non-oxidizing gas. Circulation of the gas can then be initiated and a gas sample removed and analyzed. Another evacuation and purge may be required to reduce the impurities to an acceptable level.

The gas system will be operated continuously during machine brush testing, controlling internal machine pressure, moisture content, and gas purity.

A short description of shakedown tests run to characterize the gas control system is contained in Volume II, Part A, Section 6 of this report.

12.4 CONCLUSIONS

- 1) A gas control system, capable of supplying non-oxidizing gases such as CO_2 , He, and N_2 at a preselected moisture concentration level, has been successfully designed and constructed. This system is ready for use in the development of advanced, high current density - solid brushes.
- 2) For initial testing of solid brushes in humidified carbon dioxide environments, the gas control system described in this report is adequate, providing that trace amounts of oxygen are not objectionable.
- 3) Subsequent brush testing in gas environments having hydrocarbon vapor additives will require that the activated charcoal adsorbing medium be replaced with a more suitable material, such as molecular sieve, silica gel, or other selective adsorbers, which passes the specific hydrocarbon.